

Université de Bordeaux

Ecole Doctorale des Sciences de la Vie et de la Santé

Année 2016

Thèse

Pour le

DOCTORAT DE L'UNIVERSITE DE BORDEAUX

Thesis submitted for the degree of Doctor of Philosophy (PhD)

Mention : Sciences, technologies, Santé

Option : Neurosciences

Présentée et soutenue publiquement

Le 30 Novembre 2016

Par **Steve DOS SANTOS CARVALHO**

Né le 12 Septembre 1985 à Ivry-Sur-Seine (94)

Morpho-functional impact of Vangl2 on hippocampus development

Membres du jury :

Dr. Olivier Thoumine

Dr. Fanny Mann

Dr. Froylan Calderon de Anda

Prof. Esther Stoeckli

Dr. Mireille Montcouquiol

Université de Bordeaux

Université Aix Marseille

UKE (Hamburg)

Université de Zurich (UZH)

Université de Bordeaux

Président

Rapportrice

Rapporteur

Examineur

Directrice de thèse

Acknowledgements

First of all I would like to thank to the members of the jury for accepting to evaluate this dissertation about my thesis work but also for their presence: Dr. Olivier Thoumine, Dr. Fanny Mann, Dr Froylan Calderon de Anda and Prof. Esther Stoeckli.

I would also like to thank the European Neuroscience Campus-Network, the Fondation pour la Recherche Médicale, the Agence Nationale de la Recherche and the Labex Brain foundation for the financial support of our projects.

Most importantly, I would like to thank my thesis supervisor, Dr. Mireille Montcouquiol, for all her support, guidance and brightness. She really is one of the best scientists that I ever met and I really am lucky to have had the opportunity to work with her. She was always there to pull me up and guide me into the right direction when things didn't go so well. She really is one of the persons that really changed me...for better.

Dr. Nathalie Sans, my "other boss", if I may, is another person that highly contributed to this work and also for my formation. She was always comprehensive and kind and guided me along the way as much as Mireille.

During my thesis I also had the opportunity to work with the Prof. Esther Stoeckli, at the University of Zurich, Switzerland. I had the chance to learn about and work with a totally different model: the chicken. I would like to thank her for all the knowledge that she passed to me, as well as to all the members of the team that helped me during my internship: Michael, Evely, Justin, Vlad, Beat, Irene, Tiziana, Jeannine, Laura and Tobias. All of them received me with open arms and contributed for my pleasant stay in Zurich during 6 months.

I would like to thank equally Dr. Christophe Mulle and his team, most particularly Mario Carta and Sabine Fièvre for teaching me how to culture organotypical slices and how to perform Single-Cell-Electroporations.

I also wish to thank all the members of our team as well as the ones that already left: Aysegul, Tamrat, Miki, Muna, Vera, Maureen, Nicolas, Cedric, Lea, Bénédicte, Hortense, Maité, Anne, Ben, Jerome, Ronan, Chantal, Stephanie and also our newest member Ana, for all the good

times we shared, not only in the lab but also in all the extracurricular activities. We really make a great team guys!

I could not forget all the friends that I made along the way, from the University back in Coimbra until this day in the whole Neurocampus (sorry if I didn't put your names in guys, but If I'd write down all of your names, my thesis would be twice longer as it is already!). One cannot live without friends and I can say that I have been lucky enough to have met so many different people from all over the world.

A special thank you for my family and most particularly, my Mother and my Brother, but also Joelle, Jean-Louis and Milou...their unconditional love and support has always been important...from when I was still a little boy until this very day.

Finally but certainly not last, the love of my life, my best friend, my companion, Léa, who has turned me into a better man. There are no words to describe the joy and gratefulness that I feel for having you by my side everyday.

Abstract

Planar Cell Polarity (PCP) is a signaling pathway originally known for its role in the establishment of cellular asymmetry perpendicular to the apico-basal axis, in the plane of an epithelium. PCP signaling has been shown to be crucial for many tissue patterning, including epithelial and mesenchymal tissue, but also cardiac, lung, bone, or kidney tissues, to cite a few. PCP signaling controls the regulation of cellular movement *via* the control of adhesion turnover and cytoskeleton reorganization.

Vangl2 is one of the most upstream core PCP proteins that has been implicated in the recent years in various neuronal mechanisms, such as axonal guidance, dendrite morphogenesis or synaptogenesis. However, most of these studies rely on acute downregulation of the gene *in vitro* or in the use of a mouse presenting a spontaneous mutation of this gene, called *Loop-tail* (Vangl2^{Lp}) which causes the death of the embryo at birth. Moreover, the Vangl2^{Lp} form of this protein has been described has a dominant-negative form, making it difficult to untangle the molecular mechanism leading to the many phenotypes (included neuronal ones) reported in homozygotes Looptail mice.

To bypass this problem we created a conditional knockout (cKO) mouse in which *vangl2* is deleted in the telencephalon during early embryogenesis. First, I analyzed the profile of expression of the protein during the first 3 weeks after birth, and I show that Vangl2 is specifically targeted to the arborization of granular cells (GC) of the dentate gyrus (DG) of the hippocampus, and excluded from cell bodies. Also, the protein was highly enriched in immature neurons of the subgranular zone of the DG, and in the *stratum lucidum*, a region of high-density contacts between the GC and the CA3. In this region, a special type of synapse is formed: the Mossy Fiber Bouton (MfB) / Thorny Excrescence (TE) synapse. These synapses are bigger and more complex than conventional synapses.

I then performed a structural and ultrastructural analysis of the DG/CA3 circuit in the Vangl2 cKO mice in order to understand the role of Vangl2 in the hippocampus maturation. For this, I used stereotaxic mice infection viruses, and Serial block face scanning electron microscopy (SBFsEM) with 3D reconstruction. Results show that in cKO mice, Mfs fasciculation is mildly impacted, and that the enlargement and complexification of the MfB/TE synapse is arrested, with TEs almost absent. I was able to link these morphological abnormalities to deficits in complex hippocampal-dependent learning tasks. This work demonstrates for the first time the importance of PCP signaling for the *in vivo* maturation of a specific hippocampal circuit and its specific cognitive consequences.

Next, I attempted to identify the functional consequences of *vangl2* deletion on young hippocampal neuron maturation. My results confirm that Vangl2 is expressed in young hippocampal neurons and that the deletion of the gene affected neurite outgrowth on N-cadherin substrate. I used spt-PALM-TIRF super-resolution microscopy to show that this increased neurite outgrowth was inversely proportional to a decrease in actin retrograde flow and to a decrease in the number of directed actin trajectories. These results strongly suggest that N-cadherin adhesions are affected by Vangl2 deletion. FRAP experiments demonstrated that in Vangl2 cKO neurons the recovery of N-cadherin molecules engaged in homophilic bindings (adhesion) was decreased, suggesting that the turnover of N-cadherin involved in adhesion is reduced. Altogether, I propose that Vangl2 controls the turnover/stability of N-cadherin proteins at adhesion sites to regulate local actin dynamics and consequently neuronal outgrowth.

Résumé

La Polarité Cellulaire Planaire (PCP) est une voie de signalisation originellement identifiée chez les invertébrés pour son rôle dans l'établissement d'une asymétrie cellulaire perpendiculaire à l'axe apico-basal. Elle définit une polarité dans le plan d'un épithélium et coordonne cette polarité dans tout l'épithélium. L'activation de la voie PCP conduit à une réorganisation du cytosquelette en passant par une modulation des zones d'adhésion, régulant ainsi la forme et les mouvements des cellules. La voie de signalisation de la PCP est conservée tout au long de l'évolution jusqu'au mammifères, et contrôle la morphogénèse de divers tissus dont les tissus épithéliaux et mésenchymateux, ainsi que pour les tissus cardiaques, osseux, pulmonaire ou encore rénaux, mais aussi le système nerveux pour n'en citer que quelques-uns.

Afin d'identifier le rôle de *vangl2*, un des gènes centraux de la PCP, dans la mise en place de la circuiterie hippocampale, nous avons créé un modèle murin où *vangl2* est supprimé de façon conditionnelle (cKO) dans le télencéphale à des stades précoces de l'embryogénèse.

J'ai d'abord montré que Vangl2 est enrichi dans les neurones immatures de la zone sous-granulaire du DG, ainsi que dans l'arborisation des neurites (axones et dendrites) des cellules granulaires (CG) du gyrus denté (DG) de l'hippocampe. Ainsi, Vangl2 est enrichi dans le *stratum lucidum* (sl), une région dense en contacts synaptiques entre le DG et le CA3. Dans cette région a lieu une synapse très particulière entre l'axone des CG, la fibre moussue (Mf) qui forme des boutons géants (MfB) et les excroissances épineuse (TE) issues de la partie proximale des dendrites apicaux. L'analyse structurale et ultrastructurale de ces épines démontre que l'élargissement et la complexification de la synapse MfB/TE est bloquée dans nos mutants, alors que les zones actives (PSD) des épines sont présentes, mais réorganisées. De façon intéressante, dans une zone plus distale des dendrites des neurones du CA3 (sl), les épines sont, elles, plus grosses, suggérant un remodelage complexe du réseau en l'absence de *vangl2*. Enfin, j'ai pu montrer que ces défauts morphologiques étaient corrélés à des problèmes de mémoire complexe (mémoire déclarative) qui dépendent de l'hippocampe mais aussi du cortex. Cette étude montre pour la première fois l'importance du signal PCP dans maturation *in vivo* d'un circuit hippocampique spécifique ainsi que ces conséquences cognitives.

D'autres résultats *in vitro* montrent que la suppression de *vangl2* augmente la vitesse de déplacement des cônes de croissance sur des substrats de N-cadhérine. J'ai utilisé la microscopie en super résolution spt-PALM-TIRF pour montrer que cette augmentation de croissance est inversement proportionnelle à la vitesse du flux rétrograde d'actine. Des expériences de FRAP permettent de suggérer que les molécules de N-cadhérine engagées dans des interactions hémophiliques (adhésion) est plus importante dans les mutants *vangl2*.

Je propose que Vangl2 contrôle le recyclage et la stabilité des protéines N-cadhérine dans les sites d'adhésion afin de réguler localement les dynamiques d'actine et par conséquent la croissance neuronale.

Titre Thèse en Français : Impact morpho-fonctionnel de Vangl2 sur le développement de l'hippocampe

Mots clés en français : Polarité Cellulaire Planaire, Vangl2, N-cadhérine, Cône de croissance, Croissance neuronale, Adhésion, Flux rétrograde d'actine, Embrayage Moléculaire, Hippocampe, Gyrus Denté, CA3, Fibre Moussue, Bouton Fibre Moussue, Excroissance épineuse, PSD, Mémoire de Travail, Mémoire déclarative

Mots clés en anglais : Planar Cell Polarity, Vangl2, N-cadherin, Growth cone, Neuronal outgrowth, Adhesion, Actin Retrograde Flow, Molecular Clutch, Hippocampus, Dentate Gyrus, CA3, Mossy Fiber, Mossy Fiber Bouton, Thorny Excrescence, PSD, Working Memory, Declarative Memory

Publications

Hilal, Muna L.; Moreaux, Maite M.; Racca, Claudia; Pinheiro, Vera L.; Piguel, Nicolas H.; Santoni, Marie-Josée; Dos-Santos Carvalho, Steve; Blanc, Jean-Michel; Abada, Komlayahse; Doat, Helene; Peyroutou, Ronan; Medina, Chantal; Papouin, Thomas; Vuillard, Laurent; Borg, Jean-Paul; Rachel, Rivka; Panatier, Aude; Montcouquiol, Mireille; Olié, Stéphane; Sans, Nathalie. Activity-dependent neuroplasticity induced by an enriched environment reverses cognitive deficits in Scribble1 deficient mouse. Cerebral Cortex; Manuscript in revision.

Stephanie Mauriac , Yeri-Esther Hien , Jonathan Bird , Steve Dos-Santos Carvalho , Ronan Peyroutou , Maite Moreau , Aysegül Gezer , Chantal Medina , Olivier Thoumine , Sandra Beer-Hammer , Thomas Friedman , Lukas Ruettiger , Andrew Forge , Bernd Nürnberg , Nathalie Sans, Mireille Montcouquiol. Identification of the molecular mechanism behind the Chudley McCullough syndrome reveals new function for Gpsm2/Gai3 complex in actin regulation. Nature Communications; Manuscript in revision.

Dos Santos Carvalho et al. Vangl2 inhibits neuronal outgrowth by controlling the interface between actin dynamics and adhesion. Manuscript in preparation.

Dos Santos Carvalho et al. Vangl2 controls the morphofunctional development of the DG-CA3 network of the hippocampus. Manuscript in preparation.

Posters:

- Dos Santos Carvalho S, Moreau MM Robert B, Medina C, Henderson D, Sans N, Montcouquiol M; Expression of Vangl2 in the hippocampus and validation of cKO models; Magendie Symposium, Bordeaux, October 2013.
- Dos Santos Carvalho S, Decroo M, Henderson D, Sans N, Montcouquiol M; Morphofunctional Impact of PCP signalling disruption in the hippocampus; ENC Network meeting Portugal, April 2015.
- Dos Santos Carvalho S, Decroo M, Henderson D, Sans N, Montcouquiol M; Morphofunctional Impact of PCP signalling disruption in the hippocampus; Ecole Doctorale, Bordeaux, April 2015.

- Dos Santos Carvalho S, Decroo M, Henderson D, Sans N, Montcouquiol M; Morphofunctional Impact of PCP signalling disruption in the hippocampus; Labex brain Foundation, Bordeaux, May 2015.
- Dos Santos Carvalho, Decroo M, Landmann C, Piguel N, Thoumine O, Sans N, Montcouquiol M; Vangl2: a brake in axonal growth; Magendie Symposium, Bordeaux, November 2015.
- Dos Santos Carvalho, Landmann C, Piguel N, Garcia M, Sans N, Thoumine O, Montcouquiol M; Vangl2 affects axonal outgrowth through a regulation of the molecular clutch between actin flow and N-cadherin, Ecole Doctorale, Bordeaux, April 2016.
- Dos Santos Carvalho, Landmann C, Piguel N, Garcia M, Sans N, Thoumine O, Montcouquiol M; Vangl2 affects axonal outgrowth through a regulation of the molecular clutch between actin flow and N-cadherin; 10th FENS, Copenhagen, July 2016.

Table of contents

Acknowledgements	1
Abstract	3
Résumé	5
Publications	7
Table of contents	9
Abbreviations	12
Chapter I : Introduction	16
1 Planar Cell Polarity	17
1.1 Planar Cell Polarity pathway in invertebrates	17
1.1.1 Notions of cell and non-cell autonomy	19
1.1.2 Cytoskeleton regulation	22
1.1.3 Vang-Stbm and interactions with other PCP proteins	23
1.1.4 Other PCP system: the drosophila eye and bristles	25
1.2 PCP in vertebrates and mammals	26
1.2.1 <i>Xenopus</i> / <i>Laevis</i> / <i>Zebrafish</i> and convergent extension	27
1.2.2 Core PCP and FBMN migration	29
1.2.3 Core PCP and mammals: the inner ear	29
1.2.4 Associated-PCP genes	32
1.3 PCP and the central nervous system (CNS)	32
1.4 PCP and human pathologies	36
2 Van Gogh like-2	39
2.1 Van Gogh (Vang) gene and protein	39
2.2 Vangl mutants	41
2.3 Vangl 1 and 2 functions in neurons	44
3 N-cadherin: an adhesion protein that regulates actin dynamics and tissue morphogenesis	48
3.1 Cadherin structure	48
3.2 The cadherin/catenin complex is an anchorage site for the regulation of the actin cytoskeleton	50
3.2.1 Canonical Wnt pathway	50
3.2.2 Adhesion sites	51
3.3 Cadherin expression and function in development	55

3.4	Atypical cadherins involved in PCP signaling and development	57
3.5	Adhesion molecules and PCP	57
4	<i>The neuronal growth cone: an integrative structure</i>	62
4.1	Growth cone structure	64
4.2	Stages of axonal outgrowth	66
4.3	Neuronal outgrowth: the role of adhesion sites	67
4.4	Neuronal outgrowth: cytoskeleton dynamics	69
4.4.1	Actin dynamics	69
4.4.2	Microtubules (MT) dynamics	71
4.4.3	The clutch hypothesis	73
4.4.4	Artificial pattern and super-resolution to study neuronal outgrowth	75
5	<i>The hippocampus</i>	77
5.1	Hippocampal function	77
5.2	Formation of the hippocampus and the DG/CA3 network	77
5.2.1	Neurogenesis	77
5.2.2	The CA3 mossy fiber/ pyramidal cell network	80
5.3	Maturation of the DG mossy fiber/ CA3 pyramidal cell synapse and structural plasticity	83
5.4	Adult neurogenesis	84
5.5	Specific processes strongly dependent on the EC/DG/CA3 network	86
	<i>Chapter II: Results</i>	89
	<i>Vangl2 inhibits neuronal outgrowth by controlling the interface between actin dynamics and N-cadherin adhesion</i>	90
	Summary	91
	Highlights	91
	Introduction	92
	Results	95
	Discussion	101
	Experimental Procedures	103
	Acknowledgments	108
	References	109
	Figure legends	113
	Figures	117

<i>Vangl2 controls the morphofunctional development of the DG-CA3 network of the hippocampus</i>	128
Abstract	129
Highlights	129
Introduction	130
Materials and Methods	133
Results	141
Discussion	148
References	152
Figure Legends	156
Figures	161
<i>General Discussion</i>	175
<i>General References</i>	184

Abbreviations

ABP	actin-binding protein
AD	Alzheimer's Disease
ADF	actin-depolymerizing factor
AJ	adherens junctions
AP-1	clathrin adaptor complex 1
APCAM	neural cell adhesion molecule (NCAM) ortholog in <i>Aplysia californica</i>
Arfrp1	ADP Ribosylation Factor Related Protein 1
ASD	Autism-spectrum-disorder
BP	basal progenitor
C	central domain
CA1, CA2 and CA3	horns of Ammon
CE	convergent extension
CNS	central nervous system
Co-IP	Co-immunoprecipitation
Crc	Circletail
DCX	doublecortin
DG	dentate gyrus
Dgo/ Ankrd6	Diego
Dia	diaphanous
Dlg	Discs Large
DN-cadherin	drosophila N-cadherin
DRok	Rho kinase
DnS	Down Syndrome

Ds	Dachsous
Dsh/ Dvl1-3	Dishevelled
ECs	ectodomains
EC	enthorinal cortex
ECM	extracellular matrix
ENU	N-Ethyl-N-NitrosoUrea
EPLIN	epithelial protein lost in neoplasm
ER	endoplasmic reticulum
F-actin	actin filament
FAK	Focal-adhesion kinase
FBMN	facial branchiomotor neuron
FGFR	fibroblast growth factor receptor
Fmi/ Celsr1-3	Starry Night/Flamingo
FRAP	Fluorescence-Recovery-After-Photobleaching
Fz	Frizzled
GBD:FH3	GTP-ase-binding/formin-homology 3
GCL	granule cell layer
GEF	guanine exchange factor
GFAP	glial fibrillary acidic protein
Gipc1	GAIP C-terminus interacting protein 1
GLAST	astrocyte-specific glutamate transporter
GOF	gain of function
GTPase	guanosine triphosphatase
ID	intellectual disability
IgSF	immunoglobulin superfamily
KO	knockout

LOF	loss of function
Lp	Loop-tail
LPP	Lateral Perforant Pathway
LRP5/6	lipoprotein receptor related protein
LRR	Leucine-Rich-Repeats
Mf	mossy fiber
MfB	Mf bouton
MMP14	matrix-metalloproteinase 14
MPP	Medial Perforant Pathway
MT	microtubule
Mwh	Multiple Wing Hairs
MWM	Morris water maze
NE	neuro-epithelial
NeuN	neuronal nuclear
NMDAR	N-methyl-D-aspartate-receptor
NPC	neural progenitor cell
NSC	neural stem cell
NTD	Neural tube defect
P	peripheral domain
PAR3	partitioning defective 3 homologue
PCP	Planar Cell Polarity
PDZ	PSD-95, DLG, ZO1
PDZ-BDM	PDZ - Binding Domain Motif
Pins	Partner of inscuteable
Pk	Prickle
Pk-BD	Prickle-Binding Domain

PLL	poly-l-lysine
PSA-NCAM	Polysialylated-neural cell adhesion molecule
PSD	Post-synaptic density
RGCs	radial glial cells
Sc	Schaffer collaterals
Scrib	Scribble
SFRP	Secreted-frizzled-related proteins
SGL	subgranular layer
sl	stratum lucidum
Sox2	sex determining region Y (SRY)-box 2
Spt-PALM-TIRF	Single-particle tracking - Photoactivated Laser Microscopy – Total Internal Reflection
SVZ	subventricular zone
T	transition domain
TE	Thorny excrescence
TGN	trans Golgi network
TIAM1	T lymphoma invasion and metastasis-inducing protein 1
Vangl	Vang like
Vang-Stbm	Van Gogh/Strabismus
WT	wild-type
ZO-1	zonula occludens protein 1

Chapter I : Introduction

1 Planar Cell Polarity

1.1 Planar Cell Polarity pathway in invertebrates

In epithelia, Planar Cell Polarity (PCP) is the coordinated polarization of cells or structures within the plane of a tissue. This polarity is perpendicular to the classical apico-basal polarity and is essential for the proper morphogenesis of tissues and organs. The signaling cassette controlling PCP pathway is developmentally highly conserved, from invertebrates to mammals. The most studied species is the *drosophila melanogaster*, where PCP was first identified (Vinson and Adler, 1987; reviewed in: Adler, 2012; Singh&Mlodzik, 2012; Wallingford, 2012; Strutt&Strutt, 2009).

Six core PCP proteins compose the core PCP pathway: three transmembrane proteins: Starry Night/Flamingo (Fmi), Frizzled (Fz), and Van Gogh/Strabismus (Vang-Stbm); and three cytosolic proteins: Diego (Dgo), Dishevelled (Dsh), and Prickle (Pk). Pioneer studies in simple models such as the epithelium of the *drosophila* wing have shown that these proteins have preferential interactions, and organize into specific asymmetric protein complexes within the plane of the epithelium and at cell-cell junctions (Fig. 1A,B). As such, Vang and Pk are segregated on the proximal level of the cell while Fz, Dsh and Dgo accumulate at the distal part of the cell (Fig. 1C). Fmi is present in both sides of the cells and is important not only for the stabilization of Vang and Fz at the membrane but also for the propagation of asymmetry between neighboring cells (to which Fz and Vang also participate)(Fig. 1C). It is important to notice that all the cells of a tissue express the mRNA for all 6 core genes, so that the sorting and the regulation at the protein level is crucial for this planar asymmetry to exist.

As mentioned before, PCP proteins form preferential complexes at the cell level. For these complexes to be segregated, PCP proteins are sorted through an intercellular feedback system occurring at the junction between two cells. This intercellular feedback is regulated through interaction between the different PCP proteins. Interactions between members of the proximal and distal PCP complex have been identified: Dsh and Dgo can interact with Vang and Pk (Bastock et al., 2003; Das et al., 2004; Jenny et al., 2003; Tree et al., 2002). The interaction between Pk and Dsh seems to prevent Dsh from accumulating on the proximal side, while preventing Pk from accumulating on the distal side.

Asymmetric distribution of PCP proteins precedes trichome formation

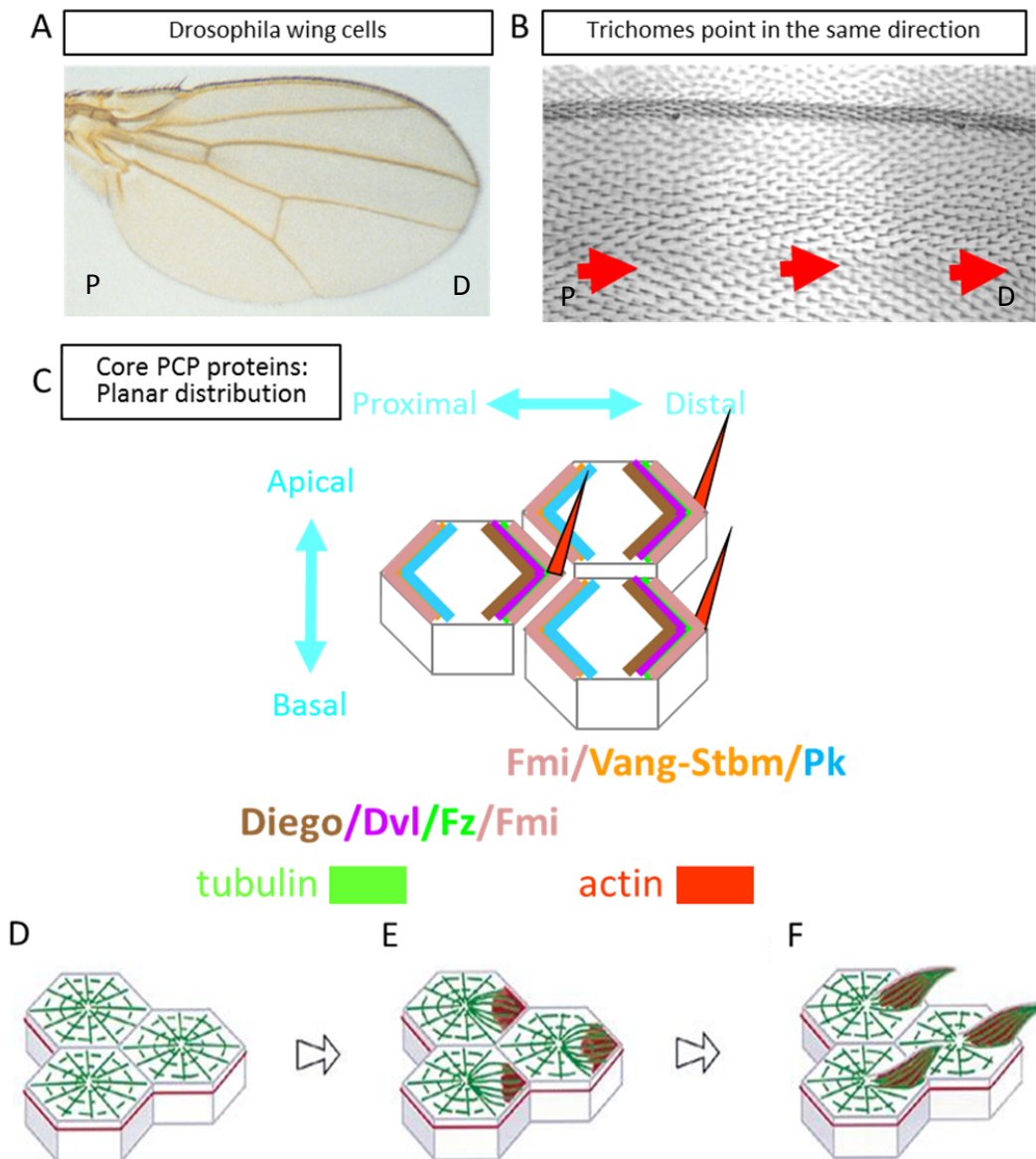


Figure 1: The asymmetric distribution of core PCP proteins precedes trichome hair formation at the distal edge in drosophila wing cells. (A,B) Drosophila wings are epithelia composed of epidermal cells with each an actin-rich hair, with the particularity that they point in the same direction, towards the distal part of the wing. (C) When PCP asymmetry is established, PCP proteins are recruited at the apical surface of wing cells, and then redistributed within the plane of the epithelium: Vang-Stbm and Pk segregate on the proximal side of wing cells while Fz, Dvl and Dgo accumulate at the opposite distal edge. This asymmetry is essential for the correct localization of the trichome at the distal edge of wing cells, and for the propagation of PCP signal across the tissue. (D,E,F) Drosophila wing cells are actin- and microtubule-rich structures. The establishment of PCP asymmetry leads to a localized recruitment of proteins that are essential for actin and microtubule polymerization to the distal edge of wing hair cells. The concentration of cytoskeleton elements leads to the formation of a trichome at the distal edge. P: proximal, D: distal. A,B: Adapted from Strutt, 2001; D-F: Adapted from Eaton, 1997.

The drosophila wing epithelium is covered with trichomes, which are actin-rich cytoplasmic extensions similar to body hair protruding at the apical surface of every hexagonal wing cell. The trichome is formed by actin and tubulin assembled in filaments that are uniformly oriented towards the distal (away) side of the cell (Fig. 1C,F) (Adler, 2002). It is this uniform orientation of all the hair within the plane of the epithelium that defines the PCP axis (proximo-distal). Mechanistically, PCP protein asymmetry happens shortly prior to any morphological manifestations of polarity, i.e. the orientation of the trichome (Fig. 1D,E,F). The asymmetric redistribution of these PCP proteins leads to the asymmetric concentration of cytoskeleton elements to the distal edge of cells, consequently leading to the formation of a trichome on the same edge (Fig. 1D,E,F).

1.1.1 Notions of cell and non-cell autonomy

PCP signaling acts at the cellular (cell autonomously) and at the tissue (non-cell autonomously) level to insure that trichomes form properly in the right location within the cell but also that all the trichomes present in the wing are uniformly oriented within the tissue (coordination between cells) (Fig. 2A).

The cell autonomous role of the PCP pathway was showed through the use of different mutants where core PCP genes were mutated. Wong & Adler in 1993 used drosophila mutants in which the expression of Fz, Dsh or Pk was suppressed and demonstrated that the disruption of PCP signaling led to the misorientation of trichomes in wing cells (Fig. 3A,B,C,D). Following research has demonstrated that PCP proteins are able to recruit effector proteins that regulate actin and microtubule polymerization (*see below in 1.1.2 section: Cytoskeleton Regulation for more details*) (Fig. 2B). Altogether, these studies suggest that the PCP pathway acts autonomously to control the position of the formation of the trichome in wing cells by dictating the site where cytoskeleton polymerization occurs.

For the non-cell autonomous effect of core PCP proteins (signal transmission), it is believed to occur before the cell autonomous one (Fig. 2A). This effect was first showed through the use of mosaic analysis of mutant clones for *fz* in chimerae: briefly some mutant wing cells (not expressing *fz*^{-/-}) are mixed in non-mutant wing cells (expressing *fz*). Surprisingly, if the mutants cells developed an expected PCP phenotype (abnormal trichome polarity), they also induced defects in the surrounding wild type cells, that displayed a PCP phenotype, such that their trichome pointed towards the mutant clone instead of away (Vinson and Adler, 1987) (Fig. 4A,B). Interestingly, the same experiments were performed with clone cells mutant for *vang* that also induced defects in non-mutant surrounding cells, but with a slight difference: now the trichomes point away from the clone (Taylor et al., 1998). The pattern displayed by both

mutants and the complementarity of the non-autonomous defects suggest that Vang and Fz participate both in non-cell autonomy (transmission of a signal), but with opposite output. Wu and Mlodzik in 2008 showed *in vitro* that the extracellular part of Fz can bind to Vang, suggesting that Fz and Vang might be able to interact extracellularly and contribute to protein asymmetry establishment and PCP signaling transmission to neighboring cells.

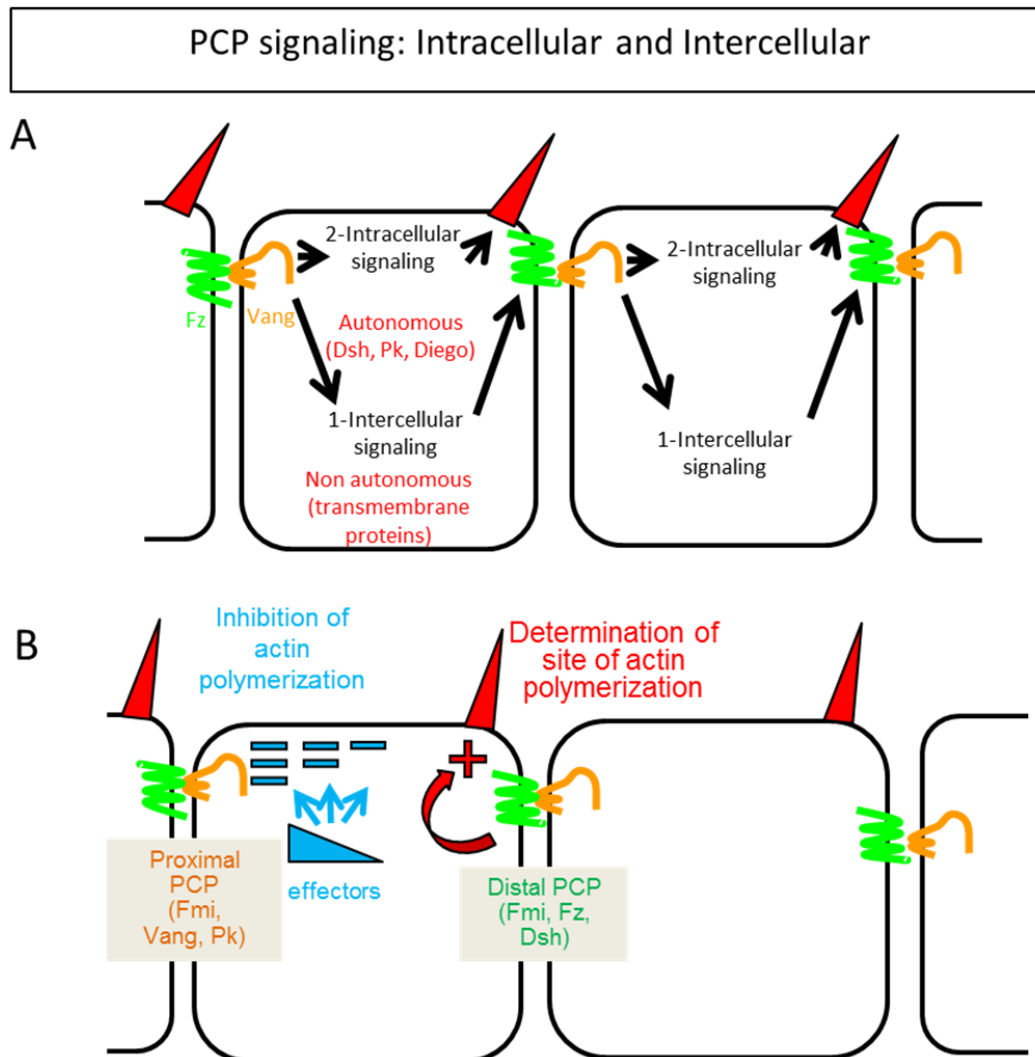


Figure 2: Non-cell autonomy (intercellular) signaling occurs prior to cell autonomy (intracellular) signaling. (A) 1- Initially, Fz and Vang-Stbm distribute distally and proximally respectively and contribute for non-cell autonomous PCP signaling: the propagation of PCP across the tissue. 2- Core PCP cytoplasmic protein asymmetry follows and stabilize the protein clusters and participates in the determination of the actin-rich hair localization: Dsh and Dgo accumulate distally while Pk accumulates proximally. (B) When PCP asymmetry is established, core PCP proteins recruit effectors in order to promote or inhibit the actin and microtubule polymerization asymmetrically, at the distal edge of wing cells (rich with Fz, Fmi and Pk). Adapted from Strutt & Strutt, 2009.

PCP signaling: Cell autonomy effect

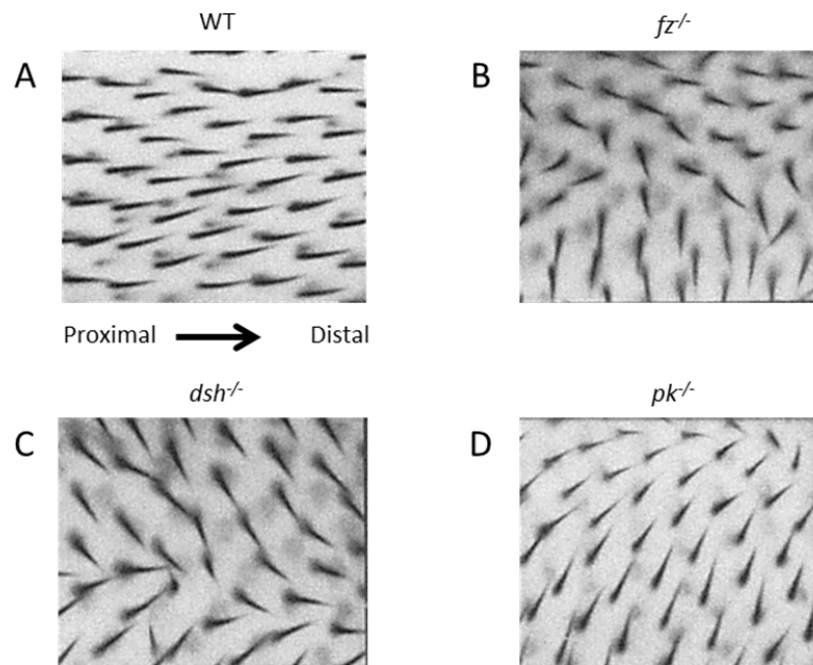


Figure 3: PCP cell-autonomous signaling is crucial for the orientation of trichomes. (A) Wild-type wing hair cells from *Drosophila* point distally to the extremity of the fly wing while disruption of core PCP signaling leads to the misorientation of trichomes in cells in which core PCP genes were mutated, such as in *fz*(B), *dsh* (C) and *pk*(D) mutants. Adapted from Wong & Adler, 1993.

PCP signaling: Non-cell autonomy effect

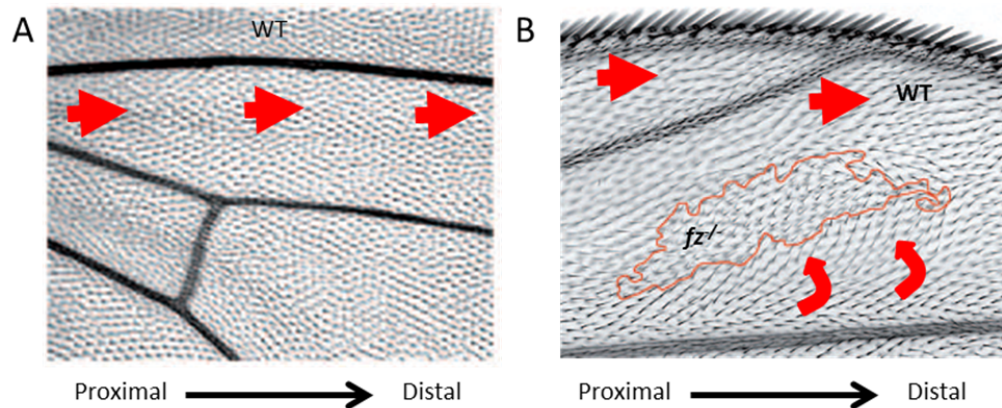


Figure 4: The non-cell autonomous role of core PCP signaling. (A) In wild-type drosophila wing, hairs point distally to the edge of the wing. Several core PCP proteins can induce the repolarization of wild-type cells located near to affected mutant cells in the drosophila wing. Core PCP proteins with these non-cell autonomous properties are all transmembrane proteins: Fz, Vang-Stbm, Fat and Dachous (Ds). In (B), *afz*^{-/-} clone (outlined in orange), surrounded by WT cells is identifiable thanks to the expression of a marker that leads to the production of multiple wing hairs (instead of the normal one) in the mutated cells. The non-cell autonomous effect is clear as the wild-type wing cells on the distal and lateral side of the mutant clone reorient themselves and point now towards the cloned cells (curved arrows). Adapted from Steifert & Moldzik, 2007.

1.1.2 Cytoskeleton regulation

Interestingly, protein asymmetry disruption does not affect trichome formation *per se* (actin polymerization is not affected) but does lead to its mislocalization at the center of the cell and its subsequent inappropriate planar orientation (Wong and Adler, 1993)(Fig.3). Because the location of the wing hair is influenced cell-autonomously by the position Fz/Dsh/Fmi complex, it is believed that core PCP proteins instruct an asymmetric distribution/activation of cytoskeleton regulators within the cell (Strutt and Warrington, 2008) (Fig. 2B). One current hypothesis is that, on the proximal side, Vang would recruit proteins that negatively regulate actin prehair formation, such as Inturned, Fuzzy and Fritz (Adler et al., 2004; Strutt and Warrington, 2008). These three proteins regulate Multiple Wing Hairs (Mwh) which is a GTP-ase-binding/formin-homology 3 (GBD:FH3) domain protein described as an actin polymerization repressor. The asymmetrical activation of this protein restricts actin nucleation to distal positions within the cell. In the absence of Mwh, ectopic actin bundles form across the apical surface and mutants display multiple wing hairs at aberrant positions without affecting the asymmetric localization of core PCP proteins (Wong and Adler, 1993). Rho and Rho kinase (DRok) have also been implicated in wing hair formation as PCP effectors: DRok for example can affect the number of trichomes formed in wing cells (Winter et al., 2001).

In drosophila wing, core PCP proteins also require actin regulators such as RhoA and the formin Diaphanous to properly form and orient trichomes. Mutations in these cytoskeletal regulators cause formation of ectopic and/or misoriented hairs (Strutt et al., 1997; Yan et al., 2009; Lu et al., 2015; Blair et al., 2006; Winter et al., 2001; Franke et al., 2010).

RhoA is required for both wing hair polarity and determination of hair number. In drosophila wing cells, *RhoA* clones exhibit a cell autonomous PCP effect, with surrounding tissue appearing phenotypically normal. *RhoA* mutation also affects PCP in drosophila eye (see below in 1.1.2 section: Other PCP system: the drosophila eye and bristles) suggesting that *RhoA* is a common factor required for the generation of polarity in all epithelial structures (Strutt et al., 1997). Adler and coll. suggest that RhoA activates Mwh and promotes its accumulation, via a direct interaction (through the GBD:FH3 domain) (Yan et al., 2009). The authors also report that RhoA has Mwh-independent functions, notably it affects Fz and Fmi asymmetric distribution, suggesting an indirect consequence of the effects of *RhoA* on DE-cadherin distribution, i. e. on cell junctions.

Formins are key regulators of actin nucleation and elongation. Diaphanous-related formins, the best-known subclass, are activated by Rho. In drosophila wing hair, the loss of function mutations and the expression of a constitutively active *diaphanous* (*dia*) gene led to cells forming both morphologically misoriented abnormal hairs and multiple hairs, suggesting then that Formins are Rho effectors (Lu & Adler, 2015). The authors proposed that the *dia* gene interacts antagonistically with *mwh* to restrict the location of actin polymerization, hence the location of the hair.

Altogether these studies indicate that regulating cytoskeleton dynamics is one important function of PCP signaling which ultimately contributes to the role of PCP signaling in cell development.

1.1.3 Vang-Stbm and interactions with other PCP proteins

PCP proteins interact with each other and these interactions contribute to their asymmetrical distribution in cells. The lab of D. Strutt showed in drosophila wing hair cells that Vang-Stbm (drosophila homologue for Vangl2) binds to Pk and Dsh to recruit these proteins to the plasma membrane and that the PDZ-BDM (PDZ-binding domain motif) is not required for this function (Bastock et al., 2003). In the absence of *vang-stbm* activity, the PCP proteins Pk and Dsh are mislocalized.

The same year, Jenny and colleagues used drosophila ommatidia as a model and showed that the interaction of Pk with Vang-Stbm was important for Vang-Stbm stabilization and clustering at the membrane (Jenny et al., 2003). By then, it was known that Pk could interact

with Dsh and antagonize Dsh by affecting its membrane localization. The authors postulated that a Vang-Stbm/Pk complex could modulate Fz-Dsh activity, resulting in a symmetry-breaking step during polarity signaling. Still in 2003, another study revealed that in *drosophila*, *fmi* and *vang-stbm* can genetically interact in early ommatidial development and that the 2 proteins colocalize (Rawls and Wolff, 2003). Years later (2006), Montcouquiol and colleagues showed that Vangl2 and Fz3 interact and that Vangl2 is important for the asymmetrical distribution of Fz3 in cochlear hair cells. This interaction was further analyzed in 2008 by Wu and Mlodzik, where it was shown in *drosophila* wing hair cells that the Fz extracellular domain could bind to Vang-Stbm. The authors postulated that Vang-Stbm can act as a Fz receptor (in trans), allowing cells to sense Fz activity/levels of their neighbors. This means that the interaction at the extracellular level could be important for establishing non cell-autonomous PCP signaling.

In 2011, an interesting paper detailed how Vang-Stbm and other PCP could be initially sorted and stabilized in membrane subdomains in *drosophila* wing cells (Strutt et al., 2011). The authors demonstrated that early on, transmembrane proteins Fmi, Fz and Vang-Stbm are trafficked and distributed to the apico-lateral regions of the membrane. At the membrane, the proteins are inserted in discrete membrane subdomains called puncta, which are asymmetric complexes. Through Fluorescence-Recovery-After-Photobleaching (FRAP) the turnover of Fmi and Fz was investigated and results showed that the localization of both proteins within the same puncta is highly stable. This local stabilization at junctions is due to cooperation between Fz and Vang-Stbm, finally resulting in two pools of Fmi at junctions: one stable due to the formation of Fz-Fmi/Fmi and Vang-Stbm -Fmi/Fmi complexes that reduce Fmi turnover, and another pool of Fmi highly unstable which is then removed from junctions by Rab5- and Dynamin-dependent processes. When preferential complexes start to form *via* homophilic Fmi interactions and Fmi-Fz or Fmi/Vang-Stbm interaction, these puncta stabilize and grow, initiating the asymmetric accumulation of proteins and contacts between neighboring cells. Finally, cytosolic PCP proteins Pk and Dsh are needed for further concentration and stabilization of these puncta into clusters, most likely by limiting lateral diffusion. This study demonstrates the importance of asymmetric complexes and their stabilization at the membrane in the turnover of membrane proteins and in the establishment of polarity between neighboring cells (Fig. 13).

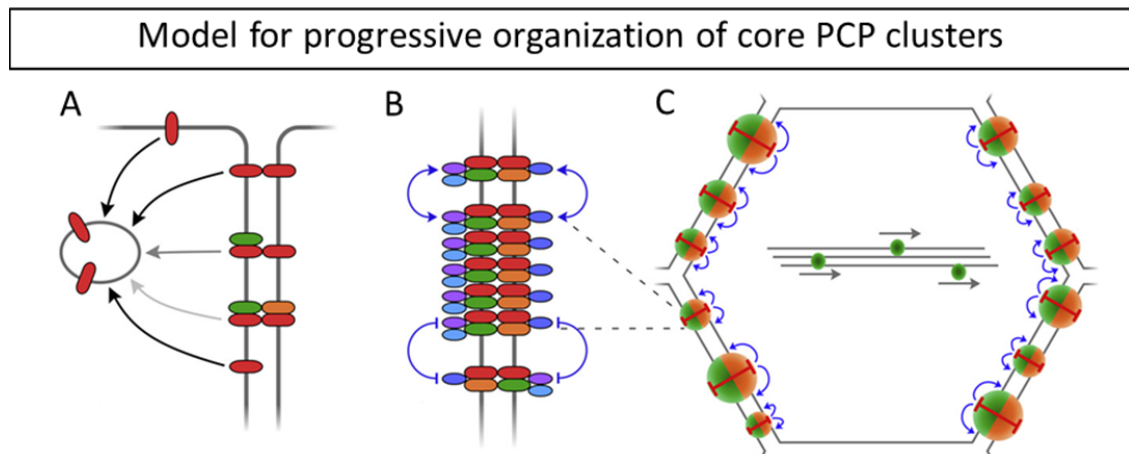


Figure 13: Model for progressive organization of core clusters and intercellular asymmetry establishment. (A) Fmi (red) localizes apically and laterally and is rapidly endocytosed (black arrows). When a complex in « *trans* » occurs (fmi-fmi/fz in green or fmi-fmi/vang in orange), endocytosis of fmi molecules is reduced, and the complex starts to stabilize. (B) PCP cytoplasmic proteins Dsh, Dgo and Pk are incorporated into these asymmetrical complexes and further promote local clustering and stability of complexes that have the same orientation either through attractive homophilic interactions or by repulsive heterophilic interactions (blue lines and arrows). (C) These asymmetric complexes might have the faculty of self-organize in order to cause cellular asymmetry by increasing individual puncta containing the same complexes, either by recruiting similar complexes or by repelling those with opposite polarity (blue arrows). (C). Due to the intrinsic asymmetry of these complexes at the intercellular level, a local self-enhancement of Fz clustering in one cell leads to the self-enhancement of Vang-Stbm in the neighboring cell. This coupled clustering acts as a long-range intercellular inhibition (red bars), ensuring that within each cell, domains containing high concentrations of Fz and Stbm form. From Strutt et al, 2011.

1.1.4 Other PCP system: the drosophila eye and bristles

Mutants for core PCP genes display various tissue-specific phenotypes, from the misorientation of hairs, to the orientation of ommatidia in the eye, to bristle orientation disruption (Adler, 2002; Strutt, 2003; Klein & Mlodzik, 2005). The drosophila eye is a well-studied system in which PCP proteins are also asymmetrically distributed. In this system, core PCP proteins localize on either side of R3/R4 photoreceptors cell boundary, and this localization will define the chirality of the rotation of the ommatidium either clockwise or anticlockwise along a midline called the equator (Singh & Mlodzik, 2012) (Fig. 5A,B). Other organs that are affected by core PCP genes mutation are the mechanosensory bristles located on the thorax/notum (Singh & Mlodzik, 2012). Mechanosensory bristles normally are patterned uniformly across the notum and oriented in the anterior-posterior axis, and in core PCP mutants, this regular pattern is randomized (Fig. 5C), similar to hair in drosophila wing.

From all these studies in the various tissues of drosophila, it is clear that the main output of PCP signaling is the modulation of cytoskeleton dynamics via effector proteins, leading to the control of cell morphology and growth.

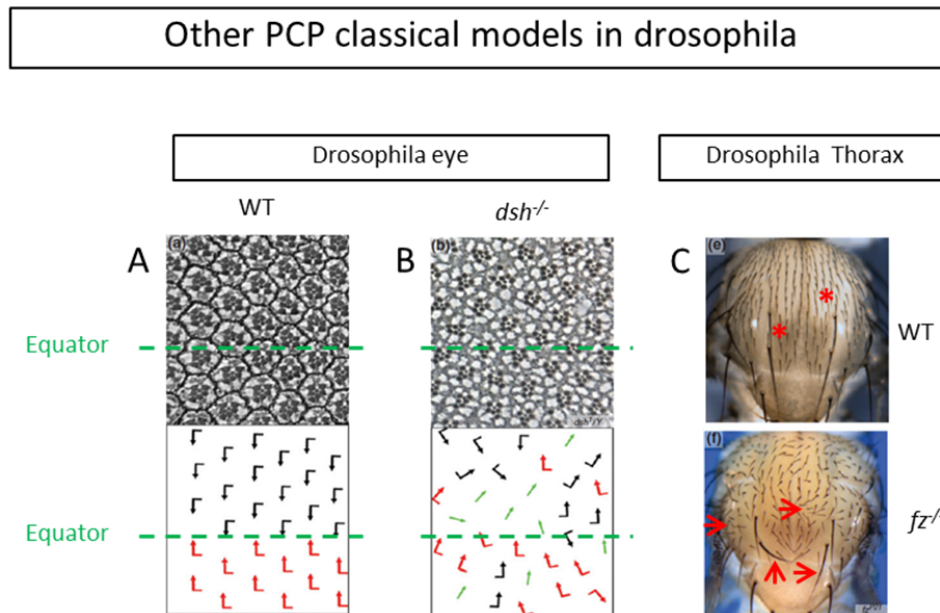


Figure 5: Other PCP classical models in drosophila tissues. (A) Drosophila eyes are composed of ommatidia (clusters of photoreceptors) which undergo a 90° chiral rotation within the plane of the epithelium depending on their position relative to the equator. Mature ommatidia are packed and planar oriented in a controlled fashion as demonstrated by the black and red arrows in the bottom panel. (B) Mutation of core PCP core proteins (*dsh* mutant here) leads to the disorganization of ommatidia. (C) Drosophila's thorax/notum is another PCP model. These body regions possess mechanosensory bristles that are uniformly oriented (asterisks in C, top panel). Mutation of PCP genes (*fz* mutant here) disrupts this organization and leads to the misorientation of bristles (arrows in C, lower panel). Adapted from Singh & Mlodzik, 2012.

1.2 PCP in vertebrates and mammals

In vertebrates the number of PCP gene orthologs is increased when compared to invertebrates such as the fly (Wallingford, 2012). For example, in mammals there are two orthologs of drosophila Vang (Vang like 1-2), three of drosophila Fmi (Celsr1-3), several of drosophila Fz (the number of Fz proteins varies between vertebrate species), three of drosophila Dsh (Dvl1-3), four of drosophila Pk (Pk1-4) and one of drosophila Dgo (Ankrd6).

1.2.1 *XenopusLaevis/Zebrafish and convergent extension*

Defining PCP in “lower” vertebrate's' tissues is more complex when compared to invertebrates such as drosophila. PCP can be understood as a process that affects cell polarity within an epithelial plane which is disrupted when at least one of the PCP genes is deleted/mutated. In xenopus and zebrafish, two animal models commonly studied, the developmental mechanism that fulfills these criteria is known as convergent extension (CE). CE is a developmental process in which the tissue of an embryo converges along a developmental axis, while elongating perpendicularly to this axis. CE is a process that has been demonstrated to occur during gastrulation in xenopus and zebrafish, and in neural tube closure in xenopus, zebrafish and mice (reviewed in Wallingford, 2012). The end result of the disruption of CE is a deficit in antero-posterior elongation, and an animal with a shorter trunk, which is the typical readout of PCP deficit in these animals (reviewed in Wang & Nathans, 2007; Wallingford, 2012).

Mechanistically, during CE, cell movements convert a short and wide array of cells into a long and skinny array of cells (Fig. 6). Typically, when CE occurs during gastrulation, cells send lamellipodia projections to form stable attachments with their mediolateral neighbors (Fig. 6B). These stable and polarized lamellipodia exert traction which results in the rearrangement of cells specifically along the mediolateral axis. Finally, these cellular movements lead to the narrowing and lengthening of the tissue, in absence of proliferation (Fig. 6A). As lamellipodia are actin-filled structures, the control of actin cytoskeleton is important in order for lamellipodia to properly form and stabilize. Moreover, the organization of the extracellular matrix (ECM) on which these lamellipodia grow is crucial for proper CE (Goto et al., 2005). CE is therefore a complex and coordinated mechanism leading to the reorganization of a tissue via cells movement. As such, it requires a dynamic coordination of adhesion and cytoskeleton motility.

Based on this lack of elongation, some proteins have been identified as PCP regulators in these animals, when they do not present the same function in drosophila (based on a deficit of the orientation of wing hair). A classical and important example of this is Wingless (Wnt in mammals) which is a ligand for Fz (in drosophila) and is not required for core PCP signaling. However, vertebrate orthologs of drosophila Wingless, such as Wnt5a and Wnt11 have been shown to play roles in a variety of PCP-mediated processes in vertebrates, as their mutation or downregulation leads to a shorter trunk.

In the 90s, two studies in xenopus were the first to show that PCP proteins play a role in the organization of tissues in vertebrates. Xenopus orthologs of Dvl2 and Fz8 were shown to specifically control CE (Deardorff et al., 1998; Sokol, 1996). In the following years many papers confirmed that most core PCP proteins (vang orthologs among them) have a role in CE

(reviewed in Wallingford, 2012). These studies along with live-cell imaging experiments in *xenopus* and zebrafish demonstrated that the manipulation of PCP proteins impacts cell behavior during CE.

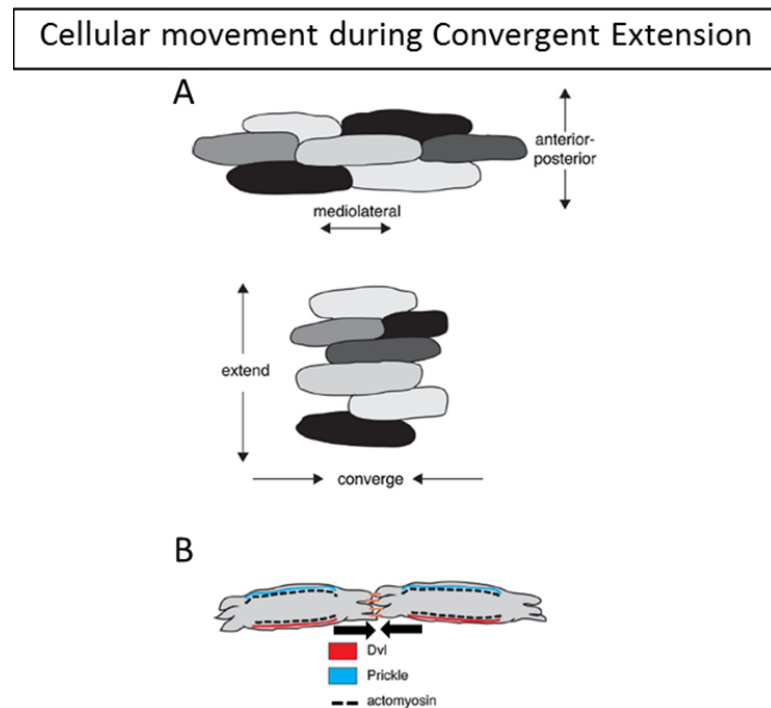


Figure 6: Convergent extension in mesenchymal tissues. (A) Mesodermal cells migrate mediolaterally and intercalate in the anterior-posterior axis, leading to the narrowing and lengthening of the body axis during developmental processes such as *xenopus* gastrulation. (B) These cells possess lamellipodia which are responsible for producing traction on their neighboring cells and for shortening the anterior-posterior cell interfaces thanks to the contractility provided by actomyosins. The asymmetrical distribution of PCP proteins is crucial for the local enrichment of actomyosins at cell interfaces and therefore contributes to convergent extension. From Devenport, 2016.

There is now a large amount of evidence showing that PCP proteins are important for CE in vertebrates (Wallingford et al., 2000; Wallingford & Harland, 2002; Wallingford & Habas, 2005). In zebrafish it was shown that the mutations of *vangl2* (*trilobite* in zebrafish) (Jessen et al., 2002), *prickle* (Veeman et al., 2003), or *wnt11* (*silberblick* in zebrafish) (Heisenberg et al., 2000) disrupted CE. Other studies showed that the disruption of PCP signaling leads to defects in both the polarity and stability of lamellipodia, in the alignment of cells along the mediolateral axis and in the formation of polarized cell intercalations (Goto & Keller, 2002; Heisenberg et al., 2000; Jessen et al., 2002; Wallingford et al., 2000).

1.2.2 Core PCP and FBMN migration

As described previously, PCP proteins can coordinate the movement of cells in order for CE to occur properly. As such, it is not a surprise that these proteins can also control cell migration in the nervous system. One of the most studied examples is the facial branchiomotor neurons (FBMNs) that migrate tangentially along the plane of the neuro-epithelium and innervate the facial musculature in zebrafish (Fig. 7). The work of Chandrasekhar is important in this sense as it explained how caudal migration of FBMN neurons in zebrafish hindbrain occurs (Chandrasekhar et al., 1997) (Fig. 7A,B). Through the use of zebrafish mutants, many PCP proteins, such as Vangl2, Scribble1, Celsr2 and Fz3, have been implicated in FBMN migration (reviewed in Wallingford, 2012). Importantly, studies with this model revealed that PCP proteins also have autonomous and non-autonomous roles in neurons in vertebrates. The non-autonomous role of PCP proteins is due to their function in the polarization of the neuro-epithelium in which these neurons migrate: if Vangl2, Fz3a (one of the two Fz3 homologs in zebrafish) or Celsr2 expression is disrupted in a neuro-epithelium, grafted-wild-type FBMNs fail to migrate (Jessen et al., 2002; Wada et al., 2005; Wada et al., 2006; Walsh et al., 2011) (Fig. 7D). On the other hand, PCP proteins owe their autonomous role in FBMNs to the fact that they control protrusive activity and cell migration (Jessen et al., 2002; Mapp et al., 2010; Rohrschneider et al., 2007; Walsh et al., 2011) (Fig. 7C). So the expression of PCP proteins is important in the environment as well as in the neurons for a correct migration. These studies were later extended to mice, where a role in the control FBMNs migration was shown for Vangl2, Scribble1, Celsr1, Celsr2 and Fz3 (Qu et al., 2010; Vivancos et al., 2009).

1.2.3 Core PCP and mammals: the inner ear

The hair bundle capping the mechano-sensory cells in the mammalian inner ear (the cochlea and the vestibular system) provides the most visually striking example of PCP in mammals. In 2003, Montcouquiol and colleagues showed that PCP genes are required for the proper patterning of mammalian tissues, in this case in the proper orientation of hair bundles capping the hair cells in the cochlea (Fig. 8), a PCP readout with strong similarities with the proper planar orientation of drosophila wing hair. The same year another study identified Celsr1 in mammalian PCP using the same tissue (Curtin et al., 2003).

The inner ear is composed of auditory and vestibular cells which possess "hairs" at their apical surface. These hairs, called stereocilia, are actin-rich and arranged in a staircase array-fashion. These stereocilia are polarized within the plane of the epithelium. This planar organization is essential for the perception of the mechanical deflection of the bundle and subsequently for the generation of an electrical signal which will be transferred to the brain

(Ezan & Montcouquiol, 2013). Mutations of core PCP genes were first associated with misorientated stereociliary bundles in the cochleae of *Vangl2^{Lp/Lp}* (Loop-tail) mouse mutants (Montcouquiol et al., 2003) (Fig. 8). The resulting mutated form of *Vangl2* (*Vangl2^{Lp}*) has been described as a dominant negative variant of *Vangl2* proteins that can disrupt *Vangl2* and *Vangl1* delivery to the membrane. Some of the phenotypes first described for the *Vangl2^{Lp/Lp}* mutants, such as *craniorachischisis*, the most severe form of neural tube defect (NTD), are shared with other core PCP genes – the flamingo ortholog *Celsr1* (Curtin et al., 2003), *Fz3/Fz6*, but also Disheveled *Dvl1-3* (Wang et al., 2006; Etheridge et al., 2008) and *Vangl1* (Torban et al., 2008). Since PCP signaling regulates CE and CE movements contribute for neural tube closure (see below in section 2.1.1: *The Looptail mutant and Vangl mutants*), it is only logical that PCP pathway disruption affects neural tube closure and causes NTDs.

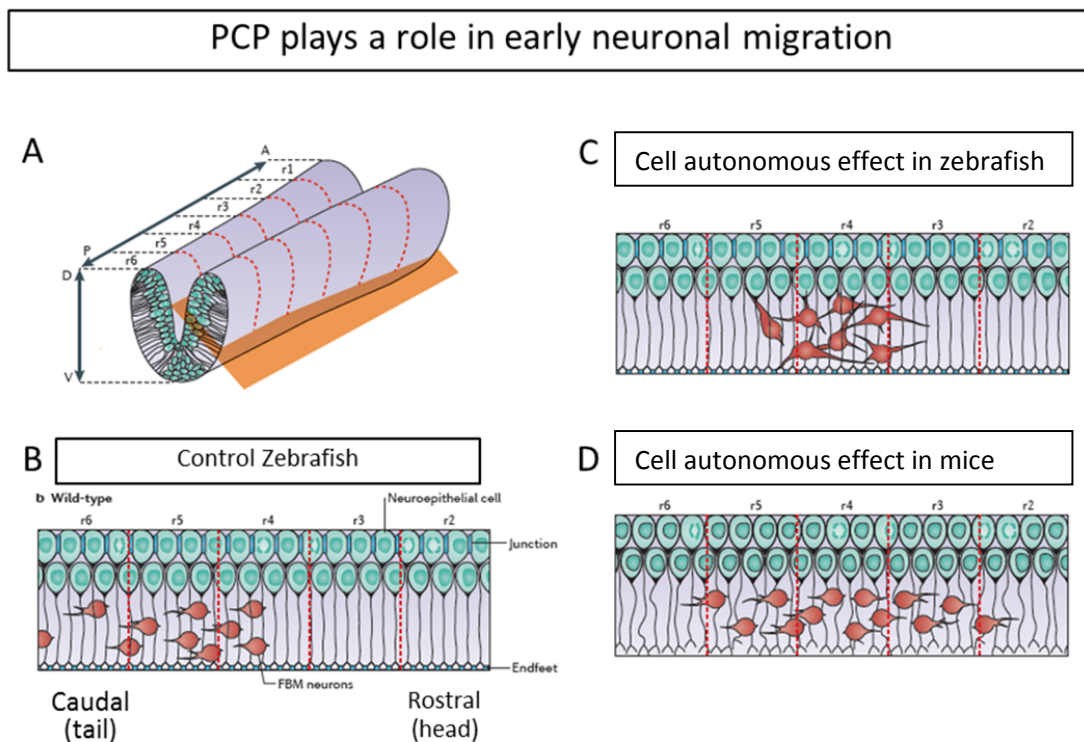


Figure 7: PCP plays a role in early neuronal migration. (A) Schematic representation of the developing rhombencephalon. (B) Facial bronchiomotor neurons (FBMNs) are generated in the rhombomere 4 (r4) and migrate caudally towards r6 in control mice. (C) In zebrafish, *prickle1b* mutated FBMNs were transplanted in wild-type rhombencephalon and failed to migrate caudally, indicating a cell-autonomous role of PCP in neuronal migration. (D) In mice, *Celsr1* (Flamingo ortholog) is expressed by the neuro-epithelial cells, the substrate for FBMNs migration, but not in FBMNs themselves. *celsr1* conditional inactivation in mice impairs FBMNs migration, in a non-cell autonomous manner similar to what is observed in corresponding zebrafish KO. Adapted from Tissir & Goffinet, 2013.

Following the seminal studies of Montcouquiol et al and Curtin et al from 2003, PCP signaling has been linked to a vast array of developmental processes and cell behaviors in very distinct mammalian cellular types, such as polarized cilia beating in the trachea (Vladar et al., 2012) and brain ventricles (Tissir et al., 2010), lung branching (Yates et al., 2010a), kidney tubular branching and glomerular maturation defects (Yates et al., 2010b), musculoskeletal system development (Stein & Mackensen, 1957), cardiac development (Henderson et al., 2001), hair follicle alignment (Devenport & Fuchs, 2008), optic nerve finding (Rachel et al., 2000) and cortical neuronal differentiation (Lake & Sokol, 2009). Altogether, these studies show that PCP is important for proper tissue morphogenesis in mammals, and suggest that disruption of PCP has numerous developmental and pathological consequences (see below).

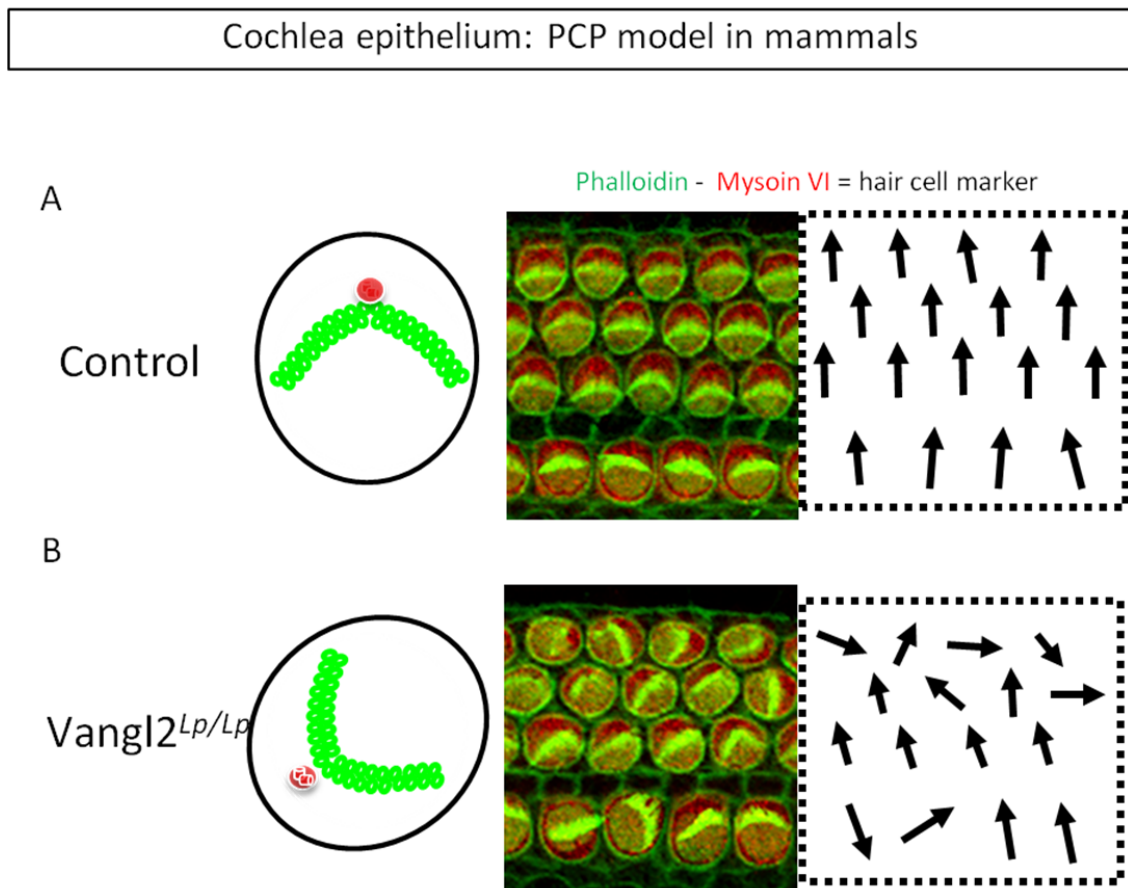


Figure 8: PCP proteins are required for the proper planar orientation of actin-rich hair bundles at the apex of cochlear hair cells. (A) Surface view of a cochlear epithelium of mouse. Stereocilia are actin-rich structures (phalloidin staining) that are arranged in a "V" shape and that display a PCP orientation perpendicular to the epithelium plan. (B) Mutation of core PCP genes such as in *Vangl2^{Lp/Lp}* mouse mutants leads to the planar misorientation of stereociliary bundles (B). Adapted from Montcouquiol et al, 2003 and Ezan & Montcouquiol, 2013.

1.2.4 Associated-PCP genes

The genome of mammals is more complex than that of *Drosophila*'s leading to a multiplication of PCP genes isoforms, but also to new regulators that appeared during evolution. Most of these "PCP-associated genes" were identified based on the development of a NTD phenotype in selected mutants, and further validated by the presence of an inner PCP phenotype, weaker than that of core PCP genes (Ezan & Montcouquiol, 2013 for review). One typical example is *Scribble1* which was associated to PCP in mammals thanks to the work of Montcouquiol and colleagues in 2003. It was reported that *Scrib1* is a binding partner for *Vangl2* and mice heterozygous for both *Vangl2*^{Lp/+} and *Scribble1*^{Crc/+} (a spontaneous mutant for *Scrib1*) present *craniorachischisis* and defects in cochlea hair bundle orientation (Montcouquiol et al., 2003). Later, the group of Marek Mlodzik confirmed a PCP role for *scribble* in fly (Courbard et al., 2009). It was one of the rare occurrences where a mammalian PCP gene led to the identification of a PCP function for a gene in invertebrate. Some of these new PCP-associated genes were identified through a screen designed to create a vast amount of mutant embryos through treatment with a mutagenic agent: N-Ethyl-N-NitrosoUrea (ENU). Embryos presenting a NTD (characteristic of PCP defects) were selected and subsequently, mutations in the genome of these embryos were sequenced in order to identify the causative genes. These screens through ENU studies were important to identify genes such as *Sec24b*, as well as *chuzhoi*, but also to identify new mutations on the *Scribble1* gene (Wansleeben et al., 2010; Merte et al., 2010; Paudyal et al., 2010). A list of these "newly" identified PCP-associated genes in mammals can be found in table 1.

1.3 PCP and the central nervous system (CNS)

The brain is a fascinating organ composed of approximately 100 billion neurons which communicate with each other through synapses. A correct synaptic communication is crucial for an optimal functioning of the brain, and for such a good communication to occur, neuronal cells need to be polarized correctly. Indeed, neurons are highly polarized cells, and are classically composed of a cell body, a dendritic tree and an axon, molecularly and anatomically different from the dendritic tree. Axons play a crucial role in the correct formation of synapses as these structures rapidly protrude and outgrow to finally contact their proper synaptic partners. Neuronal polarity and motility critically depend on cytoskeleton organization and dynamics, and a correct coordination of both will allow a proper development of the neuronal network during development, as well as during adult neurogenesis.

Table 1: New PCP genes identified in mammals

Mammal gene	Mutant name	Tissue	Reference
<i>Ptk7</i>	N/A	Inner ear	Lu et al., 2004
<i>Ror2</i>	N/A	Inner ear	Yamamoto et al, 2008
<i>Scribble1</i>	Circle-tail (Crc)	Inner ear ENU	Montcouquiol et al., 2003 Wansleebe et al., 2010
<i>Sec24b</i>	Krabbel	Inner ear ENU	Merte et al., 2010 Wansleebe et al., 2010
<i>Surf1/2</i>	N/A	Inner ear	Narimatsu et al., 2009
<i>Chuzhoi</i>	Chuzhoi (Chz)	Inner ear ENU	Paudyal et al., 2010
<i>Wnt5a</i>	N/A	Inner ear	Qian et al., 2007
<i>Fat 1-4</i>	N/A	Inner ear	Sabueri et al., 2008
<i>Ift88</i>	N/A	Inner ear	(Jones et al., 2008)
<i>Kif3a</i>	N/A	Inner ear	(Jones et al., 2008)

As described previously, PCP signaling is comprised of a number of transmembrane and cytosolic proteins acting together to influence cell shape and motility, and coordinate the development and function of many tissues. It is only logical that PCP genes - all expressed in the central nervous system (CNS) (Tissir & Goffinet, 2006) - also influence neuronal behavior.

Early studies in **invertebrates** showed that Fmi is important for the development of axonal tracts in the visual system of flies (Senti et al., 2003; Lee et al., 2003b). In this model, Fmi mediates axon-axon and axon-target interactions that are required for the guidance of photoreceptor axons. In 2000, Gao and colleagues showed in drosophila that dendritic

development, notably the elaboration of non-overlapping dendritic fields, depends on homophilic interaction of Fmi proteins, but was independent from Fz. It is interesting to note that, differently from the PCP-reported roles in drosophila epithelia, the mutation of different PCP genes in neurons does not appear to lead to the same phenotype. This means that PCP genes might have different interactions, and intervene in specific signaling pathways in different contexts. Other studies in invertebrates showed that Fmi collaborates with Pk to regulate sensory axon advance at the transition between the peripheral nervous system and the CNS (Mrkusich et al., 2011). In *C. elegans*, Fmi appears to have a similar role in axonal direction but also outgrowth (Steimel et al., 2010; Ackley, 2014).

In **mammals**, conserved core PCP genes appear to have some conserved function. In 2004, a study reported that Celsr2 was required for the maintenance of dendritic arbor as its downregulation leads to a decrease in dendritic length and in the complexity of the dendritic trees of Purkinje cells (Shima et al., 2004). Interestingly, they also noticed that the downregulation of Celsr3 had an opposite effect: dendritic overgrowth. Pk2 has also been involved in dendritic development (Sowers et al., 2013). The authors reported that Pk2 disruption in mice hippocampal neurons led to reductions in dendritic branching, synapse number and post-synaptic density (PSD) size. These morphological defects were correlated with behavioural deficits and mice with disruption in Pk2 presented altered social interaction, learning abnormalities and lack of flexibility. These behavioural and physiological deficits are consistent with Autism-spectrum-disorder (ASD)-like phenotypes detected in mouse models of ASD. In the same study, PRICKLE2 variants found in patients and transfected in mouse hippocampal neurons resulted in morphological and electrophysiological defects.

As described previously, Scribble is a PCP-associated protein and in 2010, our lab demonstrated that adult *circletail* heterozygotes mice also displayed ASD-like phenotypes. In addition to sociability deficits, the animals exhibited enhanced learning and memory abilities, two features relevant to ASD-like disorders (Moreau et al., 2010). In the lab we have shown that this protein was located in spines where it influenced actin cytoskeleton spine morphogenesis and N-methyl-D-aspartate-receptor (NMDAR) trafficking (Moreau et al., 2010; Piguel et al., 2014). In the hippocampus of these mutants, Moreau and coll. observed an increase in the total length and complexity (number of dendritic intersections) of basal dendrites of CA1 pyramidal neurons. There were no differences in the total length and number of dendritic intersections in the apical dendrites of these neurons. However, even if the number of intersections did not change, their organization did: the number of intersections close to the cell body was decreased in Scrib1^{Crc/+} mutants while the number of intersections distal to the cell body was increased.

Moreover, defects in synapse pruning associated with an increased number of enlarged spines and PSD were also identified, and a decreased number of perforated synapses (Moreau et al., 2010).

A conserved function for invertebrates PCP genes in mammalian neuronal cells is their role in axonal guidance. Two seminal studies have identified the role of Fz3 and Celsr3 (one of the flamingo orthologs) (Wang et al., 2006; Zhou et al., 2008). The inactivation of these genes leads to severe defects in the guidance of monoaminergic axons along the anterior-posterior axis (Fenstermaker et al., 2010). Work from other laboratories further found these defects in other axonal guidance models such as in the anterior turning of commissural axons in the spinal cord (Lyuksyutova et al., 2003; Avilés et al., 2015), in axon of neurons from the peripheral, sympathetic and enteric nervous system (Armstrong et al., 2011; Chai et al., 2014; Hua et al., 2013; Sasselli et al., 2013), in major axon tracts of the anterior commissure, internal capsule and the corticospinal tract (Tissir & Goffinet, 2013) (Fig. 9). Moreover, Fz3, Celsr3 but also Vangl2 are important for the anterior-posterior organization of monoaminergic axons in the brainstem and for the rostral turning of commissural axons in the spinal cord (Wang & Nathans, 2007; Price et al., 2006; Lyuksyutova et al., 2003; Shafer et al., 2011). Fz proteins are in fact the perfect example of how a PCP protein can play various roles in different contexts. J. Nathans and colleagues showed that Fz were required for PCP signaling in axonal guidance, neural tube closure as well as in the cochlea (Wang et al., 2006; Hua et al., 2014).

In the ever growing role(s) of PCP genes in neuronal cells, recently, PCP proteins were shown to be important for neuronal maturation in the context of the adult hippocampus (Schafer et al., 2015). In this study the authors used shRNA to downregulate Fz3 and Celsr1-3 in proliferative cells of the hippocampi and found that the expression of the genes was important for the maturation of adult generated granular cells of the dentate gyrus. Interestingly, they found that Celsr1-3 could control distinct aspects of PCP-mediated granular cell morphogenesis: Celsr1 regulated the direction of dendrite initiation sites while Celsr2/3 controlled the radial migration and dendritic patterning.

Altogether, these different roles for different Celsr proteins indicate that the multiplication of PCP isoforms, when compared to drosophila, led to specific functions for specific isoforms.

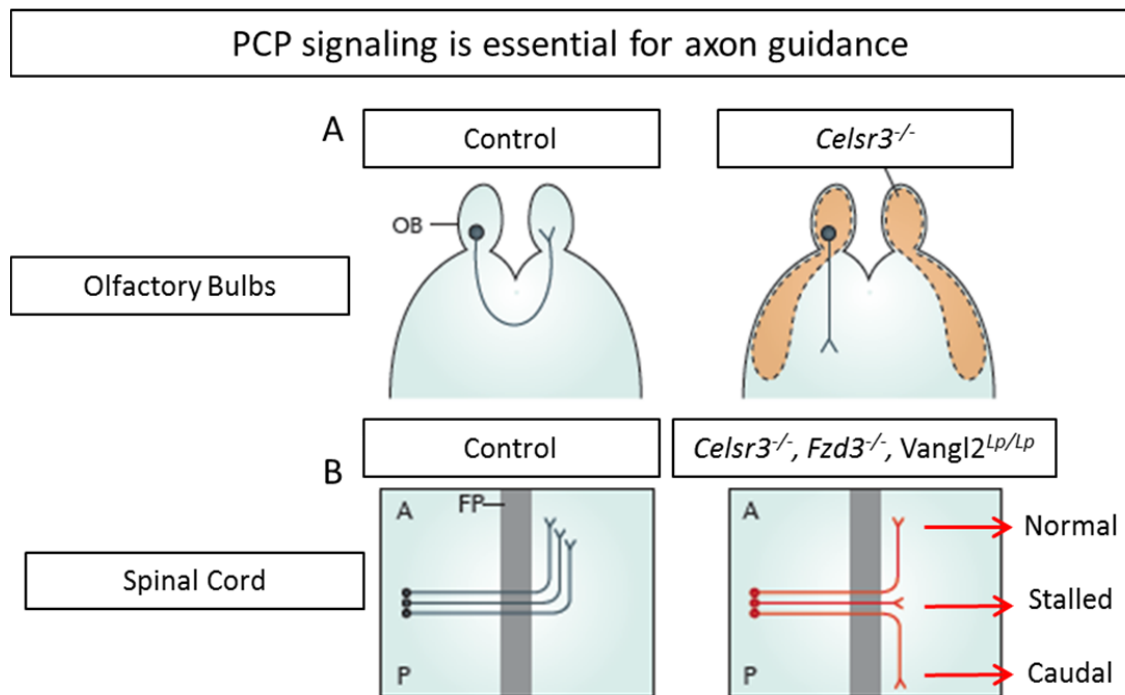


Figure 9: PCP signaling is essential for axon guidance. (A) Olfactory bulbs (OB) extend axons that cross the midline and project to the contralateral side in control mice (left panel). PCP disruption by conditional deletion of PCP genes leads to axon guidance defects which are not able to reach the contralateral side (right panel). (B) Another axon guidance model is the spinal cord commissural neurons that possess axons which turn anteriorly after crossing the floor plate (left panel). Disruption of PCP signaling leads to axon guidance errors (right panel). Adapted from Tissir & Goffinet, 2013.

1.4 PCP and human pathologies

As discussed previously, deletions and mutations in PCP genes affect many tissues in mammals: neural tube, sensory systems (hearing, vision), the skeleton, the kidney, the lung, the cardiovascular system, and a molecular link between PCP proteins and cilia-related proteins also suggest a link with ciliopathies (see Wallingford & Mitchell, 2011 for review). But a link between PCP proteins and cognitive or social deficits such as intellectual disabilities (IDs) or Autism Spectrum Disorders (ASD) is much more recent (reviewed in Sans et al., 2016).

As mentioned, *Fz3* has been implicated in axonal guidance defects (see previous section). However, the deletion/mutation of the *FZ3* gene has more profound effects in human, as this gene is positioned in the chromosomal region *8p* [*8p21.1*] which is a potential hub for neurodevelopmental disorders such as schizophrenia and autism (Tabares-Seisdedos et al., 2009). Single nucleotide mutations in the *FZ3* gene showed strong correlations with schizophrenia in the Japanese and Chinese population (Katsu et al., 2003; Kang et al., 2011). The

deletion of this gene has also been found in patients with agenesis of the *corpus callosum*, developmental delay and IDs (Sajan et al., 2013). The *FZ4* gene has been associated with familial exudative vitreoretinopathy (EVR) (hereditary disorder characterized by a failure of peripheral retinal vascularization) (Robitaille et al., 2002). The deletion of a genomic region where this gene is inserted has also been related to growth retardation, facial anomalies, abnormalities in the cleft palate, minor digital anomalies, dysmorphic craniofacial features and IDs (Li et al., 2006; Nallathambi et al., 2006). Another *FZ* gene, *FZ5*, is also important for proper human development. The deletion of genomic regions where this gene is inserted has been identified in a patient presenting developmental defects and in an autistic male presenting dysmorphic features (Roberts et al., 2014; Brandau et al., 2008). The *FZ9* gene has been associated to Williams syndrome (Wang et al., 1997; Merla et al., 2010). The children affected by this syndrome have similar characteristic facial features, cardiovascular problems, developmental delays, learning disabilities and attention deficit disorders (Martens et al., 2008). This gene is inserted in a genomic region that can be affected by the 7q11.23 duplication syndrome. The patients affected by this syndrome often suffer of IDs associated or not with delayed speech and language development, hearing impairments, macro or microcephaly (Decipher database). The Decipher database is used by the clinical community to share and compare phenotypic and genotypic data, and contains data from 21714 patients who have given consent for broad data-sharing.

Mutations of *VANGL1* cause NTD in human (Kibar et al., 2009; Iliescu et al., 2014) and is involved in cancer development (Ryu et al., 2010; Lee et al., 2011; Yoon et al., 2013), while the duplication of a chromosomal region where this gene is inserted has been associated with ASD recently (Pinto et al., 2010). Mutations in *VANGL2* also cause NTD in humans (Lei et al., 2010; Kibar et al., 2011; Iliescu et al., 2014; Iliescu et al., 2011) and is involved in cancer development (Piazzini et al., 2013). These studies show that the severe impact of the mutation of these genes during *in utero* development is probably incompatible with life, and would explain why there is still no association between the *VANGL* genes and neurodevelopmental disorders such as ASD or ID. Microduplications of the chromosomal region including *VANGL2* gene were found in the Decipher database in patients with microcephaly, IDs, delayed speech and language development, stereotypic behaviour and scoliosis.

The *DVL* genes also have a role in human development. The deletion of the chromosomal region where *DVL1* is inserted has been implicated in craniofacial dysmorphism, moderate to severe IDs, delayed growth, hypotonia, seizures, limits speech ability, malformations, hearing deficits, vision impairment and distinct facial features (Battaglia et al., 2008). *De novo* frameshift mutations in *DVL1* were also found in several individuals with Robinow syndrome (Bunn et al.,

2015; White et al., 2015). *DVL2* has been linked to lymphoma (Hegazy et al., 2013) and a deletion of the chromosomal region where it is inserted was found in patients with characteristic dysmorphic features, developmental delay and IDs (Zeesman et al., 2012). A recent paper was able to relate rare *de novo* copy number variants (CNVs) in the *Dvl2* gene with autism (Gilman et al., 2011).

PRICKLE1 has been implicated in epilepsy (Bassuk et al., 2008) and NTDs (Criscuolo et al., 2010; Bosoi et al., 2011; Tao et al., 2011) and through extensive *in vivo* and *in vitro* functional analysis this gene was defined as an ASD gene (Paemka et al., 2015). As for *PRICKLE2*, its mutation may underlie pathogenesis of human spina bifida (Wen et al., 2010), epilepsy and autism (Sowers et al., 2013). A study performed on siblings affected by ASD found two distinct heterozygous *PRICKLE2* variants that were inherited paternally. Interestingly, *Prickle2* KO mice presented some ASD-like behaviour: they had social deficits and presented enhanced spatial memory (Sowers et al., 2013).

Finally, microduplications encompassing the *Ankrd6* gene (*Diego* in drosophila) were found in the Decipher database in patients with cognitive impairment, ASD, IDs, delayed speech and language development.

All of these studies strongly suggest an important but yet poorly studied role for PCP signaling in human pathologies, and more specifically in neurological and cognitive disorders.

2 Van Gogh like-2

2.1 Van Gogh (Vang) gene and protein

Vang gene was named after the artist, van Gogh, because the swirling wing hair patterns in the drosophila mutants is reminiscent of the swirling brush strokes van Gogh used in his paintings (Taylor et al., 1998). Almost the same year, another group called the same gene *Strabismus* (*Stbm*), the medical term for 'cross-eyed', due to the drosophila mutants displaying a disrupted eye polarity (Wolff & Rubin, 1998).

In mammals, the Vangl family comprises two members: Vangl1 and Vangl2. The alignment of their amino acid sequence shows that these proteins are very similar. *van Gogh like-2* (*vangl2*) gene encodes for a tetraspanin protein. The protein contains four transmembrane domains with both the N-ter and C-ter domains located intracellularly (Kibar et al., 2001a). Vangl2 is a highly conserved protein along evolution as it has been found homologous proteins in most species, covering the entire animal kingdom. Moreover, the amino acid sequence of the protein has almost not diverged. This strong homology suggests redundancy in protein function.

Mammalian Vangl2 is composed of 521 amino-acids and has a predicted molecular weight around 60 kDa. The analysis of Vangl2's protein sequence allowed the identification of several putative domains (Kibar et al., 2001a), such as 1/a C-terminus **PSD-95, DLG, ZO1 - Binding Domain Motif** (PDZ-BDM) which is a binding domain for PDZ proteins; 2/ multiple phosphorylation sites for PKC and CK2 located in the N-terminus; 3/ membrane targeting sequences of YSGY, YHDF, NPAL and LL types respectively located in the position 7-10, 280-283, 287-290, 290-291 (Fig. 10).

Through its PDZ-BDM, Vangl2 can interact with many cytosolic proteins, as shown for Scribble1 (Scrib1) by M. Montcouquiol and colleagues in 2006. Scrib1 is a polarity protein containing a Leucine-Rich-Repeats (LRR) domain and 4 PDZ domains. The authors showed that PDZ2, PDZ3 and PDZ4 of Scrib1 can bind to Vangl2 and that in this way Scrib1 could play a direct role in asymmetric accumulation of Vangl2 at adherens junction. In 2010, Lindqvist and colleagues suggested that Vangl2 participated in the regulation of adherens junctions through Rac1 in the mouse neural tube, via direct interaction Rac1 and RhoA thanks to the PDZ-BDM of Vangl2 which is important for their interaction.

The trafficking and sorting of Vangl2 has been characterized. A mutation in the *sec24b* in mice showed for the first time the role of COPII coating protein Sec24b in the membrane targeting of a central PCP protein. It would seem that this protein is important for the assembly of Vangl2 in COPII vesicles that go from the endoplasmic reticulum (ER) to the Golgi. The mutation of this gene results in the accumulation of the Vangl2 protein in the ER (Merte et al.,

2010; Wansleebe et al., 2010). A recent study focused on the transport of Vangl2 from the trans Golgi network (TGN) in HeLa cells (Guo et al., 2013). They found that the GTP-binding protein ADP Ribosylation Factor Related Protein 1 (Arfrp1) and the clathrin adaptor complex 1 (AP-1) are required for Vangl2 transport from the TGN, but not for Fz6 (which localizes to the opposite epithelial surface from Vangl2). Arfrp1 exposes a binding site on AP-1 that recognizes the Vangl2 sorting motif for capture into a transport vesicle which will target Vangl2 to the proximal side of a polarized epithelial cell.

A recent paper from our laboratory has unveiled another trafficking interactor for Vangl: Gipc1 (GAIP C-terminus interacting protein 1). A yeast two-hybrid screen of an embryonic cochlear was performed to show that the PDZ-BDM of Vangl2 was important to bind to the PDZ domain of Gipc1. The same Vangl2 bait was used to test the interaction with other PDZ-containing proteins. Results confirmed that Gipc1, along with Scrib1, Dlg (Discs large homolog) or Magi are among the strongest interactors. Furthermore it was reported that a myosin VI-Gipc1 protein complex can regulate Vangl2 traffic in heterologous cells and that in myosin VI mutant mice, Vangl2 presence at the membrane is increased (Giese et al., 2012). Confirming some of these findings, a study on kidney mouse has determined that Vangl2 interacts with Magi-2, a protein that can be found at junctions (Babayeva et al., 2011). siRNA depletion of the core PCP gene Vangl2 was performed and reduced number of cell projections and decreased stress fibers and cell motility.

If Vangl2 degradation and presence at the membrane seems tightly controlled, the protein appears itself to be implicated in the translocation and targeting of various proteins. In 2003, Lee and colleagues showed that drosophila Dlg and Vang-Stbm are functionally linked to plasma membrane formation. Embryos with mutation either in dlg or vang-stbm presented severe defects in membrane formation, while the combined overexpression of Dlg and Vang-Stbm induced excessive plasma membrane formation (Lee et al 2003a). Moreover, they showed that the co-expression of Vang-Stbm with the mammalian Dlg homologue SAP-97-hDlg led to the translocation of SAP-97 from the cytoplasm to post-Golgi vesicles and the plasma membrane, and that this effect was specific of the Vang-Stbm/SAP-97 interaction.

More recently it was showed that Vangl2 can control the remodeling of ECM during the gastrulation of zebrafish embryos, by regulating the endocytosis of the metalloproteinase MMP14 (matrix-metalloproteinase) (Williams et al., 2012). The loss of vangl2 in trilobite mutants leads to an increase in cell surface amounts of MMP14, an abnormal remodeling of the ECM and finally disturbance of the convergent extension. This study demonstrates that Vangl2 is also important for the integration of the surrounding context in order for cells to properly

migrate over the ECM. The regulation of adhesion molecules by Vang/Vangl2 is addressed in the section 1.3: PCP and the central nervous system.

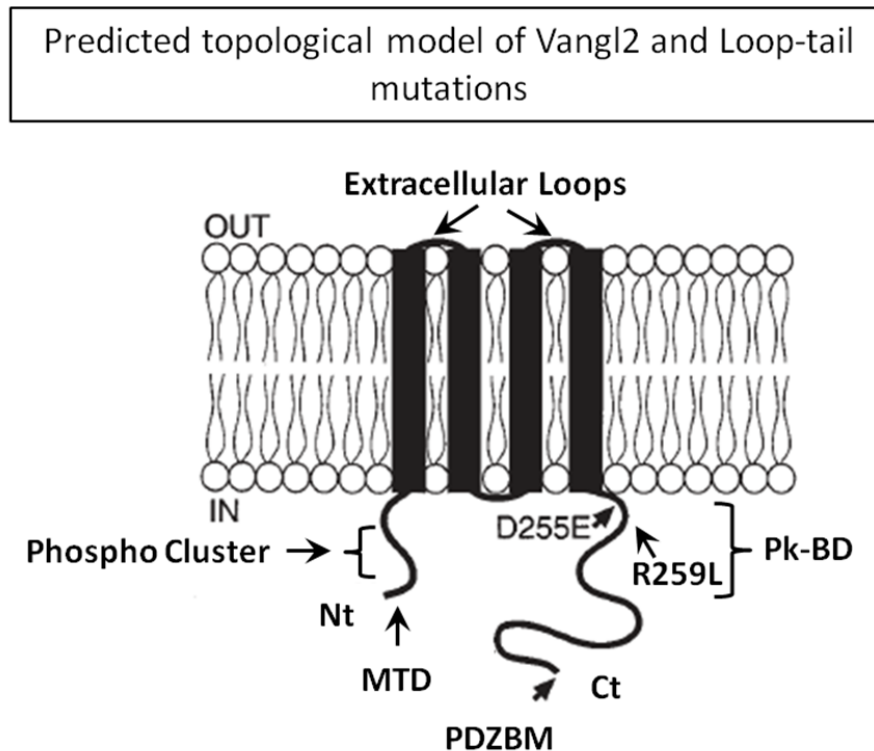


Figure 10: Predicted topological model of mammalian Vangl2. Vangl2 encodes a 521 amino-acid protein (~60 kD) that includes 4 transmembrane domains, a PDZ-Binding Motif at the C-terminus (PDZBM), a cluster of predicted PKC and CK2 phosphorylation sites and putative membrane targeting signals. The positioning of these targeting signals and the of PDZ-BM to the intracellular side suggest a topological model in which the N- and C-terminus (Nt, Ct) are located intracellularly. The C-terminus (aa 242-524) includes a conserved domain that binds to Pk (aa 298-382) (Pk-BD), which corresponds to the domain of interaction with N-cadherin (Nagaoka et al., 2014a). The N-terminus (aa 1-114) possesses several phosphorylation sites (Gao et al., 2011) (Phospho cluster). This model predicts two extracellular loops for Vangl2 which have been described to interact with the extracellular domain of Fz (Wu & Mlodzik, 2008). There are several *Loop-tail* mutations on the Vangl2 gene: Lp^{m1Jus} (D255E), Lp^{m2Jus} (R259L), and Lp (S464N). All of them result in an amino-acid substitution. MTD: Membrane-targeting domain; Pk-BD: Prickle binding domain. Adapted from Kibar et al., 2001a.

2.2 Vangl mutants

As described previously, there is a mouse strain that presents a spontaneous mutation in the *vangl2* gene called Loop-tail ($Vangl2^{Lp/Lp}$) mouse. *Loop-tail* is a semi-dominant mutation on chromosome 1 originally described by Strong et al. in 1949 (Strong & Hollander, 1949). This is a missense mutation within the Vangl2 cytoplasmic domain that affects amino acid residues otherwise conserved in the protein family: S464N (Lp) (Kibar et al., 2001a). The work of

Montcouquiol and colleagues in 2006 reported that the $Vangl2^{Lp/Lp}$ variant induces $Vangl2$ degradation as well as its mistargeting (not localized to the membrane) in heterologous cells, as well as a reduction of $Vangl2$ protein levels in the brain (biochemically by Western Blotting) and cochlea (by immunofluorescence). Torban et al. further showed that Lp -associated mutations cause $Vangl$ protein instability, reduced half-life, and increased proteasome-dependent degradation, all possibly secondary to a basic misfolding defect (Torban et al., 2012). Moreover, it has been shown that this Lp -associated variant is a dominant negative protein which is able to interact with either $Vangl1$ or $Vangl2$, form oligomers and disrupt their delivery to the cell surface (Yin et al., 2012).

A homozygous mutation of this gene leads to *craniorachischisis*, the most severe defect in NTD which ultimately results in death of the embryo in the mother's womb or at birth (Fig. 11).

Homozygous $Vangl2^{Lp/Lp}$ mutation leads to *craniorachischisis*

Wild-type

$Vangl2^{Lp/Lp}$



Figure 11: Homozygous $Vangl2^{Lp/Lp}$ mutation leads to *craniorachischisis*, the most severe form of NTD. This spontaneous mutation leads to failure of neural closure, leading to a complete exposure of the neural tube and brain. Embryos bearing a homozygous mutation of this gene die at birth but heterozygous mutants survive and have a looped tail. As mentioned before, CE mechanisms take place notably during gastrulation and neurulation. During neurulation, CE (convergent extension) movements are responsible for the narrowing and lengthening of the neural plate during neural tube closure (Torban et al., 2012) and defects in CE might contribute to NTD.

Besides NTD, *Vangl2*^{Lp/Lp} mutants also exhibit defects in lung branching, kidney tubular branching, kidney glomerular maturation, musculoskeletal morphology and in cardiac development (reviewed in Torban et al., 2012), emphasizing the role of PCP signaling, and notably *vangl2*, in these processes. Heterozygous mutants however do survive and possess a looped tail. Three alleles, *Lp*^{m1Jus}, *Lp*^{m2Jus} and *Lp*, can contribute for the *looptail* mutation (Kibar et al., 2001a; Kibar et al., 2001b; Guyot et al., 2011). Mutations on these alleles both result in amino-acid substitution: D255E (*Lp*^{m1Jus}) which consists in the substitution of an aspartate by a glutamic acid, R259L (*Lp*^{m2Jus}) consists in the substitution of an arginine by a leucine, and S464N (*Lp*), a potential phosphorylation site, where a serine is replaced by an asparagine (Fig. 10). These mutations are semi-dominant and do not impact on mRNA expression levels. Semidominant mutations lead to less severe phenotypes when compared to homozygous mutants.

Many studies in mammal identified PCP or PCP-like phenotypes or potential associated PCP members of a putative *Vangl* pathway using genetic interactions with the *vangl2* allele. To achieve this, genetic interaction experiments can be used to evaluate if the effects of one gene (here *vangl2*) are modified by one or several other genes. These experiments have been largely performed in the *Vangl2*^{Lp/Lp} mutant mouse. One of the best examples of such a genetic interaction is *vangl1*, the other isoform of the mammalian *vangl* family. Contrary to *vangl2* total knockout (KO), *vangl1* mutants do not display the severe NTD phenotypes or the defects the orientation of inner ear stereociliary bundles observed in *Vangl2*^{Lp/Lp} mutants (Torban et al., 2008; Song et al., 2010). However, *vangl1* was shown to genetically interact with *vangl2* as double heterozygous mice (*vangl1*^{gt/+}/*vangl2*^{Lp/+}) display a stronger phenotype than individual heterozygotes. These results strongly suggest that the *Vangl* pathway is exquisitely sensitive to gene dosage, with a minimum threshold level of combined *Vangl* activity required for function.

Neurulation is a Convergent Extension (CE) – dependent process

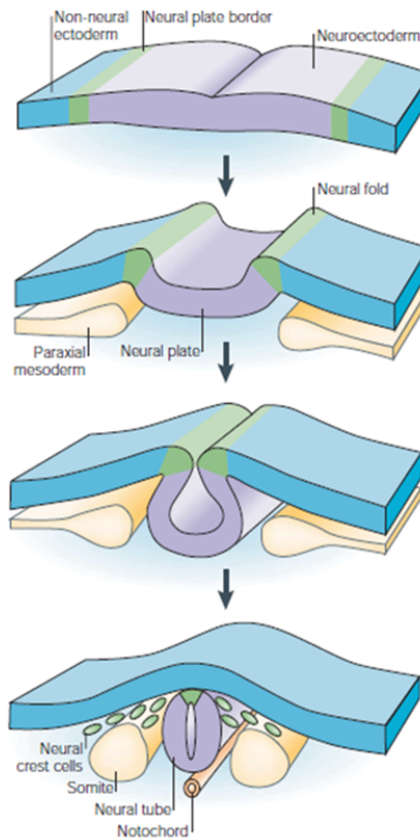


Figure 12: Neurulation is a CE-dependent process. The neuroectoderm (purple), the non-neural ectoderm (blue) and the underlying paraxial mesoderm (yellow) induce the formation of the neural plate border (green) via their combined signaling. During neurulation, the neural plate borders rise and lead to the formation of neural folds. A neural groove is then formed and its extremities fuse, causing neural tube closure. Neural crest cells delaminate from the neural folds/neural tube. This tube expands to form both the cephalic vesicle at the anterior extremity and the spinal cord. The closing of the neural tube requires CE movements (see figure 6). From Gammill & Borner-Fraser, 2003).

2.3 *Vangl 1 and 2 functions in neurons*

A work in *C. elegans* on Vang-1 and Prkl-1 (*C. elegans* orthologous of Van Gogh and Prickle proteins respectively) demonstrated that both proteins cooperated to negatively regulate neurite formation. Moreover, core components of PCP signaling are required in a subset of peripheral motor neurons to restrict neurite emergence to specific organ axis. Through loss or gain of function experiments (LOF, GOF) it was concluded that these proteins have a role in

maintaining polarized neuronal morphology by inhibiting neuronal responses to extrinsic and intrinsic cues that would otherwise promote unnecessary neurite formation (Sanchez-Alvarez et al., 2011).

In mammalian brain, comprehensive analysis of the pattern of expression of Vangl1 and Vangl2 shows both differences and overlaps (Tissir & Goffinet, 2006; Torban et al., 2008). For example, this study shows that *Vangl1* expression is restricted to the midline floor plate cells and to the notochord while *Vangl2* is more widely distributed over the entire neuroepithelium and absent from the notochord (Kibar et al., 2001a; Torban et al., 2008). Later, and in areas of the midbrain, retina and telencephalon, *Vangl2*, but not *Vangl1*, is abundantly expressed (Tissir & Goffinet, 2006). In contrast, Vangl1 and Vangl2 are colocalized in the sensory epithelia of the mouse cochlea with a similar asymmetrical localization pattern in both hair cells and supporting cells (Song et al. 2010). Altogether, these results show that in some systems, or at some developmental stages, Vangl1 and Vangl2 could interact in some specific protein complex.

As mentioned before, PCP signaling affects neuron migration, notably FBMNs (*see in section 1.2.2: Core PCP and FBMN migration*), and Vangl2 is directly implicated in this function. Sittaramane and colleagues showed in 2013 and using zebrafish that in floor plate cells *vangl2* functions largely to regulate caudal neuronal migration of FBMNs. A more recent study using the same model showed that PCP signaling is required both in FBMNs (autonomous role) and in the neuroepithelial environment in which FBMNs migrate (non-autonomous role) (Davey et al., 2016). To visualize the protrusive activity of single FBMNs at high time resolution, they utilized cell transplantation to generate embryos in which one or a few FBMNs express membrane-localized teal fluorescent protein (*Tg(isl1:mTFP)*). To determine the cell-autonomous function of Vangl2 or Fz3a (both expressing the transgene (*Tg(isl1:mTFP)*) in FBMNs the authors transplanted *vangl2* or *fz3a* mutant FBMNs into a wild type host. They found that the downregulation of Vangl2 lead to longer, more stable filopodia while Fz3a downregulation lead to less stable filopodia, with no significant change in filopodia length. To verify if these proteins also acted non-autonomously, wild-type (WT) FBMNs (expressing the transgene (*Tg(isl1:mTFP)*) were transplanted in mutant environments. This time, WT FBMNs on a *vangl2* mutant environment had less stable filopodia with no change in length, while removing Fz3a from the environment led to more stable filopodia. Altogether these results show that PCP signaling between the planar polarized environment and FBMNs is important for the selective stabilization of FBMN filopodia.

In 2009 Lake and Sokol used the Vangl2^{Lp/Lp} mutant mouse to show that these embryos presented a precocious differentiation of neural progenitors into early-born neurons at the expense of late-born neurons and glia. They reported that neural progenitors would

differentiate prematurely and loose the asymmetric distribution of Partner of inscuteable (Pins), a regulator of mitotic spindle orientation. These results along with other findings lead the authors to conclude that Vangl2 functions to maintain cortical progenitors and that it is important to regulate mitotic spindle orientation during asymmetric divisions in the mouse brain.

In another model, the mouse spinal cord, Shafer and colleagues (2011) centered their attention on commissural axon growth cones and were able to visualize that Vangl2 predominantly localized at the membrane and that it was highly enriched at the tips of filopodia as well as in patches of membrane where new filopodia emerge. Through the use of *Looptail* mutants the authors showed that after crossing the floor plate, most of the commissural axons presented guidance defects. Moreover, Vangl2 was able to reduce Fz3 phosphorylation and promote its internalization while Dvl1 exerted the opposite effect by increasing hyperphosphorylation of Fz3. The authors concluded by proposing that Vangl2 and Dvl1 had antagonistic function on the regulation of Fz3 surface levels and in this way sharpen PCP signaling locally on the tips of filopodia for sensing directional cues, ultimately causing turning of growth cones.

A role for Vangl2 in spines has also been predicted and demonstrated. A first study of Yoshioki and colleagues (2013) showed that Vangl2 can complex with PSD-95, a postsynaptic protein which only localizes at dendritic spines. In the same study it was shown that Vangl2 binds to PSD-95 through the PDZ-BM located in its C-terminus and that this binding is necessary for Vangl2's translocation into the spine. However these results were challenged two years later by a study claiming that this PDZ-BM is not absolutely required for Vangl2's localization in the synapse. Two distinct pools of Vangl2 were identified: one that has an overlapping co-localization with PSD-95 and another one that is highly correlated but complementary pattern of association with PSD-95 (Nagaoka et al., 2015). The authors postulated that only the former was significantly sensitive to the deletion of the PDZ-BM. Another interesting result of this study is that the PDZ-BM of Vangl2 enhanced the protein interactions between PSD-95 and Pk2. In a previous study the same laboratory used Vangl2^{Lp/Lp} mice and shRNA transfection in neurons to show that spine formation and synaptogenesis were impaired in the affected neurons (Nagaoka et al., 2014a). Altogether this study shows that Vangl2 determines complex formation and clustering of postsynaptic molecules for synaptogenesis. Moreover, Vangl2 has also been implied in spine formation and synaptogenesis through use of Golgi staining in *Looptail* mutant mice and shRNA against Vangl2 in cultured neurons (Nagaoka et al., 2014a). Besides this role in dendritic spines, it was shown that Vangl2 has a role in the dendritic branching of hippocampal neurons (Hagiwara et al., 2014). Through overexpression of deletion mutants, which either had

the N-terminal region or the C-terminal region of Vangl2 deleted, they showed a decrease or an increase respectively in the dendritic branching of neurons. This bidirectional regulation of dendritic branching suggests that Vangl2 is a molecular hub for neural development.

3 N-cadherin: an adhesion protein that regulates actin dynamics and tissue morphogenesis

3.1 Cadherin structure

N-cadherin belongs to the cadherin superfamily which comprises more than 80 members. This superfamily is divided in families: the **classic cadherins** (type I), the **atypical cadherins** (type II), the **desmosomal cadherins**, the **protocadherins**, the **T-cadherins**, the **Fat-like cadherins** (Fat, Dachous), the **“seven-pass transmembrane” cadherins** (Fmi), the **7D-cadherin**, the **CDH 15-23 cadherins**, the **calsyntenins** and **Ret cadherins**. All these cadherins are characterized by an extracellular part formed of ectodomains (ECs) that are structurally similar to immunoglobulins (Igs). The number of ECs varies for each cadherin (5 to 34) and at the interface between two ECs there is a binding site to Ca^{2+} . Cadherin proteins usually possess one transmembrane domain, except for the “seven-pass transmembrane” atypical cadherin which have 7 of them -like the PCP proteins Celsr1-3- and cadherin-13 which doesn't have this domain and anchors to the membrane through a glycosylphosphatidyl inositol (Nollet et al., 2000). Hence, at the exception of the cadherin-13, all cadherins possess a cytosolic domain. Interestingly this cadherin-13 has a crucial role in proper function of hippocampus and cognition, which will be further discussed in the hippocampus chapter (Fig. 14).

The family of classic cadherins can be divided into two subfamilies: type I (e.g. N-, E-cadherin) and type II (e.g. VE-cadherin, cadherin-11, but also cadherin -8, -9 which play a role in the developing hippocampus; described in the hippocampus chapter). The differences between type I and type II cadherins are apparent at the amino acid sequence level. The HAV sequence present in the EC1 domain of type I cadherins is absent in type II cadherins. Also, type I cadherins possess a single tryptophan residue at their N-terminal while type II possess two of them. Interestingly, while type I cadherins seem to be distributed broadly in tissues, type II cadherins tend to be expressed in more restricted cell populations and types (Han & Yap, 2012). For example, N-cadherin (type I) is expressed widely in the mesodermal and neural tissues, including endothelial cells, while VE-cadherin (type II) is solely expressed in the endothelial cell populations of the mesoderm (Salomon et al., 1992; Navarro et al., 1998).

E-Cadherin and N-Cadherin are type I cadherins expressed in various tissues, including epithelial tissues and the nervous system. These classical cadherins possess 5 ECs and are responsible for Ca^{2+} -dependent homotypic adhesions. They can associate laterally to form dimers in *cis* but also in an antiparallel fashion to form dimers in *trans* (Gumbiner, 2005). Ca^{2+} plays a critical role in the homophilic adhesion of cadherins and when Ca^{2+} is absent, the extracellular domain of cadherins is disorganized and a mutation in the Ca^{2+} -binding site induces reduced adhesion ability (Pertz et al., 1999; Ozawa et al., 1990). However, the adhesive

properties of cadherins are not exclusively related to their extracellular interactions. Some studies have shown that the affinity of the cadherin-cadherin is weak (Baumgartner et al., 2000; Chappuis-Flament, 2001) and that mutations in the cytoplasmic domain perturb the dimerization of cadherins and extracellular adhesion (Ozawa and Kemler, 1998; Takeda et al., 1999). Altogether these studies demonstrate that the regulation of cadherin binding ability in *cis* and *trans* is important for cellular adhesion.

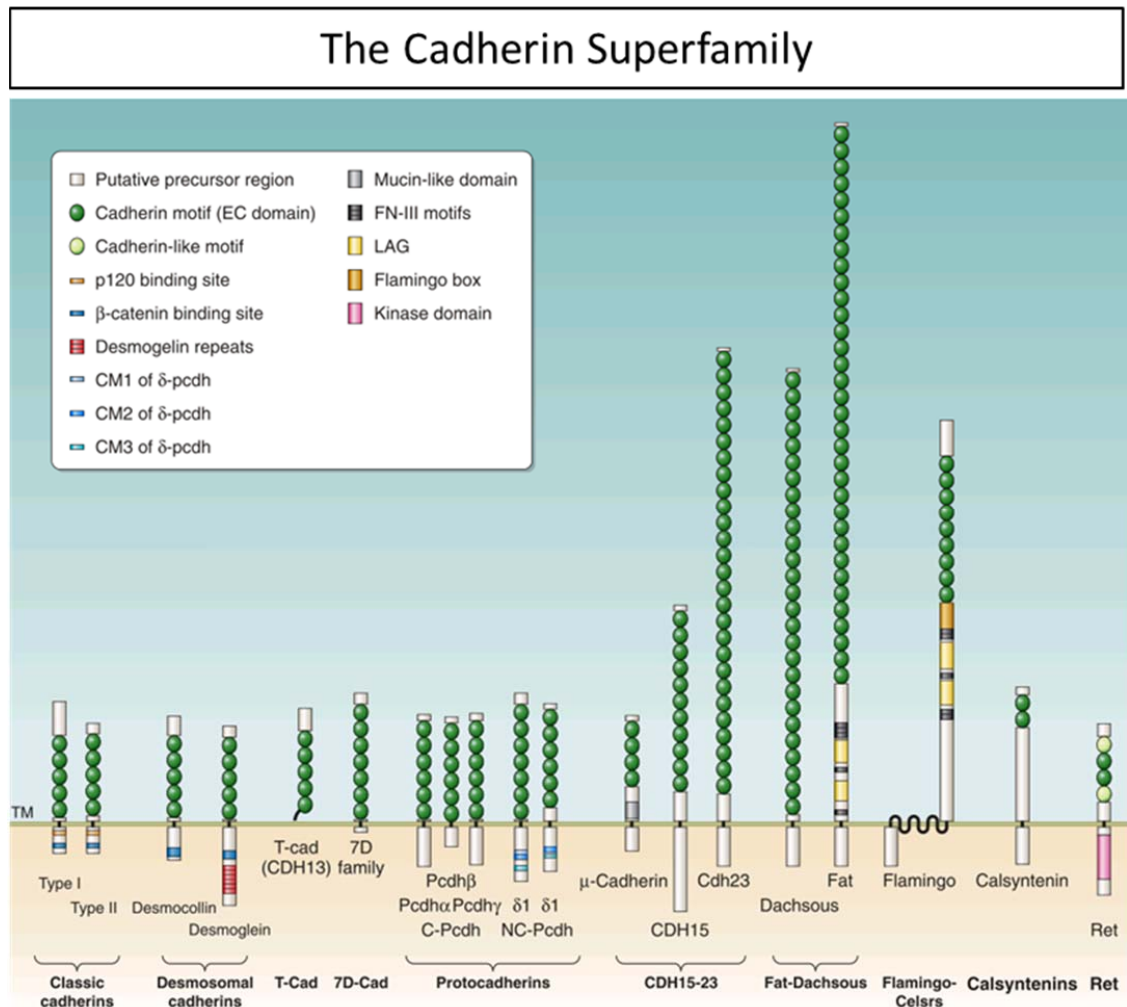


Figure 14: The Cadherin superfamily. Illustration of the different cadherin sub-families. Despite their diversity, all these cadherins possess at least one ectodomain in their extracellular domain. Every family and subfamily is classified in agreement with conserved cytoplasmic sequences. Note the presence of Fat, Dachsous and Flamingo, members of the PCP signaling. From Hirano & Takeichi, 2012.

3.2 The cadherin/catenin complex is an anchorage site for the regulation of the actin cytoskeleton

The intracellular domain of cadherins is also highly conserved in the classical sub-family. These domains allow for the intracellular interaction with catenins, which will be responsible for the link to the actin cytoskeleton (Gumbiner, 2005). β -catenin, γ -catenin and the p120-catenin are proteins which have “armadillo repeats” which are necessary for the binding to cadherins as well as to other partners. α -catenin is a protein homologous of vinculin that allows the binding to other catenins and actin. β -catenin binds to the C-terminal region of cadherins and assure the link to α -catenins, but it can also display other functions.

3.2.1 *Canonical Wnt pathway*

β -catenin participates in the targeting of cadherins at the membrane (Chen et al., 1999) and it also plays an important role in the canonical Wnt signaling pathway (Sokol, 2015; Wilson & Stoeckli, 2012). When Wnt are not bound to Fz receptors, β -catenin is phosphorylated and degraded constitutively by a protein complex comprised of GSK-3 β amongst others (Hagen & Vidal-Puig, 2002) (Fig. 15A). When a Wnt binds to a Fz receptor, β -catenin is translocated to the nucleus in order to stimulate, together with other transcription factors, the expression of specific genes involved in tissue homeostasis (Fig. 15B). The transcription occurs *via* binding of β -catenin to members of the TCF/LEF1 (T-cell factor/lymphoid enhancer-binding factor 1) family of transcription factors that bind to DNA and control the expression of specific genes (Archbold et al., 2012) (Fig. 15B). Canonical Wnt signaling is therefore a signaling depending on transcriptional activation.

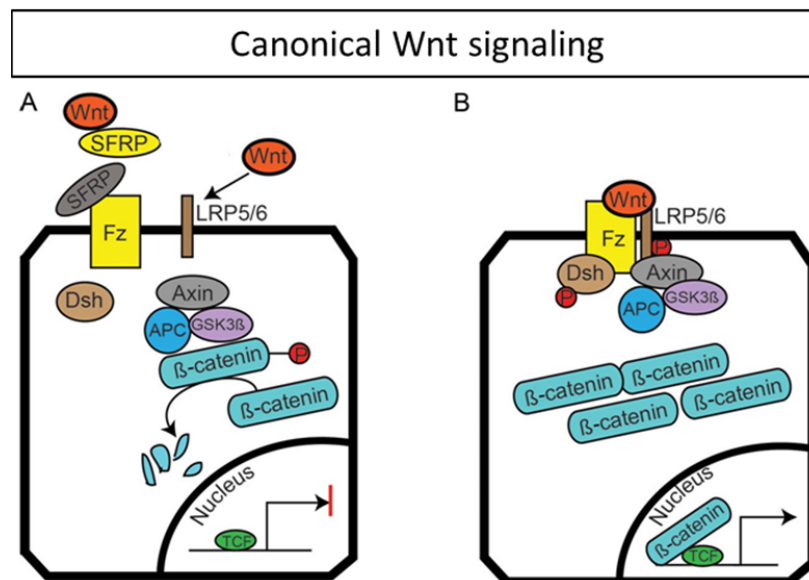


Figure 15: Canonical Wnt signaling. (A) When Wnt is not bound to Fz, β -catenin is constitutively degraded. β -catenin binds to a complex composed of Axin, APC and GSK3 β , called the destruction complex, and is phosphorylated, leading to its degradation via ubiquitination. Secreted-frizzled-related proteins (SFRP) are antagonists of Wnt that can bind either to Wnt or Fz and prevent their interaction. (B) When Wnt binds to Fz and its co-receptor lipoprotein receptor related protein (LRP)5/6, the Wnt canonical pathway is activated: Dsh is recruited and phosphorylated and Axin is now recruited near the cell membrane, preventing the formation of the destruction complex and further degradation of β -catenin. β -catenin accumulates in the cytoplasm and translocates to the nucleus where it binds to members of the TCF/LEF1 family in order to stimulate the expression of specific genes involved in tissue homeostasis. Canonical Wnt signaling is therefore a signaling depending on transcriptional activation. Adapted from Deb, 2014.

3.2.2 Adhesion sites

As α -catenin binds directly and indirectly to actin, it constitutes a point of control in actin dynamics. Hence, this protein is a hotspot that both coordinates the cadherin-cadherin adhesions and the actin cytoskeleton. Its binding domain to β -catenin is located in its N-terminal, while the domain allowing for direct binding to actin is comprised in the C-terminal (Fig. 16). This binary interaction supports a model in which α -catenin binds physically to β -catenin and actin in order to form a cadherin/ β -catenin/ α -catenin/actin quaternary complex. However many studies demonstrated that such complex does not exist, or at least, cannot be reproduced *in vitro* (Pokutta and Weis, 2000; Drees et al., 2005; Yamada et al., 2005). From these studies another model came up: when adhesion occurs, the cadherin/ β -catenin complex recruits α -catenin, therefore leading to an increase in the local concentration of α -catenin. This leads to the formation of α -catenin dimers which are then able to bind to actin. An interesting

fact is that this binding competes with the ARP2/3 nucleator (a known actin-binding proteins or ABPs) in order to inhibit the nucleation of branched actin filaments (Drees et al., 2005; Pokutta et al., 2008).

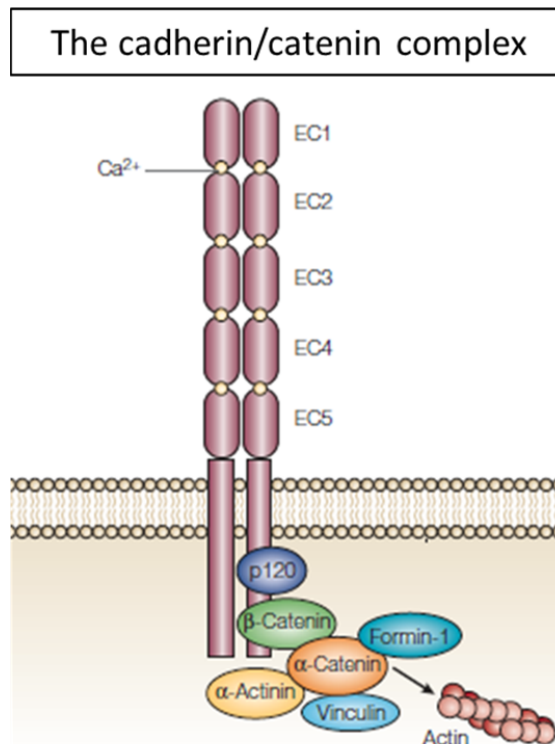


Figure 16: The cadherin/catenin complex. Schematic representation of the proteic complex formed between transmembrane cadherins and cytosolic catenins. The intracellular domain of cadherins can bind to p120 in sites located near to the transmembrane domain while β-catenin is able to bind to the C-terminus. β-catenin binds also to α-catenin which in turn binds to the actin cytoskeleton direct or indirectly. From Gumbiner, 2005.

In addition, α-catenin can bind to many proteins important for actin organization and dynamics: α-actinin (Knudsen et al., 1995), formin (Kobielak et al., 2004), vinculin (Weiss et al., 1998), zonula occludens protein 1 (ZO-1; Imamura et al., 1999), afadin (Pokutta et al., 2002) or epithelial protein lost in neoplasm (EPLIN; Abe and Takeichi, 2008). The organization of the actin cytoskeleton at adherens junctions depends on some of these proteins and their binding to α-catenin (Imamura et al., 1999; Kobielak et al., 2004; Abe and Takeichi, 2008; Benjamin et al., 2010).

It is important to note that the coupling between the cadherin/catenin complex and actin is not important only for the regulation of actin cytoskeleton, the reorganization of the actin cytoskeleton also allows the formation and stabilization of adhesion sites. For example, an

inactive mutant form of Rac1 impedes the formation of adhesive contacts (Braga et al., 1997) the inhibition of ARP2/3, formins and ENA/VASP (another ABP) perturbs the organization and formation of cellular junctions (Verma et al., 2004; Kobiela et al., 2004; Scott et al., 2006), while the small RhoGTPase is also known to have an important role in the stabilization of adherens junctions through the activation of formins and myosin (Harris and Tepass., 2010).

Altogether these studies helped Harris and Tepass to suggest a model that can explain the interaction of the actin cytoskeleton with the adhesive cadherin/catenin complex in the formation of intercellular adhesion (Fig. 17). First, the actin cytoskeleton generates a protrusion which starts a contact through the recruitment and aggregation of cadherins. This aggregation, in turn, activates the polymerization of actin filaments in order to promote membrane protrusions and to create more adhesion. These first two steps are sustained by catenin (p120-catenin) and actin nucleation through Rac1/WAVE/ARP2/3 (all ABPs) and are followed by the aggregation of cadherin/catenin complexes, which will then lead to the recruitment of α -catenin and the activation of Rho. This will in turn lead to the inhibition of the ARP2/3-dependent nucleation, the recruitment and activation of proteins such as formins, α -actinins and myosins to finally induce actin cytoskeleton reorganization and adhesion stabilization (Harris and Tepass, 2010). It is important to note that this model highlights the complexity of the reorganization of the actin cytoskeleton that depends on the temporal and spatial coordination of various ABPs, their activators and adhesion proteins.

A paper recently published reports that cadherins are included in ordered nanoclusters to control their anchoring to actin and cell-cell contact fluidity (Strale et al., 2015). The authors propose that the oligomerization of cadherins is important for the stability of junctions. Such stability would be related to their ability to form *cis* interactions which could be responsible for shifting cadherin clusters from a fluid to an ordered phase. Electronic microscopy revealed that E-cadherin molecules are organized in nanometric arrays at the cell membrane, providing the first demonstration of the existence of oligomeric cadherins at cell-cell contacts. Moreover, disruption of the *cis*-interface impeded almost completely the formation of these nanoclusters but did not affect the ability to form AJ. However, this disruption increased the mobility of E-cadherin at junctions, further affecting E-cadherin anchoring to actin and cell-cell rearrangement during collective cell migration. These results demonstrate that cadherin oligomerization is important to couple the actin cytoskeleton to the membrane. Even more interesting, this increase in actin dynamics was correlated to an increase in cell protrusion, altogether suggesting that the disruption of the *cis*-interface decreases the anchoring of E-cadherin clusters to actin.

Altogether these studies demonstrate a dynamic role of cadherin proteins in the formation of adhesion sites and how the direct and indirect interaction with cytoskeleton elements is important to control actin dynamics and cellular outgrowth.

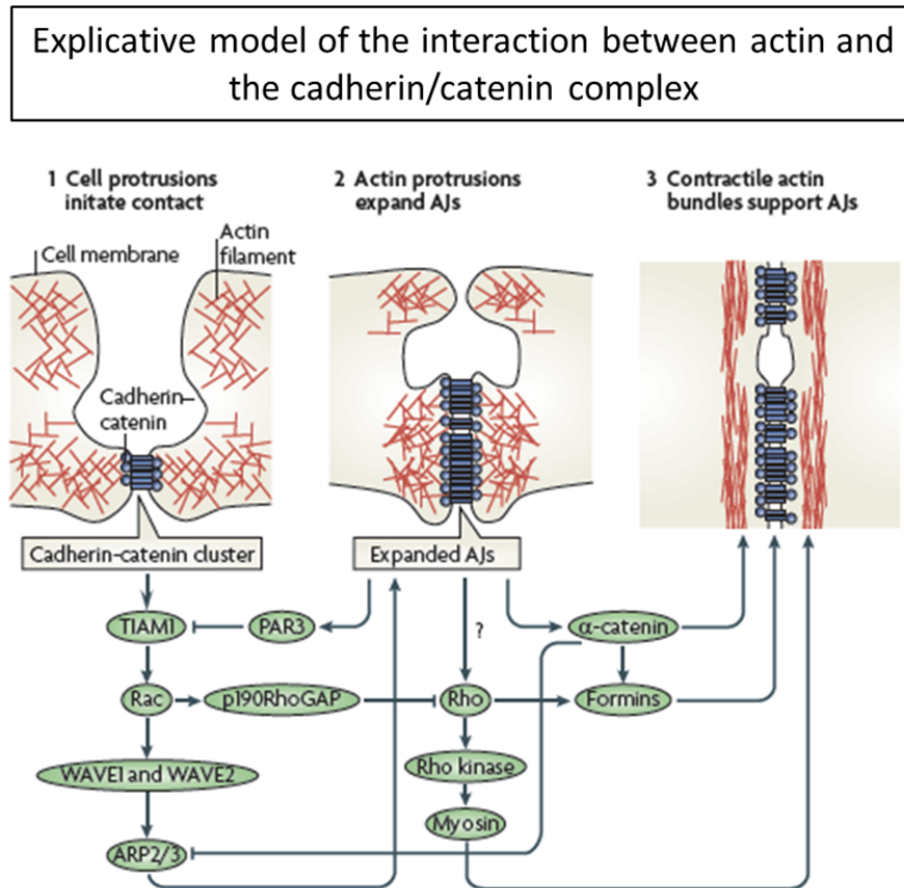


Figure 17: Explicative model of the interaction of actin cytoskeleton with the adhesive cadherin/catenin complex. (1) Two cells send out projections, promoting cell-cell contact and the local recruitment of cadherin/catenin adhesion complexes. These complexes further activated Rac which in its turn activates the actin nucleator ARP2/3, causing the expansion of actin protrusions and consequently of the adherens junction (AJ). During this first step, Rho is inhibited in order to contain the next wave of AJ signaling. (2) After the expansion of formed AJ, α -catenins and partitioning defective 3 homologue (PAR3) are recruited to this site to inhibit APR2/3 and Rac GEF T lymphoma invasion and metastasis-inducing protein 1 (TIAM1), further blocking the first wave of AJ signaling. (3) The second wave of signaling through Rho together with α -catenin related actin remodeling promotes the formation of contractile actin bundles for AJ maturation. From Harris & Tepass, 2010.

3.3 Cadherin expression and function in development

Each subtype of classical cadherins tends to be expressed at the highest levels in distinct tissue types during development (Halbleib & Neslon, 2006). E-cadherin is mostly expressed in epithelia and has a crucial role in establishing and maintaining apico-basal polarity while N-cadherin is mostly expressed in neural tissue and muscle. However, these expression patterns are not totally exclusive: in 1988 Takeichi showed that E-cadherins are expressed also in the nervous system. Other types of cadherins such as R-cadherin, P-cadherin and VE-cadherin for example are highly expressed in the forebrain and bone, the basal layer of the epidermis and in endothelial cells respectively. The fact that different cadherin subtypes can be differently expressed in different tissues confers to these proteins a role in cell sorting. This function was confirmed *in vitro* using non-adherent fibroblast, in *Drosophila* oogenesis, in *xenopus* gastrulation and vertebrate limb formation (Gumbiner, 2005).

Studies in zebrafish have shown that cadherins are crucial for tissue morphogenesis. In some of these experiments, E-cadherin adhesion was disrupted during zebrafish gastrulation and as a consequence epiblasts were still able to intercalate but failed to stabilize in the external layer and tended to de-intercalate (Kane et al., 2005; Shimizu et al., 2005). In another study, Hong & Brewster established that the deletion of N-cadherin led to the blocking of both convergence and intercalation of cells during zebrafish neurulation (Hong & Brewster, 2006). Interestingly, the deletion of N-cadherin did not affect the protrusion capability of neuro-epithelial cells but rather the stability of these protrusions.

N-cadherin is also important for neurulation in *xenopus*. In a study performed by Detrick and colleagues, cDNA encoding for N-cadherin in *xenopus* was isolated and used this cDNA to report that N-cadherin is expressed in the ectoderm of the neural tube prior to the occurrence of morphogenetic events associated with early neural development (Detrick et al., 1990). The authors further expressed N-cadherin in the ectoderm of *xenopus* embryos (GOF) and reported that some of these embryos had neural tubes that failed to properly close while others had neural tubes with hypertrophy. They also observed that N-cadherin expression was associated with disorganization in the cellular structure of the neural tube. The cells of the neural tube normally appear as a radial array of columnar epithelium, but in areas of N-cadherin misexpression, cells were often found in chaotic structures. These results show that N-cadherin plays a role in the control of morphogenetic changes that are crucial for neural tube closure.

Cadherins play a major role in the development and maintenance of the nervous system: they are differently expressed in different cells and regions of the nervous system. N-cadherin is notably important during neuronal maturation for neuronal outgrowth, axon fasciculation and

guidance, and growth cone navigation. The disruption of neuronal cadherins, such as DN-cadherin (drosophila N-cadherin), N-cadherin or PSA-NCAM (Polysialylated-neural cell adhesion molecule) in drosophila and chick embryo leads to fasciculation disruption of major axonal tracts (Iwai et al., 1997; Honig et al. 1998). Two different studies showed that N-cadherin and R-cadherin stimulate neurite outgrowth through fibroblast growth factor receptor (FGFR) activation (Redies et al., 1992; Riehl et al., 1996), while others demonstrated that Cadherin-11 and -13 can respectively promote axon elongation or act as repulsive cues for growth cones (Marthiens et al., 2005; Fredette et al., 1996). N-cadherin also plays a role in neuronal targeting in both drosophila and chick: disruption of N-cadherin adhesion results in the mis-targeting of axons in the visual system of both organisms (Inoue and Sanes, 1997; Lee et al., 2001). Interestingly, N-cadherin-mediated adhesion has also been implicated in adult neurogenesis following injury (Chen et al., 2006).

In mature neurons, several cadherins are expressed at synapses: N-cadherin, R-cadherin and Cadherin-7 (Uchida et al., 1996; Heyers et al., 2004). N-Cadherin is expressed initially at all synaptic sites but rapidly becomes restricted to a subpopulation of excitatory synaptic sites (Benson and Tanaka, 1998). These findings indicate that N-cadherin adhesion may stabilize early synapses that can then be remodeled to express a different cadherin, suggesting the possibility that expression of specific cadherin subtypes might be instructive in synapse function.

The loss of N-cadherin in mice showed that this protein is important for proper neural tube formation but is not involved in the initiation of neurulation (Radice et al., 1997), while blocking N-cadherin with a dominant-negative form leads to altered dendritic spine morphology and spine density as well as a loss of β -catenin in spines (Togashi et al., 2002). Besides their structural role at synapses, cadherins also have been implicated in synaptic plasticity as they are present in mature synapses and form junctions (*puncta adhaerentia*) that surround the active zone, where neurotransmitters are released (Fannon and Coldmann, 1996; Uchida et al., 1996). For example depolarization of neurons lead to an increase of N-cadherin-mediated adhesion (Tanaka et al., 2000). The same effect is obtained when a long term potentiation (LTP) protocol is applied (Bozdagi et al., 2000) and, remarkably, the use of antibodies directed to the extracellular domain of N-cadherin block LTP induction.

Overall these studies demonstrate the importance of cadherins in the nervous system at earlier and later stages of development and also the multitude of processes in which its role is crucial for the proper formation and function of tissues.

3.4 Atypical cadherins involved in PCP signaling and development

Specific cadherins are well represented in the PCP pathway(s). Dachsous (Ds) and Fat define a PCP pathway believed to run in parallel with the core PCP pathway (reviewed in Simons & Mlodzik, 2008). Fat and Ds are very large and atypical cadherins that possess 34 and 27 ECs respectively (Mahoney et al., 1991; Clark et al., 1995).

Ds has been implicated in cell proliferation as well as border formation in the drosophila wing disc (Clark et al., 1995; Rodriguez 2004). It binds Fat directly and inhibits its activity (Yang et al., 2002; Matakastu & Blair, 2006). Interestingly, the extracellular domain of Ds is sufficient for its PCP function, indicating that it may act as a ligand during PCP signaling (Matakastu & Blair, 2006). In drosophila ommatidia, Fat can participate in PCP signaling due to the ability to bind the transcriptional corepressor Atrophin (Fanto et al., 2003). At the opposite of Ds, it would seem that only the intracellular domain Fat is necessary for its effects on tissue growth and PCP (Matakastu & Blair, 2006). Knockdown of Fat1 increases cell proliferation in vertebrates (Hou et al., 2006).

Fmi is the only member of the entire cadherin family with a seven-pass (instead of single) transmembrane protein and a large extracellular domain with 9 ECs (Nakayama et al., 1998) (see the PCP chapter).

3.5 Adhesion molecules and PCP

Convergent extension phenomenon (may it be during gastrulation, neurulation or even during organogenesis) highly depends on cellular intercalation. There are multiple other mechanisms that can drive tissue elongation, but cell intercalation is unique in requiring that the migration and adhesion of many cells are coordinated and polarized in space and time in order to shape a tissue. Intercalation is an interesting morphogenic process which push adherens junctions (AJ) to their limits due to the fact that cells must maintain adhesion while still dynamically form and dissolve new AJs.

Cadherins (as previously described), as well as other proteins such as non-muscle myosins and Rho GTPases play a crucial role in the orchestration of tissue morphogenesis. However, in order for cells to successfully intercalate mediolaterally, they need to be polarized. Hence, cellular rearrangement highly depends on PCP pathway.

A study performed by Classen and colleagues in 2005 showed that in the drosophila wing, PCP signaling controls the assembly/disassembly of AJ by regulating the positioning of the endocytic and exocytic machinery at specific cell-cell contacts. The wing is covered by a hexagonally packed array of hairs, each constructed by a single wing epithelial cell. E-cadherin staining revealed that cells become hexagonally packed (they were irregularly arranged

previously) shortly prior hair formation (Fig. 18). Subsequently, transgenic drosophila expressing E-cadherin-GFP under its endogenous promoter were used in order to image its distribution live on a confocal microscope. The authors noticed that intercellular junctions were constantly dynamic, and shrank and grew (resembling cellular intercalation during convergent extension) during hexagonal repacking. Interestingly, through the use of a temperature-sensitive Dynamin-null mutants (*shi*) and endocytic markers, they showed that cadherin endocytosis (through Rab5) and recycling (through Rab11) are important for junction remodeling during hexagonal repacking. As hexagonal repacking occurs at the time PCP proteins polarize, it was hypothesized that PCP signaling played a role in this process. To prove this point different null-mutants for Pk, Fmi, Fz, Vang and Dgo were created and the authors quantified neighbor number and junction length variability at the time of hair outgrowth. All of these mutants impacted (although on different levels) on the hexagonal repacking of hair cells, indicating that PCP mutant cells fail to efficiently assemble boundaries with new neighbors and cannot regularize their packing geometry. Hence, it was proposed that PCP signaling affects cadherin recycling and for this purpose the authors created double mutants for Dynamin (*shi*) and several PCP genes. As the (*shi*) loss of function is temperature-induced (loss-of-function at 34°C), the authors decided to use a subrestrictive temperature (31°C). When *shi* is combined with mutations in PCP genes in these mild conditions, holes formations (due to lack of cadherin recycling in wing cells) occurred, while the *shi* mutation alone did not affect tissue formation. This experiment nicely suggests that cadherins are recycled less efficiently in the absence of PCP proteins. Finally, the authors propose that Fmi can recruit Sec5-positive vesicles (a member of the exocyst complex) containing E-cadherin to AJs: Fmi accumulates preferentially on specific regions of the wing cortex and Sec5 vesicles are particularly enriched near Fmi-positive cell boundaries. To verify if Fmi recruits Sec5, Fmi was overexpressed and results showed that Sec5 dramatically accumulated in cells overexpressing Fmi but also that large internal structures positive for Fmi and Sec5 also contained E-cadherin. This result suggest that PCP proteins may promote hexagonal packing and remodeling of AJs by polarizing membrane trafficking.

Explicative model of the hexagonal packing in drosophila pupal wing

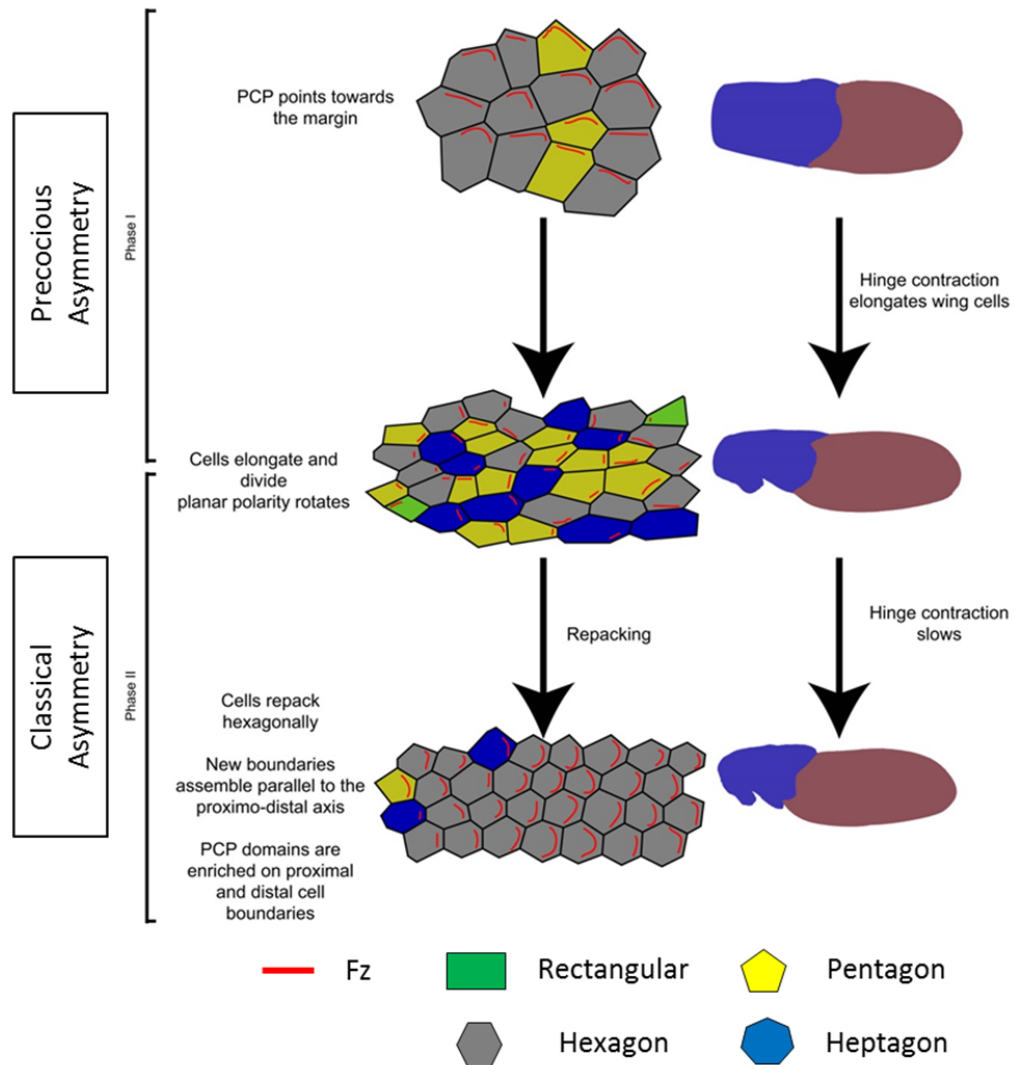


Figure 18: Model explaining the hexagonal packing of cells in drosophila pupal wings. The left panel demonstrates the cellular behavior that lead to the morphological changes that are observed during pupal wing development. Phase 1: This phase corresponds to the establishment of a precocious asymmetry, described for the first time in Agouy et al, 2010 where the authors discovered that PCP proteins were asymmetrically distributed well before the appearance of a trichome. However, the asymmetric distribution of PCP proteins is different at this stage as it was reported that Fz (Red line) enrichment site is different (90°, located apically) from where it accumulates during classical PCP asymmetry in the wing (distally). Phase2: The authors propose that in this phase, the mechanical forces deriving from the tension existing during wing lateral stretching is transmitted back to the cells, causing a redistribution of PCP proteins within the cells (from apical to distal). Colors correspond to the class of polygon described by the cells. (gray: hexagon, blue: heptagon, yellow: pentagon, green: tetragon). From Aigouy et al, 2010.

Later on, another study has emerged showing that Fz can also promote E-cadherin mobility at specific cell-cell contacts as tissue remodeling occurs in the extending drosophila germ-band (Warrington et al., 2013). Germ-band extension is a morphological process in which the germ-band, which develops into the segmented trunk of the embryo, approximately doubles in length along the anterior-posterior axis while subsequently narrowing along the dorsal-ventral axis. In this study, a novel role was reported for the core PCP pathway in promoting cell intercalation during tracheal tube morphogenesis in drosophila and that this role was due to the ability of the PCP pathway to regulate the turnover and levels of junctional E-cadherin by the guanine exchange factor RhoGEF2. Moreover, they showed that PCP pathway leads to a polarized recruitment of RhoGEF2 and E-cadherin turnover in the epidermis of both the embryonic germ-band and the pupal wing. Overall, the main idea of this paper is in accordance with the previous one (Classen et al., 2005): the PCP pathway is able to promote polarized cell rearrangements *via* remodeling of the adhesion sites.

The close relationship between cadherins and PCP proteins in the regulation of morphogenesis has also been demonstrated in vertebrates. In 2007 Harrington and colleagues injected a semi-dominant *N-cadherin* allele in zebrafish and verified that it caused the shortening of zebrafish tailbud during post-gastrulation stages (Harrington et al., 2007). Moreover, the authors injected this morpholino along with another one against *vangl2* and discovered that they interacted synergistically as the phenotypes presented by these zebrafish were worsen when compared to the injection of *N-cadherin* morpholinos only. Hence, these results suggest that *N-cadherin* and *vangl2* function synergistically and in parallel pathways to regulate CE. They did not however found a direct interaction between N-cadherin and Vangl2.

Recent studies have depicted a similar role in neurons. Nagaoka and colleagues used brain extracts and biochemically demonstrated that Vangl2 co-precipitates with PSD-95 and N-Cadherin (Nagaoka et al., 2014a). Internalization assays were used to demonstrate that Vangl2 regulates N-Cadherin internalization at the synapse level in a Rab5-dependent manner. Moreover, the authors showed that β -catenin, a known interactor of N-Cadherin, suppressed this interaction through binding competition, as it binds to N-Cadherin at the same region than Vangl2. On another hand this study demonstrated that Pk2, another core PCP protein, was also a limitation factor the Vangl2-N-Cadherin interaction as the Vangl2 domain necessary for the binding with N-Cadherin and Pk2 are the same. By downregulating Vangl2 and Pk2 separately a reduction in dendritic spine formation was observed. Altogether the authors were able to show that core PCP proteins such as Vangl2 and Pk2 can play a role in the precise formation and maturation of cell-cell adhesions at the synapse, controlling the surface levels of classic

cadherins. Two years later, the same authors published another paper in which they revisited the Vangl2/N-Cadherin interaction and function at the synapse (Nagaoka and Kishi, 2016). By silencing Vangl2 in hippocampal neurons Nagaoka showed that the clusters of PSD-95 tended to overlap with those of N-Cadherin and that the PSD-95 staining in spines was more diffused, without a significant change in the total signal. As Vangl2 can physically interact with both PSD-95 and N-Cadherin the authors postulated that a PCP-related molecular mechanism underlies the polarization of the postsynaptic regions.

The studies in drosophila and mammals strongly suggest that the selective internalization of adhesion proteins by the PCP is important for the rearrangement of cell adhesions and in the morphogenesis and function of tissues.

4 The neuronal growth cone: an integrative structure

Neurons are highly polarized cells and usually have a single long, thin axon and one or more dendrites, shorter and thicker than the axon (Fig.19). The cytoskeleton and its regulation are crucial elements in the establishment of neuronal polarity as shown by de Anda and colleagues in 2005. In this study they reported that the polarized activity of centrosomes were necessary and sufficient for neuronal polarization in the early post-mitotic stage. They showed that these organelles can polarize microtubule polymerization and membrane transport and that these events precede first neurite formation. It was also reported that neurons with more than one centrosome sprout more than one axon and that the suppression of centrosome-mediated functions impedes the first neurite formation.

At the tip of every neurites, including the axon, one can find a highly motile structure called the growth cone, whose function is also cytoskeleton-dependent. This actin-rich structure navigates throughout the environment and responds to various molecular cues (integrins, adhesion molecules, diffusible molecules) which can act as adhesive, attractive or repulsive cues. The movement of the growth cone is thus driven by the continuous reorganization and turnover of the actin and tubulin cytoskeleton in response to these cues.

Growth cones represent the major site of attachment to the outside environment in both axons and dendrites (Vitriol & Zheng, 2012). The force that drives the growth cone forward arises from the coupling between actin-rich protrusions with selective adhesion to extracellular components *via* adhesion complexes. Studies integrating every aspect s of neuronal outgrowth, including membrane turnover, cytoskeleton and adhesion to the extracellular environment, growth cone motility and guidance are few, because complex. However, the growth cone is an integrative structure under the influence of guidance and adhesive cues but also of components of the ECM that acts as the neuron substrate, making this cellular structure a major player in neuronal outgrowth and circuit formation.

For example, integrins or adhesion molecules (*i.e.* N-cadherin) can transiently induce the formation of adhesions locally in a growth cone. Adhesion sites are dynamic structures ready to immediately respond to internal and external signals (Vitriol & Zheng, 2012). As a result of their dynamics, adhesion sites remodeling will have an effect on overall migration, or even, if this alteration occurs locally in the growth cone, promote a directed movement of this structure. Focal-adhesion kinase (FAK), a tyrosine kinase, is a good example of a protein that can act as a bridge between the extracellular environment and the local regulation of cytoskeleton in the growth cone (Mitra et al., 2005; Parsons, 2003). FAK acts upstream of various signaling pathways, including regulation of Src-family kinases, Rho-GTPases, actin regulatory molecules

(Ras, Rac, Rho and Cdc42), adhesion components and microtubules (Chacon & Fazzari, 2011; Mitra et al., 2005). In neuronal adhesions, FAK is activated downstream of integrins and netrins where it regulates outgrowth and guidance in response to adhesion receptor activation (Bechara et al., 2008; Chacon & Fazzari, 2011; Li et al., 2004; Myers & Gomez, 2011; Ren et al., 2004; Robles & Gomez, 2006). Moreover, a local regulation of FAK can suffice the guidance of growth cones, when responding to locally presented attractive and repulsive cues (Bechara et al., 2008; Chacon & Fazzari, 2011; Li et al., 2004; Myers & Gomez, 2011). These studies demonstrate that the regulation of adhesion proteins is crucial for normal growth cone behavior and that disruption of adhesion proteins might be involved in abnormal circuit formation.

Molecular signaling cues (ex: netrins, ephrins, semaphorins, neurotrophins, slits) act in concert to guide the axon to its final target (Lin and Holt, 2007). Specific receptors are usually located on growth cone protrusions and are important for environment probing and for signal detection, which correspond to gradients of attractive and repulsive molecules (Tessier-Lavigne and Placzek, 1991). These signals are integrated by the growth cone and induce a local protein synthesis, finally enabling the growth cone to move towards a certain direction (Campbell and Holt, 2001). More specifically, these signals induce a rapid and localized increase/decrease in proteins levels that can bind to actin, control cytoskeleton dynamics and ultimately guide the growth cone.

As described previously, PCP proteins modulate cytoskeleton dynamics locally in cells and a disruption of PCP signaling has neurodevelopmental consequences, including disruption of axonal guidance, neuronal migration, neuronal polarity and dendrite morphogenesis (*see in section 1.3: PCP and the central nervous system*). PCP proteins are therefore good candidates to participate in cytoskeleton dynamics within the growth cone to contribute to its motility and behavior.

Neurons are polarized cells

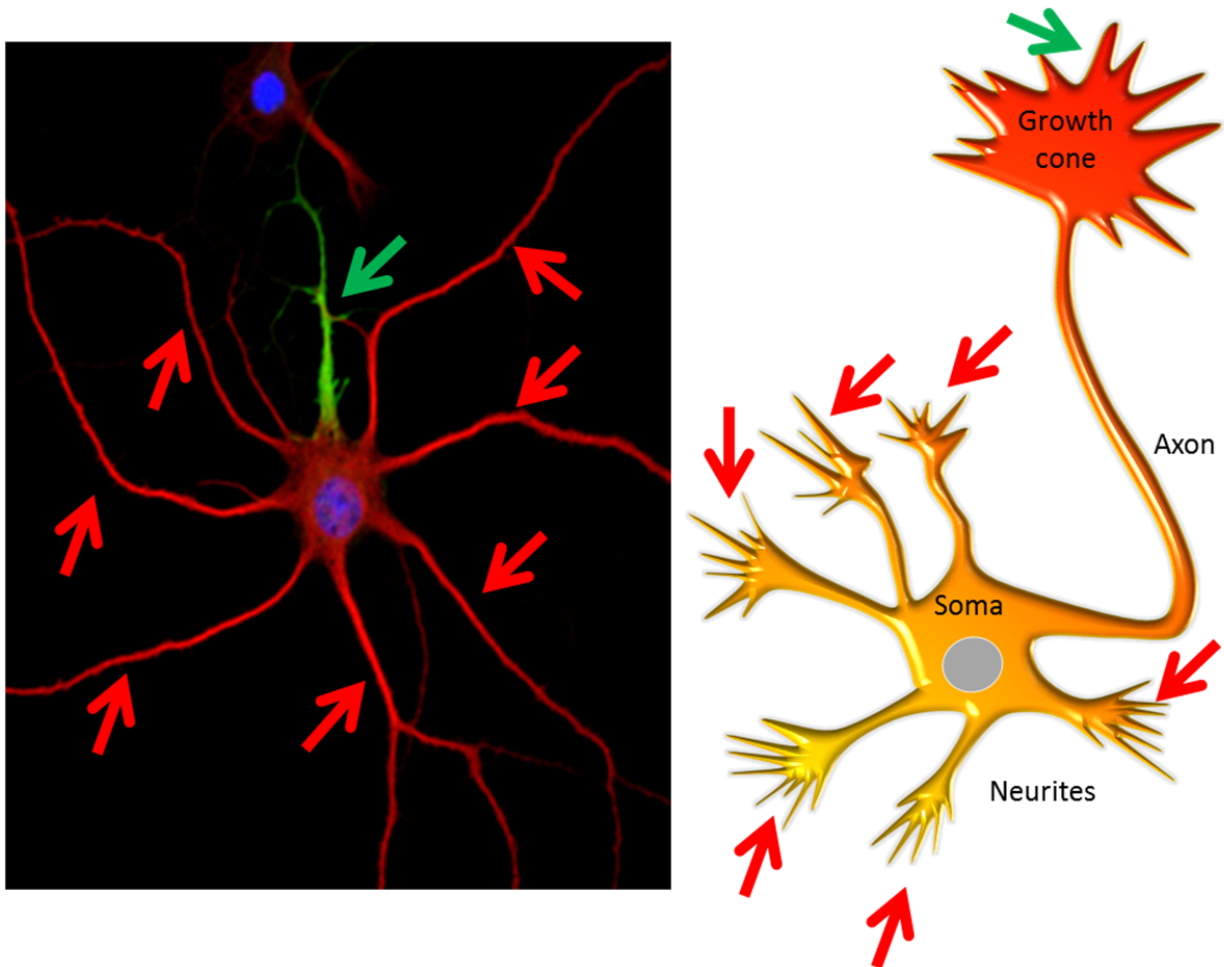


Figure 19: Neurons are polarized cells. In the left panel a picture of a neuron stained with DAPI in blue: nuclear staining, Map2 in red: a marker of dendritic microtubules, and Ankyrin-G in green: a marker of the Axonal Initial Segment, a structure that is located at the beginning of the axon. In the right panel a schematic representation of a growing neuron. Neurons possess a unique long and thin axon (green arrow) and multiple shorter and thicker dendrites (red arrows). Photo from Esther Yeri Hien.

4.1 Growth cone structure

Structurally, the growth cone can be divided in 3 domains, which are classified accordingly to their cytoskeleton composition: a central domain (C), located near to the axon and containing stable, bundled microtubules (MTs); a transition (T) domain enriched in myosin II and F-actin arcs (small actin bundles placed perpendicularly to the MTs); and a peripheral (P) domain filled with long, bundled actin filaments (F-actin bundles) which form the filopodia, as well as with

mesh-like branched F-actin networks which form lamellipodia-like structures, both highly dynamic (Lowery & Van Vactor, 2009) (Fig. 20).

Filopodia are organized in actin bundles presenting a finger-like shape which are able to elongate and retract for probing the environment. As mentioned, filopodia are composed of bundled actin filaments oriented with their fast-growing filament "plus/barbed" end (addition of G actin) toward the tip (Small et al., 1978). Actin polymerization will lead to elongation while actin depolymerization (from the "minus/pointed" end) will lead to retraction. Studies have shown that filopodia can function as points of attachment to the substrate and produce tension that is used for growth cone motility (Lowery & Van Vactor, 2009).

The P zone also is composed of a dense mesh-like branched F-actin network, the lamellipodia, located between these filopodia. As in filopodia, this structure is important for the growth cone environmental exploration and outgrowth.

The T zone of the growth cone contributes to neuronal outgrowth. In this region there is a concentration of actomyosin contractile structures that lie perpendicular to F-actin bundles and form a hemi-circumferential ring. The motor protein Myosin II is concentrated in this T zone and it has been shown that its contractility contributes to the F-actin retrograde flow. Myosin II binds to and exerts compression forces on the F-actin bundles causing their buckling, which can be enhanced by pushing forces due to actin polymerization at the leading edge (Medeiros et al., 2006). This leads to bundle severing near the proximal ends, close to the T domain, a phenomenon that has been proposed to further involve actin filament-severing proteins of the actin-depolymerizing factor (ADF)/cofilin family (Medeiros et al., 2006; Sarmiere & Bamburg, 2004). Interestingly Myosin II has also been shown to be important for severing actin filaments itself in the T zone (Medeiros et al., 2006). The severing process is important as it contributes to the recycling of actin fragments into individual actin subunits which can then be transported back to the periphery to participate in actin polymerization at the leading edge (Zicha et al., 2003).

Schematic representation of the growth cone cytoskeleton structure

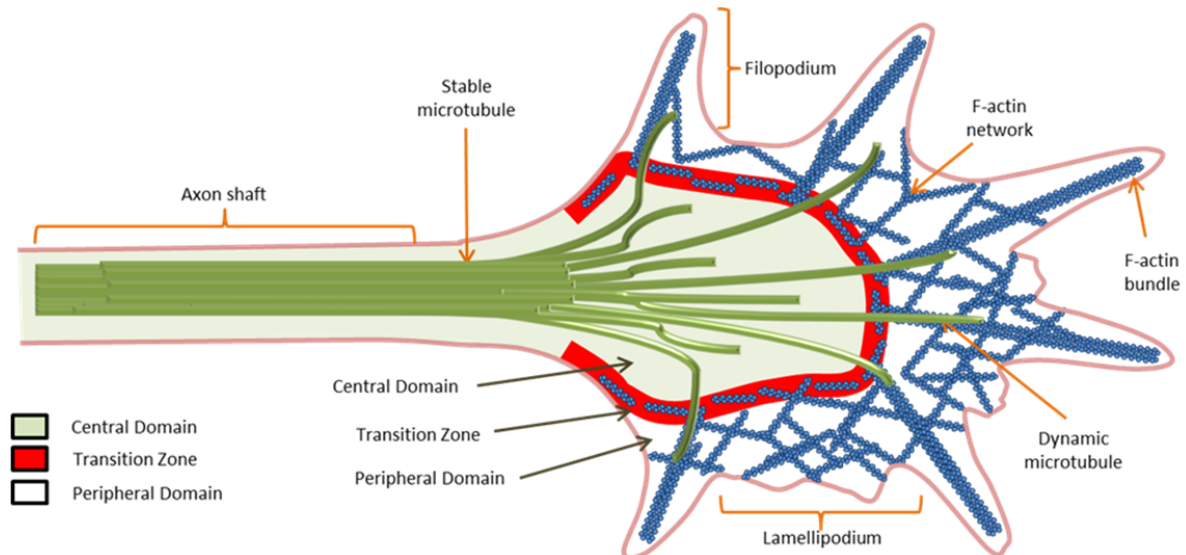


Figure 20: Schematic representation of the cytoskeleton structure of a growth cone. The growth cone can be divided in 3 sub-regions: 1) the central domain filled with bundled microtubules, 2) the transition domain which consists of F-actin arcs and actomyosin contractile structures, and 3) the peripheral domain where F-actin rich structures such as filopodia and lamellipodia protrude.

The C domain is composed of stable, bundled MTs that enter the growth cone from the axon shaft, and of numerous organelles such as vesicles and central actin bundles. The MT bundles also play a role in neuronal outgrowth and growth cone guidance (*see in section 4.4.2: Microtubules dynamics*).

In summary, the growth cone contains different cytoskeleton proteins arranged in different configurations as well as different cytoskeleton regulators and both are placed at specific subdomains of this structure. Their combined action allows growth cones to respond to guidance and adhesive cues. Hence, the correct regulation of cytoskeleton dynamics in growth cones is fundamental for proper growth cone functions. As PCP proteins modulate cytoskeleton dynamics, a role in the control of growth cone motility and behavior can be concluded.

4.2 Stages of axonal outgrowth

In order for axons to outgrow, three stages need to occur: **protrusion**, **engorgement** and **consolidation** (Dent & Gertler, 2003) (Fig. 21).

When a region of a growth cone encounters attractive adhesive substrates, receptors at its membrane will bind to the adhesion proteins present in the substrate. This binding will further activate signaling pathways and also the formation of a molecular clutch that links the

actin cytoskeleton to the substrate. While the growth cone starts to **protrude** towards this adhesive area, the clutch strengthens, leading to a decrease of F-actin retrograde flow speed. The actin is then anchored to the substrate, while F-actin polymerization still continues in front of the clutch site, causing lamellipodia and filopodia in the P domain to move towards the adhesive area and extend the leading edge. When **engorgement** occurs, actin clears of the corridor between the adhesion and the C domain and F-actin arcs reorient from the C domain towards the site of new growth (Suter & Forscher, 2001; Lee & Suter, 2008), ultimately guiding the MTs from the C domain for their invasion into the actin-cleared area. Afterwards, the new C domain **consolidates** while the proximal part of the growth cone compacts at the growth cone neck to form a new segment of axon shaft. Then myosin II-containing arcs compress the MTs in the new C-domain and filopodia retract from the adhesive area as a result of F-actin protrusive activity suppression in this region due to myosin II (Loudon et al., 2006), both promoting the axon shaft consolidation.

4.3 Neuronal outgrowth: the role of adhesion sites

Cell-cell and cell-matrix adhesions are macromolecular complexes that provide a direct linkage between the cell and its external environment, ultimately contributing to tissue morphogenesis and cell migration (Vitriol & Zheng, 2012). Together with secreted cues, adhesion proteins supply an important roadmap for the growth and guidance of axons and dendrites in order to properly form a neural circuitry (Kamiguchi, 2007; Kolodkin & Tessier-Lavigne, 2011; Maness & Schachner, 2007; Myers et al., 2011). In neuronal growth cones, adhesion sites can be composed of different receptors including integrins, cadherins and the immunoglobulin superfamily (IgSF) members. When receptors are activated at the plasma membrane, the intracellular adhesion machinery is recruited to the nascent contact in order to supply the platform needed for chemical and force-based adhesive signaling events (Huttenlocher & Horwitz, 2011).

Explicative model of different stages of axonal outgrowth

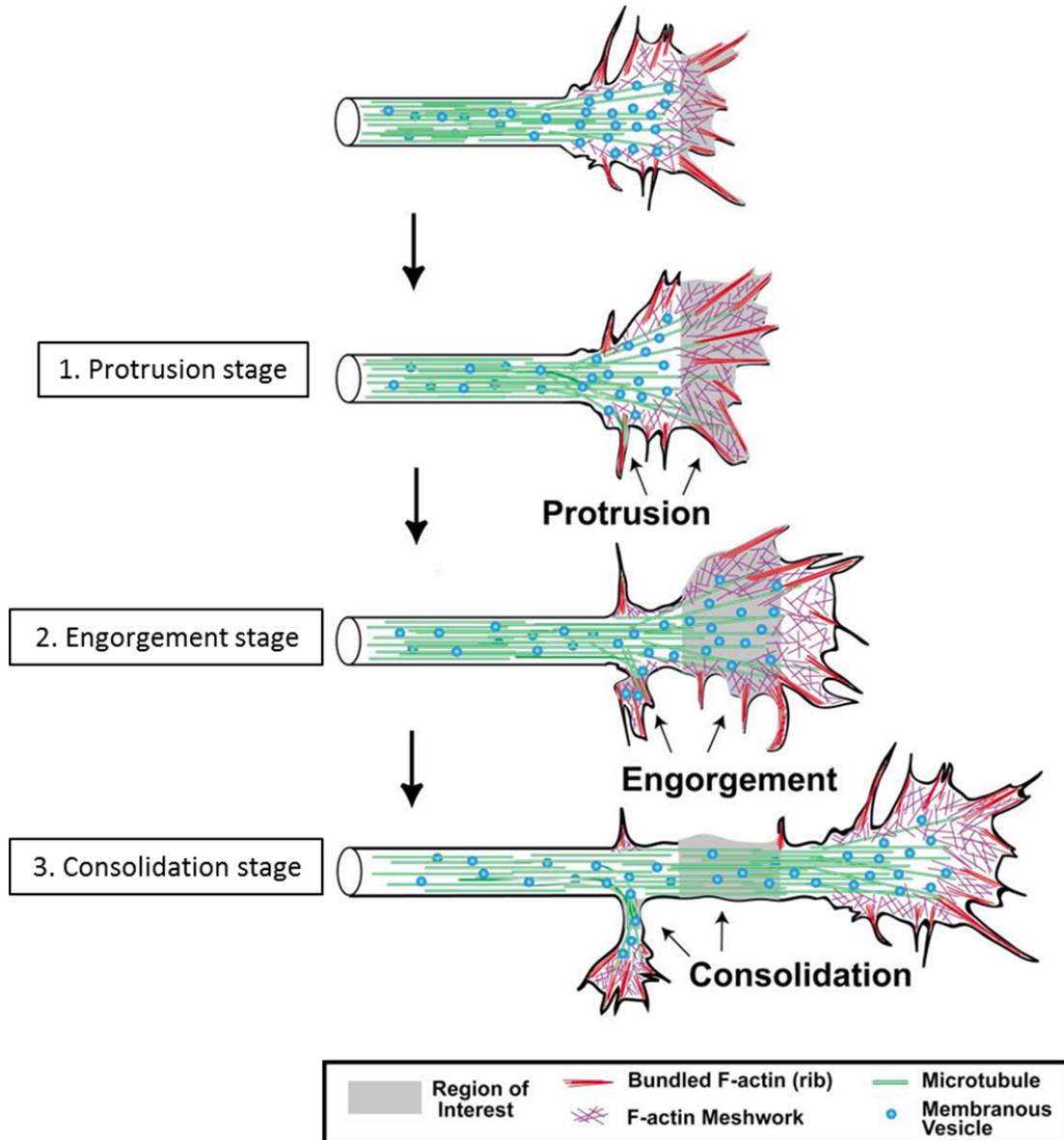


Figure 21: Explicative model of different stages of axonal outgrowth proposed by Dent & Gertler. 1) The first stage of outgrowth is protrusion where filopodia and lamellipodia protrusions are rapidly formed mainly via actin remodeling and polymerization at the edge of the growth cone. 2) As microtubules advance in the protrusion area, they bring membranous vesicles and organelles (mitochondria, endoplasmic reticulum) and engorgement occurs. 3) The last stage, consolidation, occurs when F-actin has depolymerized in the neck growth cone area, leading to a shrinking of the membrane surrounding the microtubules and finally forming a cylindrical axon shaft. From Dent & Gertler, 2003.

Adhesion sites are dynamic complexes which turnover is critical for cell movement (Huttenlocher & Horwitz, 2011). They possess the faculty of assembling and disassembling themselves, change their number, size and position (Myers & Gomez, 2011; Thoumine et al., 2008). One way for cadherins to influence growth cone motility is through the regulation of actin cytoskeleton by acting upstream of cytoskeleton regulators and adhesion components. This regulation is performed in specific growth cones subregions and allows for directed outgrowth. FAK is a good example of an adhesion protein that can induce polar effects in the migrating growth cone (described in the beginning of this chapter). APCAM (a neural cell adhesion molecule (NCAM) ortholog in *Aplysia californica*) is another good example. When APCAM-mediated adhesions are formed in the growth cone there is a local reorganization of actin leading to increased levels of localized actin that assemble at the site of adhesion. This causes a regional slowing of retrograde flow and ultimately growth cone protrusion (Suter & Forscher, 2000; Suter & Forscher, 2001; Lee & Suter, 2008).

Another way for adhesions to influence growth cone motility is through the modulation of the "molecular clutch". This subject will be discussed in more detail further in this chapter but briefly this clutch consists in the coupling between cell adhesions and actin undergoing retrograde flow. Once this molecular clutch is engaged, it will provide the mechanical resistance necessary for the actin network to overcome the actin retrograde flow, finally allowing the plasma membrane to move forward.

Altogether, the formation and dynamics of adhesion sites is important for growth cone motility. Hence, as PCP proteins are involved in the stabilization and endocytosis of adhesion proteins, they might play a crucial role in the control of neuronal outgrowth through the modulation of adhesion dynamics in growth cones.

4.4 Neuronal outgrowth: cytoskeleton dynamics

4.4.1 Actin dynamics

The actin cytoskeleton plays a crucial role in growth cone motility and guidance. Many models that explain the outgrowth of growth cones are based on the combined action of 1/ actin polymerization near the growth cone leading edge with myosin-based actin retrograde flow and with 2/ selective engagement of the "molecular clutch" at adhesion sites (Lowery & Van Vactor, 2009; Suter & Forscher, 1998).

As described previously, actin filaments result from a balance between actin polymerization at the barbed ends and depolymerization at the pointed ends. Interestingly, lamellipodia and filopodia are two-actin based structures but their overall composition is

different. Lamellipodia are formed by a meshwork of short, branched actin filaments that depend on the ARP2/3 nucleation complex, whereas filopodia are supported by long, unbranched actin filaments involving formin family of molecules and regulated by Ena/Vasp proteins (Vitriol & Zheng, 2012).

In both filopodia and lamellipodia, the constant addition and removal of G-actin generates an actin retrograde flow known as actin treadmill that provides the movement necessary to generate forces for growth cone advance (Lin and Forscher, 1993) (Fig. 22A,B). This appears as movement because the F-actin polymer as a whole changes position, but the G-actin monomers within the polymer do not. This retrograde actin flow is a Myosin II motor-driven process, present in the T domain. It continually pulls on the actin filaments until they are compressed in the T domain. As Myosin II continually exert pulling forces, the actin filaments are subjected to greater flexion forces, until these filaments finally break (Medeiros et al., 2006; Burnette et al., 2008). In conclusion, the F-actin retrograde flow is driven both by the push from F-actin polymerization at the leading edge of the growth cone and by the contractility of the motor protein Myosin II.

Capping barbed ends of actin filaments is an important mechanism for the regulation of filament elongation. Capping proteins are able to bind free barbed ends and prevent the addition or loss of actin subunits. Barbed end capping can increase the local amount of G-actin monomers that can be then nucleated by ARP2/3 and in this way promote lamellipodial protrusion (Akin & Mullins, 2008). CapZ is the predominant capping protein in most non-muscle cell types and along with the anti-capping activity of Ena/VASP proteins leads to the formation of actin bundles and filopodia (Kapustina et al., 2010; Mejillano et al., 2004; Vitriol et al., 2007). The Ena/VASP family of actin regulatory proteins acts as anti-capping actin proteins and plays a role in antagonizing actin capping. This function is important as it has been reported that the anticapping activity of Ena/VASP enhances actin polymerization and then is crucial for the initial protrusion phase (Bear et al., 2002). In filopodia ENA-VASP highly concentrates at the tips of filopodia, playing then a crucial role in the protrusive activity of filopodia.

ADF/cofilin is another family of actin-associated proteins which interestingly has been reported to have opposite effects on growth cone motile responses. ADF/cofilin can increase the rate of ADP-actin dissociation from the pointed end of actin filaments to promote depolymerization (Carlier et al., 1997). It can also work as an actin filament-severing protein, producing short filaments for their disassembly (Maciver, 1998). In lamellipodia, ADF/cofilin functions as the rear of the actin meshwork to breakdown actin filaments and recycle actin monomers for further assembly at the leading edge. Interestingly, an opposite effect of ADF/cofilin has also been proposed to occur in lamellipodia: ADF/cofilin severing of actin

filaments can create new barbed ends, which can synergize with actin polymerization factors and altogether promote filament assembly and ultimately membrane protrusion (Kuhn et al., 2000; Pollard et al., 2000). It would seem that these opposite effects are related to local concentrations of ADF/cofilin: at lower concentrations severing and disassembly are more favorable while higher concentrations favor nucleation (Andrianantoandro & Pollard., 2006). ADF/cofilin is highly expressed in the growth cone and colocalizes with F-actin (Bamburg & Bray, 1987) and its overexpression leads to increased neurite outgrowth (Meberg et al., 1998), indicating that actin turnover might promote motility (Bradke & Dotti., 1999). Again, an opposite effect has been discovered for ADF/cofilin in this context, as it has been associated with growth cone collapse (Aizawa et al., 2001; Hsieh et al., 2006; Piper et al., 2006). Interestingly, it has been shown that the local regulation of ADF/cofilin participates in growth cone local responses and consequently in growth cone steering: asymmetric ADF/cofilin inhibition mediates attractive turning whereas local ADF/cofilin activation evokes repulsion (Wen et al., 2007).

The actin cytoskeleton can also be regulated by the Rho-family GTPases which represent a key point in the connection of extracellular signals to regulated actin dynamics (BurrIDGE & Wennerberg, 2004; Hall & Nobes, 2000). As described previously (PCP and Vangl2 chapters), PCP proteins can interact with RhoGTPases to influence actin dynamics. Hence, it is possible to predict that PCP proteins can control actin dynamics in the neuronal growth cone.

4.4.2 *Microtubules (MT) dynamics*

The MT cytoskeleton is important for axonal outgrowth and guidance and it has been determined that its role depends on where these MT are located in the growth cone: if individual MTs are present in the P domain, they act as guidance sensors, if they are present as a bulk in the C domain they will be important for growth cone advance (Gordon-Weeks, 2004). MTs are dynamically instable structures and they can exist in the growth cone as individual MTs, and not only as a bulk. Interestingly, it has been reported that before growth cone protrusion, a population of individual MTs can explore the P domain (Letourneau, 1983). Moreover, if a certain adhesive cue is presented locally to a growth cone, there is an increase in the number of exploratory MTs that will interact with the adhesion site (Lee & Suter, 2008), which is why it has been proposed that these individual MTs might act as guidance sensors.

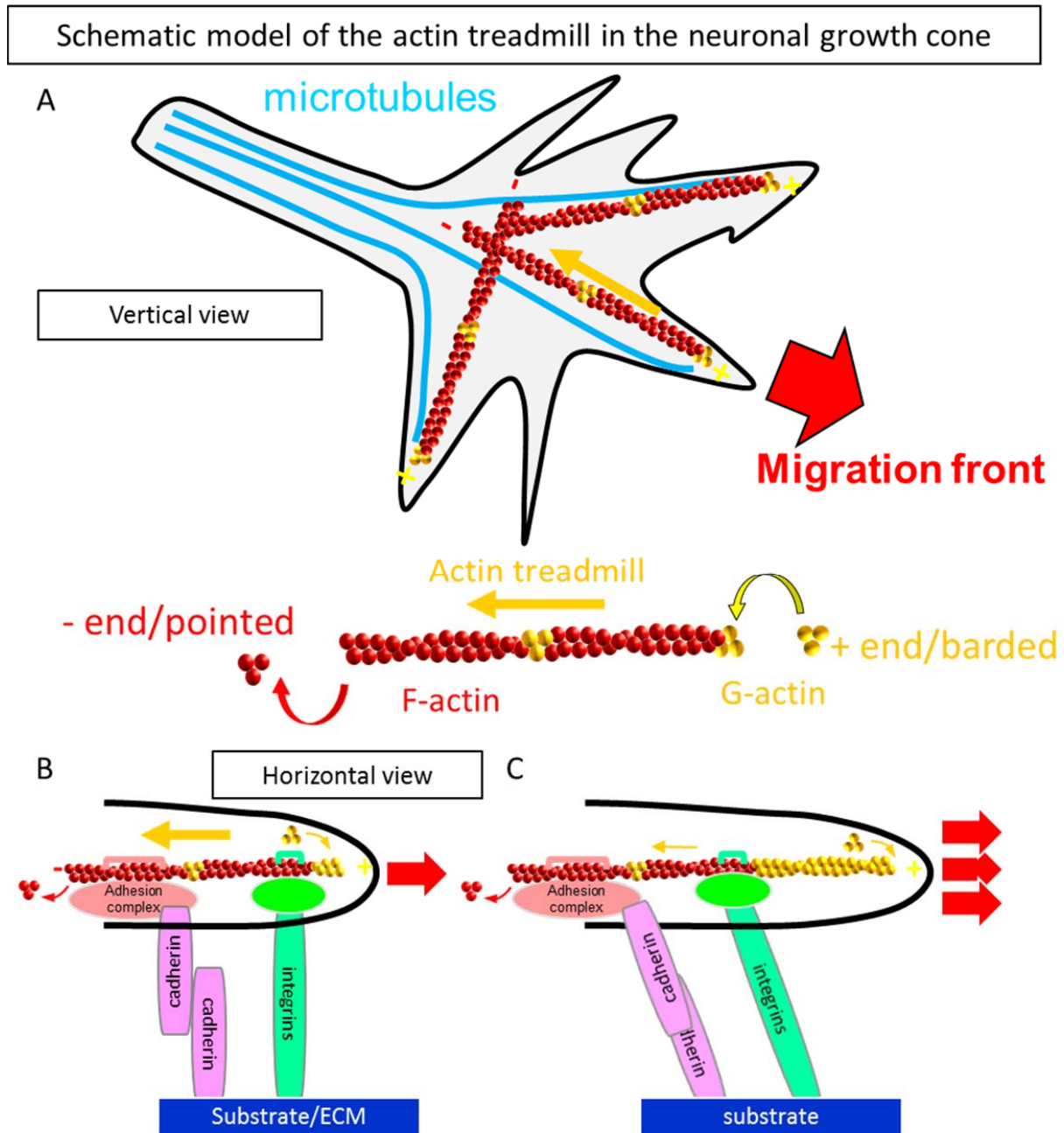


Figure 22: Schematic representation of the actin treadmill in the neuronal growth cone. (A,B) Filopodia and lamellipodia are located at the edge of moving growth cones, also known as the migration front. Filopodia and lamellipodia are constituted by F-actin bundles and meshworks respectively. These F-actin filaments are constantly undergoing actin polymerization at the barbed + end while depolymerization occurs at the pointed – end. This continuous polymerization/depolymerization leads to a phenomenon called actin treadmill. (C) When filopodia encounter adhesive cues, adhesion bounds are created between the substrate and the adhesion proteins at the membrane of filopodia. These adhesion proteins further recruit adhesion complexes that can bind directly or indirectly to the actin cytoskeleton, allowing for the transmission of traction forces from the actin retrograde flowing filaments to the substrate (clutch engaged). As the clutch is engaged, F-actin retrograde flow is reduced while the ongoing polymerization at filopodia tips promotes an inversely increased outgrowth.

In order for MTs to play their roles they need both the participation and interaction with actin (Zhou & Cohan, 2004; Rodriguez et al., 2003). Indeed, it would seem that actin plays a pivotal role in MT function in growth cones as it has been reported that actin can act both as a barrier to premature MT invasion but also as a guide for MTs during their advance (Zhou & Cohan, 2004; Burnette et al., 2007).

MTs frequently explore the peripheral area of growth cones and for that they use the trajectories defined by F-actin bundles (Letourneau et al., 1983) which are thought to guide MT into to the P domain (Zhou & Cohan, 2004). However, recent studies have shown that MT do not need F-actin bundles to advance on F-actin bundles, it is actually the ability to uncouple from these actin bundles that will determine if MT advance in the P domain or not (Burnette et al., 2007). Hence, if MT-actin uncoupling is increased, dynamic MTs can explore the growth cone periphery more frequently.

The role of the C-domain-MTs in growth cone advance/axonal steering however is not related to F-actin bundles as its disruption does not lead to an improper advance of these MTs (Burnette et al., 2007). It seems rather that the function of C-domain-MTs depends on the actin arcs that are included in the T zone, as their disruption impedes MT consolidation during axon outgrowth (Schaefer et al., 2008). Overall, it would seem that as the C domain advances towards an adhesion site, actin arcs accumulate at the sides of the C-domain and act as a barrier by capturing MTs and transporting them into the C-domain (Schaefer et al., 2008).

In summary, MTs in growth cones play a crucial role in the steering of growth cones to allow them to advance in the proper direction and their interaction with the actin cytoskeleton is important for this function. However, many studies employing different models have shown that even when the actin cytoskeleton is disrupted, MTs can still exert an effect on growth cones (Dent and Kalil, 2001; Lafont et al., 1993; Marsh and Letourneau, 1984; Bentley and Toroian-Raymond, 1986; Chien et al., 1993; Kaufmann et al., 1998). In these studies, growth cones were exposed to cytochalasin B, which induces F-actin depolymerization, and all these studies reported that growth cones continued to extend, although they were misdirected. Moreover, another study has shown that depolymerization of MTs eventually results in growth cone retraction (Yamada et al., 1971). Altogether, these studies indicate that MTs also play an important role in axon elongation.

4.4.3 The clutch hypothesis

The "molecular clutch" was proposed in the 1980s with the goal of explaining cell migration through mechanical coupling between the traction forces exerted by the actin cytoskeleton and cellular adhesions (Mitchison and Kirschner, 1988; Suter and Forscher, 1998). The F-actin

retrograde flow (the motor) is crucial in this model. The actin retrograde flow results from a balance between polymerization at the tip of the filopodia/lamellipodia and depolymerization of actin in the T domain. The membrane, which exerts tension on the polymerizing actin filaments, and myosins, which pull these filaments, both contribute to this retrograde flow as explained above (Batchelder et al., 2011; Craig et al., 2012). This flow relates to a stationary treadmill state and alone does not allow for the advance of a cell. To generate movement, the forces generated by the dynamics of actin need to be locally transmitted in a controlled-fashion to their surrounding substrate. This is accomplished *via* adaptor proteins that will promote a dynamic link between adhesion complexes stabilized at the membrane (cadherins, integrins, etc...) with the actin network (Fig. 22C). For example, when N-cadherin adhesions are formed, β -catenin is recruited, which will complex with N-cadherin at adhesion sites. Although it is not clear yet how the coupling between the N-cadherin/ β -catenin complex and α -catenin occurs, it is known that α -catenin is important to couple actin to cadherin-dependent adhesions (described previously in the N-cadherin chapter).

When the link established is strong enough, the retrograde flow is slowed down, and as actin continues to polymerize at the tip of the actin filament, cellular extensions will emerge in this area. Based on this interaction between actin and adhesion, Mitchison & Kirschner (1988) hypothesized that the speed of actin retrograde flow is inversely proportional to neuronal outgrowth. The coupling between adhesion and the cytoskeleton varies between: 1) a coupled state, 2) an uncoupled state, and 3) a "slippage" state. The latter is an intermediary state, with weak linking forces, characterized by transitory connections which are then ruptured (Chan and Odde, 2008; Bard et al., 2008). The switch between these different states can be modulated by mechanical forces. If myosin II activity is disrupted, the actin flow speed decreases while protrusion increases (Lin et al., 1996). This switch can also be controlled by cellular signaling *via* phosphorylations that can modulate the link between different adaptor proteins (Xu et al., 2004). For example, N-cadherin activity on the actin cytoskeleton at adhesion sites can only occur if β -catenin is in dephosphorylated state (β -catenin can only bind to N-cadherin if dephosphorylated).

At the growth cone the molecular clutch will enable the local and temporary coupling between the F-actin retrograde flow (the growth cone motor) and adhesion sites *via* adhesion complexes. The temporary connection of adhesion molecules, located at the membrane level, to the substrate will form a transitory binding complex with the actin filament. The strength generated by the actin flow is then transmitted to the membrane, finally causing the growth cone to advance (reviewed in Thoumine et al., 2008; Giannone et al., 2009). Because adhesion

sites in growth cones are scattered and temporary, any molecule interfering with their location and stability will interfere with neuronal outgrowth.

4.4.4 *Artificial pattern and super-resolution to study neuronal outgrowth*

N-cadherin is a main player in neuronal outgrowth. This effect was first reported by Matsunaga et al, 1988, Bixby and Zhang, 1990 and more recently by Bard and colleagues in 2008. Briefly, neurons cultured on N-cadherin substrates outgrow faster when compared to a regular and chemical poly-L-lysine substrate.

It has been more complicated to attribute an *in vivo* role for N-Cadherin in outgrowth as its mutation perturbs the overall development of the neural plate and leads to death of animals at early developmental stages (Radice et al., 1997; Lele et al., 2002). However, studies in zebrafish showed that a mutation on N-cadherin alleles affected both axonal projections of retina ganglion cells and the neuronal outgrowth of amacrin cells (Masai et al., 2003). Other studies used a dominant negative form of the protein in which the extracellular part is truncated. This truncated form competes with the endogenous N-cadherin for actin binding *via* catenins, and ultimately caused the disorganization of the cadherin/catenin complex (Nieman et al., 1999) and the perturbation in the β -catenin signaling pathway (Zhang et al., 2013). In another experiment, the same mutated form also impeded the formation as well as the elongation of axons and dendrites (Riehl et al., 1996).

In 2008, the lab of Olivier Thoumine demonstrated that N-cadherin can couple to the actin retrograde flow through catenins and that this mechanism is important for growth cone motility and neurite extension (Bard et al., 2008). In this study, neurons were cultured on N-cadherin coated coverslips and displayed an increased number of neurites, and an increased axonal length. This effect was decreased by reducing the levels of catenin, demonstrating the link between the molecular clutch and neuron outgrowth. More recently they showed that this increased neuronal outgrowth was inversely related (as expected) to actin retrograde flow speed (Garcia et al., 2015). In this study they combined spatially controlled adhesion (neurons plated on micropatterned substrates) in growth cones with single-molecule tracking and FRAP experiments. They noticed that N-cadherin/ α -catenin complexes were selectively trapped at N-cadherin micropatterns. A major fraction of actin molecules flowed rearward, making short transient pauses with immobilized N-cadherin/ α -catenin complexes, whereas a small fraction of confined actin molecules contribute to local actin rich environment. This combination of short- and long-lived interactions between the motile actin network and spatially restricted adhesive complexes represents a two-tiered clutch mechanism which would be crucial not only for

dynamic environment sensing but also to provide the necessary forces for growth cone migration.

Interestingly, it has been hypothesized that N-cadherin proteins might play a role through the same mechanism (molecular clutch) at later stages in the developing nervous system, more specifically, in the stabilization of dendritic filopodia and in morphological plasticity (Giannone et al., 2009).

N-cadherin can also promote neuronal outgrowth by activating FGF-receptors. FGF are soluble proteins involved in cellular differentiation and proliferation. It was shown that antibodies directed against FGF-receptors lead to an inhibition of cadherin-dependent neuronal outgrowth (Williams et al., 1994). It would seem that the FGF1 receptor interacts with N-cadherin through their respective extracellular domains, triggering then a signaling cascade of a second messenger that can control neuronal outgrowth (Boscher and Mège, 2008).

5 The hippocampus

5.1 Hippocampal function

In 1957, a famous epileptic patient, Henry Molaison, had a portion of his medial temporal lobe removed, including the hippocampus. This procedure left him unable to store or retrieve new memories and led for the first time to the hypothesis that the hippocampus had a role in explicit memory (Scoville and Milner, 1957). To this day, a large body of evidence has confirmed an essential role for the hippocampus in both storing and retrieving new memories as well as in spatial navigation.

In mammals, the hippocampus is divided into different regions: the subiculum, the dentate gyrus (DG) and the horns of Ammon (CA1, CA2 and CA3). The granular cells and the pyramidal cells constitute the principal cells of the DG and of the CA1/CA3, respectively. The entorhinal cortex (EC) provides the major cortical input to the DG but also CA3 and CA1 directly. The DG projects to the CA3 region via the mossy fiber (Mf) pathway, which in turn projects to the CA1 *via* the Schaffer collateral pathway. Finally, CA1 projects back to the EC, completing the loop. All these circuits constitute the main hippocampal trisynaptic circuitry. It is important to note that CA3 axons, in addition to their projections to CA1, also send collaterals that make synapses onto other CA neurons, which are called recurrent synapses (Knieriem, 2015) (Fig. 23).

5.2 Formation of the hippocampus and the DG/CA3 network

5.2.1 Neurogenesis

Neurogenesis is defined as a process of generating new neurons from neural stem cells (NSCs) or progenitor cells (Jin, 2016) (Fig. 24). During early stages of mammalian brain development, neuro-epithelial (NE) stem cells (one kind of NSCs) proliferate and generate neurons in the embryonic neural tube. After neural tube closure, NSCs are restricted to the ventricular zone, where radial glial cells (RGCs) are the major neural progenitors (Anthony et al., 2004). RGCs have self-renewal ability and can differentiate into neurons and glia (Hartfuss et al., 2001). Although NE cells and RGCs are linked, they present some differences. RGCs are thought to be elongated NE cells due to their morphologies (Alvarez-Buylla et al., 2001); express astroglial markers (glial fibrillary acidic protein (GFAP), astrocyte-specific glutamate transporter (GLAST) and brain-lipid-binding protein (Levitt & Rakic, 1980; Hartfuss et al., 2001; Kriegstein & Gotz, 2003); and their cell fate is restricted compared with NE cells. During the later stages of neurogenesis, the subventricular zone (SVZ) formed by basal progenitors (BPs) emerges outside the ventricular zone (Noctor et al., 2007). BPs can only differentiate symmetrically into two neurons and are limited compared with RGCs. They are the major source of cortical neurons

(Haubensak et al., 2004). During brain development, there is an order in the genesis of cell types: 1) first, neuronal precursors and neurons emerge, 2) glial precursors and astrocytes come next, 3) oligodendrocytes are formed last (McConnell, 1995; Timsit et al., 1995; Rao & Mayer-Proschel, 1997). This phased proliferation and differentiation process clearly demonstrates that neurogenesis and gliogenesis occur at different developmental periods.

Schematic representation of the hippocampal trisynaptic circuit

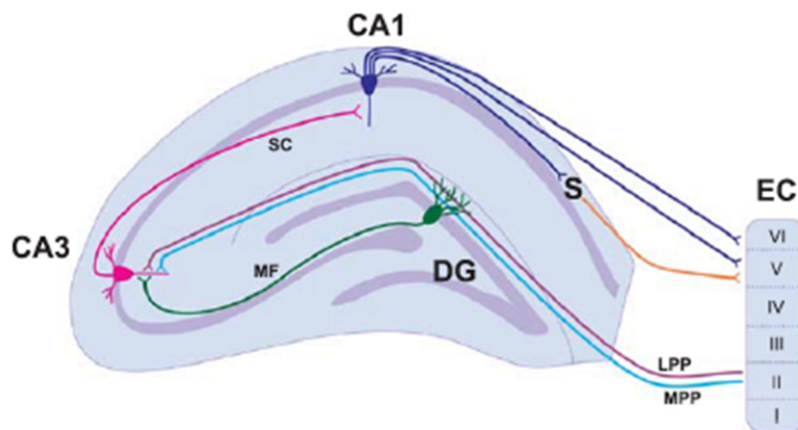


Figure 23: Schematic representation of the hippocampal trisynaptic circuit. The layer II of the entorhinal cortex contacts the granular cells of the dentate gyrus (DG) via the medial (light blue) and lateral (purple) perforant paths (MPP and LPP). The DG projects onto CA3 pyramidal neurons via the Mossy fibre (Mf) pathway (green). CA3 pyramidal neurons further project to the CA1 via the Schaffer collaterals (sc) (pink). Finally, CA1 pyramidal neurons close the circuit by projecting to both the subiculum (S) and the layers V and VI of the entorhinal cortex (EC). From Patten et al, 2015.

Initially there is a proliferation phase that precedes neurogenesis: NE cells undergo symmetric proliferative divisions, which cause a dramatic expansion of the nervous system. Then, during the first phase of neurogenesis, NE cells can either divide symmetrically or asymmetrically to generate respectively two neurons or one NE cell and one neuron (Haubensak et al., 2004; Gotz & Huttner, 2005).

At embryonic day 10 (E10), RGCs originate from NE cells either by direct transformation or by asymmetric division which simultaneously generates neurons (Noctor et al., 2002; Gotz & Huttner, 2005; Kriegstein & Alvarez-Buylla, 2009). Around E14-16 neurogenesis peaks and RGCs predominantly undergo two types of asymmetrical divisions: either a neurogenic division (one RGC, one neuron) or a differentiative division (one RGC, one BP). Interestingly, RGC can divide to generate different types of cells depending on the stage of neurogenesis of the brain: they can divide symmetrically to generate either two BPs during early stages of neurogenesis or two

neurons during later stages of neurogenesis (Zhong & Chia, 2008). Afterwards, BPs migrate into the SVZ and through symmetrical divisions contribute to neurogenesis, each BP generating two neurons or two additional BPs (Noctor et al., 2004). A subpopulation of RGCs is still present at the end of embryonic development which has the faculty to convert into adult SVZ astrocytes and SGZ radial astrocytes.

Interestingly, the hippocampus and the cerebellum are late-developing neuronal structures which only complete formation during the first 2 weeks of postnatal life in the rat (Bayer, 1980; Hauser et al., 2003). At the time of birth, the major part of neurons that constitute the different regions of the brain (including the cortex) have been already generated and the neurons are postmitotic. This is the case for CA3 and CA1 pyramidal neurons or for neurons in the cortex.

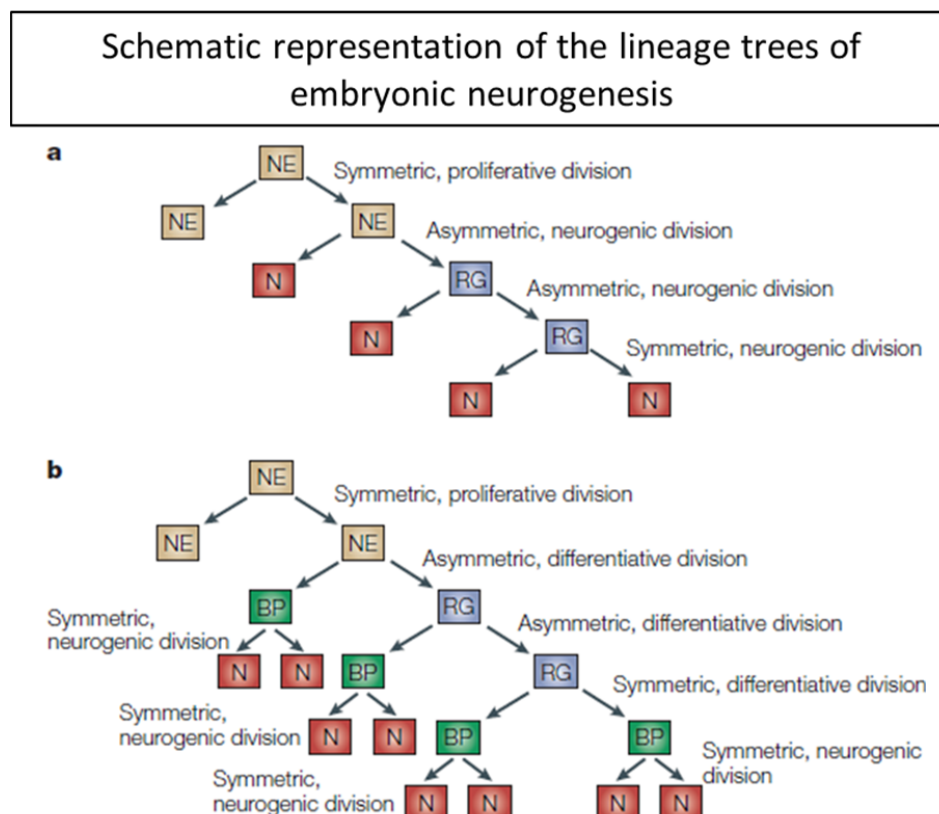


Figure 24: Schematic representation of the lineage trees of embryonic neurogenesis. This scheme demonstrates the kind of cell divisions that occur at each step as well as the relationship between neuroepithelial cells (NE), radial glial cells (RGC) and neurons (N) without (a) or with (b) basal progenitors (BP) as cellular intermediates during neurogenesis. From Götz & Huttner, 2005.

5.2.2 The CA3 mossy fiber/ pyramidal cell network

Each DG granular cell gives rise to a unique non-myelinated axon called Mf (Henze et al., 2000). After exiting the granular layer by P1 (where granular cells are compacted), the Mfs grow thin collaterals that will contact interneurons and mossy cells (excitatory neurons) located in the hilus (Acsady et al., 1998). These mossy cells contact back the granular cells ipsi- and contralaterally. At P3, the main axon of the Mf has already exited the hilus and projects itself in a very thin layer located in the CA3 *stratum lucidum* (*sl*) but they still do not possess presynaptic boutons. Around P7, Mfs make synapses *en passant* and contact CA3 pyramidal cells apically at the proximal zone of their dendrites (Gonzales et al., 2001). Pyramidal cells located in the CA3 region connect basally (not apically) with Mfs, called infrapyramidal Mfs. Besides these two regions, the proximal part of both the apical and basal dendrites, the synapses onto CA3 pyramidal distal dendrites are similar to those found on CA1 pyramidal cells. The complexity of Mf boutons (MfB) increases until P14 and the thorny excrescences (TE) only starts to emerge from the proximal dendrites of CA3 pyramidal neurons at P9. By P21, this synapse is considered mature since only few changes occur until the adult stage (420 days). During maturation, the network complexity increases until a point where each Mf forms around 10 synapses with mossy cells and contacts 11 to 18 CA3 pyramidal neurons (Henze et al., 2000). In the CA3 region, the Mf also contacts inhibitory interneurons via filopodia that emerge from their presynaptic terminal (40 to 50 synapses per Mf). The presynaptic terminal of a Mf can possess as much as 9 filopodia and their length varies throughout development. Each CA3 pyramidal cell receives approximately 50 synapses from Mfs, each of them from a different granular cell (Henze et al., 2000). The number of glutamate-release sites also increases progressively during development, starting with one active zone at P1-3 to several at adult stages (Amaral and Dent, 1981). Altogether, these morphological features demonstrate the elevated complexity of this circuit and its synapses, which might involve complex protein interactions that need to occur precisely in time and space (Fig. 25 A,B).

The molecular mechanisms that induce the restrictive laminar projection of Mfs in the *sl* are dictated by different proteins that can act as guidance cues or adhesion proteins. Plexins and Semaphorins are molecular cues necessary for the entry and guidance of Mfs along the *sl* (Suto et al., 2007). Plexin A2- and A4 constitute the receptors for Semaphorin 6A, a protein that has a repulsive effect. The expression of Plexin-A4 by Mfs allows them to not migrate in the layers where CA3 pyramidal neurons express Semaphorin 6A, meaning outside the SL. The repulsive effect of Semaphorin 6A in the *sl* is attenuated by the expression of Plexin-A2 by pyramidal cells in this region (Suto et al., 2007). Adhesion proteins such as Nectin-1 and -3 have been shown to play a role in the migration of Mfs (Honda et al., 2006) as well as neurotrophic

factors such as BDNF (Tamura et al., 2006; Tamura et al., 2009). Proteins from the cadherin superfamily also participate in the migration of these fibers. A study has shown that both cadherin-8 and N-cadherin are critical for generating the Mf pathway, but that each of them contributes differently to afferent and target differentiation (Bekirov et al., 2008). Cadherin-8 is necessary for Mf fasciculation and targeting while N-cadherin regulates Mf fasciculation but has little impact on axonal growth and targeting. However, N-cadherin is essential for CA3 dendrite arborization, which is not the case of cadherin-8. Another cadherin, the cadherin-9, has been shown to be expressed selectively in DG and CA3 neurons (Williams et al., 2011). The downregulation of cadherin-9 in CA3 neurons leads to a selective decrease in the number and size of DG synapses onto CA3 neurons. Moreover, the *in vivo* deletion of this cadherin on both the DG and CA3 causes striking defects in the formation and differentiation of the MfB/TE synapse. In another study, cadherin-13 (also known as T-cadherin or H-cadherin and a risk factor gene for attention-deficit/hyperactivity disorder - ADHD) has been shown to be expressed by hippocampal interneurons (Rivero et al., 2015). Cadherin-13 is a negative regulator of inhibitory synapses in the hippocampus and the *in vivo* deletion of this protein leads to deficits in learning and memory (classical features of ADHD).

Nikitczuk and colleagues in 2014 also studied the role of N-cadherin in mice *in vivo*. They created a conditional knockout (cKO) mouse line in which N-cadherin is not expressed in postnatal excitatory neurons. Though N-cadherin is no longer expressed in the hippocampus and β -catenin levels are reduced, they reported that the number of excitatory synapses was unchanged and that there was no impact on the number or shape of dendrites or spines, suggesting a compensatory mechanism, probably *via* other cadherins. However, they detected defects in the composition of synaptic complexes: GluA1 and PSD-95 levels were diminished and they also noticed that the loss of N-cadherin at excitatory synapses lead to an increase in the density of markers for inhibitory synapses. At a more integrated level, they reported that adult mutant mice were profoundly impaired in hippocampal-dependent memory for spatial episodes.

Altogether these studies demonstrate the importance of the diversity of cadherin expression in different hippocampal subregions for the proper formation of neuronal circuits and ultimately hippocampal-related mnemonic tasks.

Schematic representation of the morphogenesis of the DG – CA3 circuit

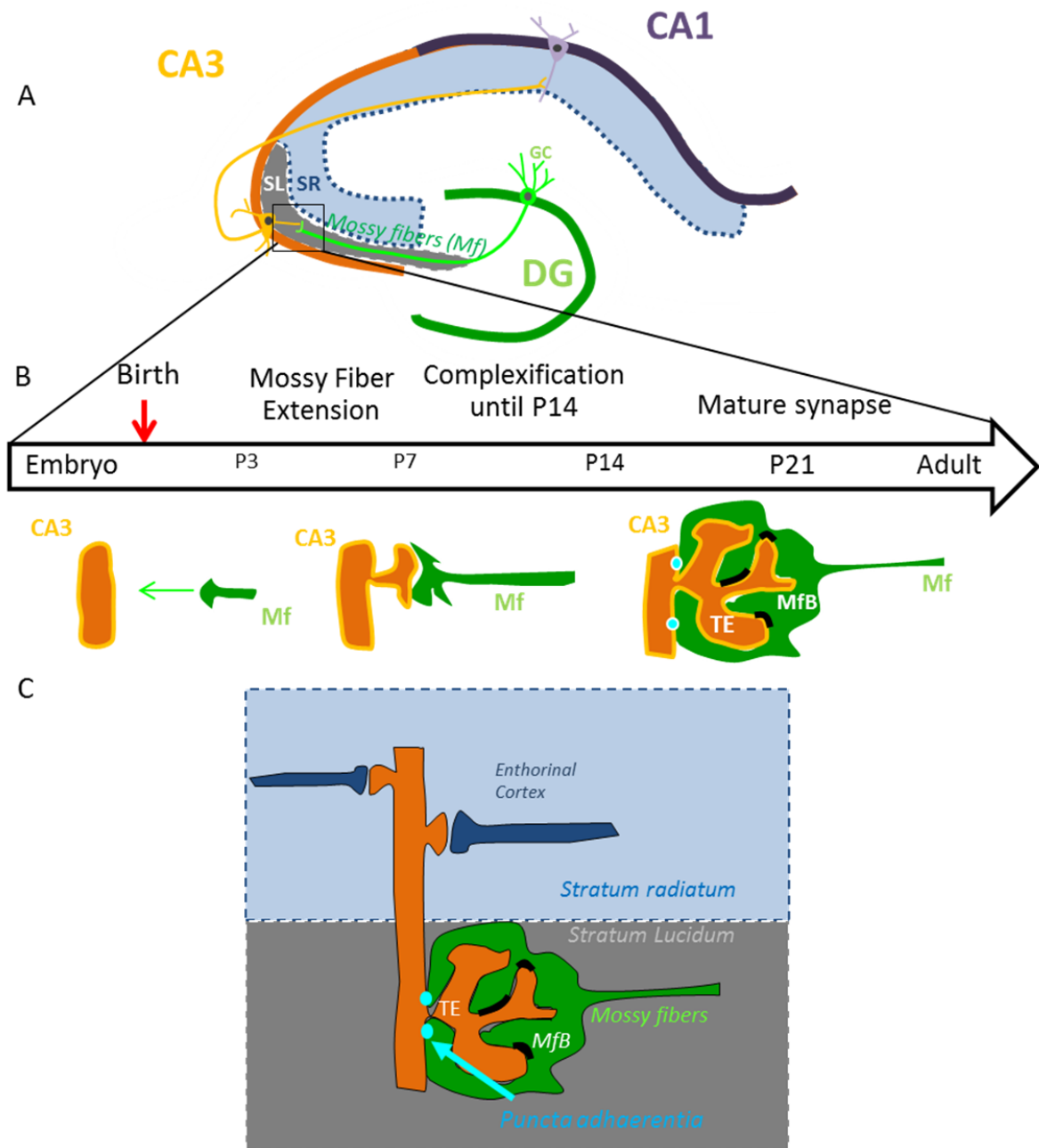


Figure 25: Schematic representation of the morphogenesis of the DG-CA3 circuit. (A,B) By P3, most GC (green cell in A) of the DG (green) have sent projections along the SL (in gray in A) in order to contact CA3 (orange) pyramidal neurons (orange cell in A). At P7, most of these axons, the Mfs, will have contacted their postsynaptic partner. Between P7 and P14 complexes morphological rearrangements occur in a way that the post-synaptic element, now called thorny excrescence (TE) (in orange in B) is completely engulfed by the pre-synaptical element, the Mf bouton (MfB) (in green in B). Morphological and electrophysiological maturation goes on until approximately P21, stage at which this synapse is considered as mature with a TE totally engulfed by a large MfB. These synapses now contain

multiple active zones/post-synaptic densities (black spots in green MfB in B) and the pre and post-synaptic elements are attached to each other *via puncta adherentia* (blue light), junction sites rich in adhesion proteins such as N-cadherin, Netrins and Afadins. (C) This scheme both demonstrates the increased size and morphological complexity of the Mf-TE synapse formed between the DG GCs and CA3 pyramidal neurons in the *stratum lucidum* vs the synaptic contacts performed by entorhinal cortical neurons on the same CA3 pyramidal neurons on another level: the *stratum radiatum*.

5.3 Maturation of the DG mossy fiber/ CA3 pyramidal cell synapse and structural plasticity

Glutamatergic excitatory synapses are asymmetrical structures composed of a presynaptic compartment containing synaptic vesicles and a postsynaptic compartment containing the postsynaptic density (PSD). These two elements are separated by the synaptic cleft. The presynaptic element contains the necessary machinery for neurotransmitter release but also scaffold proteins and signaling proteins that maintain the structure and permit the modulation of glutamate release. In the postsynaptic elements, glutamate receptors are localized in the PSD that is composed of a wide range of proteins such as adhesion proteins, cytoskeleton proteins, scaffold proteins, G proteins or signaling proteins (Sheng & Hoogenraad, 2007). The glutamatergic synapses are preferentially formed through axo-dendritic contact.

MfB/TE synapses are highly different from classical excitatory synapses morphologically. Typically, during synaptogenesis, dendritic filopodia emerge and contact passing by-axons. These filopodia are synapse precursors. Spines have been classified according to their shape as thin, stubby or mushroom (Hering and Sheng, 2001). However, thanks to the development of super-resolution microscopy, these classifications have been under discussion. The work from the laboratory of V. Nagerl suggests: 1) that common categorization schemes of spine morphology is incorrect and indicates that stubby spines are substantially over-reported in the light microscopic literature as a result of limited spatial resolution (Tonnessen et al., 2014), and 2) that it exists a more complicated developmental program for spinogenesis than the commonly held belief that larger, more distinct (“mushroom-like”) spines develop from thin and amorphously shaped (“filopodial”) structures in parallel to their functional maturation (Wijetunge et al. in 2014).

Mfs form large presynaptic boutons (4 to 10 μm diameter) that enfold a postsynaptic structure called TE (Henze et al., 2000). These two elements, the MfB and the TE, are anchored to each other through adherens junctions or *puncta adherentia*. These *puncta adherentia* contain different adhesion proteins such as nectin-1, nectin-3 (Mizoguchi, 2002), afadin (Majima et al., 2009) and N-Cadherin (Takai et al., 2003) (Fig. 25C).

In the adult, this MfB/TE complex turns into an enormous synapse composed of multiple active zones, 25 in average (between 7 and 45 usually), being that all of them face PSDs (Amaral and Dent, 1981; Rollenhagen et al., 2007). The size of these active zones varies between 0.07 and 0.17 μm^2 (0.1 μm^2 in average) and are spaced by 0.45 μm between them (Rollenhagen et al., 2007). Hence, Mfs, with all the invaginations occurring between the pre- and postsynaptic elements, differ not only in size but also in their morphologic complexity. These characteristic complex features indicate that cytoskeleton dynamics and adhesion proteins must be involved and contribute for their increased size (when compared to current synapses) and complexity.

A Mf contains 10 to 15 presynaptic boutons, each of them with a different complexity (Galimberti et al., 2006). Mice that were subjected to an enriched environment present an increase of the number and complexity of the boutons as well as a stabilization of these structures. This phenomenon is dependent of synaptic activity and more precisely of neurotransmitter release from the Mf and Protein Kinase C (PKC) activation. Moreover, these presynaptic boutons often present presynaptic “satellites”. All these satellites display the same features than a presynaptic bouton: they possess filopodia and contact CA3 pyramidal neurons. Interestingly, mice that were kept in an enriched environment presented more of these satellites. It would seem that the enriched environment-related increase in the number of synapses and complexity implies an increase in the expression and release of Wnt7a/b by the CA3 pyramidal neurons (Gogolla et al., 2009). Not all Mf possess satellites and this is due to the topographic specification of the hippocampus which is based on the position of granular cells in the DG and on EphA4 expression (Galimberti et al., 2010). Granular cells that express EphA4 present more than two satellites per bouton. Interestingly, it has been recently shown that epileptic-induced mice possessed presynaptic boutons that were bigger, more complex and with more satellites (Danzer et al., 2010) while the number of dendritic thorny excrescences on CA3 pyramidal neurons is decreased (McAuliffe et al., 2011).

Overall, these studies demonstrate the complex morphology and circuitry formed by Mfs and highlight the importance of their proper formation and maturation for hippocampus-related functions.

5.4 Adult neurogenesis

Along with the SVZ, the hippocampus is one of only a few regions in the adult brain (in rodents) that continues to produce new neurons in what is known as adult neurogenesis (Altman and Das, 1965; Kaplan and Hinds 1977; Cameron et al., 1993; Kuhn et al., 1996; Ernst et al., 2014; reviewed in Kempermaann et al., 2015; Jin et al., 2016). From the most inner part of the DG, the subgranular layer (SGL), type I NSC generate type IIa/type IIb neural progenitor cells (NPC), and

type III neuroblasts that mature into neurons and migrate into the granule cell layer (GCL) (Lazarov & Hollands, 2016). These new DG principal neurons are continuously integrated into a fully functional circuit throughout life. Adult neurogenesis (the maturation of a newly form neuron) has been estimated to take up to seven weeks to be completed and it can be divided into four phases: a precursor cell phase, an early survival phase, a postmitotic maturation and a late survival phase (reviewed in Kempermann et al., 2016). Through the use of different markers and the identification of morphological features, six different milestones were identified. It all starts with a radial glia-like precursor cell, which progresses sequentially into three identifiable progenitor stages associated with high proliferative activity and finally evolves into a postmitotic neuron. This early postmitotic neuron will on its turn pass through a maturation phase, while being integrated in the DG network and will be then considered as a granular cell (Fig. 26).

The precursor cell phase allows for the expansion of cell pools that can differentiate into neurons and glia. When these cells have exited their cell cycle, they have reached the early survival phase. Like a selection filter, most of these newborn neurons die and only a few pass to the next phase: the postmitotic maturation. This phase is associated with the establishment of functional connections, the growth of axons and dendrites and synaptogenesis. The late survival phase represents a period of fine-tuning.

These newly born neurons can account for up to ten percent of the total granule cell population (Imayoshi et al., 2008). The role of these neurons in memory formation is still controversial. Studies have shown that these adult born neurons can modulate signal processing in the DG and that they are specifically required for pattern separation, a highly complex mnesic task (for review, Aimone et al., 2011; Sahay et al., 2011a; Kropff et al., 2015). Through the combination of methods to decrease or enhance neurogenesis with behavioral tasks such as the contextual fear discrimination learning and two-choice spatial discrimination, studies demonstrated that animals with ablated neurogenesis presented deficits in the ability to discriminate between highly similar situations, while animals with increased neurogenesis were better at performing the same task (Clelland et al., 2009; Creer et al., 2010; Sahay et al., 2011b; Kheirbek et al., 2012; Nakashiba et al., 2012; Tronel et al., 2012). Altogether, these studies demonstrate how adult neurogenesis and the integration of newly-born neurons in the already-existing circuit is important for animals to properly perform mnesic tasks.

Schematic representation of neuronal differentiation during adult hippocampal neurogenesis

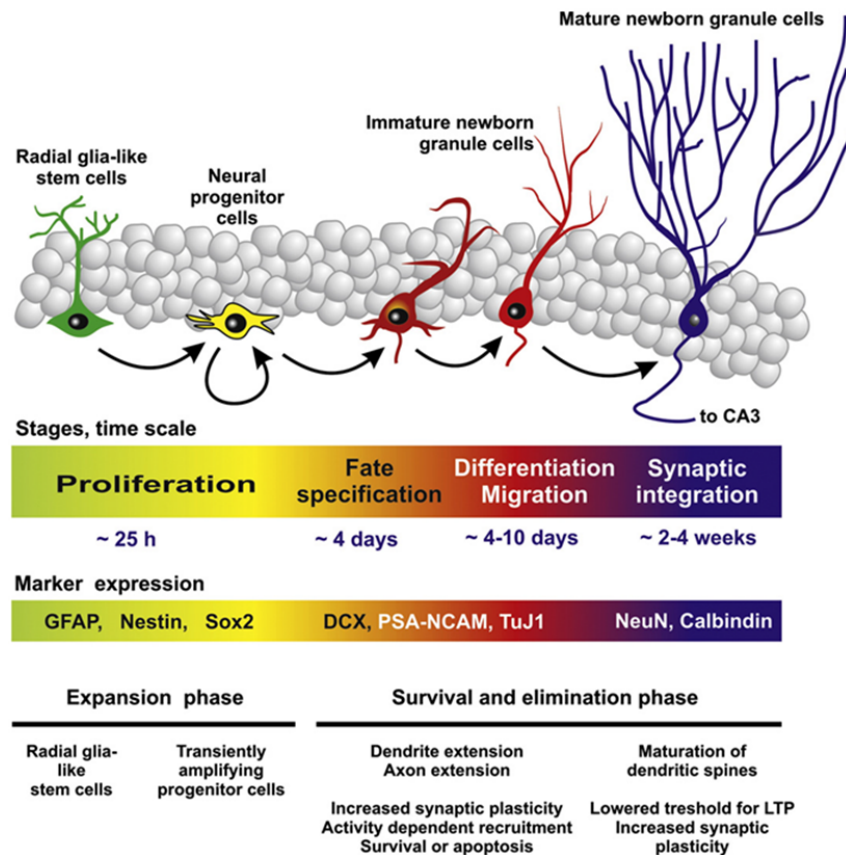


Figure 26: Schematic representation of neuronal differentiation during adult hippocampal neurogenesis. GFAP: glial fibrillary acidic protein; Sox2: sex determining region Y (SRY)-box 2; DCX: doublecortin; PSA-NCAM: polysialylated form of the neural cell adhesion molecule; TuJ1: β -tubulin III; NeuN: neuronal nuclear. Note that Nestin is a marker of neural progenitor cells, DCX is a marker of immature newborn granule cells and NeuN is a marker of mature newborn granule cells. From Lucassen et al, 2010.

5.5 Specific processes strongly dependent on the EC/DG/CA3 network

In humans, the hippocampus is associated to long-term memory, which can be subdivided into declarative and non-declarative memory. Non-declarative memory is mostly composed of procedural memory, the progressive acquisition of skills, their storage and their recall without recalling previous experiences (e.g. playing an instrument, or riding a bicycle). Declarative memory concerns information consciously accessible and that can be verbally expressed. Wixted and Squire showed in 2011 that after damage in the hippocampus, declarative memory impairment occurs. Other structures of the medial temporal lobe participate in the formation of these memories but it is believed that the hippocampus is the most important as this structure

is responsible for encoding the relations between different items of an event (Tsukiura, 2008) and for the reorganization and consolidation of the information during a long period after encoding. Communication between the hippocampus and the neocortex is crucial for declarative memory: at first, the multisensory event/experience leaves a record in the neocortical regions that process the sensed information (coding). The recollection of this event/experience depends on the hippocampus and related structures which are able to reactivate the neocortical regions that encoded this memory. Once the memory is completely consolidated, this reactivation can occur in the neocortex independently of the hippocampus (Wixted & Squire, 2011). As rodents cannot verbally express themselves, the declarative memory is rather called explicit memory in these animals, which is divided into reference and episodic-like memory. Reference memory stands for the acquisition of a unique information over several learning sessions that can be retrieved days or months after (Dudchenko, 2004). In rodents this memory is generally tested via spatial tasks, such as the Morris Water Maze or the Radial Maze which involve a long learning phase and the use of a reinforcer (negative like the water from the Water Maze, or positive like food in the Radial Maze).

The DG is known for its role in explicit memory and spatial navigation. In 2014 Rangel and colleagues showed through *in vivo* electrophysiological that DG cells selectively encode environments that are temporally distinct. Specifically, as the timeline between experiences/contexts was reduced, the proportion of cells with activity selective to a particular context was also reduced, indicating a clear temporal component of DG function. The hippocampus role in spatial navigation has also been well studied. Some CA1 and CA3 pyramidal neurons, called place cells, fire in stereotypic patterns only when an animal moves through a specific region of its environment. This phenomenon is believed to be related to the encoding of a spatial map of that region (O'Keefe & Dostrovsky, 1971, for review, Moser et al., 2008). Such process is not related to a specific topographic organization of place cells: different populations of cells can be recruited for the same environment by different individuals (Redish et al., 2001; Dombeck et al., 2010). Through combination of multiple transgenic animal lines, where specific hippocampal cell populations were affected, with various spatial learning tests including the Barnes maze task and the Morris water maze (MWM) task, experiments have shown the hippocampus does have a role in allocentric spatial mapping (Dupret et al., 2008; Imayoshi et al., 2008; Zhang et al., 2008).

The EC supplies both visual object and spatial information to the DG and CA3 through the perforant pathway. As the hippocampus is at the center of elaborated cognitive tasks such as learning and memory, the integration of contextual information encoded at the cortex into the hippocampus (through the perforant pathway) is important.

Altogether these studies highlight the complex mnemonic functions that are controlled in the hippocampus, which in some measure can be compared to the complexity of the circuitry formed between the Mfs and the CA3. As DG granular cells are continuously generated they are important for the formation of new memories, and their correct integration in the Mf-CA3 circuit is of crucial importance for the realization of complex mnemonic tasks. Hence the proper formation and regulation of this circuit both during development and later in adult stages is essential for proper learning and memory throughout an individual's life.

Chapter II: Results

Manuscript in preparation

Vangl2 inhibits neuronal outgrowth by controlling the interface between actin dynamics and N-cadherin adhesion

Steve Dos-Santos Carvalho^{1,2}, Esther Yeri Hien^{1,2}, Mikael Garcia^{3,4}, Ronan Peyroutou^{1,2}, Cedric Landmann^{1,2}, Nicolas Piguel^{1,2}, Chantal Medina¹, Deborah Anderson⁵, Nathalie Sans^{1,2}, Olivier Thoumine^{3,4*}, Mireille Montcouquiol^{1,2*}

Affiliations:

1 INSERM, Neurocentre Magendie, U1215, F-33077 Bordeaux, France

2 Univ. Bordeaux, Neurocentre Magendie, U1215, F-33077 Bordeaux, France

3 CNRS, Interdisciplinary Institute for Neuroscience, UMR 5297, F-33077 Bordeaux, France

4 Univ. Bordeaux, Interdisciplinary Institute for Neuroscience, UMR 5297, F-33077 Bordeaux, France

5 Institute of Genetic Medicine, University of Newcastle, Centre for Life, Central Parkway, Newcastle upon Tyne, NE1-3BZ, United Kingdom

Contact Information: mireille.montcouquiol@inserm.fr

Summary

Background

Planar cell polarity (PCP) proteins play a crucial role in the control of cytoskeleton dynamics in various cell types, including neurons. Data obtained in both vertebrates and mammals have suggested that Vangl2, one of the most upstream core PCP proteins, participate to tissue morphogenesis through the coordination of adhesion and cytoskeleton proteins dynamics. However, little is known about the role of Vangl2 in neuronal growth cone morphology and motility.

Results

Here we first show that Vangl2, N-cadherin and actin co-distribute in growth cones. Moreover, a spontaneous mutation or conditional deletion of *vangl2* during early brain development leads to increased neuronal outgrowth. This increase in growth cone velocity is only observed when neurons are grown on N-cadherin coated substrates, but not on laminin or poly-L-lysine substrates. By tracking single actin molecules in live growth cones, we demonstrate that the increased axonal outgrowth correlates with a decrease in the actin retrograde flow velocity and the proportion of directed trajectories in *vangl2* cKO neurons. Finally, using FRAP experiments on N-cadherin-GFP in growth cones, we show that the membrane dynamics of N-cadherin is reduced in mutant neurons compared to control counterparts.

Conclusions

Altogether, we propose that *vangl2* deletion increases the lifetime of N-cadherin molecules at the plasma membrane, thereby promoting a stronger engagement of the molecular clutch with the actin network. This consequently reduces the retrograde actin flow speed, resulting in increased neurite outgrowth. Our results demonstrate a role for Vangl2 as a molecular "brake" for neuronal outgrowth, and emphasize the importance of a tight regulation of Vangl2 levels for neuronal motility.

Highlights

- Neuronal outgrowth is increased in the absence of Vangl2
- The increase in growth cone velocity is N-cadherin dependent
- The retrograde actin flow speed is reduced in the absence of Vangl2
- N-cadherin turnover is reduced in the absence of Vangl2

Introduction

Core Planar Cell Polarity (PCP) is a conserved signaling pathway known to regulate actin dynamics and adhesion within a large variety of cell types. PCP is a key molecular pathway involved in the establishment of tissue patterning at both the tissue and individual cell levels (Goodrich, 2008; Ezan & Montcouquiol, 2013; Tissir & Goffinet, 2013; Wallingford, 2012; Walk-Shannon & Hardin, 2014). The original core PCP signaling cascade is composed of three transmembrane proteins called van gogh/strabismus (vang/stbm), flamingo/starry night (fmi/stan), frizzled (fz) and their mammalian orthologs Van gogh-like 1 and 2 (Vangl1/2), Cadherin/EGF/LAG seven-pass G-type receptor 1, 2 and 3 (Celsr1/2/3), Frizzled 1/2/3/6 (Fz1/2/3/6). Together with the three others cytosolic proteins Dishevelled (Dsh/Dvl), Prickle, and Diego (Dgo), and their mammalian orthologs (Dishevelled 1, 2 and 3 (Dvl1/2/3), Prickle 1 and 2 (Pk1/2) and Diversin/Ankrd6), these proteins define a conserved PCP signalling cassette (Klein and Mlodnick, 2004). PCP signaling has multiple roles in the morphogenesis and patterning of epithelial and mesenchymal tissues, although the precise downstream effectors are still ill-defined (Adler, 2012; Sing & Mlodnick, 2012; Wallingford, 2012). In mammals, the nervous system is severely affected by mutation of core PCP genes, with homozygous mice for mutations on *vangl2* or *celsr1* developing *craniorachischisis*, the most severe form of neural tube defect (NTD) with a completely open neural tube, and neonatal lethality of the embryo (Montcouquiol et al., 2003; Curtin et al., 2003; for review see Torban et al, 2012). Such defects have also been observed in single or double knockout mice for genes such as *frizzled3/6* (Wang et al., 2006), *vangl1* and/or *vangl2* (Song et al., 2010), or *dv1* and *dv2* (Hamblet et al., 2002; Wang et al., 2005), or associated partners such as *scrib*, *ror1/2* or *ptk7* (Wansleebe et al., 2010; Gao et al., 2011; Paudyal et al., 2010). The resulting severely disrupted central nervous system (CNS) patterning in these animals has slowed down the identification of specific molecular function of PCP proteins during CNS development. However, the analysis of Fz3 and Celsr3 single mutant mice revealed strikingly similar defects in axonal tract formation, such as in the anterior commissure and thalamocortical and corticothalamic tracts (Wang et al. 2002, 2006; Tissir et al. 2005; Zhou et al. 2008). This represents the clearest cellular function of two core PCP proteins in the mammalian CNS.

Van Gogh like-2 (Vangl2) is a four transmembrane protein, and one of the most upstream components of the core PCP signaling with Fz and Celsr (for a review see Strutt & Strutt, 2009; Torban et al, 2012). In 1949, a spontaneous missense mutation occurred in a mouse strain called Loop-tail (Vangl2^{Lp/Lp}). The gene corresponding to that mutation, later called *vangl2* was only cloned in 2001 (Strong & Hollander, 1949; Kibar et al., 2001). Like all of the core PCP gene mutants, the CNS of these mutants is severely disrupted, due to a decreased stability of the Vangl2^{Lp} protein and a dominant-negative effect of this Vangl2^{Lp} form (Montcouquiol et al., 2006; Deans et al., 2007). The severity of these anatomical defects has prevented the

identification of specific molecular functions of the protein in neurons. However, using *Vangl2*^{Lp/Lp} mice, guidance defects of mesencephalic monoaminergic and spinal commissural fibers were identified (Fenstermaker et al., 2010; Schaffer et al., 2011), while more recent results demonstrated that in double *vangl1/2* transgenic mice, no axonal guidance defects are observed (Qu et al., 2014), contrasting sharply with the deficits observed in *Fz3* and *Celsr3* mutants (Wang et al. 2002, 2006; Tissir et al. 2005; Zhou et al. 2008). Indeed, there is no evidence that all six core PCP genes interact genetically in axonal tract formation (Tissir et al. 2005, 2006). Despite this, *in situ* hybridization experiments show strong expression of the *vangl2* transcript in the forebrain, and notably in the hippocampus (Tissir & Goffinet, 2006).

A common molecular theme in epithelial and mesenchymal tissues is the spatial control of actomyosin activity and adhesion. This makes PCP signaling a strong candidate to control neuronal development, and notably the early motility of neurons. In developing neurons, a constant retrograde flow of actin, resulting from a balance between actin polymerization and depolymerization occurring in the growth cone is key to neurite elongation (Suter & Forscher, 2000). This actin retrograde flow is influenced by many cues like myosins (Medeiros et al., 2006), tensions exerted at the membrane (Batchelder et al., 2011; Craig et al., 2012), or by adhesion molecules or components of the extracellular matrix (Letourneau, 1979; Vitriol & Zheng, 2012). For growth cone movement to occur, the forces generated by the dynamics of actin and myosins need to be locally transmitted in a controlled-fashion to their surrounding substrate (Letourneau, 1979). In 1988 Mitchison and Kirschner suggested that a "molecular clutch" mechanism could explain this transmission. They hypothesized a mechanical coupling between ligand-bound adhesion receptors and the actin flow to allow traction forces to be transmitted to the substrate, resulting in local diminution of the retrograde flow and forward progression. The result is an inverse relationship between the speed of the actin retrograde flow and the strength of the adhesion to the substrate (Lin & Forscher, 1995; Suter & Forscher, 1998; Thoumine, 2008; Lowery & Van Vactor, 2009). For the particular case of cadherin-based adhesion in hippocampal neurons, it was recently shown that a N-cadherin-dependent increase in axonal outgrowth was inversely related to the actin retrograde flow in growth cones (Bard et al., 2008; Garcia et al., 2015).

In this study, we assessed the functional consequences of a deletion of *vangl2* on N-cadherin adhesion and actin dynamics in developing hippocampal neurons. Using *Vangl2* *Looptail* and cKO models, we show that the absence of *Vangl2* in young neurons leads to a N-cadherin dependent increase in growth cone motility. We use live cell single molecule tracking microscopy to show that this increase correlates with a reduced actin retrograde flow velocity. FRAP experiments further suggest that the absence of *vangl2* affects N-cadherin dynamics at the plasma membrane. Our data suggest that *Vangl2* acts as a molecular brake in growth cones,

controlling neuronal outgrowth by modulating the availability of N-cadherin adhesion molecules mediating clutch engagement with the actin network.

Results

Vangl2 and N-cadherin co-localize in neuronal growth cones and filopodia

To evaluate the endogenous expression of Vangl2 in developing neurons, we performed immunofluorescence experiments on cultured hippocampal neurons from control mice with a previously characterized custom-made antibody against Vangl2 (Montcouquiol et al., 2006). Quadruple staining of doublecortin-X (DcX), a marker of growing dendrites and migrating neurons (Burgess & Reiner, 2000), N-cadherin, Vangl2 and phalloidin showed that all three proteins were present in neuronal growth cones (Fig. 1A). Vangl2 and N-cadherin were both enriched in the cell body and the growth cone, notably in filopodia (yellow asterisks) and close to the center of growth cones (T region, red asterisk). We also observed punctate staining along the growing neurite shafts (green arrowhead) (Fig. 1A and Supplemental Information Fig. 1A). In neurons from conditional mutants for *vangl2* (Vangl2^{Emx1} mice, see Methods), the staining of Vangl2 in growth cones was absent (Fig. 1A, red arrowhead), cross-validating the antibody specificity and the efficiency of *vangl2* deletion in the cKO. Some weak non-specific staining, possibly corresponding to Vangl1, remained in the neurites and the cell body (Fig. 1A and Sup. Fig. 1B). Interestingly, the levels of N-cadherin immunostaining was not significantly different between growth cones from control and Vangl2^{Emx1} mice in these conditions, suggesting that Vangl2 does not affect the basal levels of N-cadherin in these structures. Counter staining with phalloidin revealed that the Vangl2 structures and N-cadherin puncta were localized in regions of bright phalloidin staining, suggesting a connection to the F-actin network. We further validated by Western Blot the deletion of *vangl2* in cortex and hippocampi of newborn mice (Sup. Fig. 1C). As expected, since *Emx1* is not expressed by the cerebellum and spinal cord, Vangl2 expression in these control regions remains unaffected but strongly decreased in hippocampus and cortex, of the telencephalon area (Sup. Fig. 1C).

In invertebrate's epithelial cells, Vang accumulates at adherens junctions (AJ), where it co-localizes with adhesion proteins (Classen et al., 2005). We also showed previously that the transmembrane and/or extracellular loops of Vangl2 were implicated in its oligomerization (Belotti et al., 2008), while studies in *Drosophila* support the ability of Vang/Strabismus to interact in *trans* with the extracellular domain of Frizzled receptors allowing a non-autonomous function of the proteins (Wu J & Mlodzik, 2008). This suggests two possible modes for the interaction of cadherins with Vangl2, i.e. a *trans* and a *cis* model. To evaluate the potential interplay between Vangl2 and N-cadherin at nascent cell-cell junctions respectively in *cis* and *trans*, we used a heterologous cell system (COS-7) and co-transfected them with both N-cadherin-GFP and DsRed-Vangl2 (Fig. 1B), or transfected them separately with N-cadherin-GFP or DsRed-Vangl2 before co-culture (Fig. 1C) (see Methods). Shortly after plating, neighboring co-transfected COS-7 cells often exhibit adhesion plaques (AP) (patches of attachment) in regions

of contact (Fig.1B, asterisks), or adherens junction (AJ), bands of attachment (Fig. 1B, arrows). In co-transfected cultures, N-cadherin-GFP and DsRed-Vangl2 were accumulated in these actin-rich AP (Fig. 1B, asterisks), as well as in adherens junction (AJs) (arrows). In co-cultures of COS-7 cells (Fig. 1C) with single transfection of each construct, DsRed-Vangl2 was not enriched in these AP (Fig. 1C, red arrow), while N-cadherin-GFP was still present (asterisks). These results demonstrate that while Vangl2 and N-cadherin strongly accumulate in *cis* at adhesion sites, they do not appear to be able to recruit each other in *trans*. We confirmed in co-cultures of GFP-Vangl2 and DsRed-Vangl2 that the protein were sometimes enriched at AP (Fig.1D, red asterisk), suggesting that Vangl2 is able to interact with itself in *trans* or, through interaction with other proteins, causing its local enrichment.

Absence of *vangl2* has distinct effects on neuronal outgrowth over different substrates.

The accumulation of Vangl2 in young neuronal growth cones together with N-cadherin suggests that it might affect growth cone motility, and neurites extension. To evaluate this hypothesis, we cultured hippocampal neurons from controls and Vangl2^{Emx1} mice on different types of substrates and measured the growth cone average speed at 2DIV. Results showed that after 45 min, Vangl2^{Emx1} growth cones cover a longer distance (Fig. 2A, red dotted line) when compared to controls. Over this distance, the average growth cone speed of Vangl2^{Emx1} neurons was higher ($0.66 \pm 0.06 \mu\text{m}/\text{min}$, $n=24$) when compared to controls ($0.38 \pm 0.03 \mu\text{m}/\text{min}$, $n=28$), and they paused less when compared with controls (control: 7.7 ± 0.4 pauses, $n=17$ vs Vangl2^{Emx1}: 5.8 ± 0.7 pauses, $n=15$) (Fig. 2B,C). Pauses were defined as no movement of the centroid region of growth cones during one minute or more (Fig. 2D). These results suggest that in young neurons Vangl2 acts as brake, inhibiting neuronal outgrowth. To further understand the influence of extracellular cues on growth cone motility, we repeated these experiments with neurons plated either on different substrates including laminin and poly-L-lysine (PLL). We did not find a statistical difference in growth cone displacement between Vangl2^{Emx1} and control neurons either when cultured on laminin ($0.47 \pm 0.03 \mu\text{m}/\text{min}$, $n=32$ for control vs $0.45 \pm 0.03 \mu\text{m}/\text{min}$, $n=40$ for Vangl2^{Emx1}), or on PLL at 1 mg/ml ($0.27 \pm 0.04 \mu\text{m}/\text{min}$, $n=23$ for control vs $0.22 \pm 0.03 \mu\text{m}/\text{min}$, $n=21$ for Vangl2^{Emx1}) or at 10 $\mu\text{g}/\text{ml}$ ($0.17 \pm 0.03 \mu\text{m}/\text{min}$, $n=25$ for control vs $0.15 \pm 0.02 \mu\text{m}/\text{min}$, $n=27$ for Vangl2^{Emx1}) (Fig. 2D,F,G). No difference was observed on laminin substrate in the number of pauses (control: 9.08 ± 0.66 pauses, $n=12$ vs Vangl2^{Emx1}: 9.21 ± 0.59 pauses, $n=14$) (Fig. 2E). Altogether these results show that the enhancement of growth cone velocity caused by *vangl2* deletion is dependent on N-cadherin.

Similar results were obtained using another *vangl2*-deficient mouse model (see Methods), the spontaneous mutation *Looptail* for *vangl2*, which leads to the degradation of the protein (Montcouquiol et al., 2006). In these Vangl2^{Lp/Lp} neurons, we also observed an increase in growth cone speed (Sup. Fig. 2A) and fewer pauses (Sup. Fig. 2C) when compared to wild-type growth cones ($0.60 \pm 0.04 \mu\text{m}/\text{min}$, $n=32$ and 6.8 ± 0.5 pauses, $n=12$ for control vs 0.80 ± 0.06

$\mu\text{m}/\text{min}$, $n=31$ and 5.1 ± 0.6 pauses, $n=12$ for $\text{Vangl2}^{Lp/Lp}$). Similar to $\text{Vangl2}^{\text{Emx1}}$ neurons, we saw no difference on laminin substrate ($0.31 \pm 0.03 \mu\text{m}/\text{min}$, $n=32$ and 8.2 ± 0.6 pauses, $n=21$ for control vs $0.29 \pm 0.02 \mu\text{m}/\text{min}$, $n=48$ and 7.2 ± 0.4 pauses, $n=78$ for $\text{Vangl2}^{Lp/Lp}$), indicating that the increased growth cone displacement is also N-cadherin-dependent in these neurons (Sup. Fig. 2B,D).

Altogether, these results show that the absence or a missense mutation on *vangl2* in young hippocampal neurons both increase growth cone speed and decrease the number of pauses during displacement, and that this behavior is N-cadherin-dependent. This suggests that Vangl2 and N-cadherin may act in concert to regulate growth cone migration.

The absence of Vangl2 decreases the speed of actin retrograde flow

We then hypothesized that the increase in growth cone speed displayed by $\text{Vangl2}^{\text{Emx1}}$ neurons on N-cadherin substrates was correlated to a decrease in actin retrograde flow speed. To test this hypothesis, we tracked individual actin-mEos2 molecules using live single particle tracking combined to PhotoActivation Localization Microscopy (sptPALM) (Manley et al. 2008). We further used Total Internal Reflection Fluorescence (TIRF) illumination to focus on actin molecules localized in a narrow optical section (100 nm) close to the substrate, thus likely to be involved in the coupling to adhesion (Garcia et al. 2015). By choosing a relatively slow camera frame rate (2 Hz), we were able to isolate slowly moving actin-mEos2 molecules incorporated in the filamentous actin fraction, and not fast moving actin monomers. Using dedicated image analysis software, we reconstructed single molecule trajectories and calculated their mean squared displacement (MSD) (Izzedin et al., 2012; Kechkar et al., 2013). The trajectories were then classified as directed, Brownian, or confined, according to the α exponent of a power function used to fit the MSD function over time (Fig. 3A,B, see Methods)(Garcia et al., 2015; Methods this paper).

We observed that on N-cadherin substrates mouse hippocampal neurons had on average 43% of directed trajectories, which is a little lower than what was observed in rat hippocampal growth cones (on average 56%, Garcia et al., 2015) (Fig. 3C,E). When compared to controls ($43 \pm 7\%$, $n=5$), the fraction of directed trajectories recorded in growth cones was reduced by 25% in $\text{Vangl2}^{\text{Emx1}}$ growth cones ($17 \pm 5\%$, $n=8$), while the fraction of Brownian trajectories was not affected (control: $19 \pm 2\%$, $n=5$ vs $\text{Vangl2}^{\text{Emx1}}$: $19 \pm 3\%$, $n=8$) (Fig. 3D,E). On the other hand, the proportion of the confined fraction increased significantly (control: $38 \pm 5\%$, $n=5$ vs $\text{Vangl2}^{\text{Emx1}}$: $64 \pm 6\%$, $n=8$), suggesting that most of the actin-mEos2 molecules tracked in $\text{Vangl2}^{\text{Emx1}}$ growth cones were trapped, possibly at N-cadherin adhesion sites (Fig. 3D,E,F). Next, we calculated the average speed of actin molecules that presented a directed trajectory (Fig. 3G). As expected from the clutch hypothesis, we measured a decrease in the speed of actin retrograde flow in $\text{Vangl2}^{\text{Emx1}}$ cKOs ($0.082 \pm 0.004 \mu\text{m}/\text{sec}$, $n=73$) growth cones when compared with controls

(0.119 ± 0.006 $\mu\text{m}/\text{sec}$, $n=79$). Altogether these results strongly suggest that the absence of Vangl2 in young neurons improves the mechanical coupling between N-cadherin and the actin flow, resulting in a decrease in the retrograde flow and an increase in growth cone progression.

Similar results were obtained when using Vangl2^{Lp/Lp} neurons as the speed of actin retrograde flow (wild-type: 0.149 ± 0.004 $\mu\text{m}/\text{sec}$, $n=5$ vs Vangl2^{Lp/Lp}: 0.101 ± 0.006 $\mu\text{m}/\text{sec}$, $n=11$) and the fraction of directed actin trajectories were both reduced when compared to controls (wild-type: $43 \pm 3\%$, $n=392$ vs Vangl2^{Lp/Lp}: $25 \pm 3\%$, $n=156$) (Sup. Fig. 3A,B). The decrease in actin directed trajectories was again counterbalanced by an increase in confined trajectories (wild-type: $30 \pm 3\%$, $n=5$ vs Vangl2^{Lp/Lp}: $49 \pm 4\%$, $n=11$) while Brownian trajectories remained similar (wild-type: $27 \pm 2\%$, $n=5$ vs Vangl2^{Lp/Lp}: $25 \pm 2\%$, $n=11$) (Sup. Fig. 3B,C). These results further confirm the effect of *vangl2* mutation on local actin dynamics.

To test if Vangl2 could modulate actin polymerization, we compared the ratio of F-actin to G-actin (F/G) in cultured cortical neurons from control and Vangl2^{Emx1} (see Methods). Results show that there was no statistical difference in F/G actin ratio in Vangl2^{Emx1} neurons (ratio = 0.95 ± 0.05) compared to controls (Fig. 3H). These data support the hypothesis that the influence of *vangl2* on neuronal outgrowth is not through a direct regulation of actin polymerization.

Vangl2 regulates N-cadherin dynamics at the membrane

All these results pointed to the hypothesis that Vangl2 is involved in the regulation of N-Cadherin levels and/or dynamics in the growth cone membrane. To test this hypothesis, we used Fluorescence Recovery After Photobleaching (FRAP) in order to measure the turnover of N-cadherin-GFP in moving growth cones, in controls and conditional mutants. We again used TIRF illumination to focus at the ventral surface of growth cones, on membrane N-cadherin engaged in homophilic adhesion with N-cadherin-Fc immobilized on the substrate. After photobleaching, N-cadherin-GFP recovered in two phases (Fig. 4A,B). First, we observed a rapid (initial 20 sec) recovery of around 50 % of the initial fluorescence, likely corresponding to freely diffusing N-cadherin molecules (Garcia et al. 2015). This fraction was similar in growth cones from control and Vangl2^{Emx1} neurons ($50 \pm 2\%$, $n=14$), vs $48 \pm 3\%$, $n=13$), indicating that the absence of Vangl2 has no effect on the basal N-cadherin diffusion in the plasma membrane (Fig. 4B). In control growth cones, the first rapid phase was followed by a slower recovery phase, reaching a value of $68 \pm 3\%$, ($n=14$) at the end of the recording (200 sec) (Fig. 4B). This profile is similar to what was described in rat neurons plated on micropatterned substrates coated with N-cadherin-Fc (Garcia et al., 2015), and reflects the slow turnover of N-cadherin molecules transiently trapped in adhesive interactions. In Vangl2^{Emx1} growth cones the slower recovery phase was reduced by 14% at the end of our recordings (200 sec) when compared to controls ($54 \pm 3\%$, $n=13$), indicating that the adhesive turnover of N-cadherin molecules is slower when Vangl2 is absent (Fig. 4B). In order to analyze more quantitatively the results from FRAP

experiments; data were fit by a diffusion/reaction model (Thoumine et al., 2006; Lambert et al., 2007). This model uses three parameters: the fraction of free receptors, φ (Fig. 4C), the diffusion rate taken from freely moving N-cadherin receptors, k_{diff} (Fig. 4E=D), and the turnover rate of N-cadherin adhesive interactions, k_{reac} (Fig. 4E). There were no significant differences in the fraction of free N-cadherin receptors at the membrane (control: $65 \pm 3 \%$ $n=12$ vs Vangl2^{Emx1}: $63 \pm 3 \%$ $n=13$) and consequently in the fraction of N-cadherin receptors engaged in homophilic bonds (control: 35% $n=12$ vs Vangl2^{Emx1}: 37% $n=13$) (Fig. 4C). Moreover, the diffusion rate of freely moving N-cadherin receptors is also not affected by Vangl2 deletion (control: $22 \pm 3 \text{ min}^{-1}$ $n=12$ vs Vangl2^{Emx1}: $23.18 \pm 3.49 \text{ min}^{-1}$ $n=13$) (Fig. 4D). However, we found a significant difference in the turnover rate of N-cadherin receptors involved in homophilic bonds (control: $0.18 \pm 0.05 \text{ min}^{-1}$ $n=12$ vs Vangl2^{Emx1}: $0.03 \pm 0.01 \text{ min}^{-1}$ $n=13$) (Fig. 4E). These results strongly suggest that the exchange of N-cadherin molecules involved adhesive turnover is reduced in Vangl2^{Emx1} growth cones potentially by an effect on the affinity of cadherin homophilic bonds. Altogether, these results suggest that in absence of vangl2, N-cadherin is more immobilized at the substrate level, and can thus serve as a stable anchor for engagement of a clutch mechanism with the actin flow, which would then promote neuronal growth.

Perspective:

Our data strongly suggest that Vangl2 affects the level of N-cadherin engaged in the clutch mechanism, so that in its absence, more N-cadherin is available. To refine our FRAP data, we want to culture hippocampal neurons on micropatterned coverslip, as used in Garcia et al. (2015). By creating artificial adhesion-like spots, enriched with N-cadherin, we will be able to FRAP N-cadherin-GFP within and outside "adhesion zones", in controls and Vangl2^{Emx1} neurons. We will then be able to compare the role of Vangl2 on N-cadherin stability within and outside an adhesion zone, similar to what Warrington et al. did in drosophila wing cells (2013). In this study, the authors showed that E-cadherin levels were increased at cell-cell junction enriched with Vang, but that at junction with no enrichment E-cadherin levels were unchanged. We also wish to further investigate how Vangl2 affects N-cadherin dynamics when this adhesion molecule is engaged vs when it is not, and for this purpose we will track N-cadherin particles through spt-PALM-TIRF on neurons plated on N-cadherin micropatterns. We will also use the micropatterned coverslip to correlate the enrichment of proteins of the clutch complex on N-cadherin spot in presence/absence of Vangl2 (notably α -catenin).

Finally, using the same micropattern, we want to evaluate if adhesion-like spots, enriched with N-cadherin, will in turn affect Vangl2 motility. For this, we will measure mEOS2-Vangl2 trajectories on micropatterned coverslips with N-cadherin or a variant lacking the extracellular domain.

Another important experiment would be to do acquisition of N-cadherin-GFP in stream mode and in TIRF, in order to rule out the presence of vesicular recycling (endocytosis/exocytosis) in the growth cone.

One of the consequences of a looser regulation of neuronal outgrowth and decreased number of pauses could be a growth cone more error prone. Pauses are necessary for the growth cone to integrate environmental cues. It would be of interest to use a tightly controlled microfluidic system to impose chemotactic gradients, to address the impact of a deletion of *vangl2* on hippocampal axon guidance, to correlate its effect on axonal outgrowth to guidance defects.

Discussion

In this study, using two different transgenic mice, we find that Vangl2 restrains neuronal outgrowth, most likely via the regulation/engagement of N-cadherin at the plasma membrane of young neurons, and the regulation of the actin retrograde flow speed. Our results demonstrate that PCP signaling is important for the motility of young neurons, and most probably participates in the fine-tuning of brain connectivity.

First, we show that Vangl2 is endogenously expressed in young developing hippocampal neurons, and is notably enriched in growth cones and filopodia, where it colocalizes with N-cadherin. We further show that the spontaneous (Vangl2^{Lp}) or conditional (Vangl2^{Emx1}) deletion of *vangl2* lead to an increase in growth cone displacement. In neurons, N-cadherin or integrins affects actin dynamics and growth cone displacement by creating a mechanical coupling between adhesion proteins or molecules of the extracellular matrix and the actin retrograde flow via an adhesive complex (Mitchison and Kirschner, 1988). This "molecular clutch" mechanism, when active, results in traction forces to be transmitted to the substrate, resulting in local diminution of the retrograde flow and forward progression of the growth cone (Fig. 5), and as polymerization continues at the tip of filopodia and lamellipodia, cellular protrusion. The obvious mechanical consequence of such a mechanism is an inversely proportional relationship between the speed of the actin retrograde flow and the strength of the adhesion to the substrate (Lin & Forscher, 1995; Suter & Forscher, 1998; Thoumine, 2008; Lowery & Van Vactor, 2009). Using single-actin particle-tracking, we were able to correlate the observed increased growth cone displacement in both mutants to a decreased actin retrograde flow speed in the peripheral region of growth cones and a reduced number of directed trajectories. These results are consistent with a stronger engagement of cadherins or integrins in the clutch mechanism, and we further show that this increase is N-cadherin-dependent, as we see no effect on PLL or laminin substrates, the latter a known permissive substrate. These results suggest that the slower actin retrograde flow and bigger entrapment of actin molecules is related to abnormally high levels of N-cadherins at the plasma membrane engaged in the molecular clutch, an hypothesis further supported by recent studies showing that increasing concentrations of N-cadherin in the substrate leads to increased outgrowth and decreased actin retrograde flow speed (Garcia et al., 2015). To confirm this hypothesis, we monitored the recovery of N-cadherin-GFP in control and Vangl2^{Emx1} neurons after FRAP. We showed that, in absence of Vangl2, the late phase of fluorescence recovery of N-cadherin-GFP in Vangl2^{Emx1} neurons never reached the same levels as the controls. It has been proposed that this second phase of recovery is related to N-cadherin molecules involved in homophilic bonds at adhesion sites (Garcia et al., 2015).

The interplay between core PCP proteins, cytoskeleton and adhesion molecules has been intensively studied in tissue undergoing intense remodeling, such as zebrafish posterior body formation (Harrington et al., 2007), or the drosophila germband extension (Warrington et al., 2013). In drosophila wing epithelium, Classen and colleagues suggested that PCP signalling controls the assembly/disassembly of adherens junctions by regulating the trafficking of cadherin-containing exocysts vesicles during junction remodeling, and notably that cadherins recycle less efficiently in the absence of PCP proteins (Classens et al., 2005). This hypothesis was confirmed by a more recent study by Warrington et al. demonstrating that core PCP activity promotes E-cad turnover from junctions (Warrington et al., 2013). Moreover, in drosophila epithelium, *vang* (the orthologue to *vangl2* in drosophila) participates in the rearrangement of cell adhesions and is important for the formation of protein clusters at the membrane and for their stabilization at adhesion sites (Strutt et al., 2011). This is of interest as it has been recently shown that cadherin clustering at the membrane is important for the anchoring of cadherins to actin and for cell-cell rearrangement during collective cell migration (Strale et al., 2015). Based on these studies in invertebrates and epithelia, a recent study suggested that Vangl2 directly binds N-cadherin and enhances its internalization in a Rab5-dependent manner in mature neurons (Nagaoka et al., 2014). Using Vangl2^{4p} mutant and shRNA, the authors proposed that Vangl2 regulates N-cadherin surface expression at synapses and that the deletion of *vangl2* leads to decreased spine formation and synaptogenesis in mature neurons (Nagaoka et al., 2014).

For a growth cone to advance, it must not only be able to stick to the substrate but also to dynamically disassemble and reassemble adhesion complexes (Vitriol & Zheng, 2012). Since PCP signaling has the ability of controlling cadherin turnover at junctions and since Vangl2 induces N-cadherin endocytosis, we believe that the deletion of *vangl2* impacts on the turnover of N-cadherin molecules involved in adhesions. As a result, these homophically-bound molecules are less recycled and stabilize at the membrane, ultimately decreasing the turnover of adherens junction. Altogether we propose that Vangl2 regulates the number of N-cadherin molecules engaged in the clutch mechanism, and consequently plays a pivotal role in neuronal outgrowth. This increased outgrowth may have a negative effect on the control of migration of growth cones and consequently their connectivity.

Experimental Procedures

Transgenic mice used in this study

This study was performed according to the European Communities Council Directives (2010/63/EU) with local ethical approval. The *Vangl2* flox transgenic is detailed in Ramsbottom et al. 2014. *Emx1*^{B6.129S2-*Emx1*^{tm1}(cre)Krl/J} (*Emx1*-Cre) stocks were obtained from the Jackson Laboratory (Bar Harbor, ME). The *vangl2* conditional knockout line (cKO) was generated by crossing *vangl2* flox/flox animals with *Emx1*-cre animals (*Vangl2*^{*Emx1*}), effectively deleting full-length *Vangl2* in the telecephalon as early as E10.5 (Gorski et al., 2002). The recombination following the expression of Cre is predicted to produce a premature stop codon that gives rise to an 8 KDa protein, which lacks the four trans-membrane domains and C-terminal domain. The *Vangl2*^{*Emx1*} cKO is detailed in another manuscript (Carvalho et al., in preparation). Looptail (*Vangl2*^{Lp}) mutant mice on the LPT/Le stock were obtained from The Jackson Laboratory (Bar Harbor, ME).

Western Blotting

The cortex, hippocampi, cerebellum and spinal cord from at least three P0/1 mice were dissected, pooled and weighted. A buffer A solution containing TrisHCl 50mM (Gibco) and a mix of proteases inhibitors (Roche) was added to the tissues according to their weight. Samples were homogenized and sonicated and protein concentration was evaluated through BCA analysis (BCA protein Assay Kit from Thermo Scientific). Protein concentration was adjusted for each sample by adding the necessary quantity of buffer A. Samples were diluted with 4X SDS loading buffer containing 5% β -mercaptoethanol, as previously described (Ezan et al., 2013). Proteins were loaded on a 8% acrylamide gels and ran at 125V for 1h30. The proteins are then transferred for 2h30 to a PVDF Immobilon membrane (Millipore). The membranes are saturated with a TBS (25mM Tris, pH7.5 + 137mM NaCl + KCl 3mM + MilliQwater up to 2L) solution containing 8% milk overnight (ON) at 4°C. The following day membranes were rinsed and incubated with a rabbit anti-*Vangl2* (Montcouquiol et al., 2006) and a mouse anti-GAPDH (Millipore) followed by secondary antibodies (donkey anti-rabbit or anti-mouse IgG conjugated to horseradish peroxidase, GE Healthcare UK). The membranes were processed with chemiluminescence (ECL, Thermo Scientific).

cDNA constructs

N-cadherin-GFP used for COS-7 cells immunocytochemistry experiments was a kind gift from Cécile Gauthier-Rouvière (CRBM/CNRS, Montpellier). DsRed-*Vangl2*, was originated by inserting mouse CDS *Vangl2* (Montcouquiol et al., 2006) in a commercially available pDsRed-C1 vector. Actin-mEOS2 and N-cadherin-GFP were previously described (Thoumine et al., MBOC 2006; Garcia et al., PNAS 2015).

Neuronal cell culture and immunofluorescence

Regular 18-mm glass coverslips were incubated for 2 h at 37 °C with 1 mg/ml poly-L-lysine (PLL) in borate buffer, rinsed with H₂O, then incubated 2 hr at 37 °C with 4 µg/cover of goat anti-human Fc (Jackson ImmunoResearch) in 0.2 M boric acid (pH 8.5), before another incubation overnight (ON) at 4°C with 0.2 µg/cover (stp-PALM and FRAP) and 0.6 µg/cover (time-lapse of N-cadherin-Fc). Before use, the coverslips were rinsed again with boric acid 0.2 M. For laminin, coverslips were coated with 1 mg/ml PLL and then laminin ON at 4°C (5µg/cover).

Hippocampal neurons were harvested from P0/P1 Vangl2^{Emx1} or Vangl2^{Lp} and control mice and recovered in a HBSS solution containing antibiotics, trypsin and HEPES. After 14 min incubation at 37°C, hippocampi were rinsed with the medium that will be further used for neuron plating called Plating Medium (PM), which contains: neurobasal medium, B27 supplement (50X, Gibco), 2 mM Glutamine, 0.3 % Glucose, 37.5 mM NaCl and 5% of Fetal Bovine Serum (FBS). This medium was filtered before FBS addition. Another medium (serum free medium – SFM) was prepared with the same ingredients (except for the FBS) which will be used 2 h after neuron plating to dilute the 5 % FBS present in the PM. After PM rinsing, hippocampi were dissociated by gently performing up and down movements with a pipette. After counting (Malassez cell), the required quantity of neurons was centrifuged at 1 rpm, 5 min at room temperature (RT). These neurons were further diluted in 1 ml of PM and plated on the previously prepared coverslips.

For immunocytochemistry experiments approximately 200,000 cells were plated on coverslips treated with 0.1 mg/ml of poly-lysine followed by 2 hr incubation with 1 µg/ml of laminin. After two days, neurons were fixed 10 min with 4 % PFA/sucrose at room temperature, then pre-incubated 30 min in permeabilization buffer (PBS, 10% NGS, 0.1% triton). Cells were then incubated at room temperature (RT) for 1 h with mouse anti-N-cadherin (610921, from BD Transduction Laboratories), rabbit anti-Vangl2 (Montcouquiol et al., 2006), guinea pig anti-Doublecortin-X (AB2253 from Millipore) and Phalloidin Coumarin (P2495, from Sigma). Coverslips were then mounted with Prolong Gold antifade reagent (P36930 from Life Technologies). Fluorescent images of the neurons were obtained using an epifluorescence microscope (Zeiss Imager.Z1), using Axiovision software for image acquisition and further processed with Adobe Photoshop.

Proteins localization in COS-7 cells

COS-7 cells were plated on glass coverslips and cultured in DMEM solution (4.5g/L D-Glucose, 0.11 g/L Sodium Pyruvate, L-Glutamine free, ref #21969-035) with 10 % SVF, 1x Pen/Strep and 1x L-Glutamine (DMEM complete solution). For co-transfection experiments, cells were transfected 24 hr after plating with different constructs (2µg total DNA) diluted in the transfection mix (12.5 µl of CaCl₂ 1M, 100µl of HBS 2X, and H₂O up till 200µl). Cells are

incubated overnight (ON) at 37°C, then rinsed with DMEM and finally cultured in DMEM complete solution. Twenty-four hr after the cells are processed for immunofluorescence. For co-culture experiments, the transfected cells are harvested, mixed 1:1 or 1.5:1.5 ratio, and re-plated on 15 mm coverslips treated with 5 µg/mL PLL for another 24 hr before immunocytochemistry.

For immunofluorescence, the cells were rinsed with PBS and fixed with 4 % PFA 15 min at RT. After permeabilization with PBS/Triton 0,25 %, we blocked non-specific sites for 1 hr at RT with 10 % goat serum in PBS, then incubate with the primary antibodies (chicken anti-GFP, ab13970 from Abcam and rabbit anti-DsRed, 32496 from Clontech) 1 hr at RT. Cells are rinsed with PBS and secondary antibodies are added 40 min at RT (Alexa Invitrogen anti-Rabbit-546, A11011 and Alexa Fluor anti-Chicken-488, 103-545-155 from Jackson ImmunoResearch) with Phalloidin-Atto 647N (65906 from Sigma) with 4,6-Diamidino-2-phenylindole (DAPI) (D1306, Invitrogen). Finally cells are rinsed with PBS and mounted with Fluoromount (17984-25 from Electron Microscopy Sciences).

Video-microscopy

For video-microscopy experiments (neuronal outgrowth), hippocampal neurons from newborn (P0/1) pups were plated at a density of 50,000 cells per coverslip. Coverslips were coated with different substrates, as described above. Neurons were used after 2 days in vitro (DIV2). Images were acquired every 1 min for 45 min using an Orca Flash 4.0 camera (Hamamatsu Photonics, Hamamatsu City, Japan) driven by the MetaMorph software (Molecular Devices, Sunnyvale, USA). Neurons were covered with 1 ml of Tyrode solution (120 NaCl mM, 5 KCl mM, 2 MgCl₂ mM, 2 CaCl₂ mM, 25 mM 4-(2-hydroxyethyl)-1-piperazineethanesulfonic acid, and 30 mM d-glucose, pH 7.4), and observed under the same setup used for sptPALM-TIRF. We used an oil 63x/1.40 N.A objective and differential interference contrast illumination (DIC) on Nikon Eclipse TiE equipped with autofocus and motorized 2D stage. The multi-position recordings were performed with Metamorph Multi-Dimensional Acquisition Module. Temperature was maintained at 37°C. Quantification of neuron growth cone speed was performed using ImageJ software plugin “manual tracking”. Quantification of the number of pauses was performed for neurons that presented a speed of displacement close to the average value for each condition (mean ± SEM).

For Videomicroscopy experiments on Vangl2^{Emx1} neurons and their littermate controls we quantified: 1) **on N-cadherin substrates**: 28 control neurons vs 24 Vangl2^{Emx1} neurons, from 8 different mice and from 3 independent experiments; 32 wild-type neurons vs 31 Vangl2^{Lp/Lp} neurons, from 9 different mice and from 5 independent experiments; 2) **on laminin substrates** 32 control neurons vs 40 Vangl2^{Emx1} neurons, from 6 different mice and from 2 independent experiments. 48 wild-type neurons vs 78 Vangl2^{Lp/Lp} neurons, from 6 different mice and from 3

independent experiments; 3) **on PLL**: at 1mg/ml: 23 control neurons vs 21 Vangl2^{Emx1} neurons, from 6 different mice and from 2 independent experiments; at 10µg/ml: 25 control neurons vs 27 Vangl2^{Emx1} neurons, from 9 different mice and from 2 independent experiments.

Spt-PALM acquisition

The SptPALM experiments were done as described in Garcia et al. (2015). Briefly, hippocampal neurons were electroporated with the Amaxa system (Lonza) (200,000 cells per cuvette) with 4 µg of actin-mEos2 and 1 µg pEGFP-C3, and plated on N-cadherin-Fc-coated coverslips at a density of 100,000 cells per coverslip. Images were acquired on a Nikon Ti Eclipse (Nikon France S.A.S., Champigny-sur-Marne, France) with a TIRF arm and using objective Apo TIRF 100 X oil NA 1.49 and a sensitive Evolve EMCCD camera (Photometrics, Tucson, USA). Photoactivation was done at 405nm, while the images were taken using the laser 561 nm (diode lasers). For actin-mEos2, sequences of 360 images were acquired using 250 msec exposure time and at 2 Hz frequency (1 image every 0.5 sec) in order to visualize long trajectories reflecting the slow movements of actin filaments. Our spt-PALM-TIRF experiments were performed on genetically modified mice while the study to which we refer (Garcia et al., 2015) obtained their results from rat growth cones. There are differences between these two models, mainly growth cone size and the number of actin particles activated by lasers. We had to be more rigorous in defining what we considered to be the peripheral region of the growth cone in order to avoid contamination by actin particles that are located more centrally in the growth cone. Due to the low activation of actin-mEOS2 particles in mice growth cones (when compared to rat), the imaged growth cones present less trajectories than in rat growth cones. For spt-PALM-TIRF experiments were conducted on 6 control neurons vs 10 Vangl2^{Emx1} neurons from 3 independent experiments.

Speed and trajectories analysis

Actin trajectories recorded by spt-PALM were computed and analyzed using custom-made algorithms written as a MetaMorph plug-in as described in Garcia et al. (2015). Single-molecule localization was performed using a wavelet-based algorithm, and trajectories were computed using a simulated annealing algorithm. Trajectories longer than seven frames in regions of interest were reconstructed, and the mean squared displacement (MSD) function was computed over time. To classify actin-mEOS2 trajectories in Control and cKO neurons, individual MSDs were fitted by the power law $4Dt\alpha$ using Kaleidagraph 4.1, where α is a power exponent between 0 and 2. The distribution of α exponents was computed for all trajectories: trajectories with $\alpha < 0.8$ were classified as confined, trajectories with $0.8 < \alpha < 1.2$ were treated as Brownian, and trajectories with $\alpha > 1.2$ were called directed (Garcia et al., 2015). Statistical analyses were carried out using Prism statistical package (GraphPad). Normality of distribution and homogeneity of variance were validated and Statistical significance between means

was calculated using Student's t test or Mann & Whitney Rank Sum Test in the case where normality test failed. $p < 0.05$ was considered significant.

For Vangl2Emx1 trajectories classification, we analyzed 184 different trajectories from control neurons vs 440 in Vangl2Emx1 and for actin flow speed 73 different trajectories from control neurons vs 78 in Vangl2Emx1 were quantified.

For Vangl2Lp/Lp trajectories classification, we analyzed 917 different trajectories from wild-type neurons vs 640 in Vangl2Lp/Lp and for actin flow speed 392 different trajectories from wild-type neurons vs 156 in Vangl2Lp/Lp were quantified.

FRAP

FRAP experiments were done as described in Garcia et al. (2015). Briefly, hippocampal neurons were electroporated with the Amaxa system (Lonza) (200,000 cells per cuvette) with 1 μ g of C-terminally GFP-tagged WT chicken N-cadherin (generous gift from our O. Thoumine) and plated on N-cadherin-Fc-coated coverslips at a density of 100,000 cells per coverslip. Experiments were runned under the same setup used for sptPALM-TIRF. The four-color laser bench (405 nm, 488 nm, 561 nm, and 642 nm; 100mW each) used for sptPALM-TIRF experiments has a second optical fiber output connected to an illumination device containing galvanometric scanning mirrors (iLas; Roper Scientific). Switching between the two fibers for alternating between imaging and bleaching is performed in the millisecond range using a mirror. After acquiring a 10 sec baseline at a frame rate of 1 Hz, rapid photobleaching of the selected region in a growth cone was achieved at higher laser power (50-mW output), during 200-300 msec. Fluorescence recovery was further recorded for 200 sec at a frame rate of 0.5-2 Hz. For FRAP-TIRF experiments were conducted on 14 control neurons vs 13 Vangl2^{Emx1} neurons from 3 independent experiments.

Actin polymerization assay

The amount of F-actin and G-actin was according to the Cytoskeleton Actin Polymerization Assay Kit (BK037, Cytoskeleton) protocol and as previously described (Durand et al., 2012). Cortical and hippocampal neurons from P0 controls and Vangl2^{Emx1} mice were dissociated and plated at a density of 200,000 cells per dish, and stimulated with KCl before harvesting at DIV3. For neurons stimulation, we used 20mM KCl at 37°C for 1 min, then collected the neurons in cold PBS before pelleted them at 3,000 x g for 5 min at 4°C, and stored at -80°C. To separate F-actin (pellet) from G-actin (supernatant) a 1 hr centrifugation at 100.000 x g was performed on the lysate, then the pellet was resuspended in a volume equivalent to the supernatant using F-actin depolymerizing buffer. Actin levels were quantified by immunoblot using an anti-actin antibody (Cytoskeleton). For each condition we pooled 3 petri dishes. The expression levels were determined using a Bio-Rad Quantity One system with a GS800 calibrated densitometer,

and represented as a percentage of control band intensity. We used a total of 8 controls and 8 Vangl2^{Emx1} mice.

Acknowledgments

We thank the «animal and genotyping facilities» members of the Neurocentre Magendie for technical assistance, notably S. Laumond, D. Gonzales and co-workers, the “Biochemistry and Biophysics Facility” of Bordeaux Neurocampus funded by the Labex B.R.A.I.N.

The microscopy was done in the Bordeaux Imaging Center a service unit of the CNRS-INSERM and Bordeaux University, member of the national infrastructure France BioImaging. The help of Christel Poujol, Sébastien Marais and Patrice Mascachi is acknowledged.

This work was supported by INSERM, the University of Bordeaux, Conseil Régional d’Aquitaine (NS/MM), Neurocampus program (MM), ANR MossyPCP ANR-12-BSV4-0016-01 (NS) and the LABEX BRAIN. SDSC is supported by an ENC Neurasmus Ph.D. fellowship. NHP was supported by the Conseil Régional d’Aquitaine/INSERM during his Ph.D. and the FRM “Bourse de soudure” fellowship. The Montcouquiol/Sans & Thoumine labs are members of the Labex B.R.A.I.N.

References

- Ackley, B.D. (2014). Wnt-signaling and planar cell polarity genes regulate axon guidance along the anteroposterior axis in *C. elegans*. *Devel Neurobio* 74, 781–796.
- Bard, L., Boscher, C., Lambert, M., Mège, R.-M., Choquet, D., and Thoumine, O. (2008). A Molecular Clutch between the Actin Flow and N-Cadherin Adhesions Drives Growth Cone Migration. *J. Neurosci.* 28, 5879–5890.
- Batchelder, E.L., Hollopeter, G., Campillo, C., Mezanges, X., Jorgensen, E.M., Nassoy, P., Sens, P., and Plastino, J. (2011). Membrane tension regulates motility by controlling lamellipodium organization. *PNAS* 108, 11429–11434.
- Bekirov, I.H., Nagy, V., Svoronos, A., Huntley, G.W., and Benson, D.L. (2008). Cadherin-8 and N-cadherin differentially regulate pre- and postsynaptic development of the hippocampal mossy fiber pathway. *Hippocampus* 18, 349–363.
- Bixby, J.L., and Zhang, R. (1990). Purified N-cadherin is a potent substrate for the rapid induction of neurite outgrowth. *J Cell Biol* 110, 1253–1260.
- Craig, E.M., Van Goor, D., Forscher, P., and Mogilner, A. (2012). Membrane Tension, Myosin Force, and Actin Turnover Maintain Actin Treadmill in the Nerve Growth Cone. *Biophysical Journal* 102, 1503–1513.
- Gao, F.-B., Kohwi, M., Brenman, J.E., Jan, L.Y., and Jan, Y.N. (2000). Control of Dendritic Field Formation in *Drosophila*: The Roles of Flamingo and Competition between Homologous Neurons. *Neuron* 28, 91–101.
- Garcia, M., Leduc, C., Lagardère, M., Argento, A., Sibarita, J.-B., and Thoumine, O. (2015). Two-tiered coupling between flowing actin and immobilized N-cadherin/catenin complexes in neuronal growth cones. *PNAS* 112, 6997–7002.
- Gorski, J.A., Talley, T., Qiu, M., Puelles, L., Rubenstein, J.L.R., and Jones, K.R. (2002). Cortical Excitatory Neurons and Glia, But Not GABAergic Neurons, Are Produced in the *Emx1*-Expressing Lineage. *J. Neurosci.* 22, 6309–6314.
- Gumbiner, B.M. (2005). Regulation of cadherin-mediated adhesion in morphogenesis. *Nat Rev Mol Cell Biol* 6, 622–634.
- Harrington, M.J., Hong, E., Fasanmi, O., and Brewster, R. (2007). Cadherin-mediated adhesion regulates posterior body formation. *BMC Developmental Biology* 7, 130.
- Izeddin, I. et al. Wavelet analysis for single molecule localization microscopy. *Opt. Express* 20, 2081–2095 (2012).

- Jessen, J.R., Topczewski, J., Bingham, S., Sepich, D.S., Marlow, F., Chandrasekhar, A., and Solnica-Krezel, L. (2002). Zebrafish trilobite identifies new roles for Strabismus in gastrulation and neuronal movements. *Nat Cell Biol* 4, 610–615.
- Kechkar, A., Nair, D., Heilemann, M., Choquet, D. & Sibarita, J. B. Real-time analysis and visualization for single-molecule based super-resolution microscopy. *PLoS ONE* 8, e62918 (2013).
- Keller, R., Shih, J., and Domingo, C. (1992). The patterning and functioning of protrusive activity during convergence and extension of the *Xenopus* organiser. *Development* 116, 81–91.
- Kibar, Z., Vogan, K.J., Groulx, N., Justice, M.J., Underhill, D.A., and Gros, P. (2001a). Ltap, a mammalian homolog of *Drosophila* Strabismus/Van Gogh, is altered in the mouse neural tube mutant Loop-tail. *Nat Genet* 28, 251–255.
- Lake, B.B., and Sokol, S.Y. (2009). Strabismus regulates asymmetric cell divisions and cell fate determination in the mouse brain. *J Cell Biol* 185, 59–66.
- Lee, R.C., Clandinin, T.R., Lee, C.-H., Chen, P.-L., Meinertzhagen, I.A., and Zipursky, S.L. (2003). The protocadherin Flamingo is required for axon target selection in the *Drosophila* visual system. *Nat Neurosci* 6, 557–563.
- Letourneau, P.C. (1979). Cell-substratum adhesion of neurite growth cones, and its role in neurite elongation. *Exp Cell Res* 124, 127–138.
- Lowery, L.A., and Vactor, D.V. (2009). The trip of the tip: understanding the growth cone machinery. *Nat Rev Mol Cell Biol* 10, 332–343.
- Mapp, O.M., Walsh, G.S., Moens, C.B., Tada, M., and Prince, V.E. (2011). Zebrafish Prickle1b mediates facial branchiomotor neuron migration via a farnesylation-dependent nuclear activity. *Development* 138, 2121–2132.
- Manley S, et al. (2008) High-density mapping of single-molecule trajectories with photoactivated localization microscopy. *Nat Methods* 5(2):155–157.
- Matsunaga, M., Hatta, K., Nagafuchi, A., and Takeichi, M. (1988). Guidance of optic nerve fibres by N-cadherin adhesion molecules. *Nature* 334, 62–64.
- Mitchison, T., and Kirschner, M. (1988). Cytoskeletal dynamics and nerve growth. *Neuron* 1, 761–772.
- Montcouquiol, M., Sans, N., Huss, D., Kach, J., Dickman, J.D., Forge, A., Rachel, R.A., Copeland, N.G., Jenkins, N.A., Bogani, D., et al. (2006). Asymmetric Localization of Vangl2 and Fz3 Indicate Novel Mechanisms for Planar Cell Polarity in Mammals. *J. Neurosci.* 26, 5265–5275.
- Nagaoka, T., and Kishi, M. (2016). The planar cell polarity protein Vangl2 is involved in postsynaptic compartmentalization. *Neuroscience Letters* 612, 251–255.

- Nagaoka, T., Inutsuka, A., Begum, K., Hafiz, K. Musabbir bin, and Kishi, M. (2014b). Vangl2 Regulates E-Cadherin in Epithelial Cells. *Scientific Reports* 4, 6940.
- Nagaoka, T., Ohashi, R., Inutsuka, A., Sakai, S., Fujisawa, N., Yokoyama, M., Huang, Y.H., Igarashi, M., and Kishi, M. (2014a). The Wnt/Planar Cell Polarity Pathway Component Vangl2 Induces Synapse Formation through Direct Control of N-Cadherin. *Cell Reports* 6, 916–927.
- Ramsbottom, S.A., Sharma, V., Rhee, H.J., Eley, L., Phillips, H.M., Rigby, H.F., Dean, C., Chaudhry, B., and Henderson, D.J. (2014). Vangl2-regulated polarisation of second heart field-derived cells is required for outflow tract lengthening during cardiac development. *PLoS Genet.* 10, e1004871.
- Rohrschneider, M.R., Elsen, G.E., and Prince, V.E. (2007). Zebrafish Hoxb1a regulates multiple downstream genes including prick1b. *Developmental Biology* 309, 358–372.
- Schafer, S.T., Han, J., Pena, M., Halbach, O. von B. und, Peters, J., and Gage, F.H. (2015). The Wnt Adaptor Protein ATP6AP2 Regulates Multiple Stages of Adult Hippocampal Neurogenesis. *J. Neurosci.* 35, 4983–4998.
- Senti, K.-A., Usui, T., Boucke, K., Greber, U., Uemura, T., and Dickson, B.J. (2003). Flamingo Regulates R8 Axon-Axon and Axon-Target Interactions in the Drosophila Visual System. *Current Biology* 13, 828–832.
- Shih, J., and Keller, R. (1992). Cell motility driving mediolateral intercalation in explants of *Xenopus laevis*. *Development* 116, 901–914.
- Steimel, A., Wong, L., Najarro, E.H., Ackley, B.D., Garriga, G., and Hutter, H. (2010). The Flamingo ortholog FMI-1 controls pioneer-dependent navigation of follower axons in *C. elegans*. *Development* 137, 3663–3673.
- Strale, P.-O., Duchesne, L., Peyret, G., Montel, L., Nguyen, T., Png, E., Tampé, R., Troyanovsky, S., Hénon, S., Ladoux, B., et al. (2015). The formation of ordered nanoclusters controls cadherin anchoring to actin and cell–cell contact fluidity. *J Cell Biol* 210, 333–346.
- Strutt, H., Warrington, S.J., and Strutt, D. (2011). Dynamics of Core Planar Polarity Protein Turnover and Stable Assembly into Discrete Membrane Subdomains. *Developmental Cell* 20, 511–525.
- Suter, D.M., and Forscher, P. (1998). An emerging link between cytoskeletal dynamics and cell adhesion molecules in growth cone guidance. *Current Opinion in Neurobiology* 8, 106–116.
- Suter, D.M., and Forscher, P. (2000). Substrate-cytoskeletal coupling as a mechanism for the regulation of growth cone motility and guidance. *Journal of Neurobiology* 44, 97–113.
- Thoumine, O. (2008). Interplay between adhesion turnover and cytoskeleton dynamics in the control of growth cone migration. *Cell Adhesion & Migration* 2, 263.

- Tissir, F., and Goffinet, A.M. (2006). Expression of planar cell polarity genes during development of the mouse CNS. *European Journal of Neuroscience* 23, 597–607.
- Torban, E., Iliescu, A., and Gros, P. (2012). Chapter Ten - An Expanding Role of Vangl Proteins in Embryonic Development. In *Current Topics in Developmental Biology*, Y. Yang, ed. (Academic Press), pp. 237–261.
- Vitriol, E.A., and Zheng, J.Q. (2012). Growth Cone Travel in Space and Time: the Cellular Ensemble of Cytoskeleton, Adhesion, and Membrane. *Neuron* 73, 1068–1081.
- Wada, H., Iwasaki, M., Sato, T., Masai, I., Nishiwaki, Y., Tanaka, H., Sato, A., Nojima, Y., and Okamoto, H. (2005). Dual roles of zygotic and maternal Scribble1 in neural migration and convergent extension movements in zebrafish embryos. *Development* 132, 2273–2285.
- Wada, H., Tanaka, H., Nakayama, S., Iwasaki, M., and Okamoto, H. (2006). Frizzled3a and Celsr2 function in the neuroepithelium to regulate migration of facial motor neurons in the developing zebrafish hindbrain. *Development* 133, 4749–4759.
- Walsh, G.S., Grant, P.K., Morgan, J.A., and Moens, C.B. (2011). Planar polarity pathway and Nance-Horan syndrome-like 1b have essential cell-autonomous functions in neuronal migration. *Development* 138, 3033–3042.
- Wang, Y., Zhang, J., Mori, S., and Nathans, J. (2006). Axonal Growth and Guidance Defects in Frizzled3 Knock-Out Mice: A Comparison of Diffusion Tensor Magnetic Resonance Imaging, Neurofilament Staining, and Genetically Directed Cell Labeling. *J. Neurosci.* 26, 355–364.
- Williams, B.B., Cantrell, V.A., Mundell, N.A., Bennett, A.C., Quick, R.E., and Jessen, J.R. (2012). VANGL2 regulates membrane trafficking of MMP14 to control cell polarity and migration. *J Cell Sci* 125, 2141–2147.
- Wilson, P., and Keller, R. (1991). Cell rearrangement during gastrulation of *Xenopus*: direct observation of cultured explants. *Development* 112, 289–300.

Figure legends

Figure 1: Vangl2 and N-cadherin co-localize in neuronal growth cones and filopodia, and at cellular junction. (A) We validated the deletion of *vangl2* on DIV2 cultured hippocampal neurons both from control and Vangl2^{Emx1} cKO mice. In controls (top panels), neurites and growth cones labeled by the microtubule-associated protein DCX, Vangl2 is enriched in the growth cones (red asterisk) and notably in filopodia (yellow asterisk), where it co-localizes with N-Cadherin (green) and filamentous actin (Phalloidin, white). Some vesicles labeled for both Vangl2 and N-cadherin are present along the neurite (green arrows). In cKO neurons (bottom panels), most of the staining in neurite and growth cone is absent. Scale bar: 10µm (B) Co-transfection of GFP-N-Cadherin and DsRed-Vangl2 in COS-7 cells shows that both proteins are enriched and co-localize at adhesion contacts (arrow) and plaques (arrow). (C) Co-culture of DsRed-Vangl2 and GFP-Vangl2-transfected cells. Vangl2 accumulates at adhesion plaques and junctions (asterisks) in *cis* (green) but also in *trans* (red). Scale bar: 10 µm (B-C) and 3 µm in zoom boxes.

Figure 2: Deletion of *vangl2* increases growth cone velocity. (A,B) Comparison of the extension of a dendrite (outlined in blue) between control Vangl2^{Emx1} cKO neurons during a 45 min time-lapse recording. The growth cone control covers less distance (red dotted line) than the Vangl2^{Emx1} cKO with an average speed of growth cones displacement almost twice faster (0,66 µm/min, n=24 for Vangl2^{Emx1} and 0,38 µm/min, n=28 for controls). (C) Quantifications of pauses during 45 min of neuronal outgrowth show that Vangl2^{Emx1} growth cones (n=17 neurons) pause less times than control growth cones (n=15 neurons). (D) Graphic showing the cumulated distance covered by control and Vangl2^{Emx1} growth cones. Pauses were defined as no movement of the centroid region of growth cones during one minute or more (blue light arrows). Vangl2^{Emx1} growth cones tend to pause fewer times and for shorter period of time when compared to controls. (E-H) On laminin (n=32 for control and n= 40 for Vangl2^{Emx1}) or PLL substrate at 1 mg/ml (n=23 for control and n= 21 for Vangl2^{Emx1}) or 10 mg/ml (n=25 for control and n= 27 for Vangl2^{Emx1}) we observe no changes in neuronal outgrowth. Scale bar: 1µm. Data are presented as mean ± SEM; *p<0,05; **p<0,01; ***p<0,001

Figure 3: Deletion of *vangl2* decreases actin treadmilling. (A,B) Schematic representations of trajectories according to their α values, as measured in Methods (A), and representation of typical curves obtained for each trajectory type after fitting the MSD values by the power law $4Dt^\alpha$ (B). (C,D) Example of the projection of 3 min recording of actin particles trajectories recorded in a typical growth cone from control (C) and Vangl2^{Emx1} (D) neurons retraced by PALM-TRACER in Metamorph. (E,F) The proportion of directed actin trajectories is decreased in Vangl2^{Emx1} neurons (43% directed trajectories in control neurons vs 17% in Vangl2^{Emx1} neurons;

n=184 trajectories for 5 control neurons and n=440 for 8 Vangl2^{Emx1} neurons). The histogram of distribution according to the α value highlights the increase in values ≥ 1.2 . (G) The measured speed of the actin retrograde flow in Vangl2^{Emx1} neurons is statistically lower (0.082 $\mu\text{m/s}$, from 73 directed trajectories, n=8 neurons) when compared to controls (0.119 $\mu\text{m/s}$, from 79 directed trajectories, n=5 neurons). (H) The F/G actin ratio measured in control (n= 8 cultures from 8 different mice) and Vangl2^{Emx1} (n= 8 cultures from 8 different mice) cortical neurons is not different at DIV3, suggesting no major actin polymerization deficits. Data are presented as mean \pm SEM; *p<0,05; **p<0,01; ***p<0,001

Figure 4: GFP-N-cadherin turnover is reduced in absence of Vangl2. (A) Representative images of the recovery of GFP-N-cadherin observed by TIRF illumination in growth cones from controls (upper panels) and Vangl2^{Emx1} (lower panels) neurons during a 200 sec recovery. The growth cones were photobleached in the selected area with a $\sim 300\text{ms}$ laser pulse at 0 sec, and the fluorescence recovery was recorded during the following 200s (color coding). (B) Mean FRAP curves of GFP-N-cadherin fluorescence recovery over time containing individual data points with \pm SEM for each experiment. In absence of *vangl2* expression, the initial recovery is similar to control but the total recovery is statistically lower (n=14 control growth cones vs n=13 Vangl2^{Emx1} growth cone from 3 different experiments). The solid line represents the fit made by the diffusion-reaction model previously described in Thoumine et al, 2006 and in Lambert et al, 2007. (C) Quantification of the GFP-N-cadherin fraction freely moving at the membrane shows no difference between control (65 %, n=12) and Vangl2^{Emx1} (63 %, n=13) growth cones. (D) Quantification of the diffusion rate of GFP-N-cadherin molecules freely moving at the membrane shows no difference between control (22 min^{-1} , n=12) and Vangl2^{Emx1} (23 min^{-1} , n=13) growth cones. (E) Quantification of the turnover rate of GFP-N-cadherin molecules involved in homophilic bonds at the membrane shows that the protein turnover is reduced by approximately 17% in Vangl2^{Emx1} (0.03 min^{-1} , n=13) growth cones when compared to controls (0.18 min^{-1} , n=12). Data are presented as mean \pm SEM; *p<0,05; **p<0,01; ***p<0,001

Figure 5: Vangl2 inhibits neuronal outgrowth by regulating N-Cadherin engagement in the clutch mechanism. (A) The actin retrograde flow is generated by constant polymerization (at the tip of filopodia) and depolymerization (at the base) of actin monomers along a filamentous filament (F-actin), and participates to the extension and retraction of filopodia. (B) When permissive substrates such as N-cadherin or laminin are present in the environment they bind to cell surface receptors at the plasma membrane, which recruit specific adhesion complexes, creating a molecular link between the adhesion proteins and the F-actin filaments within the growth cone. This “molecular clutch”, leads to the local entrapment of actin retrograde flow, finally causing a decrease in its speed and a proportional increased in neuronal outgrowth (due to the ongoing actin polymerization at the tip of filopodia). If no permissive substrate is present

(PLL), the link is absent, and the outgrowth is slow, while the retrograde flow is fast. (C) The absence of Vangl2 leads to an increased presence/stabilization of N-cadherin at the plasma membrane, and the engagement of more N-cadherin molecules which in its turn increases the molecular clutch strength. As a result, a decreased actin retrograde flow speed and an increased neuronal outgrowth is observed.

Supplemental Figure 1: Vangl2 and N-cadherin co-localize in neuronal growth cones and fillopodia. (A-B) Low magnification of Figure 1, showing DCx, N-cadherin and Vangl2 staining in DIV2 cultured neurons from control and Vangl2^{Emx1} mice (red arrowhead). (C) Validation of the deletion of Vangl2 in various tissues by Western Blot. We isolated the cortex, hippocampi, cerebellum and spinal cord of P0/P1 control and Vangl2^{Emx1} mice and validated the absence of expression of Vangl2 in brain regions expressing the Cre recombinase (Cre) under the Emx1 promoter, the cortex and the hippocampus, and the presence of Vangl2 in tissues not expressing the Cre, the cerebellum and the spinal cord. Scale bar: 10µm.

Supplemental Figure 2: Looptail mutation increases growth cone velocity

(A) Results show that in Vangl2^{Lp/Lp} mice the speed of growth cones displacement is increased (0,80 µm/min, n=32) compared to controls (0,60 µm/min, n=31 growth cones). (B) No difference is detectable when neurons migrate on laminin substrates (control: 0,31 µm/min, n=48 growth cones vs Vangl2^{Lp/Lp}: 0,29µm/min, n=78 growth cones). (C,D) Quantifications of pauses during neuronal outgrowth show that Vangl2^{Lp/Lp} growth cones pause less (5,1 pauses, n=25 growth cones) than control growth cones (6,8 pauses, n=12 growth cones) but not on laminin. Data are presented as mean ± SEM; *p<0,05; **p<0,01; ***p<0,001.

Supplemental Figure 3: Looptail mutation decreases actin treadmill

(A,B) The proportion of directed actin trajectories is decreased in Vangl2^{Lp/Lp} neurons (43% directed trajectories in wild-type neurons vs 25% in Vangl2^{Lp/Lp} neurons; n=5 neurons for wild-type and n=11 for Vangl2^{Emx1} neurons). The histogram of distribution according to the α value highlights the increase in values ≥ 1.2. (C) The measured speed of the actin retrograde flow in Vangl2^{Lp/Lp} neurons is statistically lower (0.101 um/s, from 156 directed trajectories, n=11 neurons) when compared to wild-type (0,149 um/s, from 392 directed trajectories, n=5 neurons). Data are presented as mean ± SEM; **p<0,01; ***p<0,001

Supplemental Figure 4: N-cadherin micropatterned substrates

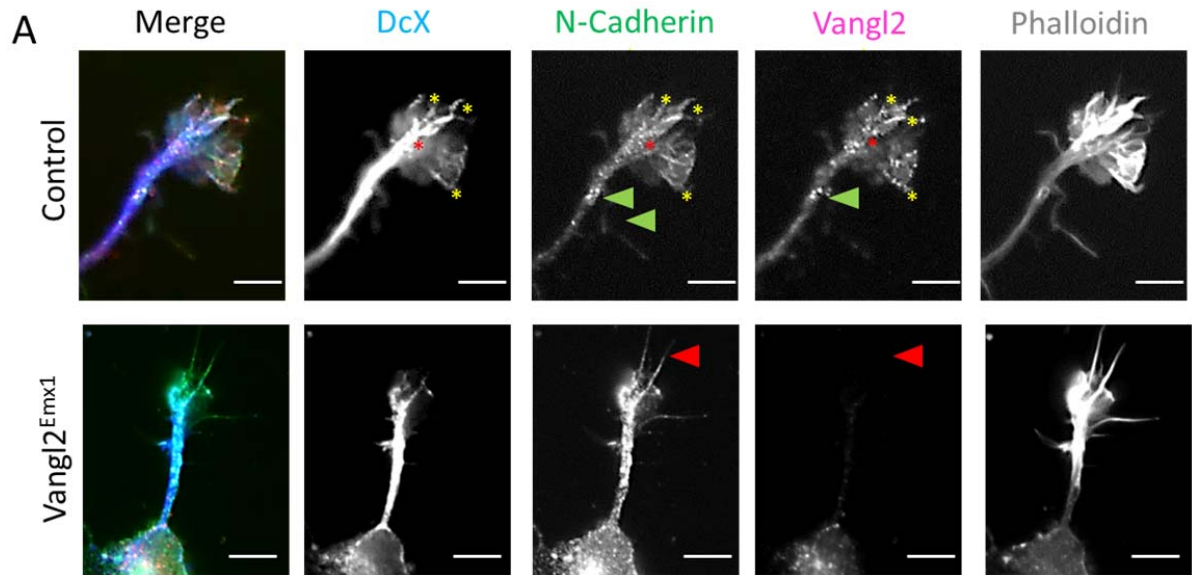
(A) Low magnification of an example of a micropatterned N-cadherin substrate on which hippocampal neurons (in red) were cultured. N-cadherin substrate should only be present in blue spots. (B) High magnification of another example of a micropatterned N-cadherin substrate on which hippocampal neurons (in green) were cultured. In both A and B it is possible to observe

that neurite projections preferentially follow these patterns and avoid the extracellular space between these dots.

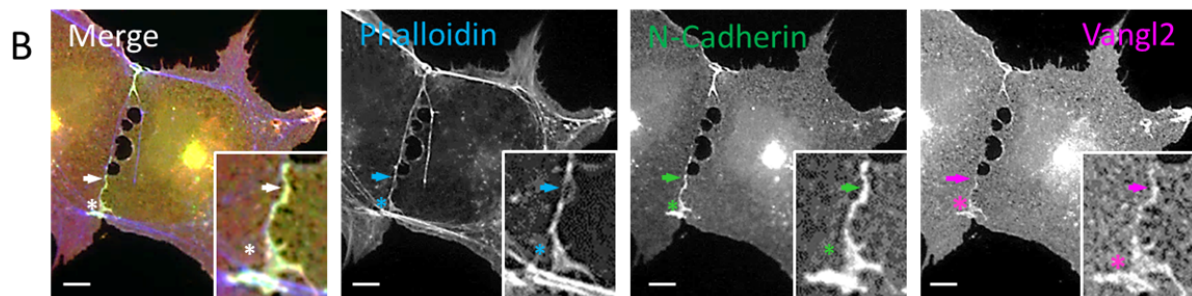
Figures

Figure 1

DIV2 mouse hippocampal neurons



COS7 co-transfected with N-Cadherin-GFP & DsRed-Vangl2



Co-culture of GFP-Vangl2 COS7 cells with DsRed-Vangl2 COS7 cells

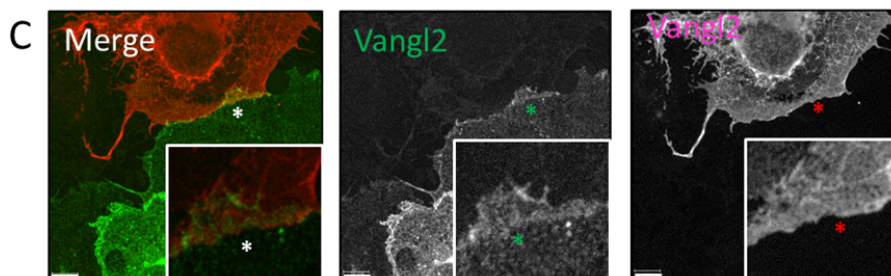


Figure 2

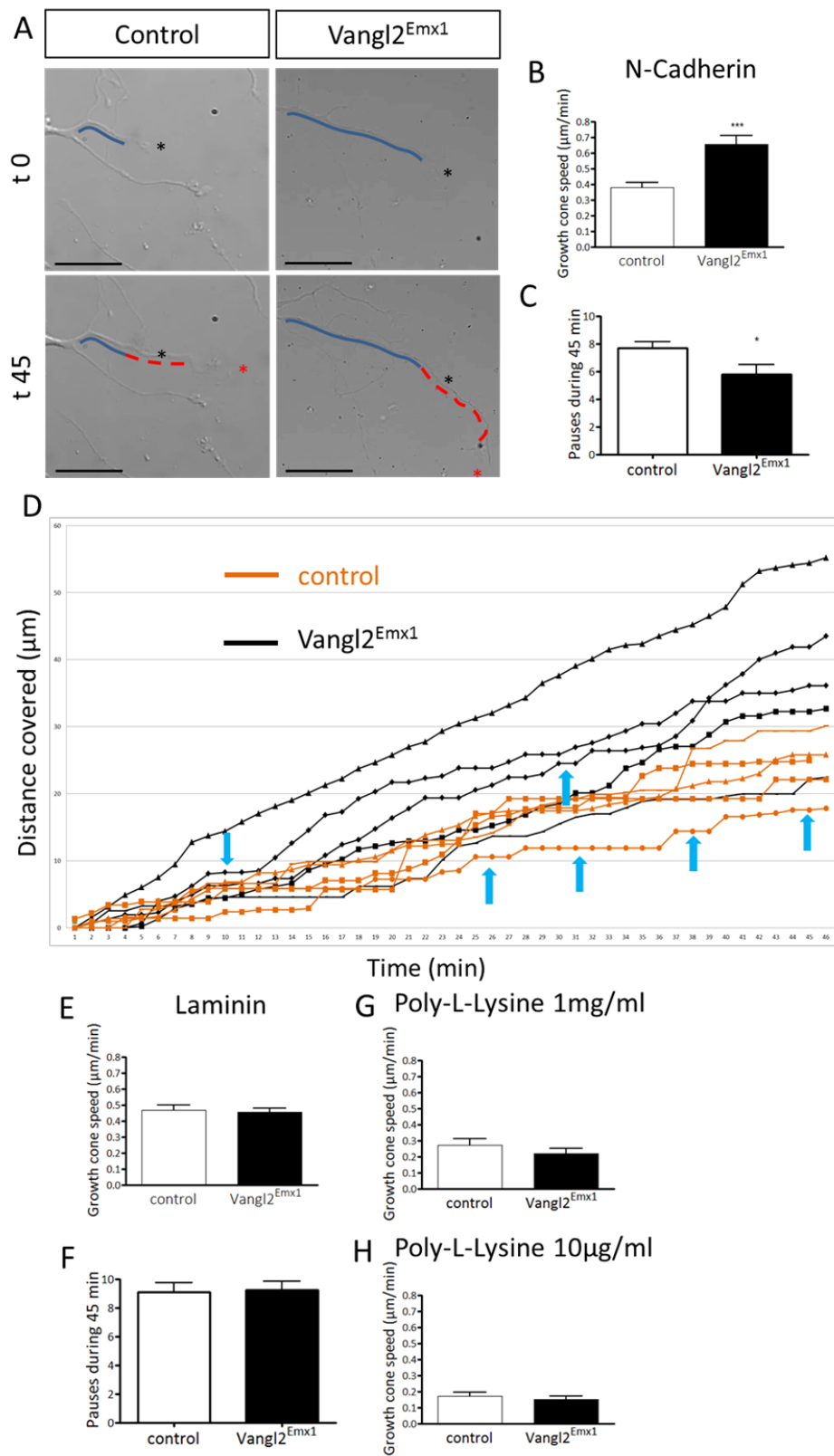


Figure 3

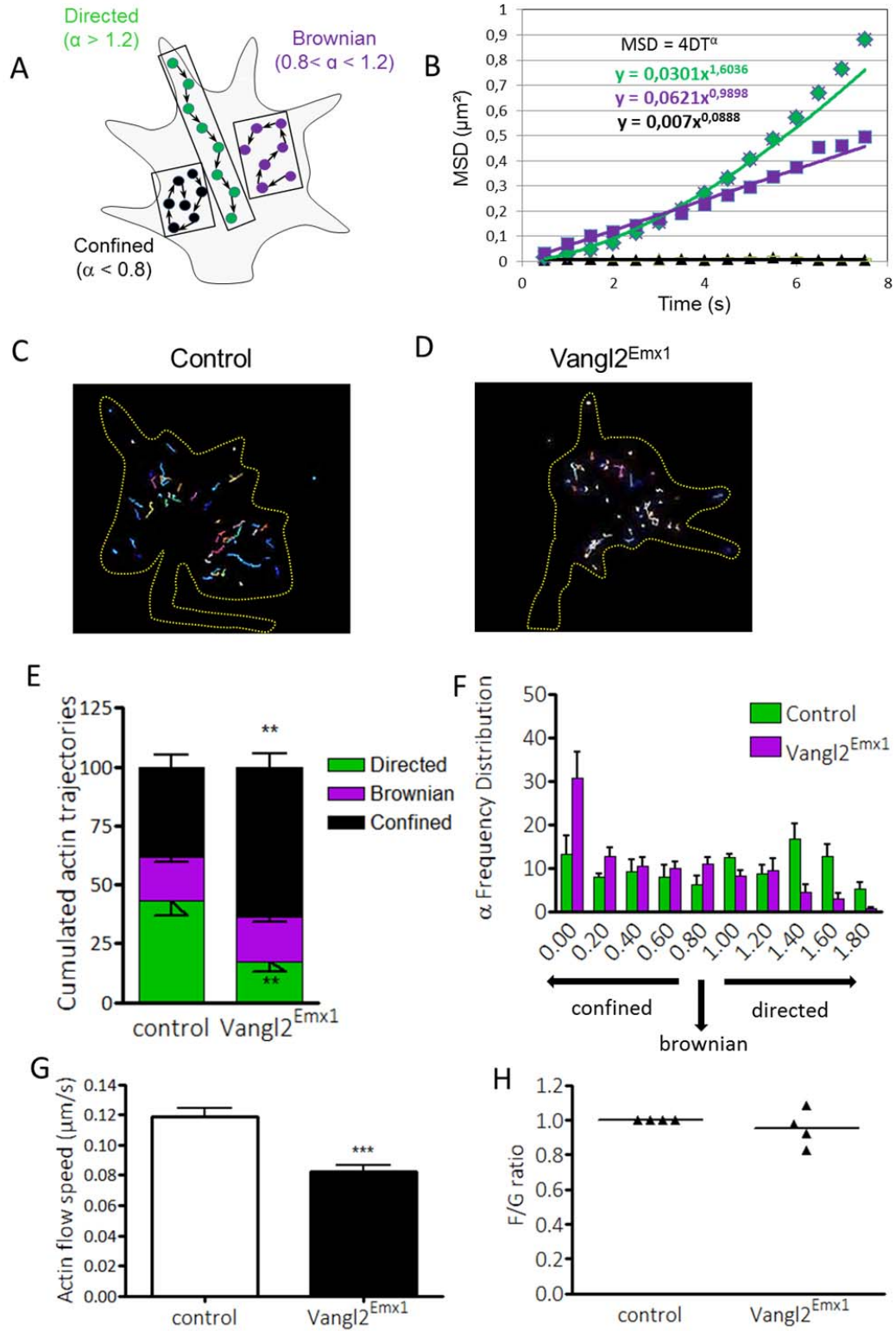


Figure 4

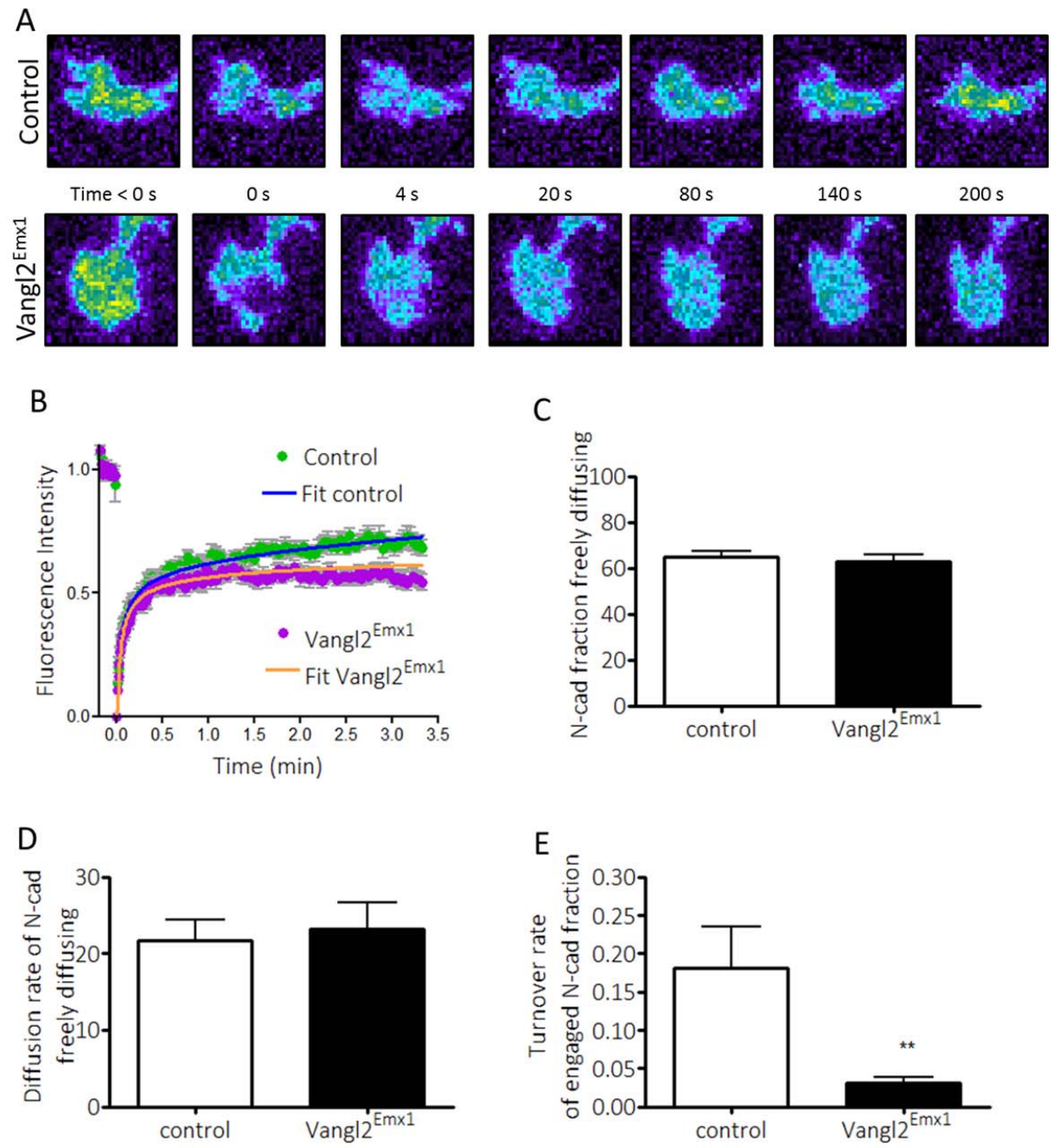
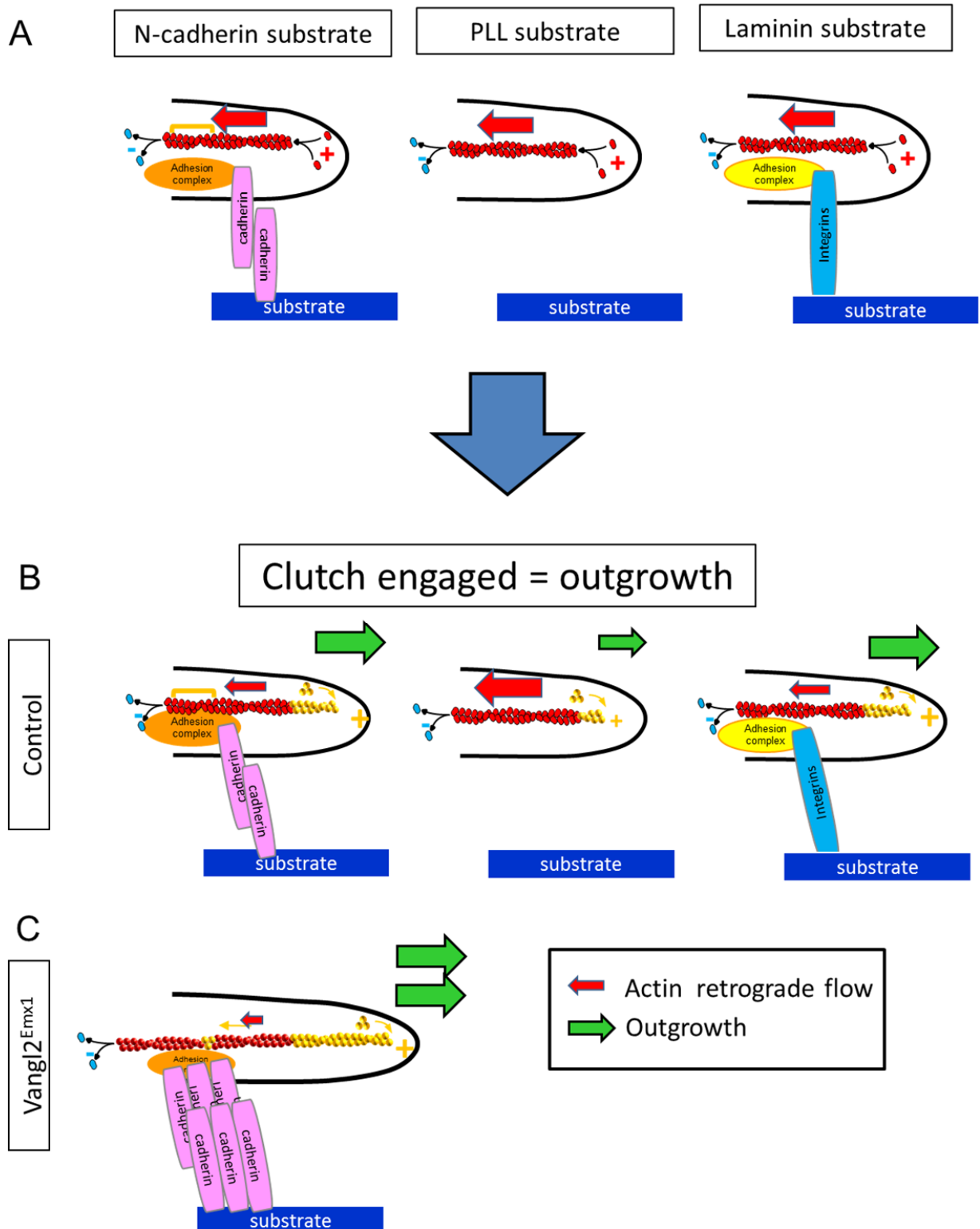
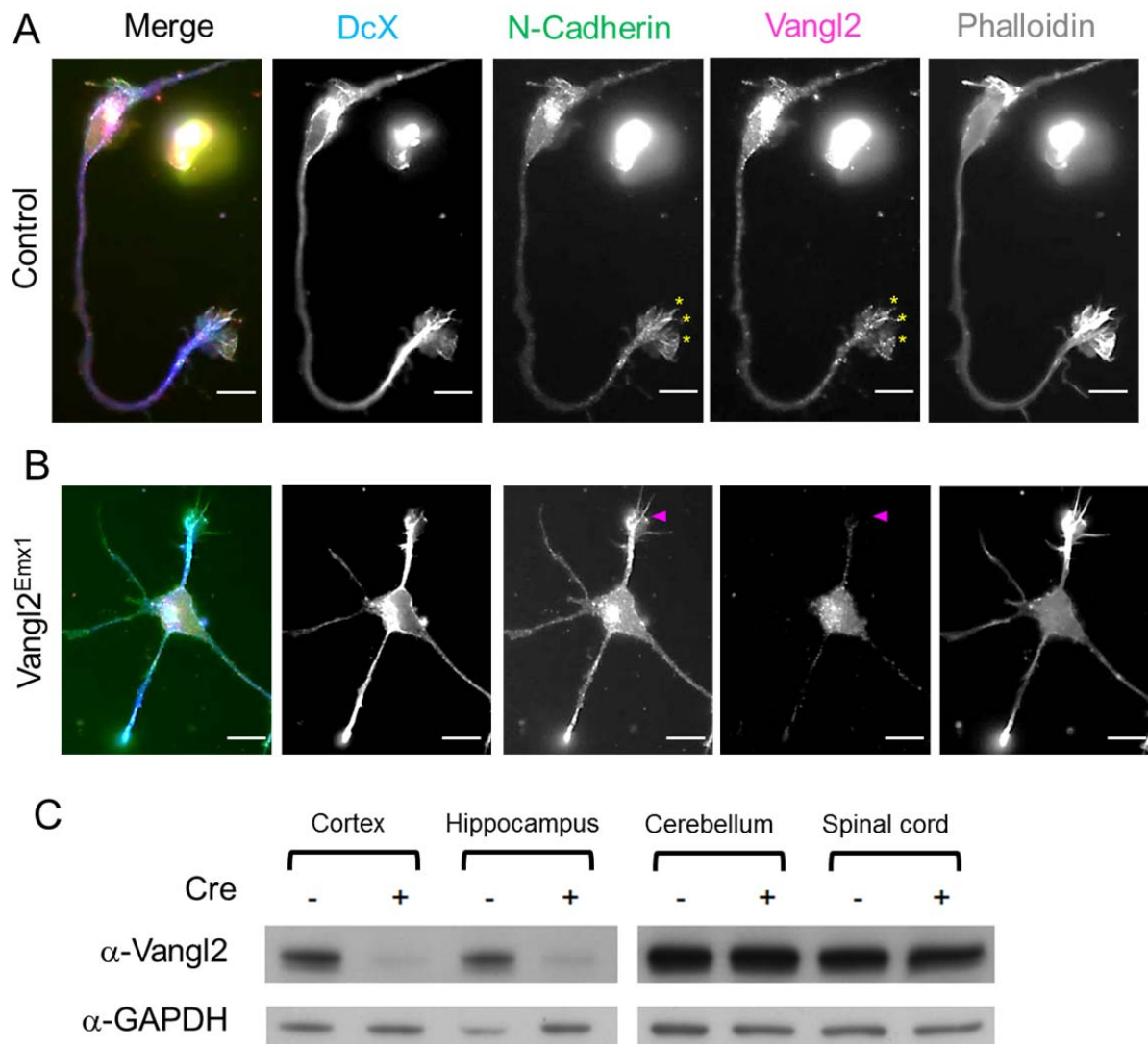


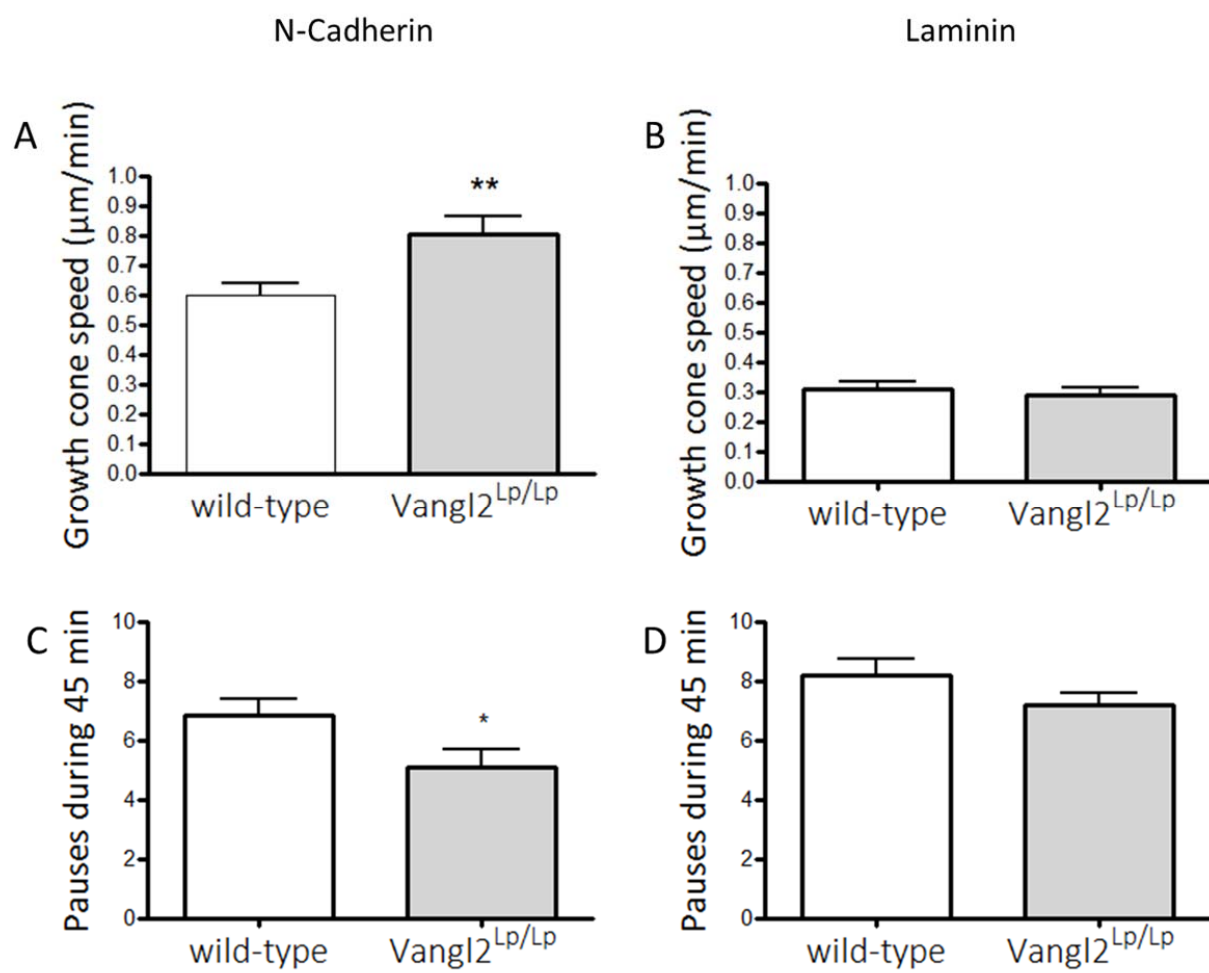
Figure 5



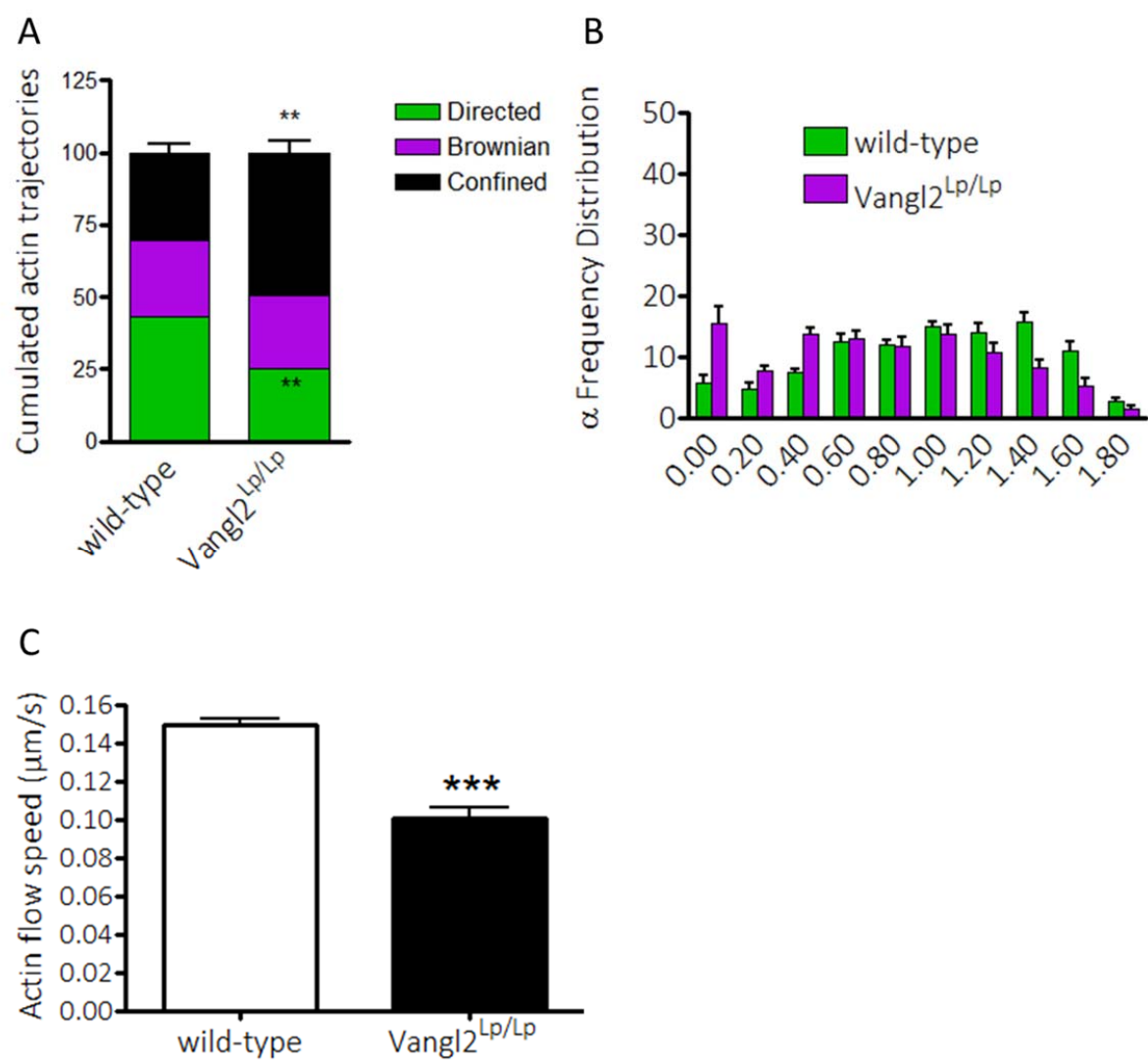
Supplemental Figure 1



Supplemental Figure 2

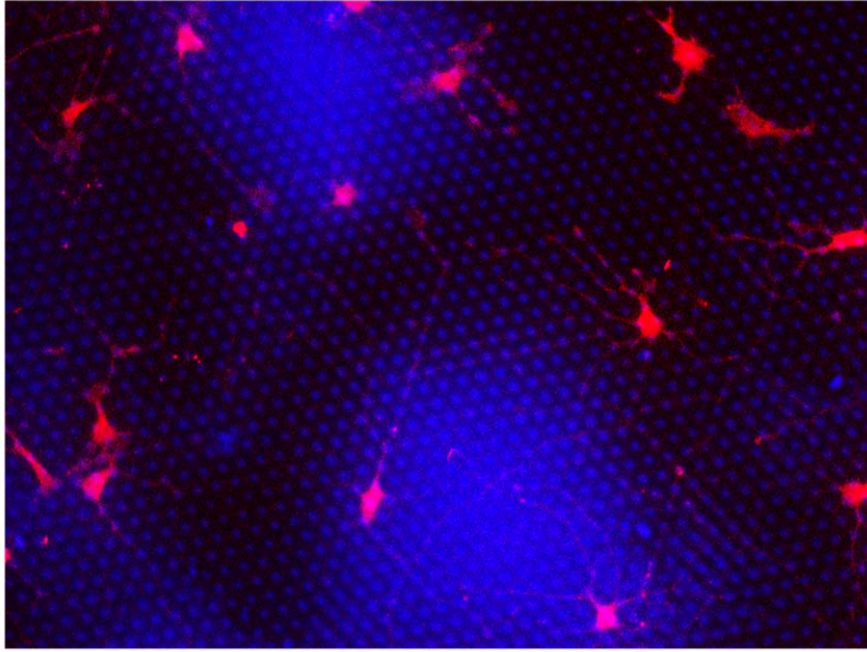


Supplemental Figure 3

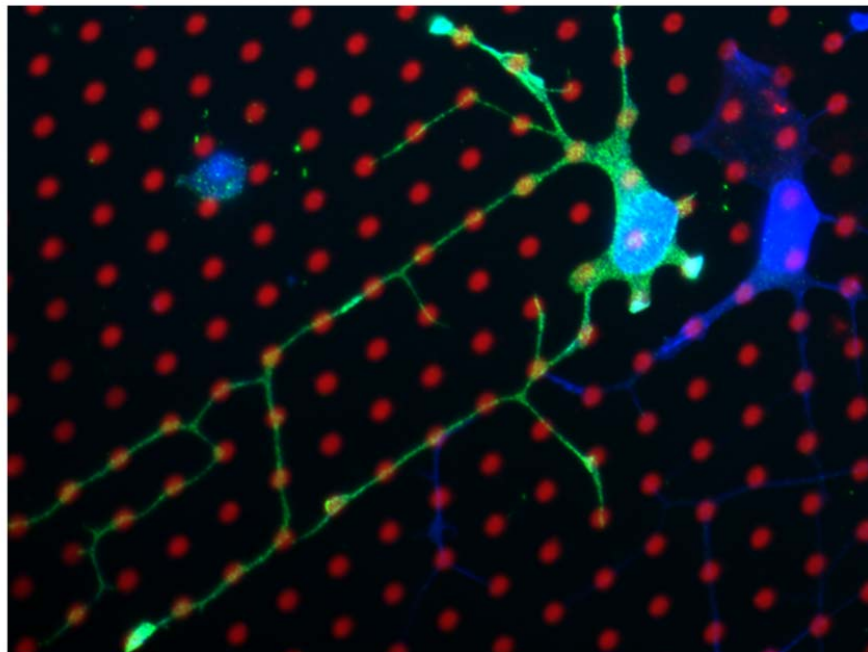


Supplemental Figure 4

A



B



Manuscript in preparation

Vangl2 controls the morphofunctional development of the DG-CA3 network of the hippocampus

This manuscript was done in collaboration with Dr Claudia Racca (Institute of Neuroscience, Newcastle University) for the electronic microscopy and 3D analysis) and Dr. Aline Marighetto for the behavioural analysis (Neurocentre Magendie, Team: Pathophysiology of declarative memory).

The behavioural experiments were conducted by Anne Quiedeville and Maité Moreau (Neurocentre Magendie, Team: Planar Polarity and Plasticity).

Contact Information: mireille.montcouquiol@inserm.fr

Abstract

Background

Planar cell polarity (PCP) signaling controls cytoskeleton and adhesion dynamics in various tissues, but its role in shaping the brain, and notably its postnatal connectivity, has not been addressed. One distinctive connection of the hippocampus is found between the granular cells of the dentate gyrus (DG) and neurons of the CA3 region, at the mossy fiber bouton/thorny excrescence (MfB/TE) synapses. These synapses, enriched in a region called the *stratum lucidum* (sl), have unique features in terms of size, morphology, molecular composition, and function. As the hippocampus is a key region of the brain controlling learning and memory, we sought to investigate whether core PCP signaling affect its development and function.

Results

Here we show that Vangl2 is widely expressed in the developing hippocampus, and notably enriched in the sl, at a stage that coincides with its increasing morphological complexity of the MfB/TE synapse, suggesting this protein could be crucial for the establishing of proper connectivity between DG Mfs and the dendrites of CA3 pyramidal neurons. We created a conditional *vangl2* KO mutant in which the protein is no longer expressed from early on during brain development. Results show *vangl2* deletion affects axon fasciculation and the morphological growth in complexity of the MfB/TE synapse. We were able to link these morphological defaults to behavioral deficits, as cKO mice were less performant than control mice when challenged with complex memory tasks.

Conclusions

Altogether we show that Vangl2 early developmental profile of expression correlates with the maturation of the Mf/CA3 hippocampal circuit, and that an early deletion of *vangl2* strongly reduced the morphological complexity of the MfB/TE synapse. Functionally, *vangl2* early deletion leads to impairments in certain aspect of memory abilities known to depend on the hippocampus.

Highlights

- Vangl2 is enriched in the hippocampal DG subgranular zone and in the *stratum lucidum*
- Vangl2 deletion affects axon fasciculation and growth in complexity of the MfB/TE synapse
- Vangl2 enrichment in the hippocampus is important for learning complex tasks

Introduction

Vangl2 is a component of the planar cell polarity (PCP) pathway that controls tissue shape and patterning (Walk-Shannon & Hardin, 2014; Wallingford, 2012; Singh & Mlodzik, 2012). Spontaneous mutants for vangl2 (called Loop-tail) present a number of neurological defects including the most severe form of neural tube defects (NTD) in mammals, craniorachischisis, leading to a complete disruption of brain patterning and early lethality (Strong & Hollander, 1949; Kibar et al., 2001; Montcouquiol et al., 2003, Torban et al., 2012). In human, *vangl2* mutations account for 0.4-2.5% of cases, and characterised mutations affect conserved amino acid residues at the cytoplasmic C-terminal PDZ-binding domain, diminishing protein-protein interactions essential for function (Lei et al., 2010; Seo et al., 2015). *Vangl1* mutations are similarly considered a risk factor, affecting conserved residues with missense mutations (Kibar et al., 2009).

Vangl2 is broadly expressed throughout the neuroectoderm during early neurogenesis where it controls morphogenesis, patterning of axial midline structures, and the developing neural plate (Kibar et al., 2001; Wang & Nathans, 2007; Walk-Shannon & Hardin, 2014; Tissir & Goffinet, 2013). Its expression is maintained in the entire CNS, as assessed by in situ hybridization, including the hippocampus (Tissir & Goffinet, 2006; Torban et al., 2007). In contrast the specific protein distribution at critical periods of brain maturation or the functional consequences of its deletion on learning and memory have not been described.

The hippocampus is a late-developing brain structure which only completes formation during the first two weeks of postnatal life in rats (Bayer, 1980). The granular cells (GC) of the dentate gyrus (DG) are distinguished by their late time of formation during brain development, and in rats, approximately 85% are generated after birth (Bayer & Altman, 1974). The GC precursors remain in a subgranular zone (SGZ) that becomes progressively thinner as the DG grows, but these precursor cells are retained in adult mammals. These sparsely scattered cells constantly generate GC neurons, and they continue to do so throughout the life of the animal (Jin, 2016). The hippocampus is a highly laminated structure and this lamination into well-defined strata is crucial for the proper migration/guidance of axonal fibres along these strata and consequently for the correct formation of circuits between different hippocampal sub-regions, as well as for the connectivity with other cerebral regions (Förster et al., 2006). Due to this lamination, the hippocampal CA3 region receives inputs from different brain regions via different *strata*. One important input comes from the entorhinal cortex which connects with the CA3 in the *stratum radiatum* (*sr*) via the perforant pathway. Another main input into CA3 is the Mossy fibers (Mf), which are axonal projections of DG GC that migrate along a specific hippocampus layer called *stratum lucidum* (*sl*). Mfs are distinctive unmyelinated axons arising from GC in the DG, they

have unusually large “giant” mossy fibre boutons (MfB) of 3-5 μ m in diameter (Henze et al., 2000). The majority of Mf extend and migrate along *the sl* where they bundle together, to eventually project into their target, the CA3 region. During their migration along the *sl*, each Mf sends fine collaterals that allow these axons to form “en passant” excitatory synapses with mossy cells located in the hilus, as well as with excitatory and inhibitory neurons located in the CA3 area. CA3 pyramidal neurons of the hippocampus also form specialized and complex synaptic structures called thorny excrescences (TE) that emerge from the proximal apical dendritic shaft (Amaral & Dent, 1981; Rollenhagen et al., 2007) and contact MfBs. The synapses between the CA3 pyramidal neurons and the Mfs are morphologically more complex than classical excitatory synapses. During the first three postnatal weeks, these synapses enlarge and undergo strong morphogenesis to form large presynaptic boutons that enfold and contact complex corresponding postsynaptic structures, the TE. Each MfB forms 11 to 18 synapses with the proximal apical dendrites of CA3 pyramidal neurons (Acsady et al., 1998; Claiborne et al., 1986; Gonzales et al., 2001), while MfB filopodial extensions synaptically contact the neighbouring inhibitory interneurons (40-50 synapses per Mf), which contact back the CA3 pyramidal neurons, and together form an elaborated synaptic complex (Henze et al., 2000). Thus, Mfs provide robust signalling to the proximo-apical dendrites of CA3 pyramidal neurons but also to interneurons that have dendrites in the *sl*. These synapses possess multiple active zones (14 active zones in average per MfB) facing their associated post-synaptic densities (Henze et al., 2000). Since CA3 pyramidal neurons can be contacted by 50 MfB (Amaral et al., 1990), each CA3 pyramidal neuron can be associated with an average of 700 active zones (only related with DG Mfs). This translates in a strong excitatory drive from Mfs to dendritic regions proximal to the soma and to the region of action potential generation in CA3 pyramidal neurons.

MfBs and TEs are a complex and multifaceted structure both morphologically and electrochemically. They appear almost unique within the brain in these regards, and represent an important component of the hippocampal circuitry, with important cognitive roles (Knierim, 2015; Lazarov & Hollands, 2016). Such a morphological and functional complexity does not exist in the more distal spines of CA3 pyramidal neurons located in the *sr*, which morphologically resemble more to CA1 spines. The spines from CA3 distal dendrites receive input from cortical regions such as the medial (MEC) and lateral (LEC) entorhinal cortex. Both the MEC and LEC target CA3 as well as the DG, and present projections that overlap, indicating that the DG and CA3 can combine the information conveyed by these inputs (Knierim, 2015). Since these cortical areas are essential not only for sensing and coding information coming from the environment but also to transmit the coded, sensed information to other cerebral regions, the inputs from these cortical regions to the hippocampus are important for memory and learning tasks that depend on the combined activity of the hippocampus and cortex.

In this study we generated a conditional mutant for Vangl2 (Vangl2^{Emx1}) to bypass early lethality and anatomical defects, as well as utilised GC-specific deletion of Vangl2 via viral injection to examine Vangl2 function in the developing hippocampus. We show that Vangl2 is enriched in the dendrites and axons of GCs of the DG. Conditional deletion of Vangl2 leads to defects in the maturation of Mf, and a decrease in the complexity of MfBs. Finally, using a version of the eight-arm radial maze task assessing hippocampus-dependent flexibility of spatial memory as a model of declarative memory in mice, we correlated the anatomical defects induced by the mutation to a specific impairment of declarative memory.

Altogether, our data demonstrate the role of Vangl2 as a maturation factor for the DG/CA3 network of the hippocampus, and highlight specific anatomical and cognitive consequences to its early deletion.

Materials and Methods

Generation of transgenic mice. This study was performed according to the European Communities Council Directives (2010/63/EU) with local ethical approval. The conditional knockout line (cKO) was generated by crossing Vangl2 flox/flox animals (Ramsbottom et al., 2014) with Emx1B6.129S2-Emx1tm1(cre)Krl/J (Emx1-Cre) mice. The recombination is predicted to produce a premature stop codon that gives rise to a small 8 KDa protein, which lacks the four trans-membrane domains and C-terminal PDZ-binding domain. Emx1 is expressed in the entire telencephalon as early as E10.5 (Gorski et al., 2002). Looptail stocks were obtained from the Jackson Laboratory (Bar Harbor, ME).

Immunofluorescence on brain sections. Terminal anaesthesia was induced by injection with pentobarbital (4ml/kg). Afterwards, mice were perfused transcardially with 4% paraformaldehyde (PFA) in 0.1M phosphate buffer saline (PBS), pH 7.4. Brains were harvested, post-fixed in 4% PFA, 2h at 4°C and cut into serial sections using a vibratome (40µm). The sections were rinsed with PBS/0.3% Triton X-100 (Triton) and then blocked with PBS/5% NGS (Normal Goat Serum)/0.3% Triton, 1h at room temperature (RT). Sections were then rinsed and incubated with primary antibodies (see below) overnight (on) at 4°C. The sections were rinsed and incubated with secondary antibodies (see below) and DAPI (1/10000) for 1h. Sections were rinsed again and mounted on slides with ProLong Gold Antifade mounting medium (ThermoFischer). Control and Vangl2^{Emx1} brain sections were treated simultaneously. Control experiments, in which the primary antibody was omitted, gave no signal. Images were acquired with an epifluorescence microscope (Zeiss Axio Imager.M2) with Axiovision software.

Quantifications of vangl2 cKO hippocampal phenotypes. Mf density was assessed in rectangular region of interests (ROIs) in the SP (see Figure 2A) using ImageJ software. DAPI staining allowed us to precisely delineate the CA3 pyramidal neurons in the SP and create a mask with them. The mask was then placed on Synaptopodin and NF-H images of the same ROI and the corresponding area of fluorescence was retrieved. This area was divided by the total area of DAPI staining in the SP, thus giving the Mf density and synaptic density in the SP. For quantification of Synaptopodin and Bassoon fluorescence staining in the sl images of CA3 areas were taken and then ran through a custom macro in ImageJ, which automatically quantified fluorescence intensity in the sl only. Levels of fluorescence for each Vangl2^{Emx1} mouse were compared to those for a littermate control mouse. For quantification of Mf density and levels of fluorescence, 3 to 5 brain sections from at least 4 different animals for each condition were quantified. The results in control and Vangl2^{Emx1} are presented as the mean ± SEM.

Antibodies. Antibodies were used as follows: anti-Vangl2 (0.84 µg/ml; Montcouquiol et al., 2006); anti-Synaptoporin (1/200; 102002, Synaptic Systems); anti-Doublecortin X (1/2000; AB2253, Millipore); anti-NeuN (1 µg/ml; clone A60, MAB377, Millipore); anti-Map2 (2 µg/ml; MAB 364, Millipore), anti-Bassoon (1/5000; SAP7F407, Stressgen); anti-NF-H (1/500; 2H3, the Hybridoma Bank, University of Iowa, Iowa City); anti-Znt3 (3.33 µg/ml; 197 011, Synaptic Systems), anti-N-cadherin (1.25µg/ml; 610921, BD Transduction Laboratories), anti-Nestin (2µg/ml; ab6142, Abcam) and anti-DsRed (1/1000; 632496, Clontech Living Colors). Secondary antibodies, used at 1/1000 and all made in goat and cross-adsorbed, were the following: anti-rabbit, anti-mouse and anti-guinea pig conjugated to AlexaFluor 546 and 488 (Invitrogen).

Stereotaxic viral injection into neonatal mice. Under sterile conditions, mouse pups (P5) were beforehand anesthetized by hypothermia (2-4 min on crushed ice bedding carefully packed flat). The pups were considered anesthetized when all movement stops. Cryoanesthetized pups were then secured in a digital stereotaxic frame with neonatal mice adaptor (World Precision Instruments, Inc., Sarasota, FL, USA), maintained on isofluorane inhalation (0.2%) and crushed ice bedding to provide more constant level of hypothermia. Before performing the surgical incision, 5µl of lidocaine (5 mg/kg, intradermal) was injected at the incision site for local anesthesia. Holes of the size of the injection needle were drilled with a fine needle into the skull, and injections were distributed using a 30G Nanofil needle attached to a Nanofil syringe (World Precision Instruments, Inc., Sarasota, FL, USA) coupled with a UMP3 UltraMicroPump (WPI). To label mossy fibers of the dentate gyrus, 100nl of AAV2/9-CaMKII -mCherry-WPRE virus (titer of 1.9×10^{12} genome copies/ml diluted in sterile PBS, Vector Biolabs) were injected bilaterally in the dentate gyrus zone (Y: ~0.5mm from lambda; X: ±0.75 mm; Z: 1.65 mm). After surgery, neonates were allowed to recover on a warm heating pad and, then, returned to their mother.

Confocal imaging and analysis of infected hippocampi. Confocal image stacks of PFA-fixed brain sections were acquired with a Leica DM2500 TCS SPE laser-scanning microscope with 561nm excitation wavelength using 63x Leica oil objective. Images of the mossy fiber termination zone in the CA3 sl region of the hippocampus were captured with an interval of 300nm in the z-axis. Camera aperture, magnification, light power, and exposure time were fixed for all images. A minimum of ten stacks from each animals of each genotype and age were acquired randomly. High-resolution 3D stacks were generated using Imaris 7.1.1 software (Bitplane) to characterize and analyze presynaptic terminals as individual objects. In order to be sure the analysis of TE, only large elements were considered (elements smaller than $5\mu\text{m}^3$ in volume were excluded). For of each 3D mossy fiber bouton, we then determined the volume, the index of complexity (determined by dividing bouton volume by its area) and the number of filopodial extensions per MfB. Values are presented as mean \pm SEM of n experiments. For statistical analysis, after checking the assumption of Normality, unpaired t-test was used for comparison of two groups. Statistical differences were considered as significant when $p \leq 0.05$.

Serial block face scanning electron microscopy (SBFsEM), 3D reconstruction and quantifications. P21 male mice were terminally anesthetized by brief inhalation of isoflurane (0.05% in air), followed by an intramuscular injection of ketamine (100 mg/ kg) and xylazine (10 mg/kg). Subsequently mice were perfused intracardially with 1 ml 5000U Heparin dissolved in phosphate buffer saline (PBS: 0.1 M, pH 7.2), followed by 200ml 2% paraformaldehyde + 2.5% glutaraldehyde in PBS, cooled to 4C. Then the brain was dissected and placed in the same fixative and stored at 4C until shipping. For shipping brains were transferred to 1x PBS + 0.01% Na Azide, at 4C, and restored to 2% paraformaldehyde + 2.5% glutaraldehyde in PBS at 4C upon arrival. All procedures were performed in full accordance with recommendations of the European Communities Council Directives (86/609/EEC), the French national Committee (87/848) and the requirements of the United Kingdom Animals (Scientific Procedures) Act 1986, AWERB Newcastle University (ID: 374). Note that, at all time the experimenters were blind to the mouse genotype. The code was only broken once all the modelling and analyses were finalized.

Sectioning was performed on a vibratome (Leica VT1000 S, Leica Biosystems) in PBS, producing 100 μm sections which were trimmed down to include the region of interest, and stored in glass vials with PBS at 4C. Osmium impregnation began with rinsing samples in PBS five times for three minutes each, then 3% potassium ferrocyanide in 2% osmium tetroxide in PBS at 4C for 1 hour. Samples were rinsed in ddH₂O at room temperature 5 times for 3 minutes each, and incubated in freshly prepared and filtered 1% (w/v) thiocarbohydrazide (TCH) for no longer than 20 minutes to avoid crystal formation and precipitation. They were then rinsed 5 times for 3 minutes each in ddH₂O followed by 2% osmium tetroxide in ddH₂O for 30 minutes, rinsed 5 times for 3 minutes and en bloc stained in 1% uranyl acetate in ddH₂O, at 4C overnight.

The next day samples were rinsed 5 times for 3 minutes each in ddH₂O, placed in Walton's lead aspartate solution at 60°C for 30 minutes, then rinsed in ddH₂O as before at room temperature. Dehydration via a graded ethanol series: 25%, then 10 mins at 4°C each change (1 x 50%, 1 x 70%, 1 x 90%, 2 x 100%), followed by 3 times in 100% Acetone for 30 minutes at room temperature. Samples were infiltrated by embedding in increasing concentrations of TAAB 812 epon resin (TAAB) mixed with acetone, beginning at 50% TAAB 812 resin rising to 70% after 30 minutes and 90% after a further 30 minutes, at room temperature. The samples were then transferred to aluminium boats filled with 100% TAAB 812 resin for 4 hours at room temperature. Sections were flat embedded and polymerised at 60°C for 48 hours. Specimens containing the ROI were then prepared on metal stubs for SBFsEM (Tapia et al. 2012, Wilke et al. 2013). Specimens were imaged on a Zeiss Sigma VP Scanning Electron Microscope with Gatan 3View to gather images using 50nm z-steps for control samples and 60nm for KO using the same parameters as in Wilke et al. (2013).

3D models were produced from the SBFsEM image stacks using the publically available Microscope Image Browser (MIB; <http://mib.helsinki.fi>) software (Belevich et al., 2016). The resultant 3D profiles were used to produce volumetric reconstructions of, and to provide statistics on the volume of, pre- and postsynaptic structures of interest. A total of 2 datasets were completed. In each dataset a postsynaptic dendrite was first traced in its entirety within the block and reconstructed. Then the spines, PSD, and presynaptic elements were similarly isolated individually and reconstructed. Spines and TEs were defined as a protrusion from the dendritic shaft, typically with a narrow neck. PSDs were defined as an increased electron density and thickening of the postsynaptic membrane at an interface between presynaptic and postsynaptic structures. MfB were defined visually by their structure surrounding the TE/spines isolated previously. Only synapses and structures perpendicular to the plane of sectioning could be reconstructed, and reconstructions were constrained by the edges of the image block. The statistics tool included in MIB was used to provide measurements for volume of the isolated structures. Final 3D models were rendered at full resolution through Amira 3D software (FEI, ThermoFisher).

Quantitative Statistical Analysis of SBFsEM. The quantitative statistical analysis was performed using Sigmaplot12.5 (Systat Software) for Windows. Data of volumes of dendrite, spines or TE, postsynaptic densities and MfB were analysed. Using these data, two additional parameters were evaluated: TE or Spine density (N°. TE or spine/ μm^3) and Ratio of total TE or Spine volume/total dendrite volume. When single data populations had a Gaussian distribution according to the Shapiro-Wilk test, we reported parametric statistical features (mean \pm SEM); otherwise we performed the nonparametric statistical one-sample Kolmogorov-Smirnov test. Additionally, skewness values were also assessed to determine whether the distribution of the sample data were symmetric or not; and Kurtosis values to find whether the sample data were heavy-tailed with lots of outliers, or light-tailed with respect to a normal distribution. To assess statistical significance between two groups (wt vs KO), we tested for normality with Shapiro-Wilk test, if this passed, we followed it by Equal Variance test. If the normality test failed, we tested with Mann–Whitney rank sum to assess statistical significance between the groups. $P < 0.05$ was considered statistically significant. To assess correlation between groups, we applied a Spearman rank order test followed by a linear regression test. $P < 0.05$ was considered statistically significant.

Culture of Hippocampal organotypical slices and Single-Cell-Electroporation (SCE). P5 rats were decapitated and the hippocampi were retrieved for organotypical culture. Briefly, brains were dissected in a GBSS medium (Sigma) containing 2.5M D-Glucose (Sigma) and 1% Penicillin/Streptomycin antibiotics. The retrieved hippocampi were cut with a McIlwain Tissue Chopper and the slices were further placed on membranes located in 6 well-plates containing an Opti-MEM (Gibco) medium with 25% HBSS (Gibco) and 2.5M D-Glucose. After 3 days in vitro (DIV3), the medium was retrieved and a Neurobasal (Gibco) medium containing 200mM Glutamine (Gibco), 2% B27 (Gibco) and 2.5M D-Glucose. All the solutions were filtered and Horse Serum was further added to the Opti-MEM and Neurobasal solutions. At DIV7, neurons were electroporated with a pEGFP-C3 cDNA construct containing only expressing Vangl2 or with a pEGFP-C3-Vangl2 cDNA construct that will produce a form of GFP-tagged Vangl2. At DIV15-16, slices were fixed with 4% PFA 37°C and mounted on slides with Prolong Gold. The organotypical slices were imaged with a confocal microscope, reconstructed with a Leica software and finally manipulated with Volocity PerkinELmer).

Behavioral analysis.

All experimental manipulations were approved by the Committee on Animal Health and Care of the local governmental body and performed in strict compliance with the EEC recommendations for the care and use of laboratory animals. Experiments were done using control and Vangl2^{EMX1} littermates. All animals were adult male mice of 10-12 weeks of age at the start of behavioral tests that were housed under standard laboratory conditions with a 12h light/12h dark cycle (light on at 07:00) with food and water supplied ad libitum. Two cohorts of animals were used

for the behavioral tests. The most stressful essays were administered last to minimize interference. One group of 15 control and 15 Vangl2^{EMX1} mice was tested in locomotor activity, plus-maze, black and white box, Y-maze and water maze test. A second group of 15 control and 15 Vangl2^{EMX1} mice was tested in radial maze. All tests were performed during the light phase of the light/dark cycle.

Locomotor activity. Locomotor activity was assessed in photocell-based activity chambers under light-dark environmental conditions, using inter-connected Plexiglas individual chambers equipped with infra-red sensors as published previously (Moreau et al., 2010). Chambers are inter-connected and linked to a computer using an electronic interface (Imetronic, Bordeaux, France). Rearing and horizontal activity data were collected for each mouse over a 3hr time course (response to novelty in 10-min bouts).

Elevated plus-maze. The Plexiglas plus-maze apparatus had two open and two enclosed arms radiating outward from a central open square and was 60 cm above the floor. The maze was illuminated by halogen light at 100 lux in the central open square. Mice were briefly handled for 2 consecutive days prior to elevated plus-maze experiment to habituate them. They were placed in the center of the maze and allowed free access to all arms for 5min.

Dark/light exploration assay. The dark/light was conducted in a two-chamber shuttle box with an opaque divider in the middle. The walls of the dark chamber were made of black Plexiglas while the light chamber was white and illuminated by halogen light at 300 lux. Mice were first placed into the dark chamber and allowed to freely travel between the chambers for 5 min. For each tests, a video tracking system (Ethovision version 11, Noldus Technology, Wageningen, The Netherlands) was used to analyze the mouse movements, the percentage of time spent and the number of entries in the open arms or light chamber.

Spontaneous alteration in the Y maze. Spontaneous alternation was assessed in a grey, plastic Y-maze, placed on a table 80 cm above the floor and located in the middle of a room containing a variety of extra-maze cues. The three arms of the Y-maze were similar in appearance, spaced at 120° from each other and were illuminated with a same light. Mice were placed at the end of one of the arms and allowed to explore the maze for 5 min. Allocation of the start arm was counterbalanced within experimental groups. An entry into one of the arms was scored when all four paws of the animal were placed inside this arm. Spontaneous alternation, expressed as a percentage, refers to the proportion of arm choices differing from the two previous choices. Thus, if an animal made the following sequence of arm choices: A, B, C, B, A, B, C, A, the total number of alternation opportunities would be six (total entries minus two) and the percentage alternation would be 67% (four out of six).

Spatial learning and memory in the Morris water maze. Spatial memory was tested in a circular

pool (diameter 150 cm) filled with water maintained at 19-20°C and opaque by the adjunction of a non-toxic cosmetic adjuvant. Mice were trained to swim to a 14 cm diameter platform in order to escape from the water. Data were collected using a video camera fixed to the ceiling of the room and connected to a computerized tracking system (Viewpoint, Lyon, France) located in an adjacent room. To measure performance in hidden trials, the escape latency, distance to the target, and swim speed were analysed as outcome measures for each session. During the test, mice were trained for two series of three trials per day: 3 trials in the morning and 3 trials in the afternoon, with a cut-off of 60 s, 5 min intertrials interval and 3 hr interseries interval. If the mice found the platform, they were allowed to remain on it for 15s (reinforcement); mice that failed to find the platform within 60s were led to the platform by the experimenter where they were allowed to stay for 15s. Mice were released from different starting point at each trial, and different sequences of starting points were used each day. Visual training: During 5 consecutive sessions, mice were trained to swim to unsubmerged platform indicated by a ball suspended with a transparent thread at 7.5cm above the platform. Spatial training: Mice were trained during 10 days to swim to a submerged platform (1.5 cm below the water surface) using spatial cues located in the room (posters on the walls). Probe testing: The probe trials were designed to examine the extent of spatial discrimination learning (spatial bias) at day 10 during the spatial training. To do this, the platform was removed from the pool 24 hr after the last hidden platform training trial. The number of crossings of the platform location, and the time that mice spent swimming in the target quadrant (where the platform was located during hidden platform training) were measured over a 60 s trial.

Relational/Declarative memory in the radial maze. One week before the beginning and until the end of the experiments, mice were submitted to partial food deprivation (82-85% of their free feeding weight) and handled daily. We used three identical fully automatized 8-arm radial-mazes made of grey Plexiglas. Only extra-maze cues were available (posters on the walls). Habituation: Each mouse was submitted to two days of habituation, where all the arms are baited and open, and must visit each arm and eat all the pellets to complete the session. Training: Each mouse was assigned three pairs of adjacent arms for all the training (pairs A, B and C). One arm of each pair is always baited (the right arm for pairs A and B, the left one for pair C). Within each daily training session, the mouse was submitted to 20 successive presentations (trials) of the three pairs, in a pseudo-random order, separated by an inter-trials interval of 20s (Fig. 7A). A trial was considered successful when the mouse chose the baited arm. The training lasted at least 5 days, and ended when a mouse achieved a mean performance of 72.5% on two days for all three pairs. Mice, which failed to complete each daily session in a maximum of one hour, and mice, which did not finish the training in 12 days, were excluded from the analysis (here, 3 control and 3 Vangl2^{EMX1} mice were excluded). Test. When a mouse completed the training, it was submitted to a test session of 20 trials. During this session, each mouse was assigned three pairs of arms. One was already known (the pair C, that will

serve as a control pair), one was totally new (pair N, composed of two adjacent arms never visited during the training), and one pair was recombined using the unbaited arm of the pair A and the baited arm of the pair B (pair AB). The percentage of performance obtained for this pair AB served as an index of memory flexibility, which is a cardinal characteristic of relational/declarative memory (Marighetto et al, 1999; Etchamendy et al.2003; Mingaud et al, 2007) for the animal.

Statistical analysis of the behavioural tests. All data were presented as mean \pm SEM, and $p \leq 0.05$ was considered statistically significant. When necessary, we have checked the assumption of Normality. One-way ANOVA was used for analyzing the effect of genotype on time spent in each quadrant of the water maze in the probe test. Two-ways ANOVA was used for analyzing the effect of days of training and genotype in the declarative and working memory performance of the radial maze test. The Bonferroni posthoc test was used when appropriate. The Student's t-test was used for comparing control and Vangl2^{EMX1} mice in the plus-maze; dark/light test; locomotor rearing and Y-maze test and declarative memory. All calculations were performed using GraphPad Prism version 4 for Windows.

Results

Vangl2 expression profile follows the DG/CA3 network maturation

We first evaluated the profile of expression of vangl2 mRNA during the early postnatal maturation of the hippocampus. Results show that at birth (P0), vangl2 mRNA is highly expressed in the whole developing hippocampal CA1-3 and DG regions (Fig. 1A, asterisk). High levels of transcripts are also present in the surrounding areas, including the ventricular zones, the neocortex and the thalamus (Fig. 1A). At P7, vangl2 mRNAs are present in the same regions, and strongly enriched in the hippocampus, with a now formed DG (Fig. 1B). At P21, vangl2 mRNA levels are decreased, though still present in the DG and CA3 regions (Fig. 1C). Of note, in order to allow the comparison of expression levels through development (P0-P21), the images in Fig. 1 were all processed with identical concentration of probe and timing of development of the coloration and imaged with the same exposure time and light intensity. Results show a weaker staining in P21, when compared to the other stages, suggesting that vangl2 mRNA levels decrease in the hippocampus during development.

At the protein level, at 14 days after birth (P14), Vangl2 was strongly expressed in the entire hippocampus, notably in the DG (Fig. 2A). The dendrites of GC were strongly labelled, and we observed a strong accumulation in the SGZ and all along the *sl*, where Mf contact apico-proximal dendrites of CA3 pyramidal cells (Fig. 2A). Vangl2 labelling was also found in other regions (e.g. the thalamus) (Fig. 2, yellow asterisk), and the ependymal cells (Fig. 2, red asterisk). At P21, Vangl2 expression was maintained in all the aforementioned regions, with a reduction of the staining in the GC layer (Fig. 2B). To identify the cellular type expressing Vangl2 we performed a series of double-stainings with various markers at P21. Results show good co-localization of Vangl2 with DCX, a marker of GC late neural progenitor (Fig. 2D, Sup. Fig. 1A), but not with NeuN or Kv2.1, markers of mature GC (Fig. 2E, Sup. Fig. 2A). The accumulation of Vangl2 in the SGZ at P21 appeared reduced compared to P14, correlating with the increased maturation of the GC and decreased DCX staining (data not shown). We saw no co-localization with nestin, a marker of early progenitors at this stage of development (Sup. Fig. 2B).

At P21 Vangl2 enriched in the *sl* in the CA3 region, where it co-localizes with DCX (which labels Mf projections arising from immature GC) and Tau (a marker of axonal microtubules) but not with Znt3, Map2 and PSD-95 (Fig. 2D,F, Sup. Fig. 1B,C,D,E,G & 2C,D,E) suggesting that at this stage Vangl2 is mostly enriched in Mf axons. This profile is decreased but maintained in adult (data not shown). Finally, we observed expression of Vangl2 in GC dendrites and their spines as illustrated by the good co-localization with Map2 and PSD-95 in the *stratum moleculare* (*sm*, Fig. 2G, Sup. Fig. 1F & 2F). A similar co-localization is observed with N-cadherin, both in the dendrites and in the SGZ (Fig. 2H).

Altogether these results show that Vangl2 expression is enriched in immature GC of the DG at the time of their maturation, and is preferentially enriched in GC neurites rather than in the somata of mature neurons.

Vangl2 deletion leads to deficits in DG/CA3 network maturation

As presented in Figure 2, Vangl2 is enriched in the CA3 *sl*. To assess whether Vangl2 is required for Mf pathway development and MfB-TE synaptogenesis, we created a conditional Vangl2 knockout mouse (Vangl2^{Emx1}). This conditional deletion leads to the suppression of Vangl2 expression in neuron and glia progenitors during embryogenesis in the telencephalon, before the formation of the DG-CA3 network. At P21, when the DG-CA3 network is considered mature, Vangl2 is no longer present in the hippocampus of Vangl2^{Emx1} mice while it remains present in the thalamus (diencephalon) (Figure 2A).

When Mfs migrate from the DG hilus to find their future synaptic partner, they migrate throughout the *sl* and contact the proximal part of the apical dendrites of CA3 pyramidal neurons. If Mfs migrate properly, they rarely cross the *stratum pyramidale* (*sp*) (where CA3 pyramidal cell somata are packed) and also rarely make synaptic contact with the cell bodies of these neurons. To quantify migrating "errors" that Mfs might have made during development, we performed immunofluorescence assays for Neurofilament-H (which stains axonal projections) and Synaptoporin (a protein that is highly enriched at MfB) (Fig. 3B). After multichannel image acquisition of a defined region in the CA3 *sp* emerging from the DG hilus (depicted in blue in Fig. 3B), we used a macro in ImageJ which allowed us to estimate the fluorescence level of each marker in the defined area. The fluorescence level for each marker was then divided by the total superficial area of the *sp* region selected (defined by the DAPI staining); the value obtained represented the Mf density in the selected SP region. Quantification of Mf density in this region showed a significant increase in Vangl2^{Emx1} hippocampus when compared to control, for both NF-H (control: 0.30 ± 0.02 , n=17 hippocampi from 4 different mice; Vangl2^{Emx1}: 0.35 ± 0.02 , n=21 hippocampi from 4 different Vangl2^{Emx1} mice; p=0.03) and Synaptoporin (control: 0.30 ± 0.02 , n=17, 4 mice; Vangl2^{Emx1}: 0.38 ± 0.02 , n=21, 4 Vangl2^{Emx1} mice; p=0.02) (Fig. 3C). These results suggest that Vangl2^{Emx1} Mfs are more errors prone not only during their migration along the *sl* but also that they erratically connect to more cell bodies of CA3 pyramidal neurons, when compared to controls.

These errors in Mf lamination could reflect a decrease in the content of Mf boutons in the *sl* that properly connect to their correct synaptic partner: the proximal part of the apical dendrites of CA3 pyramidal neurons. To verify our hypothesis we evaluated Bassoon and Synaptoporin staining (Fig. 3D), two proteins that are enriched at MfB. Using a custom-made macro (ImageJ), we showed that the levels of fluorescence for both these markers were decreased in Vangl2^{Emx1} *sl*, when compared to controls (Bassoon: $89.3 \pm 2.99\%$, n=5 different mice for each condition, p=0.023; Synaptoporin: $88.6 \pm 3.63\%$, n=5 different mice for each condition, p=0.035) (Fig. 3E). We did not discriminate whether this decrease in fluorescence of

MfB proteins was related to a reduction in the number of MfBs in the *sl*, or of the protein content in each MfB, due to maturation deficits, or both of these options.

Vangl2 deletion affects the morphogenesis of the DG/CA3 synapses

We used two morphometric approaches to characterize the eventual structural changes of the pre- and postsynaptic elements of the DG/CA3 network. First, we infected the GCs of the DG of mice pups with a construct expressing a fluorescent tag and quantified the morphological characteristics of MfBs at P25 (see Methods, Fig. 4A,B,C). Initial observations suggested an overall decreased number and/or size of MfB in the *sl* of *Vangl2^{Emx1}* mice compared to controls (Fig. 4D,E). We chose to quantify only the volume of very large remaining MfBs (volume $\geq 5 \mu\text{m}^3$) at P25, and confirmed a statistically significant reduction of large MfB volume in *Vangl2^{Emx1}* mice compared to their control (control: $37.48 \pm 2.77 \mu\text{m}^3$, $n=47$ boutons; *Vangl2^{Emx1}*: $26.62 \pm 2.07 \mu\text{m}^3$, $n=57$ boutons, $p<0.01$; Fig. 4D,E,F). As the MfBs mature, they grow and become more complex, notably by the presence of multiple filopodia (Lanore et al., 2012). Consequently, we determined both MfBs complexity index (see Methods) and the number of filopodial extensions per MfB, and showed that both MfB complexity (control: 0.25 ± 0.005 , $n=47$ boutons; *Vangl2^{Emx1}*: 0.18 ± 0.01 , $n=57$ boutons, $p<0.0001$; Fig. 4F), and the number of filopodia per bouton were decreased in *Vangl2^{Emx1}* mice (control: 2.55 ± 0.28 , $n=47$ boutons; *Vangl2^{Emx1}*: 1.22 ± 0.18 , $n=57$ boutons, $p<0.0001$; Fig. 4F). Consistent with a delayed morphological maturation in *Vangl2^{Emx1}* mice, the percentage of boutons showing filopodia was decreased as compared with control mice at P25 (control: 79.24%, $n=47$ boutons; *Vangl2^{Emx1}* mice: 54.4%, $n=57$ boutons; Fig. 4F). Altogether these results demonstrate that in *Vangl2^{Emx1}* mice, MfB are structurally smaller and less complex, suggesting an immaturity of the presynaptic compartment.

Viral infection in the DG limited the imaging and analysis to the presynaptic side of the MfB/TE junction. To evaluate the impact of *vangl2* deletion on the entire synapse, we used serial block face scanning electron microscopy (SBFsEM) and 3D reconstruction of *Vangl2^{Emx1}* samples (Sup. Fig. 3). Preliminary analysis of the image stacks showed a dramatic difference in the morphology of control and *Vangl2^{Emx1}* samples in the *sl*. In control, as expected, we observed large MfBs contacting TEs which emerged from CA3 pyramidal cell dendrites, while in *Vangl2^{Emx1}* we only observed smaller boutons and spine-like structures which appeared to also be in higher number than the MfB/TE in control (Fig. 5A,A',A'',B,B',B''). *sr* shows subtler but inversed changes between control and *Vangl2^{Emx1}*, with increased spines volumes in *vangl2* cKO (Suppl. Fig. 3A,B). The 3D models confirmed and revealed even greater morphological differences. In controls, the structures of the MfBs were large and complex and quantifications show that in *Vangl2^{Emx1}* mice the average volume of MfB is significantly decreased (control: $8.29 \pm 2.32 \mu\text{m}^3$, $n=9$ MfB from one mouse vs *Vangl2^{Emx1}*: $0.41 \pm 0.13 \mu\text{m}^3$, $n=5$ MfB from one mouse; $p<0.001$) (Table 1 & Fig. 5A,B,C). Our quantifications are comparable to those observed in wild type mice (Wilke et al., 2013). In *sl*, the TE-spine volume between control and *Vangl2^{Emx1}* was also significantly smaller, demonstrating that the whole MfB/TE synapse morphology is affected

by Vangl2 deletion (control: $0.56 \pm 0.09 \mu\text{m}^3$, $n=19$ TE from one mouse vs Vangl2^{Emx1}: $0.1 \pm 0.01 \mu\text{m}^3$, $n=180$ TE-spine from one mouse; $p<0.001$) (Table 1 & Fig. 5C,D).

On several occasions in control samples, a single MfB was observed to make contact with two or more TEs on the same dendrite and make multiple synaptic connections with each TE. The dendritic shaft found between MfB/TE synapses was smooth (black asterisk in Fig. 5A). CA3 proximal apical dendrites were mostly of uniform thickness along their length, and three out of four 3D reconstructed dendrites split into two separate, but similarly sized branches. In Vangl2^{Emx1}, both pre- and postsynaptic-structures were smaller and resembled classic bouton/spine structures and the CA3 proximal apical dendrites had a spinous appearance (yellow asterisk in Fig. 5B). In Vangl2^{Emx1}, we observed a higher number of spines than control (Table 1). Quantitative analysis of the two sets of data showed that in control *sl*, the 19 TEs we reconstructed had a total of 83 PSDs, meaning each TE formed an average of 4-5 synapses (Table 1 & Fig. 5E). Vangl2^{Emx1} had fewer PSDs (150) than spines (180), indicating some spine-like structures do not form synapses. In the *sr* however both control and Vangl2^{Emx1} have more PSDs than spines (Sup. Fig. 3C). These results demonstrate that in addition to the size of the MfB/TE synapse, another distinctive feature of this MfB/TE synapse is affected by *vangl2* deletion: the contact between one MfB and multiple TEs.

The PSD volume of the TE in *sl* were significantly bigger ($p=0.022$) in Vangl2^{Emx1} compared to control (control: $0.0057 \pm 0.0004 \mu\text{m}^3$, $n=83$ TE from one mouse vs Vangl2^{Emx1}: $0.0065 \pm 0.0002 \mu\text{m}^3$, $n=150$ TE from one mouse; $p<0.001$) (Table 1 & Fig. 5E), while no differences were found in PSD volume of spines in *sr* (control: $0.0058 \pm 0.0005 \mu\text{m}^3$, $n=43$ spines from one mouse vs Vangl2^{Emx1}: $0.0059 \pm 0.0005 \mu\text{m}^3$, $n=73$ spines from one mouse) (Sup. Fig. 3D). TE-Spine density ($n.$ TE-spine/ μm^3 of dendritic volume) was also higher in Vangl2^{Emx1} compared to the density of TE-spine in controls ($p=0.029$) (Table 1). Altogether, the increase in PSD size and spine density indicate that the deletion of Vangl2 also affects overall spino- and synaptogenesis of CA3 pyramidal neurons in addition to the already described defects on MfB/TE morphology. Altogether, our results show that in Vangl2^{Emx1} cKOs, the number of TE was increased, but their size was comparable to those of classical spines, while their synaptic densities (PSDs) were bigger, but fewer. In the *sr* the number of spines is also increased, but the size of the PSDs is unchanged.

PCP proteins have been shown to affect cellular shape and growth when downregulated (loss of function – LOF) but also when they are overexpressed (gain of function – GOF) (Lee et al., 2003). Hence we sought to determine if Vangl2 overexpression could also affect the MfB/TE synapse morphology. To answer this question we used single-cell-electroporation on CA3 pyramidal neurons from hippocampal organotypical slices (Sup. Fig. 5A) to express "low doses" (50 ng/ml) of tagged *vangl2* cDNA. The expressed protein accumulated in TE-like structures located near to the cell body of the CA3 neurons in the *sl* (Sup. Fig. 5C,D green arrows), while a construct expressing GFP alone did not accumulate in these post-synaptic compartments (Sup.

Fig. 5B). Moreover, when we increased the concentration of electroporated *vangl2* cDNA (200 ng/ml) in these neurons, we observed a dramatic increase in the arborisation complexity of these neurons, with increased neurites, more branching and more structures resembling TEs (Sup. Fig. 5E). Due to technical limitations we could not test if *Vangl2* overexpression in GCs could also affect the morphology of the pre-synaptic element: the MfB. Altogether, these GOF experiments demonstrate that *Vangl2* is targeted at post-synaptic structures and that overexpression of *Vangl2* enhances neurons arborisation, suggesting that *Vangl2* overexpression participate in the maturity of the CA3 pyramidal neurons.

***Vangl2* is not required for spatial learning but is required for declarative memory assessed by flexible expression of spatial memory.**

To determine the functional consequence of a loss of *vangl2* in the forebrain, we tested *Vangl2*^{Emx1} mice and their littermate controls in a series of tasks measuring emotional, exploratory and cognitive behaviors. We first performed elevated plus-maze and dark/light experiments to test anxiety-like behavior. Compared to their control littermates, *Vangl2*^{Emx1} mice spent a normal amount of time in the open arms of the elevated plus-maze (*t*-test, $t_{28}=1.66$, n.s; Fig. 6A), as well as a comparable percentage of time in the white box of the dark/light test (*t*-test, $t_{28}=1.33$, n.s; Fig. 6B). Thus the *Vangl2*^{Emx1} mice did not display alteration of anxiety-like behavior. In addition, locomotion was also unaltered in *Vangl2*^{Emx1} mice, which displayed normal rearing behavior (*t*-test, $t_{28}=1.16$, n.s; Fig. 6C) and horizontal units of activity (main effect of genotype, $F_{(1,476)} < 1$, n.s; Fig. 6C). Next, we tested spontaneous alternation in the Y-maze, based on the natural tendency of mice to explore a novel environment. Namely, a mouse spontaneously alternates its visits among the arms, given that the successive visits are temporarily kept in short-term memory. Alternation can therefore be taken as an index of short-term/working memory. The analysis showed a significant difference between *Vangl2*^{Emx1} mice and their control in the percentage of alternation (*t*-test; $t_{24}=2.1$; $p = 0.045$; Figure 6D). The *Vangl2*^{Emx1} mice did not perform above the chance level of 50% (one group *t*-test, $t_{12}=2.2$; n.s; Fig. 6D), while the control group had a 67% alternation score (one group *t*-test, $t_{12}=4.8$; $p < 0.001$; Fig. 6D). These data suggest that the *Vangl2*^{Emx1} mice displayed poor spatial working memory.

We next analyzed the effect of *vangl2* loss on spatial learning and memory in the Morris water maze, known as a typical "hippocampus-dependent" test. During visual acquisition of the task, we found no impairment in the *Vangl2*^{Emx1} mice. Similarly, the *Vangl2*^{Emx1} mice were also indistinguishable from control during the acquisition of the standard spatial reference memory version of the Morris water maze task (Fig. 6E). Analysis of the latency to reach the platform during spatial training revealed that the two groups of mice acquired the task at the same rate (main effect of days, $F_{(18,513)} = 15.25$; $p < 0.0001$; main effect of genotype, $F_{(1,513)} < 1$; n.s; genotype-by-days interaction, $F_{(18,513)} < 1$; n.s) (Fig. 6E). The performances were also assessed

during probe test conducted 24hr after the last trial of the 10th day. Analysis of the distribution of time spent in the four quadrants of the pool revealed a significant effect of quadrant for the probe tests of control mice (ANOVA, $F_{(3,56)} = 28.07$, $p < 0.0001$; target vs. others quadrants, Bonferroni comparison, all t -test $p < 0.001$) but also for the Vang2^{EMX1} mice (ANOVA, $F_{(3,56)} = 21.32$, $p < 0.0001$; target vs. others quadrants, Bonferroni comparison, all t -test $p < 0.001$) (Fig. 6F). Similarly, inspection of annulus crossings data revealed equivalent learning in two groups of mice for the probe test (data not shown). In this spatial memory task, control and Vang2^{EMX1} mice learned the location of the platform to the same extent.

Despite the fact that MfB morphology was affected, Vang2^{EMX1} mice displayed normal anxiety-like behavior, activity and spatial learning and memory; nevertheless the reduction of spontaneous alternation is suggestive of a deficit in the short-term term (working) component of spatial memory.

We next tested another aspect of spatial memory, its flexibility taken as a model of declarative memory, using a specific version of the radial maze task. The acquisition phase of this task evaluates the capability to learn constant food locations within the maze, i.e. acquisition of reference spatial memory. The maze arms are repeatedly presented by pairs (3 invariant pairs A, B, C), and the test phase evaluates the capability to flexibly express learned information, a distinctive feature of declarative memory, by recombining into a novel pairing two of the pairs learnt in the acquisition phase. During the acquisition, we found no impairment in the Vang2^{EMX1} mice as they reached the learning criterion as quickly as control mice (t -test, $t_{24}=1.4$, n.s; Fig. 7B), and had similar levels of performance during the first five days of training (main effect of days, $F_{(4,96)} = 11.7$; $p < 0.0001$; main effect of genotype, $F_{(1,96)} < 1$; n.s; genotype-by-days interaction, $F_{(4,96)} < 1$; n.s) or the last five days of training (main effect of days, $F_{(4,96)} = 35.95$; $p < 0.0001$; main effect of genotype, $F_{(1,96)} < 1$; n.s; genotype-by-days interaction, $F_{(4,108)} < 1$; n.s). Both groups thus displayed equally good abilities to acquire spatial (reference) memory. To analyze the results of the test, we compared the performance on the last day of training (D-1) to the performance in the test day. There was no difference between D-1 and test whatever the genotype regarding the control pair C (main effect of days, $F_{(1,48)} < 1$; n.s; main effect of genotype, $F_{(1,48)} = 2.85$; n.s; genotype-by-days interaction, $F_{(1,48)} < 1$; n.s; Fig. 7C), showing that both control and Vang2^{EMX1} expressed equally well their memory when the testing situation was unchanged. In contrast, regarding the recombined pair AB, the analysis showed that performance significantly declined between the end of acquisition D-1 and the test in Vang2^{EMX1} mice only (main effect of days, $F_{(1,48)} = 14.57$; $p < 0.01$; main effect of genotype, $F_{(1,48)} = 1.61$; n.s; genotype-by-days interaction, $F_{(1,48)} = 4.06$; n.s; Bonferroni comparison D-1 vs. test: control $p > 0.05$; Vang2^{EMX1} $p < 0.001$; Fig. 7C). Hence, while control mice could flexibly express their memories in a modified testing, Vang2^{EMX1} mice failed to do so hence showing memory inflexibility. As expected for the Novel pair, performances did not differ from chance level (50% correct) whichever the genotype (one group t -test vs. 50%, control $t_{10} = 1.1$; n.s; Vang2^{EMX1} $t_{14} =$

0.56; n.s; Fig. 7C.). All together, these data show that Vang2^{EMX1} mice are not grossly impaired as they can normally learn and express spatial memories in unvarying situations, but they are not capable to use their spatial memory with flexibility in a changed situation, hence displaying a selective impairment of relational/declarative memory.

Altogether our data demonstrated that an early deletion of vangl2 does not result in a general impairment of spatial learning and memory but suggest that it selectively affects certain mnemonic components, including short-term/working memory (spontaneous alternation) and flexible memory expression, a cardinal characteristic of declarative memory.

Discussion

In this study we show that *Vangl2* is expressed early in the hippocampus and is enriched in the SGZ of the DG and the CA3 *s/l* at stages that coincide with the maturation of the MfB/CA3 circuit. Early conditional deletion of *Vangl2* affects the morphological complexification of the MfB/TE synapse, with a striking absence of the characteristic large TE in the CA3 *s/l*. These morphological deficits do not grossly affect spatial memory abilities known to depend on hippocampal function, but are associated with specific impairments in certain aspects of this memory, especially a loss of flexibility indicative of a declarative memory decline. Overall, these results show for the first time that *Vangl2* is crucial for the proper establishment of a hippocampal circuit (DG/CA3 circuit) and is consequently important for hippocampus-related cognitive function.

PCP genes are well known for their role in tissue morphogenesis during development, notably in epithelial and mesenchymal cells, but also during cardiac (Henderson et al., 2001), lung (Yates et al., 2001b), bone (Stein & Mackensen, 1957), and kidney (Yates et al., 2001a) development to cite a few. All core PCP genes, and many associated PCP genes (Ezan and Montcouquiol, 2013), are expressed early in central nervous system (CNS) development (Tissir & Goffinet, 2006, 2013), but studies of the specific localization of core PCP proteins, their role in CNS patterning or the cognitive functional consequences of genes deletion are still few, and mostly rely on the spontaneous mutant *Loop-tail* or downregulation via shRNA. Previous work from Lake and Sokol (2009) demonstrated that the deletion of *Vangl2* in mice presenting a spontaneous mutation in the *vangl2* gene (*Loop-tail* mutation) leads to precocious differentiation of neural precursor cells (NPCs) into early-born neurons at the expense of progenitor population regeneration, further causing a reduced brain-size in mutant mice. Our data revealed no major defects in the hippocampus of the *Vangl2*^{Emx1} cKOs regarding the structural development of the DG. This difference might be due to the fact that *Vangl2* does not play a similar role in DG neurogenesis, or that the effect described by Lake and Sokol is related to the reported negative-dominant effect of the *Vangl2*^{Lp} protein form produced by the *Loop-tail* mutation (Yin et al., 2012), or that there might be compensation either through *Vangl1* or another PCP protein.

We found that *vangl2*, one of the most upstream core PCP genes, is strongly expressed in the early postnatal CNS, and enriched in the DG and the CA3 subregions of the hippocampus. This is consistent with previous mRNA characterization (Tissir & Goffinet, 2006). *Vangl2* protein distribution profile matches mRNA distribution, with a strong enrichment in the subgranular zone (SGZ) of the DG and the *s/l* of the CA3. Specific co-localization with DCX in the SGZ but exclusion from nestin-positive cells demonstrates that *Vangl2* is expressed by late neuronal progenitor or immature GC of the DG. Co-localization with MAP2 and PSD-95 in the DG and with

Tau and DCX in the *sl* show enrichment in neurites (both dendrites and axons, respectively) of GC of the DG, with little accumulation in the cells body.

In epithelial but also mesenchymal cells one characteristic feature of core PCP proteins is their asymmetric distribution, and tightly controlled targeting and regulation (Strutt & Strutt, 2009). Our results suggest a similar tight control of Vangl2 traffic in neurons, with an almost complete targeting of the protein to the arborisation of the cells, supporting a role for the protein during neurons maturation and establishment of their connectivity. The *sl* CA3 enrichment was notably striking, as this region receives the axonal projections of the GC, the Mfs, which contact the proximal apical dendrites of CA3 pyramidal cells. When these synapses are established, they undergo dramatic morphogenesis and growth in complexity during the first three weeks after birth, morphing into a large presynaptic contact (MfB) and its mirror-shaped postsynaptic structure (TE). The unusual large size of these synaptic contacts requires intense cytoskeleton remodelling, a function consistent with PCP signalling role, as the main output of PCP signalling in invertebrates and throughout evolution is the control of actin polymerization and adhesion sites, in order to coordinate tissue patterning. The profile of Vangl2 expression is consistent with a role in the establishment of MfB/TE morphological complexity, with strong enrichment in the *sl* at P14, and a decreased expression as development proceeds. The maintenance of this staining in adult stages also suggests a maintenance role.

On the other hand, we did not find a co-localization with Znt3, a marker of presynaptic MfBs contacting CA3 pyramidal dendrites, and with postsynaptic markers (PSD-95) in TEs, whereas previous studies have reported Vangl2 expression at mature neuronal synapses, where it co-localizes with PSD-95 (Nagaoka et al., 2014; Yoshioka et al., 2013). The discrepancies with our results might be related to developmental stages differences or simply to technical differences, as we used immunohistochemistry on hippocampal tissue sections, whereas the previous reports are on dissociated neurons and PSD fraction.

Despite the absence of staining with pre- or postsynaptic markers, the structural and ultrastructural analysis of MfB/TE morphology revealed striking phenotypes in Vangl2^{Emx1} cKO. The absence of Vangl2 expression prevents the morphogenesis of the MfB/TE synapse into large and complex elements typical of these connections, reducing the size of these synaptic elements to the same of that of more classical spines (see Table 1). On the other hand, the size of spines in the *sr* was slightly increased suggesting a more general but also more complex role for Vangl2 in the maturation/morphogenesis of spines, depending on the area of the brain. Another possibility is that this discrepancy is due to a morpho-functional compensatory mechanism of the circuit, to adapt the loss of *vangl2*.

In both the *sl* and the *sr*, the number of spines was increased, contradicting previous reports that *vangl2* downregulation in neurons leads to a reduction in the number and density of spines

(Hagiwara et al., 2014). These discrepancies might be related to *in vitro* versus *in vivo* models differences, or to the difference in the systems used for Vangl2 (downregulation versus deletion), or even to a difference in the type of hippocampal neurons that were studied (the authors did not specify).

On the other hand, synaptic contacts are still present in Vangl2^{Emx1} cKO mice, suggesting that Vangl2 is either not necessary, or not the only PCP protein involved in their formation. It has to be seen whether such synapses in the cKO have similar or different functional properties than those of controls.

Interestingly, the connections formed between Mfs and TEs were monosynaptic in Vangl2^{Emx1} cKO mice, their PSDs were bigger as well as more numerous, while in control MFBs, we observed multisynaptic contacts with TEs. Again, this increase in both spine density and PSD volume may be a compensatory mechanism for the loss of the MFB/TE structures. In a different model system, the absence of *vangl2* led to a reduced size and complexity of glomerular podocytes of the kidney (Rocque et al., 2015). Interestingly, these structures were still able to perform their task although less efficiently and they were more susceptible to damage. Similarly, MFB/TEs synapses in Vangl2^{Emx1} cKO mice might be still functional but the loss of the complexity of this structure may deprive it from its “detonator synapse” properties and thus reduce the influence that DG GCs can exert over CA3 pyramidal neurons.

We first demonstrated that the conditional deletion of Vangl2 impacted the maturation of the MFB/TE synapse and subsequently demonstrated that overexpression of the same protein impacts the CA3 dendrite and TE morphology. We showed that Vangl2 overexpression in CA3 pyramidal neurons increased the complexity of the neurites, and seem to affect the number and size of TEs, hence causing a complete opposite phenotype to the one induced by *vangl2* conditional deletion. Despite their differences, LOF and GOF of *vangl2* had the same phenotypical readout: an alteration of the MFB/TE morphology/maturation, probably via a similar mechanism related to the local regulation of adhesion and cytoskeleton dynamics.

A previous study on the MFB/TE synapse reported that the disruption of this structure impacts on animal behaviour (Wilke et al., 2014). Interestingly, the magnitude of the morphological abnormalities reported was smaller when compared with the defects we present in this report. Our behavioural experiments revealed no major differences in the locomotor activity and anxiety in these mice. They also acquired and retained spatial learning tasks known to depend on the hippocampus, with the same efficiency as their controls. Nevertheless, Vangl2^{Emx1} cKO mice failed when challenged with a modified testing situation that requires flexible use of spatial memories. Such a loss in memory flexibility is taken as evidence for deterioration in relational memory, the equivalent in animals of declarative memory in humans. Previously observed in old mice (e.g. Marighetto et al., 1999; Etchamendy et al., 2001; Mingaud et al.,

2008) and in old humans (Etchamendy et al., 2011), the loss of flexible memory expression was shown to be related to functional alterations of the hippocampus and prefrontal cortex (Etchamendy et al., 2011; Touzani et al., 2003, Mingaud et al., 2007; 2008). Interestingly the mutation also produced a deficit in spontaneous spatial alternation, shown to depend on the hippocampus and prefrontal cortex. Hence Vangl2 appears to be a critical player for the development of the neuronal circuitry within the hippocampus but might also be important for the circuitry between the hippocampus and the prefrontal cortex, needed for higher order cognitive function.

References

- Acsády, L., Katona, I., Gulyás, A. i., Shigemoto, R., and Freund, T. f. (1997). Immunostaining for substance P receptor labels GABAergic cells with distinct termination patterns in the hippocampus. *J. Comp. Neurol.* 378, 320–336.
- Amaral, D.G., and Dent, J.A. (1981). Development of the mossy fibers of the dentate gyrus: I. A light and electron microscopic study of the mossy fibers and their expansions. *J. Comp. Neurol.* 195, 51–86.
- Amaral, D.G., Ishizuka, N., and Claiborne, B. (1990). Neurons, numbers and the hippocampal network. *Prog. Brain Res.* 83, 1–11.
- Bayer, S.A. (1980). Development of the hippocampal region in the rat II. Morphogenesis during embryonic and early postnatal life. *J. Comp. Neurol.* 190, 115–134.
- Bayer, S.A., and Altman, J. (1974). Hippocampal development in the rat: cytogenesis and morphogenesis examined with autoradiography and low-level X-irradiation. *J. Comp. Neurol.* 158, 55–79.
- Belevich, I., Joensuu, M., Kumar, D., Vihinen, H., and Jokitalo, E. (2016). Microscopy Image Browser: A Platform for Segmentation and Analysis of Multidimensional Datasets. *PLoS Biol.* 14, e1002340.
- Claiborne, B.J., Amaral, D.G., and Cowan, W.M. (1986). A light and electron microscopic analysis of the mossy fibers of the rat dentate gyrus. *J. Comp. Neurol.* 246, 435–458.
- Etchamendy, N., Enderlin, V., Marighetto, A., Vouimba, R.M., Pallet, V., Jaffard, R., and Higeret, P. (2001). Alleviation of a selective age-related relational memory deficit in mice by pharmacologically induced normalization of brain retinoid signaling. *J. Neurosci.* 21, 6423–6429.
- Etchamendy, N., Konishi, K., Pike, G.B., Marighetto, A., and Bohbot, V.D. (2012). Evidence for a virtual human analog of a rodent relational memory task: a study of aging and fMRI in young adults. *Hippocampus* 22, 869–880.
- Ezan, J., and Montcouquiol, M. (2013). Revisiting planar cell polarity in the inner ear. *Seminars in Cell & Developmental Biology* 24, 499–506.
- Förster, E., Zhao, S., and Frotscher, M. (2006). Laminating the hippocampus. *Nat. Rev. Neurosci.* 7, 259–267.

- Gonzales, R.B., DeLeon Galvan, C.J., Rangel, Y.M., and Claiborne, B.J. (2001). Distribution of thorny excrescences on CA3 pyramidal neurons in the rat hippocampus. *J. Comp. Neurol.* 430, 357–368.
- Gorski, J.A., Talley, T., Qiu, M., Puellas, L., Rubenstein, J.L.R., and Jones, K.R. (2002). Cortical Excitatory Neurons and Glia, But Not GABAergic Neurons, Are Produced in the Emx1-Expressing Lineage. *J. Neurosci.* 22, 6309–6314.
- Henderson, D.J., Conway, S.J., Greene, N.D.E., Gerrelli, D., Murdoch, J.N., Anderson, R.H., and Copp, A.J. (2001). Cardiovascular Defects Associated With Abnormalities in Midline Development in the Loop-tail Mouse Mutant. *Circ Res* 89, 6–12.
- Henze, D.A., Urban, N.N., and Barrionuevo, G. (2000). The multifarious hippocampal mossy fiber pathway: a review. *Neuroscience* 98, 407–427.
- Jin, X. (2016). The role of neurogenesis during development and in the adult brain. *Eur J Neurosci* n/a-n/a.
- Kibar, Z., Bosoi, C.M., Kooistra, M., Salem, S., Finnell, R.H., De Marco, P., Merello, E., Bassuk, A.G., Capra, V., and Gros, P. (2009). Novel mutations in VANG1 in neural tube defects. *Hum. Mutat.* 30, E706–E715.
- Kibar, Z., Vogan, K.J., Groulx, N., Justice, M.J., Underhill, D.A., and Gros, P. (2001a). Ltap, a mammalian homolog of Drosophila Strabismus/Van Gogh, is altered in the mouse neural tube mutant Loop-tail. *Nat Genet* 28, 251–255.
- Knierim, J.J. (2015). The hippocampus. *Current Biology* 25, R1116–R1121.
- Lanore, F., Labrousse, V.F., Szabo, Z., Normand, E., Blanchet, C., and Mulle, C. (2012). Deficits in morphofunctional maturation of hippocampal mossy fiber synapses in a mouse model of intellectual disability. *J. Neurosci.* 32, 17882–17893.
- Lazarov, O., and Hollands, C. (2016). Hippocampal neurogenesis: Learning to remember. *Progress in Neurobiology* 138–140, 1–18.
- Lee, O.-K., Frese, K.K., James, J.S., Chadda, D., Chen, Z.-H., Javier, R.T., and Cho, K.-O. (2003). Discs-Large and Strabismus are functionally linked to plasma membrane formation. *Nat Cell Biol* 5, 987–993.
- Lei, Y.-P., Zhang, T., Li, H., Wu, B.-L., Jin, L., and Wang, H.-Y. (2010). VANG2 Mutations in Human Cranial Neural-Tube Defects. *New England Journal of Medicine* 362, 2232–2235.

- Marighetto, A., Etchamendy, N., Touzani, K., Torrea, C.C., Yee, B.K., Rawlins, J.N., and Jaffard, R. (1999). Knowing which and knowing what: a potential mouse model for age-related human declarative memory decline. *Eur. J. Neurosci.* 11, 3312–3322.
- Mingaud, F., Le Moine, C., Etchamendy, N., Mormède, C., Jaffard, R., and Marighetto, A. (2007). The hippocampus plays a critical role at encoding discontinuous events for subsequent declarative memory expression in mice. *Hippocampus* 17, 264–270.
- Mingaud, F., Mormede, C., Etchamendy, N., Mons, N., Niedergang, B., Wietrzyk, M., Pallet, V., Jaffard, R., Krezel, W., Higuieret, P., et al. (2008). Retinoid hyposignaling contributes to aging-related decline in hippocampal function in short-term/working memory organization and long-term declarative memory encoding in mice. *J. Neurosci.* 28, 279–291.
- Nagaoka, T., Ohashi, R., Inutsuka, A., Sakai, S., Fujisawa, N., Yokoyama, M., Huang, Y.H., Igarashi, M., and Kishi, M. (2014a). The Wnt/Planar Cell Polarity Pathway Component Vangl2 Induces Synapse Formation through Direct Control of N-Cadherin. *Cell Reports* 6, 916–927.
- Ramsbottom, S.A., Sharma, V., Rhee, H.J., Eley, L., Phillips, H.M., Rigby, H.F., Dean, C., Chaudhry, B., and Henderson, D.J. (2014). Vangl2-regulated polarisation of second heart field-derived cells is required for outflow tract lengthening during cardiac development. *PLoS Genet.* 10, e1004871.
- Rollenhagen, A., Sätzler, K., Rodríguez, E.P., Jonas, P., Frotscher, M., and Lübke, J.H.R. (2007). Structural Determinants of Transmission at Large Hippocampal Mossy Fiber Synapses. *J. Neurosci.* 27, 10434–10444.
- Seo, J.H., Zilber, Y., Babayeva, S., Liu, J., Kyriakopoulos, P., Marco, P.D., Merello, E., Capra, V., Gros, P., and Torban, E. (2015). Mutations in the planar cell polarity gene, Fuzzy, are associated with neural tube defects in humans. *Hum. Mol. Genet.* 24, 3893–3893.
- Singh, J., and Mlodzik, M. (2012). Planar cell polarity signaling: coordination of cellular orientation across tissues. *WIREs Dev Biol* 1, 479–499.
- Stein, K.F., and Mackensen, J.A. (1957). Abnormal development of the thoracic skeleton in mice homozygous for the gene for looped-tail. *Am. J. Anat.* 100, 205–223.
- Strong, L.C., and Hollander, W.F. (1949). Hereditary loop-tail in the house mouse accompanied by imperforate vagina and with lethal craniorachischisis when homozygous. *Journal of Heredity* 40, 329–334.
- Strutt, H., and Strutt, D. (2009). Asymmetric localisation of planar polarity proteins: Mechanisms and consequences. *Seminars in Cell & Developmental Biology* 20, 957–963.

- Tissir, F., and Goffinet, A.M. (2006). Expression of planar cell polarity genes during development of the mouse CNS. *European Journal of Neuroscience* 23, 597–607.
- Tissir, F., and Goffinet, A.M. (2013). Shaping the nervous system: role of the core planar cell polarity genes. *Nat Rev Neurosci* 14, 525–535.
- Torban, E., Iliescu, A., and Gros, P. (2012). Chapter Ten - An Expanding Role of Vangl Proteins in Embryonic Development. In *Current Topics in Developmental Biology*, Y. Yang, ed. (Academic Press), pp. 237–261.
- Torban, E., Wang, H.-J., Patenaude, A.-M., Riccomagno, M., Daniels, E., Epstein, D., and Gros, P. (2007). Tissue, cellular and sub-cellular localization of the Vangl2 protein during embryonic development: effect of the Lp mutation. *Gene Expr. Patterns* 7, 346–354.
- Touzani, K., Marighetto, A., and Jaffard, R. (2003). Fos imaging reveals ageing-related changes in hippocampal response to radial maze discrimination testing in mice. *Eur. J. Neurosci.* 17, 628–640.
- Walck-Shannon, E., and Hardin, J. (2014). Cell intercalation from top to bottom. *Nat Rev Mol Cell Biol* 15, 34–48.
- Wallingford, J.B. (2012). Planar cell polarity and the developmental control of cell behavior in vertebrate embryos. *Annu. Rev. Cell Dev. Biol.* 28, 627–653.
- Wang, Y., and Nathans, J. (2007). Tissue/planar cell polarity in vertebrates: new insights and new questions. *Development* 134, 647–658.
- Wilke, S.A., Antonios, J.K., Bushong, E.A., Badkoobehi, A., Malek, E., Hwang, M., Terada, M., Ellisman, M.H., and Ghosh, A. (2013). Deconstructing complexity: serial block-face electron microscopic analysis of the hippocampal mossy fiber synapse. *J. Neurosci.* 33, 507–522.
- Yates, L.L., Papakrivopoulou, J., Long, D.A., Goggolidou, P., Connolly, J.O., Woolf, A.S., and Dean, C.H. (2010a). The planar cell polarity gene Vangl2 is required for mammalian kidney-branching morphogenesis and glomerular maturation. *Hum. Mol. Genet.* 19, 4663–4676.
- Yates, L.L., Schnatwinkel, C., Murdoch, J.N., Bogani, D., Formstone, C.J., Townsend, S., Greenfield, A., Niswander, L.A., and Dean, C.H. (2010b). The PCP genes Celsr1 and Vangl2 are required for normal lung branching morphogenesis. *Hum. Mol. Genet.* 19, 2251–2267.
- Yoshioka, T., Hagiwara, A., Hida, Y., and Ohtsuka, T. (2013). Vangl2, the planar cell polarity protein, is complexed with postsynaptic density protein PSD-95. *FEBS Letters* 587, 1453–1459.

Figure Legends

Figure 1. Vangl2 mRNA is expressed in the developing mouse hippocampus. A, In situ hybridization of *vangl2* in newborn mice (P0) shows that Vangl2 mRNA is expressed throughout the brain but is enriched in the Cortex (Cx), CA1, CA3 and Dentate Gyrus (DG) regions of the hippocampus, the thalamus (Th) and in the Habenula (Hb). B, At P7 *vangl2* mRNA profile is similar, but a bit more restricted compared with P0 mice. C, At P21, *vangl2* mRNA expression is weaker when compared to younger stages (P0 & P7) and it still expressed in the hippocampus where it appears to be stronger in the DG when compared to CA1 and CA3. All three stages were processed simultaneously to allow comparison.

Figure 2: Vangl2 is enriched in DG neurites projections. A, Immunostaining against endogenous Vangl2 in P14 mouse brain shows that Vangl2 protein is present in the entire hippocampus, and enriched in the dentate gyrus (DG) subgranular zone (SGZ) and in the CA3 *stratum lucidum* (*sl*) of the hippocampus. B, At P21 Vangl2 protein expression is more confined than in P14 mice brains and Vangl2 but still enriched in the DG SGZ as well as in areas where DG neurites (axons and dendrites) project: the *stratum moleculare* (*sm*) and the *sl*. Note that Vangl2 is also expressed in the corpus callosum (CC), in the ependymal cells lining the ventricles (Ep) (red asterisk), as well as in more ventral regions such as the Hb and the Th (yellow asterisk), but not much in the hippocampal fimbria (Fb). Compared to mRNAs expression, the protein is excluded from the cell bodies of the GC, and targeted to the neurites. C, Schematic representation of the morphogenesis of the DG-CA3 circuit. At P21, the MfB/TE synapse is considered morphologically mature with a TE engulfed by a large MfB. These synapses contain multiple active zones/post-synaptic densities (PSD)(magenta spots in green MfB) and the pre- and post-synaptic elements are attached to each other via *puncta adhaerentia* (blue light), junction sites rich in adhesion proteins such as N-cadherin, Nectins and Afadins. This schematic demonstrates the increased size and morphological complexity of the MfB-TE synapse formed between the DG GCs and CA3 pyramidal neurons in the *sl* (in gray), but also the synaptic contacts formed by enthorinal cortical neurons on the same CA3 pyramidal neurons in the *stratum radiatum* (*sr*) (depicted in light blue). D, High-magnification image of Vangl2 (red) and DCX (green) in the hippocampus shows that these proteins colocalize in the SGZ of the DG as well as in the CA3 *sl*. E, Vangl2 (red) and NeuN (green) do not colocalize in the granular cell layer (GCL) of the DG and the pyramidal CA3 areas. F, Vangl2 (red) and Znt3 (green) are both present in the CA3 *sl* but do not colocalize. G, Vangl2 (red) and Map2 (green) colocalize in the dendritic region of the DG, the *sm*. H, Vangl2 (red) and N-cadherin (green) colocalize in the dendrites (in the *sm*) and the SGZ of the DG.

Figure 3: Conditional deletion of Vangl2 affects the development of the hippocampus. A, Vangl2 is expressed in mouse hippocampus and enriched in the dentate gyrus (DG) and CA3 *sl*. We validated *in vivo* the deletion of *vangl2* in the hippocampus of Vangl2^{Emx1} mice at P21. Note that Vangl2 staining in more ventral regions (midbrain) devoid of Cre recombinase expression such as the thalamus (yellow asterisk) is still present in the Vangl2^{Emx1} mouse, confirming both the specificity of our antibody and the precise deletion of *vangl2* in more dorsal regions of the brain (telencephalon). B, In absence of *vangl2* we observed an increase of Synaptoporin and Neurofilament staining in the CA3 *stratum pyramidale* (*sp*) (between the depicted blue lines) which can be interpreted as a probable default in axonal guidance or fasciculation. C, Quantifications of Fiber density of Neurofilament and Synaptoporin staining in the *sp* show a significant increase in Vangl2^{Emx1} mice. D, In Vangl2^{Emx1} mice, Bassoon and Synaptoporin fluorescence are reduced in the CA3 *sl* (between the depicted blue lines) suggesting a decrease in the synaptic content or a decrease of molecule content per synapse, or both. E, Quantifications of normalized Fluorescence Intensity normalized for Bassoon and Synaptoporin in the *sl* show a significant decrease. For axon guidance/bundling defaults: NF-H: control: n=17 hippocampi from 4 different mice, Vangl2^{Emx1}: n=21 hippocampi from 4 different Vangl2^{Emx1} mice; and Synaptoporin: control: n=17 hippocampi from 4 mice; Vangl2^{Emx1}: n=21, 4 Vangl2^{Emx1} mice. For staining quantification in the SL: Bassoon: n=5 different mice for each condition, Synaptoporin: n=5 different mice for each condition. Unpaired *t*-test: **p*<0,05.

Figure 4. The presynaptic mossy fibers boutons (MfBs) are smaller in Vangl2^{Emx1} mice. A, Schematic representation of the experimental procedure. AAV-CaMKII-mCherry virus is injected bilaterally in the DG granular cells layer in pups (P5). After 20 days, tissues were prepared for imaging. B, Pictures of the hippocampus (left top panel, false green color) and the mossy fibers (Mf) labeled with mcherry in the *sl* (right top panel). The dotted zone represents the zone of synaptic boutons and the arrow shows a synaptic bouton. The bottom panels show the projection of 3D-reconstructed confocal image stacks of presynaptic MfB labeled by virus infection at P25 in control mice. Green: image projection of Mf reconstructed with Imaris software, red: presynaptic boutons reconstructed with surface rendering. C,D,E Examples of presynaptic terminals reconstructed with Imaris software for control and Vangl2^{Emx1} mice at P25. F, Graph of the presynaptic terminal volume, the index of complexity calculated by dividing the volume by the area, the number of filopodia per presynaptic bouton and the percentage of boutons with filopodia at P25 for control and Vangl2^{Emx1} mice. Number of boutons: control: n=47, Vangl2^{Emx1}: n=57; Student *t*-test: ***p*<0.01, ****p*<0.001.

Figure 5. The MfB/TE synapse is smaller in Vangl2^{Emx1} mice. A, Control *sl*, showing large, smooth dendrites (in green), and well defined Mossy fiber Boutons (MfBs) contactin one or more Thorny excrescences (TE) (in yellow and light blue). B, In Vangl2^{Emx1} mice, the structure

and organization of the section lacks large MfBs and Thorny Excrescences (TEs) in the *sl*. A, 3D rendering of the entire EM stack of one dendrite in control mice. Large MfBs (in yellow, orange and blue light) are seen to interdigitate with TEs and cover part of the dendrite surface (in green). Although not visible in these images synaptic structures between TE and MfB are also present, buried within. At several points TE can be seen to partly emerge from the edges of MfBs (magenta arrows) and are differentiated by their color being distinct from their MfB (red spot in the yellow MfB, blue light spot in the orange MfB and yellow spot in the blue light MfB). Note also the smooth structure of the dendrites outside the MfB/TE region (black asterisk). A', another 3D rendering from a neighboring dendrite in a control mouse. Again, MfBs are present (dark blue, purple) with TE partly emerging from these boutons (blue light spot in dark MfB, grey, blue light and red spots in the purple MfB) and dendrites (beige) are smooth. A'', 3D rendering of the entire EM stack of an entire dendritic region region in control mice. B, B' In $Vangl2^{Emx1}$ mice simple spines (yellow asterisk) appear in place of the digitated TEs and are more numerous, visible along the entire length of both the blue (B) and green (B') dendrites with a single PSD at the tip (red spots indicated by yellow arrows in B). Lastly small Mf are also present and rendered in pink, red, light blue and orange, their synapses are not the large complex structures they were in control animal. B'', 3D rendering of the entire EM stack of an entire dendritic region in $Vangl2^{Emx1}$ mice. C, Quantifications of the average volume of TEs and MfBs show a significant decrease in both parameters in $Vangl2^{Emx1}$ mice. D, Cumulative distribution of TE volume shows that $Vangl2^{Emx1}$ mice have a large range of spines volumes in contrast with a much narrower range of TEs in control mice, mostly large. E, Graph showing the distribution of PSD volume for control and $Vangl2^{Emx1}$ mice and quantifications of post-synaptic densities (PSD) show that there is a larger number of PSDs in $Vangl2^{Emx1}$ samples. Moreover, the distribution of values shows a more negative skew for $Vangl2^{Emx1}$ mice and is reflected in the bigger average volume for these mice. The ratio of PSDs per TEs confirm that in $Vangl2^{Emx1}$ mice there is a significant reduction of the number of PSDs in TEs. Average PSD volume of TEs in the *sl* demonstrates that in $Vangl2^{Emx1}$ mice the PSD volumes are higher when compared to controls. Number of boutons: control: n=9, $Vangl2^{Emx1}$: n=5; Number of TEs: control: n=19, $Vangl2^{Emx1}$: n=180; Number of PSDs: control: n=83, $Vangl2^{Emx1}$: n=150. Unpaired t-test: *** $p < 0.0001$.

Figure 6. Anxiety, locomotor activity and spatial memory were not affected by $Vangl2$ mutation in mice.

A, Graph of the time spent and the latency to the first entry in the open arms of the plus-maze test. B, Graph of the time spent in the white box of the dark/light test. C, Graph of the number of rearings and activity during the locomotor activity. D, Graph of the percentage of alternations in the spontaneous working memory Y-maze test. E, Latency to escape of the water maze test during the visual, spatial and reversal acquisition. F, Time spent in the four quadrants of the water maze during the probe test at 10 days during the spatial acquisition. T: target, A.L:

adjacent left, O: opposite, A.R: adjacent right. Number of animals: control: n=15, Vangl2^{Emx1}: n=15; One sample *t*-test: #*p*<0.05.

Figure 7. Vangl2^{Emx1} mice displayed a deficit in flexibility of relational/declarative memory.

A, Schematic representation of the radial maze protocol. B, Graph of the number of days to meet the acquisition criterion, and of the percentage of correct responses during the first five days and the last five days of training. C, Graph of the evolution of percentage of correct responses between the last day of acquisition (D-1) and the Test for the critical pairs (left: Pairs A and B recombined into Pair AB in the Test, representing the critical flexibility probe) and control pairs (middle: Pair C is an “unchanged learnt” control; right: Pair N is an “unlearned” control appearing in Test only). Number of animals: control: n=11, Vangl2^{Emx1}: n=18; Bonferroni comparison, D-1 versus Test for control mice : *p*>0.05; Vangl2^{Emx1} mice: *** *p*<0.001.

Table1: Table showing detailed volume data of MfB and TE 3D reconstructions with SBFsEM.

Supplementary Figure 1: Linescans of double-immunohistochemical staining in the hippocampus. In order to better illustrate co-localization of protein in the DG we traced a line crossing the entire upper part of the DG, from the hilus to the *stratum moleculare* (*sm*) (yellow line in Sup. Fig. 2A). A, Results show that in the DG, Vangl2 and DCX present an almost identical profile throughout the DG and the surrounding layers in the subgranular zone (SGZ) (black arrow) and in the *sm* (light blue). B, In the CA3 upper part (blue light line in Sup. Fig. 2D), close to the CA2 region, starting in the *stratum radiatum* (*sr*) until the *stratum pyramidale*, where pyramidal cells are packed. We traced such line carefully so that the line crossed both axonal projections and synaptic terminals located in the *sl*. In the CA3, both Vangl2 and DcX proteins are enriched in the *stratum lucidum* (*sl*), as demonstrated in the respective linescan (black arrow). C, Linescan in the CA3 for Vangl2 and Tau staining demonstrates that these proteins are enriched in the *sl* and have similar profile of expression (black arrows). D, Linescan in the CA3 for Vangl2 and Znt3 staining shows that these proteins expression profile does not overlap (black arrows). E, Linescan in the CA3 for Vangl2 and PSD-95 staining shows that these proteins expression profile does not overlap in this region (black arrows). F, Linescan in the DG for Vangl2 and PSD-95 staining shows that these proteins have similar expression profiles in both the SGZ (black arrow) and the *sm* (blue light arrow). G, Linescan in the CA3 for Vangl2 and Map2 staining shows that these proteins expression profile does not overlap (black arrows).

Supplementary Figure 2: Vangl2 is enriched in DG neurite projections. A, High-magnification acquisition of double-immunostainings against Vangl2 (red) and Kv2.1 (green) in the dentate gyrus (DG) shows that these proteins do not co-localize in the granular cell layer (GCL). The yellow line illustrates how linescans were drawn in the DG to analyze protein expression profiles. B, Double-immunostaining against Vangl2 (red) and Nestin (green) shows that these

proteins do not co-localize in the subgranular zone (SGZ) of the DG. C, Vangl2 (red) and Tau (green) proteins co-localize in the *stratum lucidum* (sl). D, Vangl2 (red) and Map2 (green) staining shows that these proteins do not co-localize in the sl. The blue light line illustrates how linescans were drawn in the CA3 to analyze protein expression profiles. E, Vangl2 (red) and PSD-95 (green) staining shows that these proteins do not co-localize in the sl. High-magnification acquisition of double-immunostainings against Vangl2 (red) and PSD-95 (green) in the DG shows that these proteins co-localize in the DG SGZ as well as in GC dendrites in the *stratum moleculare* (sm).

Supplementary Figure 3: Example of EM images of control and Vangl2^{Emx1} samples. These EM images were used to create the 3D renders that are shown in Fig.3.

Supplementary Figure 4: Analysis of classical spine morphology in the hippocampal *stratum radiatum* of Vangl2^{Emx1} mice. A, Example of EM images in the *stratum radiatum* (sr). Three dendrites were modelled (red, green and blue), in addition the spines for the blue dendrite are shown in yellow, adjacent. PSD are visible at some spine tips. 3D rendering of an entire EM stack. In Vangl2^{Emx1} three dendrites are shown (red, green, dark blue) with their associated spines (yellow, orange a light blue respectively). B, Quantification of the average volume of spines show a significant increase in Vangl2^{Emx1} mice, with the cumulative distribution of spine volume in cKO presenting a shift rightward when compared to controls. C, This graph demonstrates that the PSDs in controls have a larger range that in Vangl2^{Emx1} samples. Moreover, cKO have an overall larger number of PSDs throughout the sample. Statistical analysis of PSDs volume of spines located in the sr demonstrates that there are no differences between control and Vangl2^{Emx1} mice. D, Quantification of PSDs per spine in the sr shows that there is no difference in number between control and cKO samples. Number of spines: control: n=56, Vangl2^{Emx1}: n=81; Number of PSDs: control: n=43, Vangl2^{Emx1}: n=73. Unpaired *t*-test: ****p*<0.0001.

Supplementary Figure 5: Vangl2 overexpression via Single-cell-electroporation in CA3 induces morphological changes in neuron morphology. A, Schematic representation of single-cell electroporation (SCE). B, Image showing a CA3 pyramidal neuron electroporated via SCE with a plasmid expressing GFP only. C-D Images showing a CA3 pyramidal neuron electroporated via SCE with a construct expressing GFP-Vangl2 at 50 ng/ml. GFP-Vangl2 is enriched in large and complex structures (green arrows) located near to the neuron cell body that resemble TEs. E, Image showing a CA3 pyramidal neuron electroporated via SCE with 200 ng/ml of a plasmid expressing GFP-Vangl2. At this concentration, Vangl2 increases the complexity of the neurites of infected CA3 cells.

Figures

Figure 1

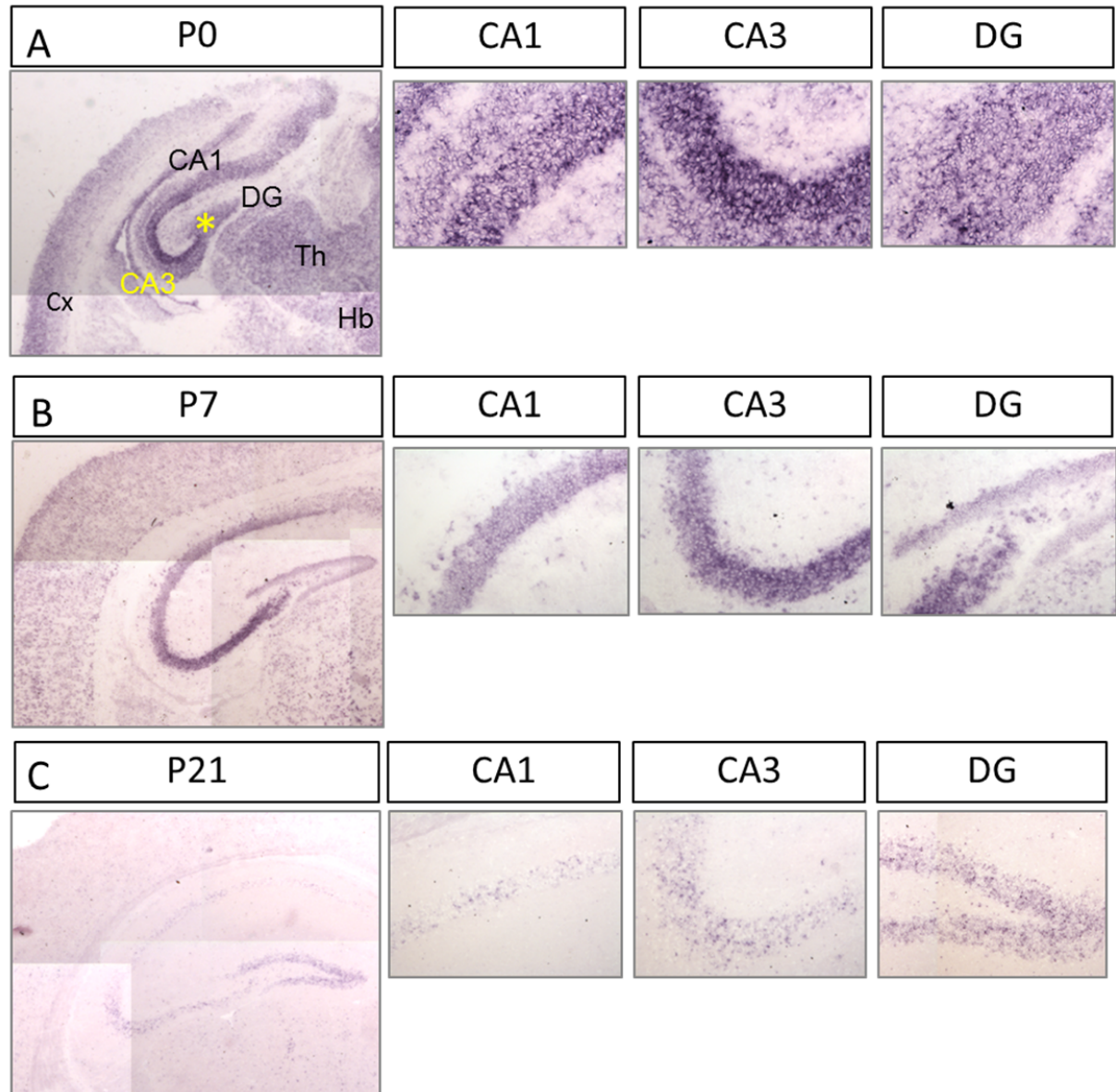


Figure 2

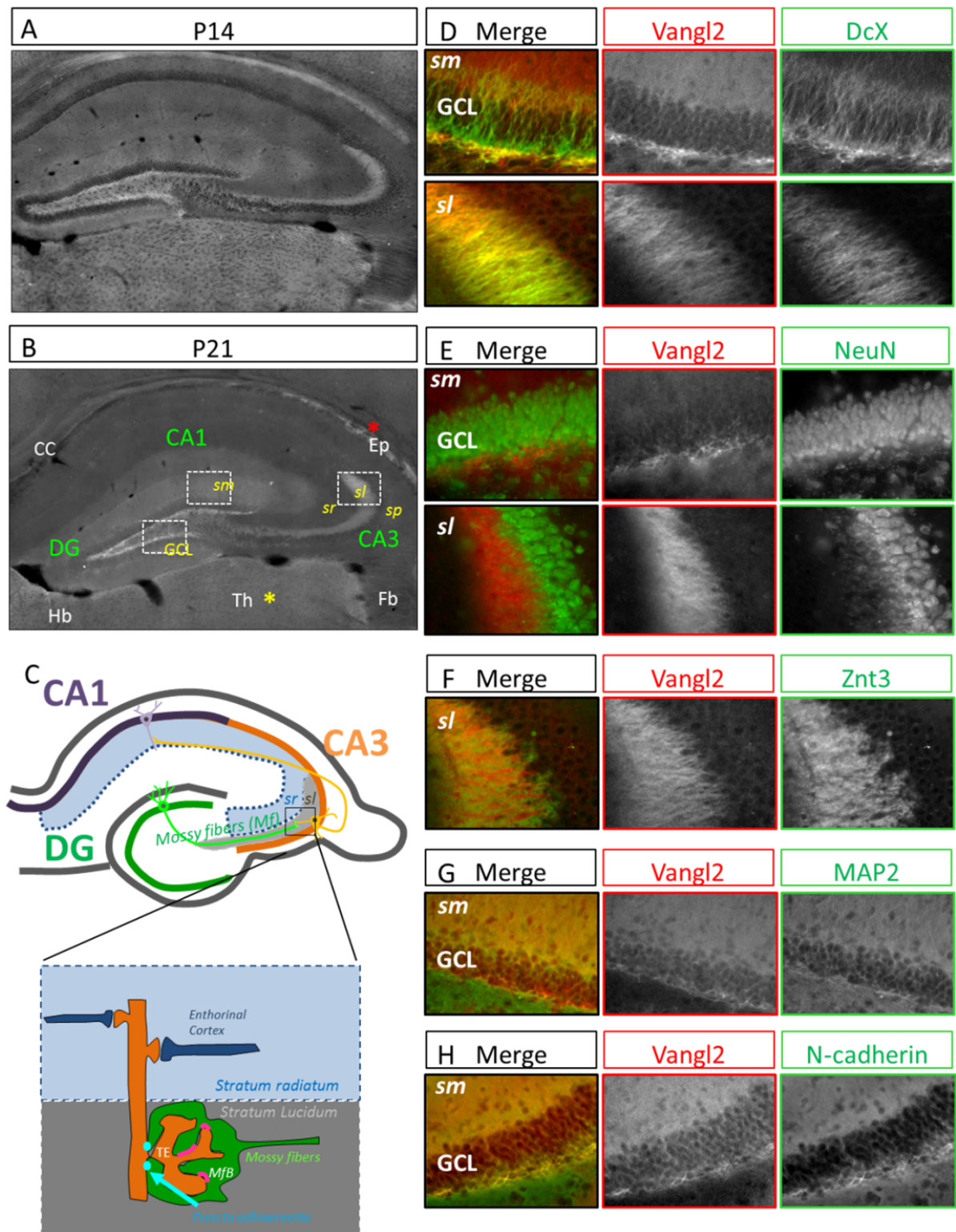


Figure 3

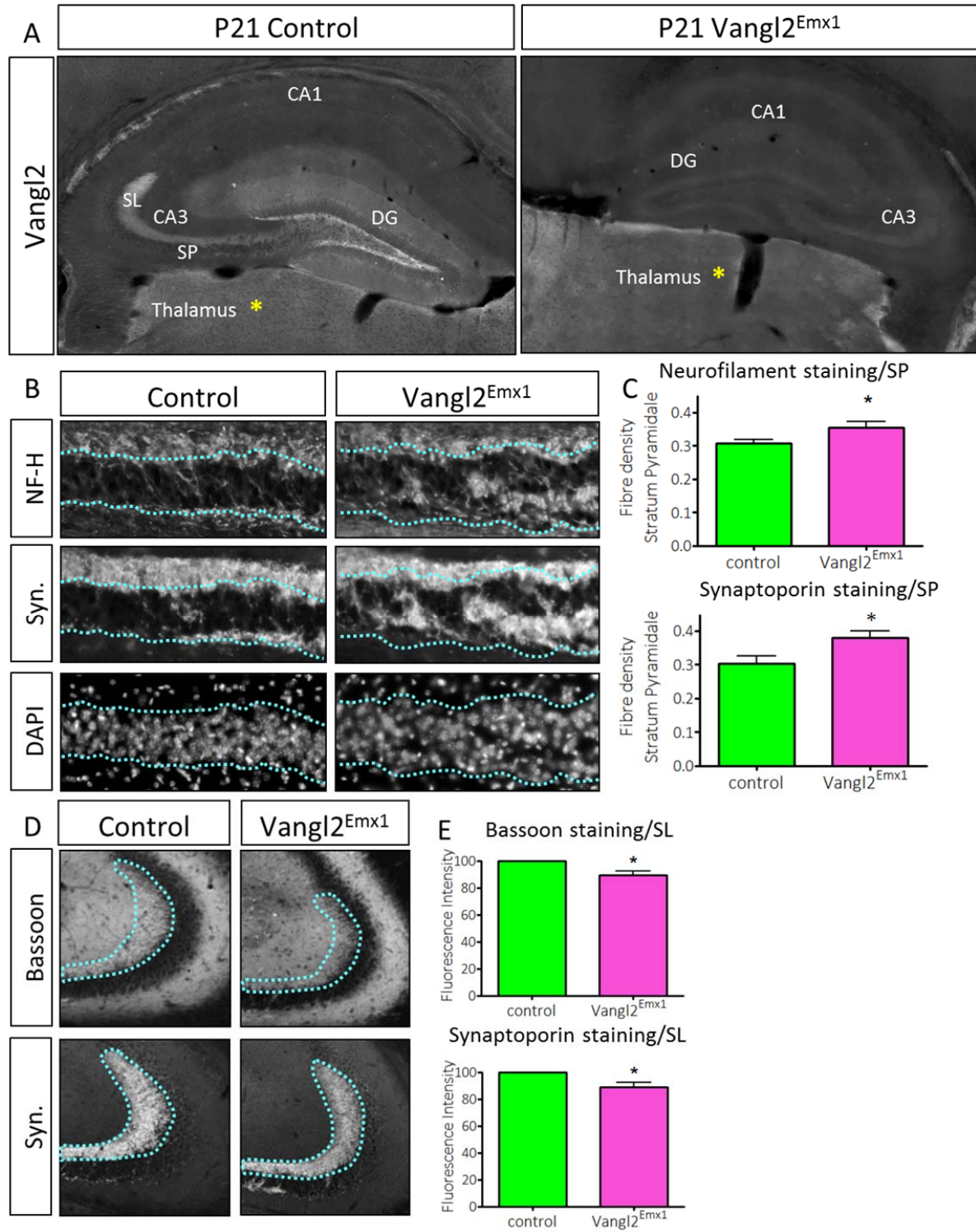


Figure 4

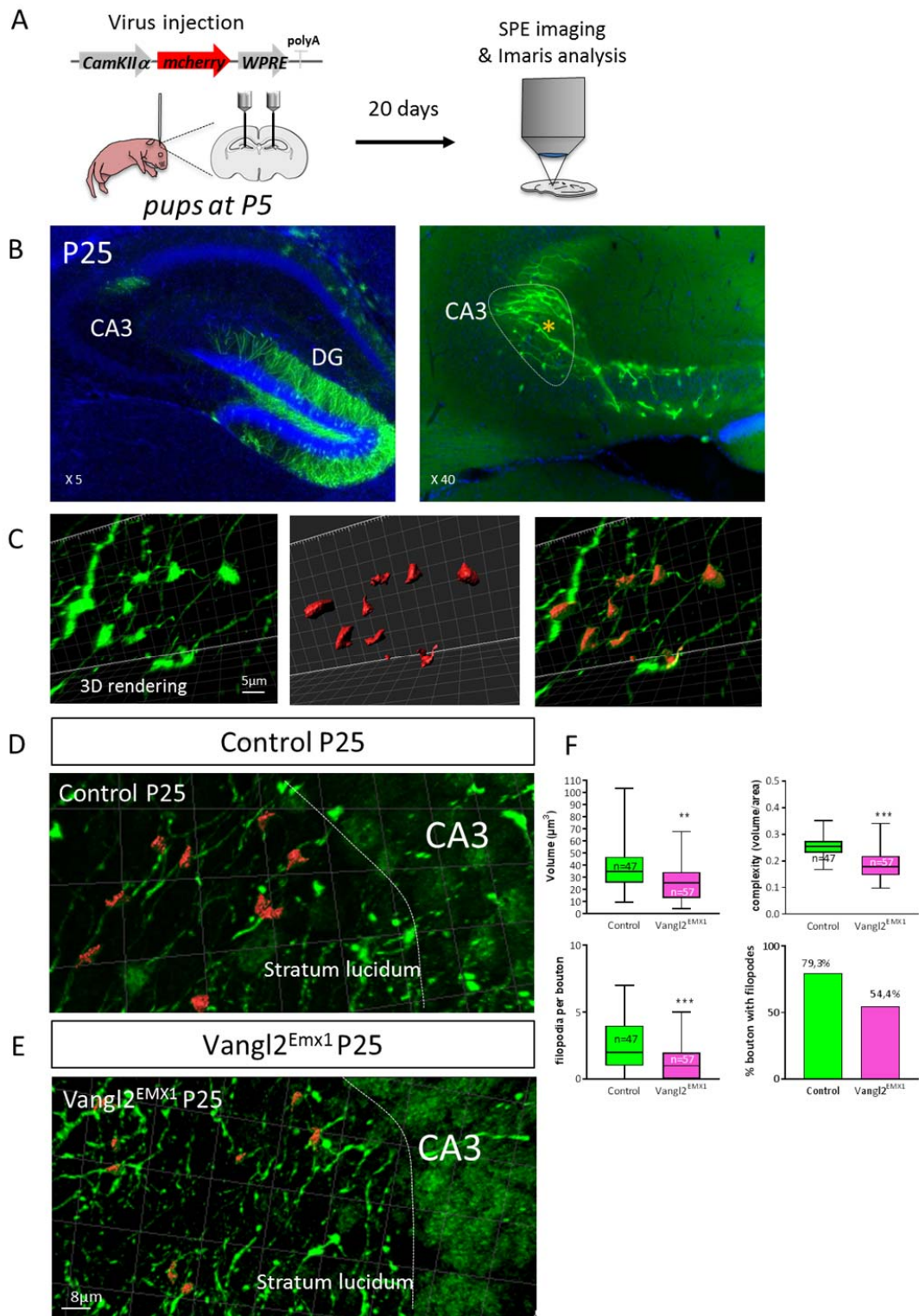


Figure 5

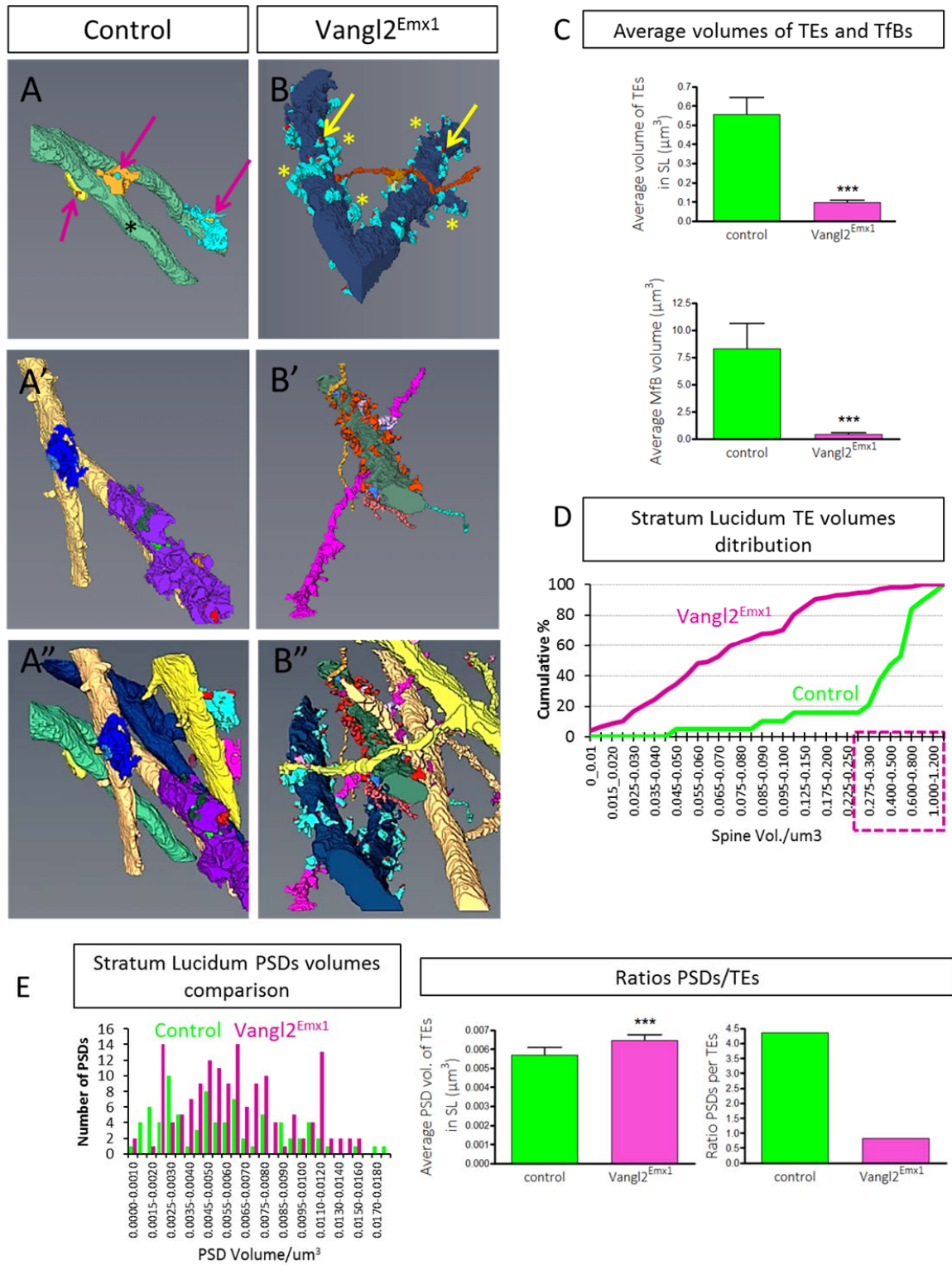


Figure 6

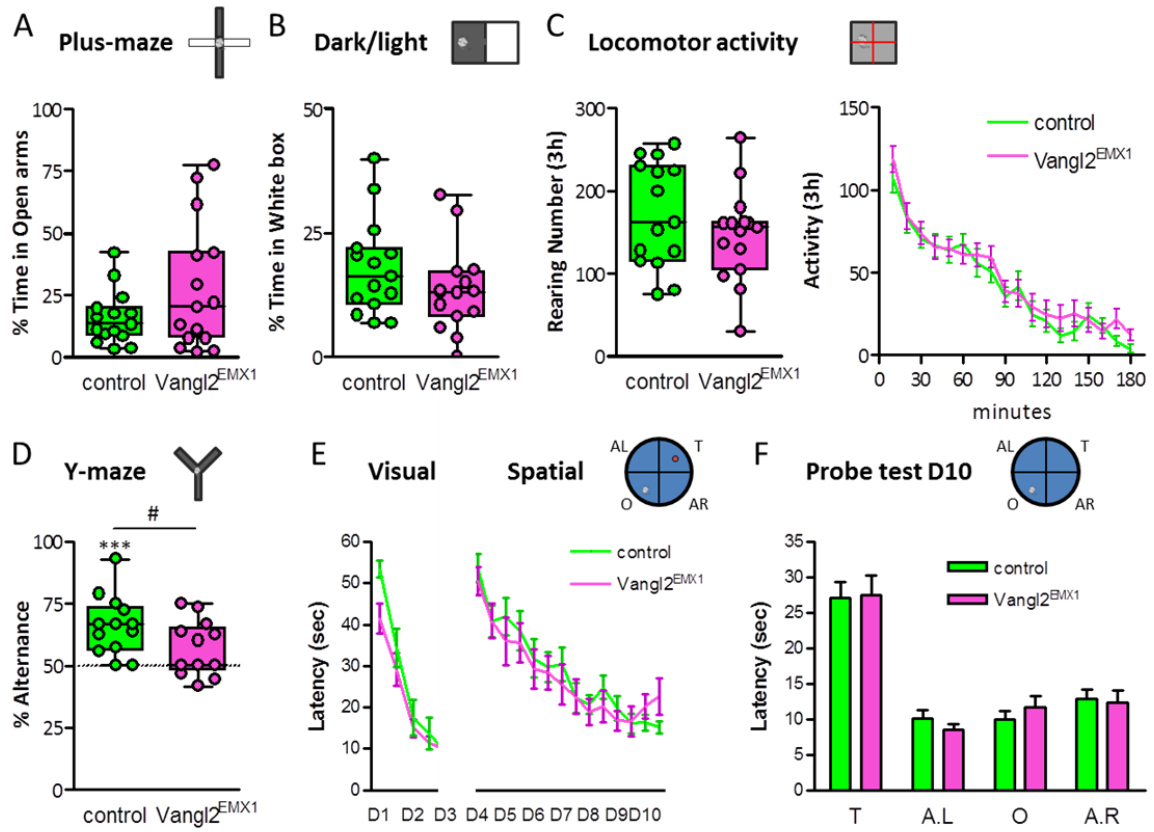


Figure 7

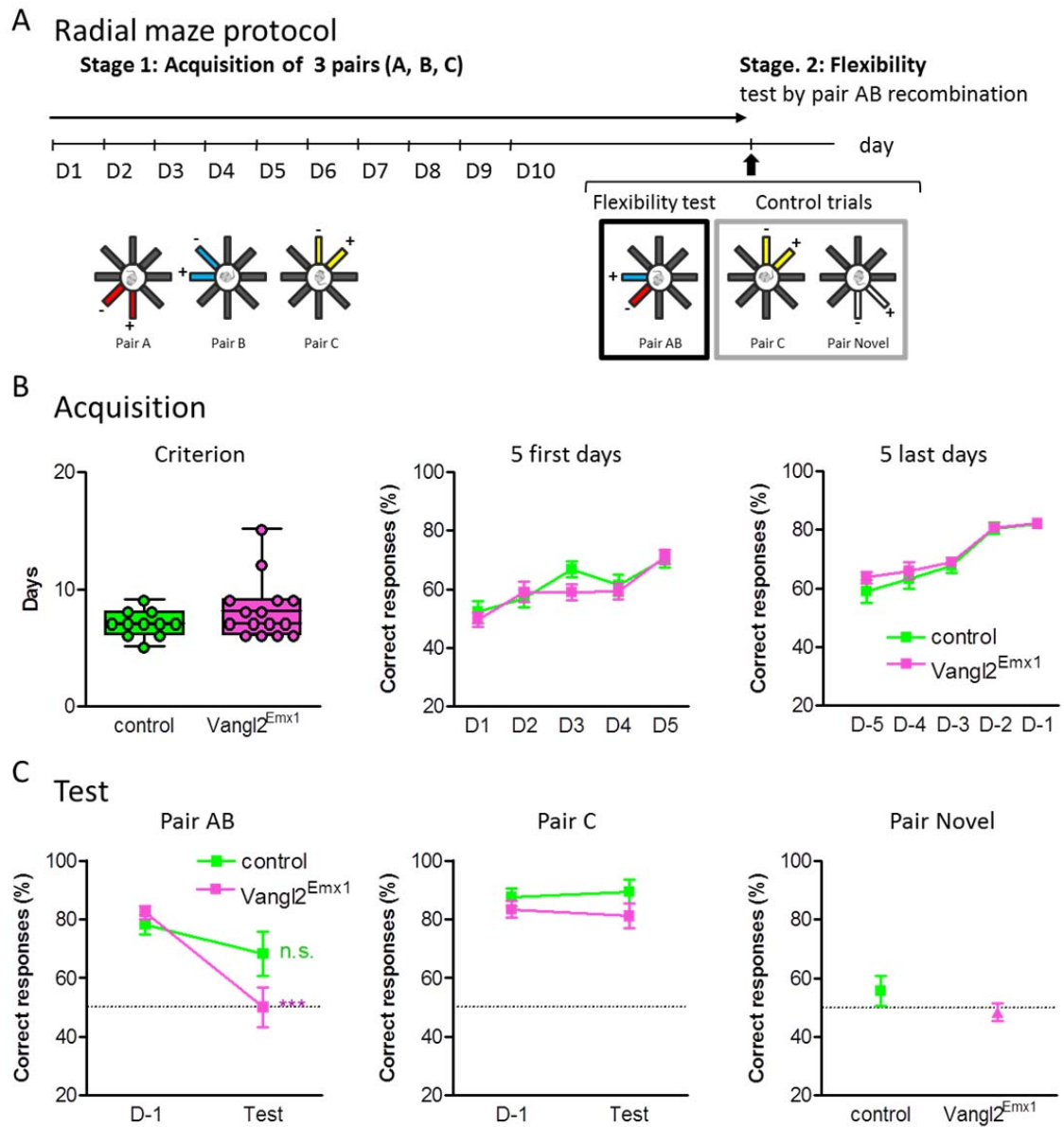
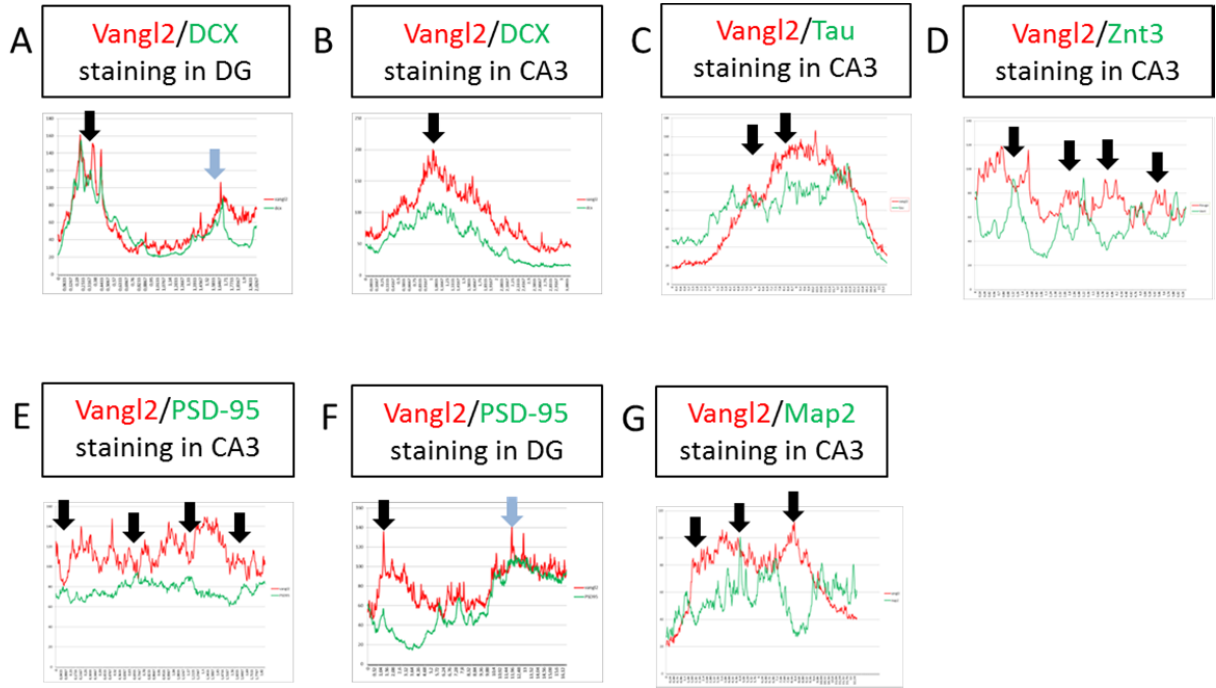


Table1

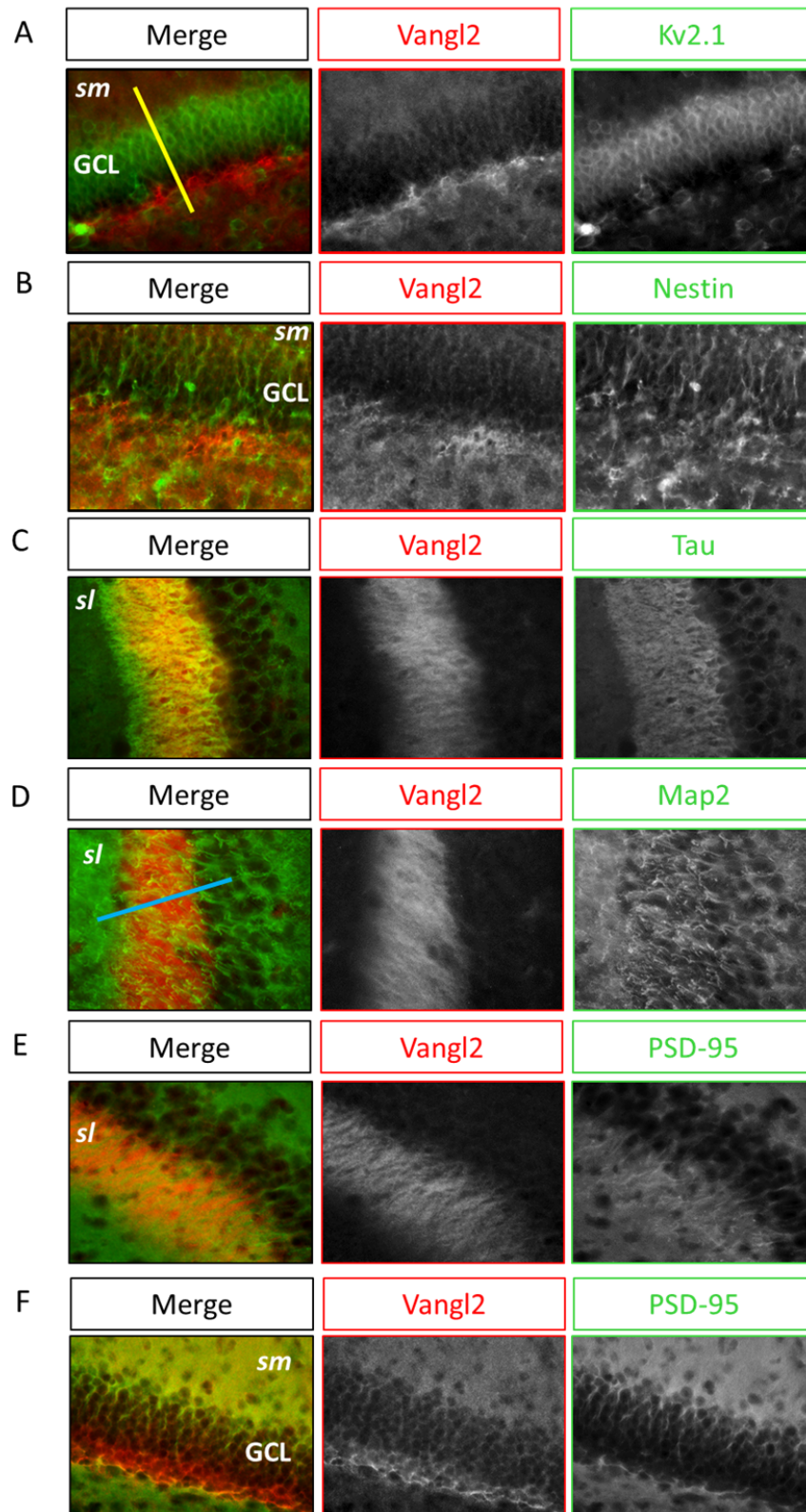
Morphometric data, significant differences are marked ‘’*

	Stratum Lucidum		Stratum Radiatum	
	Control	Vangl2^{Emx1}	Control	Vangl2^{Emx1}
Number of TE	19	180	56	81
Average Spine Vol. (μm^3) \pm SEM	*0.5560 \pm 0.086	0.0982 \pm 0.00941	*0.0899 \pm 0.0128	0.4450 \pm 0.0656
Average Density of TE or Spines \pm SEM	*0.0430 \pm 0.0155	0.5960 \pm 0.168	*0.5040 \pm 0.120	1,0260 \pm 0.134
Number of PSD	83	150	43	73
Average PSD Vol. (μm^3) \pm SEM	*0.00568 \pm 0.0004	0.00648 \pm 0.000263	0.00578 \pm 0.000519	0.00588 \pm 0.00050
MfB Volume (μm^3) \pm SEM	*8.287 \pm 2.315	0.409 \pm 0.133	N/A	N/A

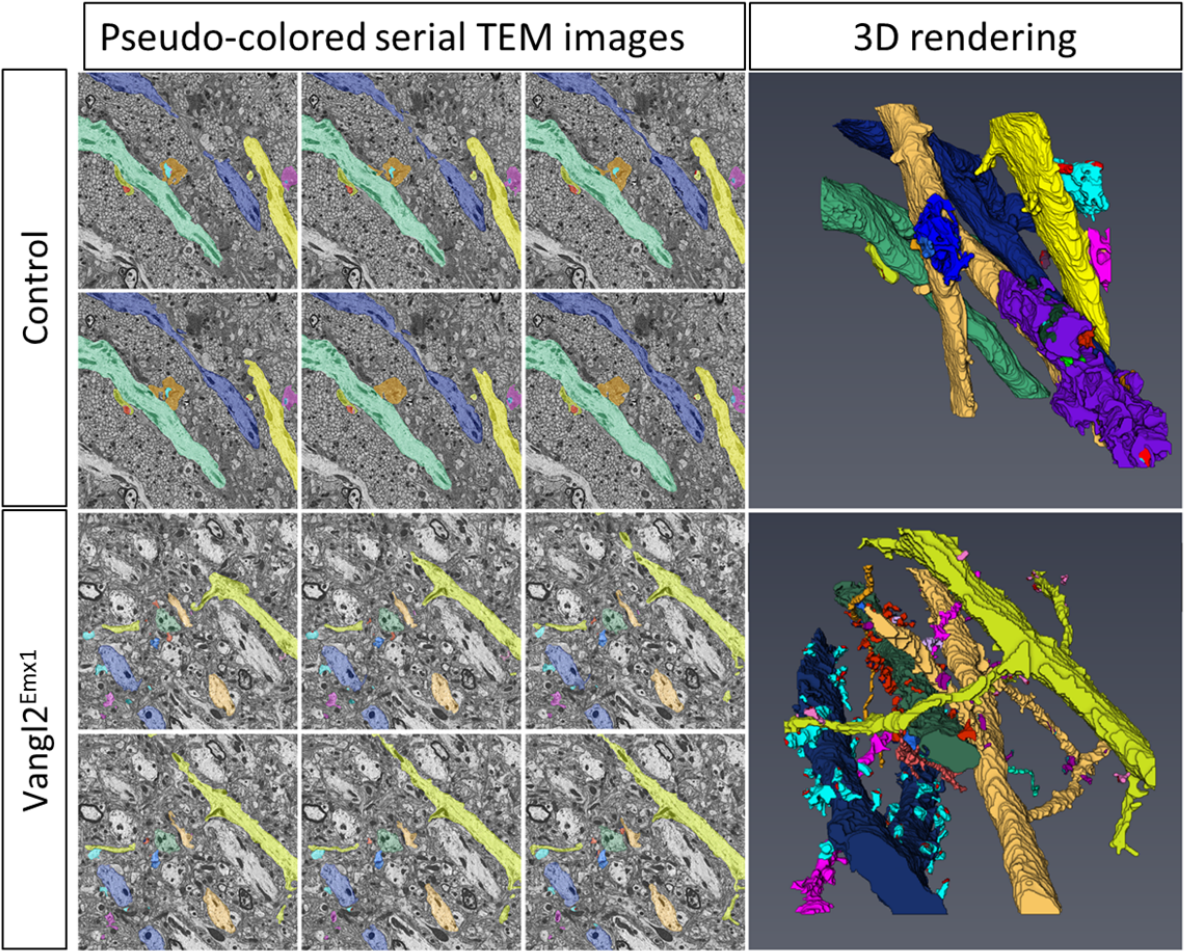
Supplementary Figure 1



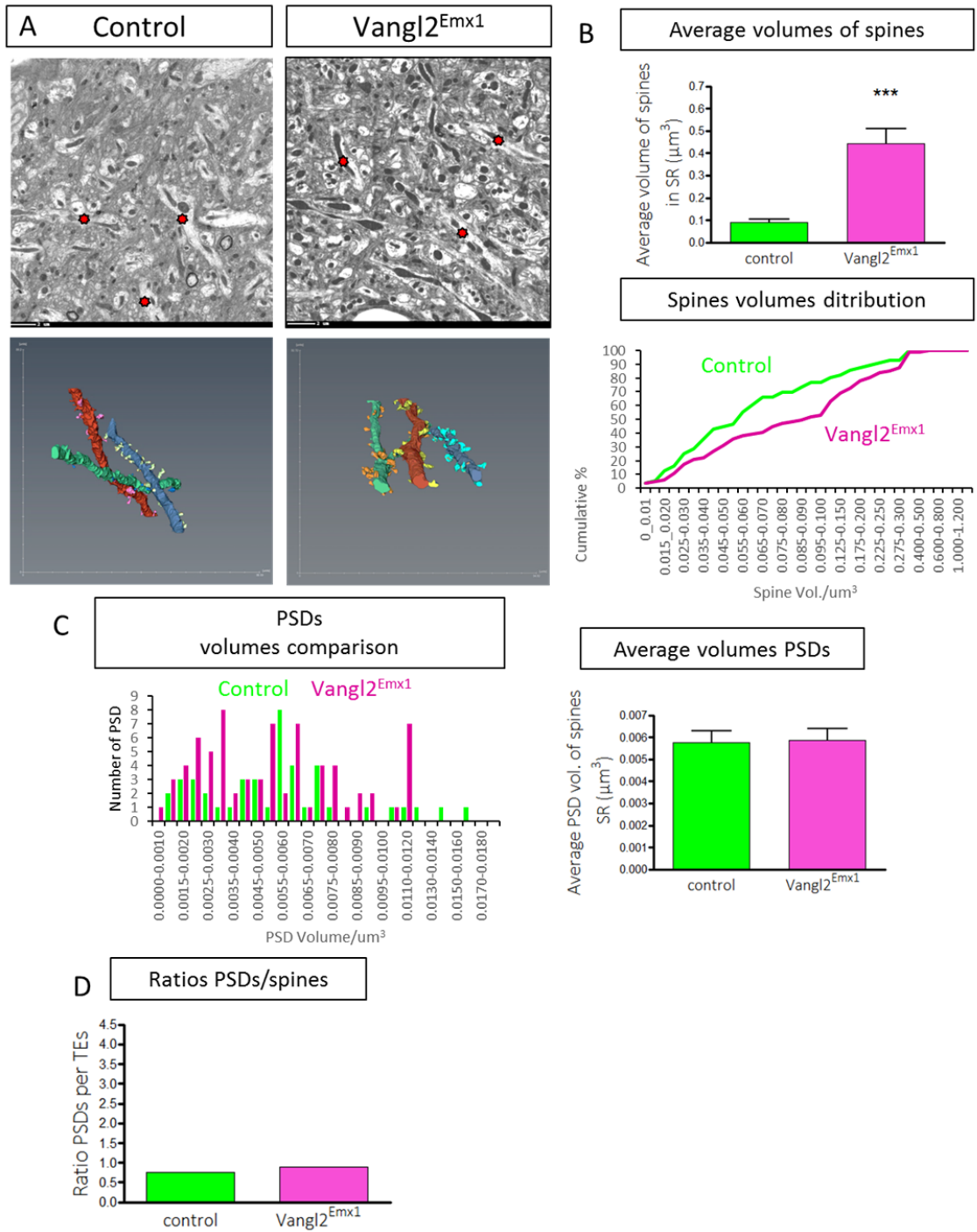
Supplementary Figure 2



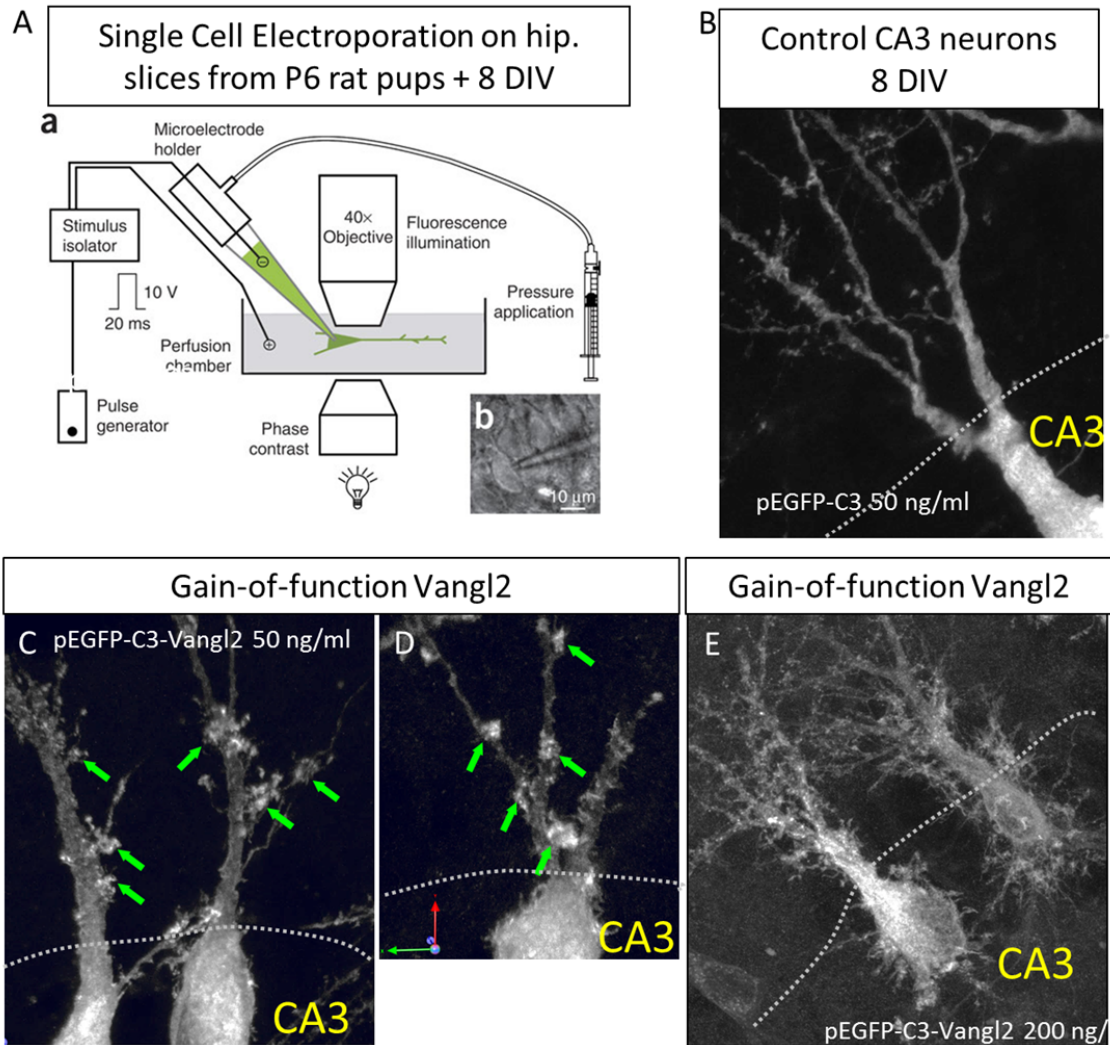
Supplementary Figure 3



Supplementary Figure 4



Supplementary Figure 5



General Discussion

Studies in *Drosophila* demonstrated that PCP signaling is involved in axonal guidance, dendrite morphogenesis and synaptogenesis. In vertebrates, such as *Xenopus*, zebrafish and mice, this signaling pathway is implicated in convergent extension movements during neurulation. The zebrafish model is also significant as it showed for the first time that PCP core proteins are important for neuronal migration, both autonomously and non-autonomously.

Importantly, core PCP proteins are highly conserved proteins along development, and studies in mammals revealed that PCP signaling role in neuronal development is maintained throughout evolution. Also, in the last ten years, links between PCP signaling and neurodevelopmental pathologies such as Autism Spectrum Disorders (ASD), have emerged. All these studies reveal that PCP proteins are crucial for the proper function of neurons and the brain. However, little is known about the molecular mechanisms that underlie the functions of this signaling pathway during neuronal development, and specific roles of core PCP proteins in shaping specific brain regions and their function are few.

It was my objective to investigate the role of one of these core PCP proteins - Vangl2 - in the development of a specific brain region - the hippocampus.

Most of the work reported so far about a role for Vangl2 in the mammalian nervous system was performed on mice carrying a spontaneous mutation on the *vangl2* gene, called *Loop-tail*. Animals carrying a homozygote mutation for this gene die at birth making it impossible to study the effect of the absence of Vangl2 postnatally. Moreover, the Vangl2^{LP} form produced by this mutation has a dominant negative effect (Yin et al., 2012), making it hard to conclude if previous studies using these animals were actually reporting an effect related to the absence of Vangl2 or rather to the dominant-negative properties of Vangl2^{LP}. The use of a conditional knockout mouse model was then necessary to allow discriminating between these, and assessing the "pure" effect of *vangl2*. I was then able not only to investigate the postnatal morphological effect of Vangl2 deletion in a specific brain region, but also to determine the molecular mechanisms that might underlie eventual structural abnormalities and finally to assess at a more integrated level the impact of *vangl2* in cognitive events.

In my first study I demonstrated that *vangl2* deletion affected neuronal outgrowth in a N-cadherin dependent manner. The reported increase in neuronal outgrowth was correlated to a decrease of actin retrograde flow and actin directed trajectories, suggesting that actin dynamics was perturbed in these neurons. I put forward the hypothesis that these results are due to an increase in the fraction of immobilized N-cadherin molecules at the substrate level, thus serving as a stable anchor for engagement of a clutch mechanism. To demonstrate this point, I used FRAP technique and showed that in Vangl2 cKO neurons, N-cadherin proteins

engaged in homophilic adhesions had a lower turnover than in controls. Altogether, I was able to show for the first time that the role of PCP signaling over adhesion turnover impacts actin dynamics and as a consequence, neuronal outgrowth.

Previous studies had reported such role in adhesion regulation/turnover for PCP proteins in *drosophila* epithelia and in lower vertebrate mesenchymal tissue. For example, Classen and colleagues demonstrated in 2005 in *drosophila* fixed tissue that PCP proteins (Vang included) affected the turnover of E-cadherin at the membrane of pupal wing cells (Classen et al., 2005). More importantly they showed that the regulation of PCP proteins at adhesion sites was important to regulate adhesion formation and turnover, and ultimately to control the dynamic morphology of these epithelial cells during remodeling. In 2013, Warrington and colleagues demonstrated that PCP signaling was important to promote cell intercalation during tracheal tube morphogenesis in *drosophila* and that this role was due to Fz (another core PCP protein) locally promoting the turnover of E-cadherin at adhesion sites (Warrington et al., 2013). Although they were able to show in live cells the turnover of E-cadherin *via* FRAP experiments, they did not correlate these effects to a local regulation of cytoskeleton dynamics. Increased E-cadherin levels in epithelial tissues can lead to increased adhesion and reduced cellular outgrowth (Stockinger et al., 2001). However, another study on retinal ganglion cells also demonstrated that inhibition of E-cadherin *via* antibody-blocking reduced neurite outgrowth (Oblander et al., 2007). These studies suggest that the role of cadherins on adhesion and outgrowth is context-dependent, and therefore needs to be studied on a case by case basis.

There are important differences between epithelial cells during tissue remodeling and young moving neuronal cells, as growth cones are highly dynamic structures that need to be constantly creating and destructing adhesions sites in order to advance (or retract). Hence, adhesion spots in these structures present a shorter life-time, allowing the growth cones to quickly respond to the surrounding context on which they are growing. Growth cones are constantly forming adhesions and destructing them until they find their post-synaptic partner, and a tight regulation of the adhesion/outgrowth balance is crucial for the proper connectivity of neurons. My data suggest that the role of Vangl2 resides in the modulation of adhesion site dynamics in growth cones, and is specifically used by the neuron as a brake, regulating the speed of movement. A good example of this is the number of pauses performed by Vangl2 cKO moving neurons that is reduced when compared with controls. Pauses are important in order for growth cones to integrate the information of the surrounding context on which they are growing. In the case of Vangl2 cKOs neurons, the growth cones have less time to sample the local environment and integrate the various cues of the environment on which they grow. They might not answer correctly to constantly changing molecular cues, and hence present defaults

in axon outgrowth and guidance. *In vivo* results showed that Mfs from GC do not display major defects during their migration along the *sl*, suggesting either that Vangl2 does not play a role in axonal guidance in this context, or that the surrounding molecular context in which these fibers migrate is so strong that it manages to bypass eventual deficits due to Vangl2 deletion. Several studies have suggested a role for Vangl2 in the axonal guidance, in brainstem monoaminergic axons (Fenstermaker et al., 2010), or in dorsal commissural neurons in mice (Shafer et al., 2011) and chicken (Avilés et al., 2015). On the other hand, another study using a double KO for *vangl1* and *vangl2* did not display axonal guidance deficits in the anterior commissure, thalamocortical, corticothalamic, and corticospinal tracts, but had an absence of *corpus callosum* (Qu et al, 2014 Figure 3). However, the authors do not mention this phenotype in their study, maybe because the conditional mutant was generated using a Foxg1-Cre line, notorious for its impact of axonal tract on C57BL/6J background. In our conditional mutant, generated by an Emx1-Cre line, we observed a dorsal agenesis of the *corpus callosum*. The literature on the role of core PCP genes and axonal guidance is controversial and appears to be gene- and context-dependent. To evaluate whether Vangl2 is essential for axonal guidance of hippocampal neurons, an experiment would be to culture Vangl2 cKO neurons on N-cadherin substrates and use a microfluidic chamber in order to challenge these neurons with different molecular cues and observe if they present axon guidance mistakes. On the other hand, during our immunohistochemical experiments, we noticed that the *corpus callosum* in the caudal region of the brain of Vangl2^{Emx1} mice was absent, similar to the Chai et al. study (2014), indicating that Vangl2 can affect the formation of axonal tracts. Since our results on hippocampal neurons show that the neurites of Vangl2^{Emx1} neurons migrate faster than those of control neurons, this phenotype could also be occurring in neurites of cortical neurons. The growth cones of these neurites would then miss crucial molecular cues that would guide them until their final and correct target. Cortical neuron cultures and time-lapse imaging could help us to confirm this. The specific *corpus callosum* phenotype (with no other commissural deficit) suggests that Vangl2 effect on axonal guidance might be context-dependent. Finally, despite the fact that *in situ hybridization* does not show an overlapping profile of expression of *vangl2* and *vangl1* (Tissir & Goffinet, 2006), compensation by Vangl1 or another PCP protein could also explain the lack of major axonal guidance defects.

The results from this first study are very promising but some data are still missing in order to fully understand the basis of the molecular and cellular interactions between Vangl2 and N-cadherin. For this purpose I used micropatterned coverslips coated with N-cadherin. These micropatterns not only allowed the creation of artificial "adhesion spots" but also

permitted to compare the interplay between Vangl2 and N-cadherin in a *trans*- configuration (on these spots vs the extracellular space which does not have N-cadherin). We were able to study N-cadherin dynamics on control and Vangl2 cKO neurons and compare this dynamics within and outside "adhesion spots". Notably, I performed FRAP experiments on regions of growth cones within and outside adhesive spots and compare the recovery of N-cadherin-GFP signal between control and Vangl2^{Emx1} neurons. These data are crucial to confirm if the role of Vangl2 on N-cadherin turnover is solely related to molecules engaged in adhesion or if such regulation occurs throughout the whole growth cone.

It has been shown that N-cadherin substrates can affect actin dynamics via their interaction with catenins (Garcia et al., 2015). More specifically, this paper showed that the recovery of α -catenin-GFP had a similar profile to N-cadherin-GFP and that α -catenin molecules are more confined at N-cadherin patterned spots. These data suggest that at N-cadherin adhesions sites there is an interaction between these two proteins, forming a stable complex at the membrane important for actin dynamics regulation *via* α -catenins. In order to confirm that the deletion of *vangl2* leads to an increased life-time of molecules involved in the molecular clutch, I will perform FRAP experiments with a tagged α -catenin. I will evaluate if in absence of Vangl2 these proteins present a lower recovery as we showed for N-cadherin. After understanding how Vangl2 impacts on N-cadherin dynamics and the engagement of the molecular clutch, it would also be essential to understand how/if Vangl2 dynamics is affected at adhesion spots and also if the N-cadherin-dependent effect on actin treadmill and cytoskeleton outgrowth is due to *cis*- or *trans*- or even both kind of interactions of Vangl2 with N-cadherin.

Wu & Mlodzik previously reported in 2008 that Vangl2 could bind to Fz in a *trans*-configuration (on an adjacent cell) *via* its extracellular loops, suggesting that the extracellular domain of Vangl2 might play a role in the transmission of PCP signaling throughout the tissue. This *trans*- interaction could participate in an eventual non-cell autonomous role of Vangl2, such as PCP signaling transmission between neighboring cells. We could imagine that Vangl2 regulates N-cadherin dynamics in *trans*-, and that one consequence of *vangl2* deletion might ultimately impact axon fasciculation, as N-cadherin is important for axon fasciculation of hippocampal neurons (Bekirov et al., 2008). Such mechanism could explain the fasciculation deficits that we reported in Vangl2 cKO mice *in vivo* in our second work.

Interestingly, a paper recently published reported an interaction between Vangl2 and N-cadherin in neurons, although on a different neuronal structure: the spine (Nagaoka et al., 2014a). In this report, the authors showed that Vangl2 is enriched in neuronal spines and more precisely in PSDs, and reported a positive co-IP (co-ImmunoPrecipitation) between the two proteins. In our second work, we reported that we could not detect positive colocalization of

Vangl2 with postsynaptic (PSD95) or presynaptic (Bassoon) markers in the *sl* of the CA3. This was true at any developmental stage studied, including P21, which is comparable to the neuronal cultures kept 21 days *in vitro*. On the other hand, we did find good colocalization between PSD95 and Vangl2 in the *stratum moleculare*, where the dendrites of the GC project, suggesting that the Vangl2/PSD95 colocalization is specific to some synapses, or maybe simply easier to image for certain neuronal populations/connections, emphasizing the importance of tissue-specific analysis. The Vangl2-antibody we used in our studies is different from the one used in their report. We demonstrated the specificity of our antibody *in vivo* using *vangl2* cKO mouse, while Nagaoka and colleagues demonstrated specificity for their Vangl2 antibody in cultured neurons after acute downregulation with shRNA. However, they cultured neurons from the entire hippocampus and they did not identify cellular types *via* immunohistochemical staining, which makes it impossible to know if all neurons or only a specific subtype present: 1) specific Vangl2 staining in spines, and 2) colocalization with PSD95. Hence, the specificity of their antibody remains elusive. Also, the technical procedures before immunohistochemical staining were different as the authors used cryo-preserved slices post-fixed with methanol while we transcardially perfused the brains and post-fixed with PFA. We tried to replicate their technical conditions in both control and cKO mice. With their protocol, we detected some puncta that resembled synaptic staining in the dendrites of CA1 and CA3 pyramidal neurons. However, such punctas were still present in cKO mice, indicating that this staining might not be Vangl2-specific. Another result of their study was an observed reduction in spine density number and in the density of synaptic markers in dissociated cultured neurons transfected with shRNA. Similar results on spine density were further confirmed *in vivo* in the hippocampal CA1 region of heterozygous *Loop-tail* mice. The EM data from our second study partially corroborate these results, while revealing a more complex picture. More specifically, we showed that the deletion of *vangl2* leads to a decrease in the density of TE in the CA3 *stratum lucidum* (*sl*). However, the density of spines in the CA3 *stratum radiatum* (*sr*) was increased by Vangl2 deletion. A common effect on both *strata* was the increase of PSDs, contrary to what Nagaoka and colleagues reported. These results indicate that in absence of *vangl2*, spinogenesis occurs, but the morphogenesis of spines, and their number and density is abnormal, but in a region-specific manner.

Finally the authors revisited the interaction of PCP proteins with cadherins in neuronal spines, and added a new spin to it: a direct interaction between Vangl2 and N-cadherin. Briefly, Nagaoka and colleagues reported *via* co-IP that Vangl2 and N-cadherin interacted, and that Vangl2 levels affected the presence/absence of N-cadherin at the plasma membrane in the spines of neurons. Through the use of neuron cultures and either overexpression or

downregulation of *vangl2* they demonstrated that N-cadherin levels at the membrane were either reduced or increased respectively. Finally, they used heterologous cell systems (HEK and MDCK cells) to show that the effect of Vangl2 on N-cadherin endocytosis occurs in a Rab5-dependent manner. Altogether, they concluded that the crosstalk between Vangl2 and N-cadherin is crucial for the formation and maturation of cadherin-based cell-cell junctions at the synapse. Such a role for core PCP signaling in the regulation of adhesion turnover *via* Rab proteins and recycling was previously demonstrated by Classen and colleagues (2005) in drosophila wing cells. Later, the study of Warrington et al (2013) in drosophila germband confirmed such a mechanism, and reported that PCP proteins regulated the levels and turnover of E-cadherin at junctions, but this time via RhoGEF2. Altogether, these results might explain our own data showing that the recovery of N-cadherin-GFP molecules engaged in homophilic bindings was lower in Vangl2^{Emx1} neurons. More specifically, it could be that a Rab5-dependent endocytosis mechanism is involved in our model and that in this way N-cadherin molecules are more immobilized at the substrate. This means that overall levels of N-cadherin molecules, the ones involved in homophilic adhesions and the ones freely diffusing at the membrane should be reduced. However, we showed in our first study that the recovery of N-cadherin-GFP molecules freely exchanging at the membrane is not impacted by *vangl2* deletion.

In my second work, I carefully analyzed the morpho-functional consequences of the deletion of *vangl2* in a specific context: the DG-CA3 hippocampal circuit. For this study, I had the help of a specialist of the brain ultrastructure, Claudia Racca (Institute of Neuroscience, The Medical School, Newcastle University, Newcastle upon Tyne, United Kingdom), and of a specialist of mammalian memories and their associated pathologies, Aline Marighetto (Neurocentre Magendie, Team: Pathophysiology of declarative memory, Bordeaux, France). We started by demonstrating that Vangl2 has a very unique profile of expression in the hippocampus, with an enrichment in the DG subgranular layer, as well as in neurites (both axons and dendrites) of the hippocampal granular cells. Using double-immunohistochemical assays I determined that Vangl2 is present in the granular cells (GC) Mfs but not in their synaptic terminals, the boutons. I was not able to detect Vangl2 in the dendrites and spines of CA3 pyramidal neurons. However, double-immunohistochemical stainings in the DG *stratum moleculare* show that Vangl2 and PSD95 colocalize. Moreover, our single-cell-electroporation experiments demonstrate that Vangl2 is targeted to structures that resemble to Thorny Excrescences (TE). These results suggest either that Vangl2 protein levels in the MfB/TE synapse and at P21 are too low to be detected by immunofluorescence, or that these discrepancies are related to a technical issue.

The structural and ultrastructural analysis of the hippocampus of cKO mice show for the first time that a core PCP protein affects the correct formation/maturation of a hippocampal circuit, and consequently induces specific memory deficits. We show that in these animals both the pre- and post-synaptic elements of the MfB-TE synapses are morphologically abnormal regarding their size and complexity. *vangl2* deletion also impacted the organization of these synapses. Classically, one MfB contacts TE that contains 4 to 5 PSDs (active zones), while in cKOs, we observed that one MfB contacted TE presenting only one PSD. Overall the synapses in the *sl* of in *vangl2* cKOs resembled classical synapses in size and PSD content, suggesting that they failed to mature and develop the complex morphological traits that they normally present. Interestingly, the overexpression of Vangl2 led to another phenotype, where neurons presented a highly complex morphology, with increased neurites branching and increased number of TE-like structures. As one of the main readouts of PCP signaling is local cytoskeleton reorganization, it is reasonable to think that an important function of Vangl2 is to locally control actin dynamics and participates in the morphological complexification of the pre- and postsynaptic element of this synapse and consequently in its maturation.

On another hand, PCP core proteins regulate adhesion protein dynamics and control adhesion stability/turnover (including in neurons, as demonstrated in our first work), and MfB/TE synapses are particularly interesting as they are enriched with N-cadherin, Nectins and Afadins. These proteins concentrate in *puncta adhaerentia*, structures that act like strong *adherens junctions* and are crucial to maintain adhesion between the MfB and the TE. *Puncta adhaerentia* only form if the MfB/TE synapse is correctly formed and mature. Hence, *vangl2* deletion could affect the molecular integrity and maturation of these adhesion sites, and this would participate in MfB/TE abnormal morphology.

Another original result from our *in vivo* study is the failure of Vangl2^{Emx1} mice to use previously learned spatial information flexibly. A previous study on the MfB/TE synapse reported that the disruption of this structure impacts the morphology of this synapse in a mouse model (FAD) of Alzheimer's disease (AD) (Wilke et al., 2014). They showed that MfBs were smaller (~50%), contacted fewer postsynaptic spines and had greater numbers of presynaptic filopodial processes. Thorny excrescences were smaller (less than 50%) in the FAD mutant condition and presented reduced complexity and significantly smaller sites of synaptic contact. Significantly, there was no change in the volume of classical dendritic spines at neighboring inputs to CA3 neurons suggesting input-specific defects in the early course of AD related pathology. Another paper showed in a mouse model of Down Syndrome (DS) that TEs were morphologically affected, with reduction of spine density (~15%) and number of thorns per TE (~45%) (Popov et al., 2011). In both papers, the magnitude of the morphological

abnormalities reported was smaller compared with the morphological deficits we show in this report. These studies suggest that the correct formation and maturation of MfB/TE synapses is impacted in two neuropathological mice models, and that such morphological defects can contribute to the phenotypes that characterize each clinical condition. Together with our work, these studies show that a proper maturation of the MfB/TE synapse is important for hippocampal-dependent mnemonic tasks such as memory, learning and behavior.

On the other hand, neither these studies nor ours have demonstrated that the cognitive deficits specific to each mouse model is causally related to the structural deficits observed in the CA3. In our study, we saw no differences between cKOs and controls in the hippocampal-dependent water maze test, despite the enrichment of Vangl2 in the DG/CA3 network, and despite the structural deficits in the CA3 region. On the other hand, studies have shown that the loss of flexible memory expression was related to functional alterations of the hippocampus but also in the prefrontal cortex (Etchamendy et al., 2011; Touzani et al., 2003; Mingaud et al., 2007; 2008). In our study, *vangl2* mutation produced a deficit in spontaneous spatial alternation, also known to depend on the hippocampus and prefrontal cortex. These results suggest that input from the cortex play a substantial role in the observed deficit. So if Vangl2 is a critical player for the development of the neuronal circuitry within the hippocampus, it also appears to be important for the circuitry between the hippocampus and the prefrontal cortex, needed for higher order cognitive function. All of this, obviously, remains to be tested. Lastly, because the loss of flexible memory expression has been reported in old mice (Marighetto et al., 1999; Etchamendy et al., 2001; Mingaud et al., 2008) and in old humans (Etchamendy et al., 2011), and *vangl2* expression decreases over time, it is tempting to suggest that the core PCP proteins could participate in some ageing process. It would be interesting to evaluate *vangl2* levels of expression in the hippocampus of old animals, or correlatively, to increase the levels of *vangl2* in old animals *via* viral infection, and assess their flexible memory expression.

Altogether, my two distinct works point out to one common function for Vangl2 in neuronal function. They demonstrate that Vangl2 is a fundamental element in the precise control of neuronal maturation, which is important for time- and space-precise formation of connections between neurons or even between the neuron and its substrate. As a consequence, Vangl2 is important for the correct communication between neurons or even between brain regions. Altogether, it means that the precise regulation of Vangl2 levels in the hippocampus (and other cerebral regions as the cortex *p.e.*) is crucial for proper neuronal morphogenesis, brain activity and memory.

General References

- Abe, K., and Takeichi, M. (2008). EPLIN mediates linkage of the cadherin–catenin complex to F-actin and stabilizes the circumferential actin belt. *PNAS* *105*, 13–19.
- Ackley, B.D. (2014). Wnt-signaling and planar cell polarity genes regulate axon guidance along the anteroposterior axis in *C. elegans*. *Devel Neurobio* *74*, 781–796.
- Acsády, L., Katona, I., Gulyás, A. i., Shigemoto, R., and Freund, T. f. (1997). Immunostaining for substance P receptor labels GABAergic cells with distinct termination patterns in the hippocampus. *J. Comp. Neurol.* *378*, 320–336.
- Adler, P.N. (2002). Planar Signaling and Morphogenesis in *Drosophila*. *Developmental Cell* *2*, 525–535.
- Adler, P.N. (2012). Chapter One - The frizzled/stan Pathway and Planar Cell Polarity in the *Drosophila* Wing. In *Current Topics in Developmental Biology*, Y. Yang, ed. (Academic Press), pp. 1–31.
- Adler, P.N., Zhu, C., and Stone, D. (2004). Inturned Localizes to the Proximal Side of Wing Cells under the Instruction of Upstream Planar Polarity Proteins. *Current Biology* *14*, 2046–2051.
- Aigouy, B., Farhadifar, R., Staple, D.B., Sagner, A., Röper, J.-C., Jülicher, F., and Eaton, S. (2010). Cell Flow Reorients the Axis of Planar Polarity in the Wing Epithelium of *Drosophila*. *Cell* *142*, 773–786.
- Aimone, J.B., Deng, W., and Gage, F.H. (2011). Resolving New Memories: A Critical Look at the Dentate Gyrus, Adult Neurogenesis, and Pattern Separation. *Neuron* *70*, 589–596.
- Aizawa, H., Kishi, Y., Iida, K., Sameshima, M., and Yahara, I. (2001). Cofilin-2, a novel type of cofilin, is expressed specifically at aggregation stage of *Dictyostelium discoideum* development. *Genes to Cells* *6*, 913–921.
- Akin, O., and Mullins, R.D. (2008). Capping Protein Increases the Rate of Actin-Based Motility by Promoting Filament Nucleation by the Arp2/3 Complex. *Cell* *133*, 841–851.
- Altman, J., and Das, G.D. (1965). Autoradiographic and histological evidence of postnatal hippocampal neurogenesis in rats. *J. Comp. Neurol.* *124*, 319–335.
- Alvarez-Buylla, A., García-Verdugo, J.M., and Tramontin, A.D. (2001). A unified hypothesis on the lineage of neural stem cells. *Nat Rev Neurosci* *2*, 287–293.

- Amaral, D.G., and Dent, J.A. (1981). Development of the mossy fibers of the dentate gyrus: I. A light and electron microscopic study of the mossy fibers and their expansions. *J. Comp. Neurol.* **195**, 51–86.
- Andrianantoandro, E., and Pollard, T.D. (2006). Mechanism of Actin Filament Turnover by Severing and Nucleation at Different Concentrations of ADF/Cofilin. *Molecular Cell* **24**, 13–23.
- Anthony, T.E., Klein, C., Fishell, G., and Heintz, N. (2004). Radial Glia Serve as Neuronal Progenitors in All Regions of the Central Nervous System. *Neuron* **41**, 881–890.
- Archbold, H.C., Yang, Y.X., Chen, L., and Cadigan, K.M. (2012). How do they do Wnt they do?: regulation of transcription by the Wnt/ β -catenin pathway. *Acta Physiologica* **204**, 74–109.
- Armstrong, A., Ryu, Y.K., Chieco, D., and Kuruvilla, R. (2011). Frizzled3 Is Required for Neurogenesis and Target Innervation during Sympathetic Nervous System Development. *Journal of Neuroscience* **31**, 2371–2381.
- Avilés, E.C., and Stoeckli, E.T. (2016). Canonical wnt signaling is required for commissural axon guidance. *Devel Neurobio* **76**, 190–208.
- Babayeva, S., Zilber, Y., and Torban, E. (2011). Planar cell polarity pathway regulates actin rearrangement, cell shape, motility, and nephrin distribution in podocytes. *American Journal of Physiology - Renal Physiology* **300**, F549–F560.
- Bamburg, J.R., and Bray, D. (1987). Distribution and cellular localization of actin depolymerizing factor. *J Cell Biol* **105**, 2817–2825.
- Bard, L., Boscher, C., Lambert, M., Mège, R.-M., Choquet, D., and Thoumine, O. (2008). A Molecular Clutch between the Actin Flow and N-Cadherin Adhesions Drives Growth Cone Migration. *J. Neurosci.* **28**, 5879–5890.
- Bastock, R., Strutt, H., and Strutt, D. (2003). Strabismus is asymmetrically localised and binds to Prickle and Dishevelled during Drosophila planar polarity patterning. *Development* **130**, 3007–3014.
- Batchelder, E.L., Hollopeter, G., Campillo, C., Mezanges, X., Jorgensen, E.M., Nassoy, P., Sens, P., and Plastino, J. (2011). Membrane tension regulates motility by controlling lamellipodium organization. *PNAS* **108**, 11429–11434.

- Battaglia, A., Hoyme, H.E., Dallapiccola, B., Zackai, E., Hudgins, L., McDonald-McGinn, D., Bahi-Buisson, N., Romano, C., Williams, C.A., Brailey, L.L., et al. (2008). Further Delineation of Deletion 1p36 Syndrome in 60 Patients: A Recognizable Phenotype and Common Cause of Developmental Delay and Mental Retardation. *Pediatrics* 121, 404–410.
- Baumgartner, W., Hinterdorfer, P., Ness, W., Raab, A., Vestweber, D., Schindler, H., and Drenckhahn, D. (2000). Cadherin interaction probed by atomic force microscopy. *PNAS* 97, 4005–4010.
- Bayer, S.A. (1980). Development of the hippocampal region in the rat II. Morphogenesis during embryonic and early postnatal life. *J. Comp. Neurol.* 190, 115–134.
- Bear, J.E., Svitkina, T.M., Krause, M., Schafer, D.A., Loureiro, J.J., Strasser, G.A., Maly, I.V., Chaga, O.Y., Cooper, J.A., Borisov, G.G., et al. (2002). Antagonism between Ena/VASP Proteins and Actin Filament Capping Regulates Fibroblast Motility. *Cell* 109, 509–521.
- Bechara, A., Nawabi, H., Moret, F., Yaron, A., Weaver, E., Bozon, M., Abouzid, K., Guan, J.-L., Tessier-Lavigne, M., Lemmon, V., et al. (2008). FAK–MAPK-dependent adhesion disassembly downstream of L1 contributes to semaphorin3A-induced collapse. *The EMBO Journal* 27, 1549–1562.
- Bekirov, I.H., Nagy, V., Svoronos, A., Huntley, G.W., and Benson, D.L. (2008). Cadherin-8 and N-cadherin differentially regulate pre- and postsynaptic development of the hippocampal mossy fiber pathway. *Hippocampus* 18, 349–363.
- Benjamin, J.M., Kwiatkowski, A.V., Yang, C., Korobova, F., Pokutta, S., Svitkina, T., Weis, W.I., and Nelson, W.J. (2010). α E-catenin regulates actin dynamics independently of cadherin-mediated cell–cell adhesion. *J Cell Biol* 189, 339–352.
- Benson, D.L., and Tanaka, H. (1998). N-Cadherin Redistribution during Synaptogenesis in Hippocampal Neurons. *J. Neurosci.* 18, 6892–6904.
- Bentley, D., and Toroian-Raymond, A. (1986). Disoriented pathfinding by pioneer neurone growth cones deprived of filopodia by cytochalasin treatment. *Nature* 323, 712–715.
- Bixby, J.L., and Zhang, R. (1990). Purified N-cadherin is a potent substrate for the rapid induction of neurite outgrowth. *J Cell Biol* 110, 1253–1260.

- Blair, A., Tomlinson, A., Pham, H., Gunsalus, K.C., Goldberg, M.L., and Laski, F.A. (2006). Twinstar, the *Drosophila* homolog of cofilin/ADF, is required for planar cell polarity patterning. *Development* 133, 1789–1797.
- Boscher, C., and Mège, R.-M. (2008). Cadherin-11 interacts with the FGF receptor and induces neurite outgrowth through associated downstream signalling. *Cellular Signalling* 20, 1061–1072.
- Bosoi, C.M., Capra, V., Allache, R., Trinh, V.Q.-H., De Marco, P., Merello, E., Drapeau, P., Bassuk, A.G., and Kibar, Z. (2011). Identification and characterization of novel rare mutations in the planar cell polarity gene PRICKLE1 in human neural tube defects. *Hum. Mutat.* 32, 1371–1375.
- Bozdagi, O., Shan, W., Tanaka, H., Benson, D.L., and Huntley, G.W. (2000). Increasing Numbers of Synaptic Puncta during Late-Phase LTP: N-Cadherin Is Synthesized, Recruited to Synaptic Sites, and Required for Potentiation. *Neuron* 28, 245–259.
- Bradke, F., and Dotti, C.G. (1999). The Role of Local Actin Instability in Axon Formation. *Science* 283, 1931–1934.
- Braga, V.M.M., Machesky, L.M., Hall, A., and Hotchin, N.A. (1997). The Small GTPases Rho and Rac Are Required for the Establishment of Cadherin-dependent Cell–Cell Contacts. *J Cell Biol* 137, 1421–1431.
- Brandau, D.T., Lund, M., Cooley, L.D., Sanger, W.G., and Butler, M.G. (2008). Autistic and dysmorphic features associated with a submicroscopic 2q33.3–q34 interstitial deletion detected by array comparative genomic hybridization. *Am. J. Med. Genet.* 146A, 521–524.
- Bunn, K.J., Daniel, P., Rösken, H.S., O'Neill, A.C., Cameron-Christie, S.R., Morgan, T., Brunner, H.G., Lai, A., Kunst, H.P.M., Markie, D.M., et al. (2015). Mutations in DVL1 Cause an Osteosclerotic Form of Robinow Syndrome. *The American Journal of Human Genetics* 96, 623–630.
- Burnette, D.T., Schaefer, A.W., Ji, L., Danuser, G., and Forscher, P. (2007). Filopodial actin bundles are not necessary for microtubule advance into the peripheral domain of *Aplysia* neuronal growth cones. *Nat Cell Biol* 9, 1360–1369.
- Burnette, D.T., Ji, L., Schaefer, A.W., Medeiros, N.A., Danuser, G., and Forscher, P. (2008). Myosin II Activity Facilitates Microtubule Bundling in the Neuronal Growth Cone Neck. *Developmental Cell* 15, 163–169.

- Burridge, K., and Wennerberg, K. (2004). Rho and Rac Take Center Stage. *Cell* 116, 167–179.
- Cameron, H.A., Woolley, C.S., McEwen, B.S., and Gould, E. (1993). Differentiation of newly born neurons and glia in the dentate gyrus of the adult rat. *Neuroscience* 56, 337–344.
- Campbell, D.S., and Holt, C.E. (2001). Chemotropic Responses of Retinal Growth Cones Mediated by Rapid Local Protein Synthesis and Degradation. *Neuron* 32, 1013–1026.
- Chacón, M.R., and Fazzari, P. (2011). Fak. *Cell Adhesion & Migration* 5, 52–55.
- Chai, G., Zhou, L., Manto, M., Helmbacher, F., Clotman, F., Goffinet, A.M., and Tissir, F. (2014). Celsr3 is required in motor neurons to steer their axons in the hindlimb. *Nat Neurosci* 17, 1171–1179.
- Chan, C.E., and Odde, D.J. (2008). Traction Dynamics of Filopodia on Compliant Substrates. *Science* 322, 1687–1691.
- Chandrasekhar, A., Moens, C.B., Warren, J.T., Kimmel, C.B., and Kuwada, J.Y. (1997). Development of branchiomotor neurons in zebrafish. *Development* 124, 2633–2644.
- Chappuis-Flament, S., Wong, E., Hicks, L.D., Kay, C.M., and Gumbiner, B.M. (2001). Multiple cadherin extracellular repeats mediate homophilic binding and adhesion. *J Cell Biol* 154, 231–243.
- Chen, J., Zacharek, A., Li, Y., Li, A., Wang, L., Katakowski, M., Roberts, C., Lu, M., and Chopp, M. (2006). N-cadherin mediates nitric oxide-induced neurogenesis in young and retired breeder neurospheres. *Neuroscience* 140, 377–388.
- Chen, Y.-T., Stewart, D.B., and Nelson, W.J. (1999). Coupling Assembly of the E-Cadherin/ β -Catenin Complex to Efficient Endoplasmic Reticulum Exit and Basal-lateral Membrane Targeting of E-Cadherin in Polarized MDCK Cells. *J Cell Biol* 144, 687–699.
- Chien, C.-B., Rosenthal, D.E., Harris, W.A., and Holt, C.E. (1993). Navigational errors made by growth cones without filopodia in the embryonic xenopus brain. *Neuron* 11, 237–251.
- ChuanYuan, K., Li, Z., Hua, L., and JianZhong, Y. (2011). Association study of the frizzled 3 gene with Chinese Va schizophrenia. *Neuroscience Letters* 505, 196–199.

- Clark, H.F., Brentrup, D., Schneitz, K., Bieber, A., Goodman, C., and Noll, M. (1995). Dachshous encodes a member of the cadherin superfamily that controls imaginal disc morphogenesis in *Drosophila*. *Genes Dev.* 9, 1530–1542.
- Classen, A.-K., Anderson, K.I., Marois, E., and Eaton, S. (2005). Hexagonal Packing of *Drosophila* Wing Epithelial Cells by the Planar Cell Polarity Pathway. *Developmental Cell* 9, 805–817.
- Clelland, C.D., Choi, M., Romberg, C., Clemenson, G.D., Fragniere, A., Tyers, P., Jessberger, S., Saksida, L.M., Barker, R.A., Gage, F.H., et al. (2009). A Functional Role for Adult Hippocampal Neurogenesis in Spatial Pattern Separation. *Science* 325, 210–213.
- Courbard, J.-R., Djiane, A., Wu, J., and Mlodzik, M. (2009). The apical/basal-polarity determinant Scribble cooperates with the PCP core factor Stbm/Vang and functions as one of its effectors. *Developmental Biology* 333, 67–77.
- Craig, E.M., Van Goor, D., Forscher, P., and Mogilner, A. (2012). Membrane Tension, Myosin Force, and Actin Turnover Maintain Actin Treadmill in the Nerve Growth Cone. *Biophysical Journal* 102, 1503–1513.
- Creer, D.J., Romberg, C., Saksida, L.M., Praag, H. van, and Bussey, T.J. (2010). Running enhances spatial pattern separation in mice. *PNAS* 107, 2367–2372.
- Criscuolo, C., de Leva, M. f., Sorrentino, P., Piro, R., Carbone, R., Guacci, A., De Michele, G., and Filla, A. (2010). PRICKLE1 progressive myoclonus epilepsy in Southern Italy. *Mov. Disord.* 25, 2686–2687.
- Curtin, J.A., Quint, E., Tshipouri, V., Arkell, R.M., Cattanach, B., Copp, A.J., Henderson, D.J., Spurr, N., Stanier, P., Fisher, E.M., et al. (2003). Mutation of *Celsr1* Disrupts Planar Polarity of Inner Ear Hair Cells and Causes Severe Neural Tube Defects in the Mouse. *Current Biology* 13, 1129–1133.
- Danzer, S.C., He, X., Loepke, A.W., and McNamara, J.O. (2010). Structural plasticity of dentate granule cell mossy fibers during the development of limbic epilepsy. *Hippocampus* 20, 113–124.
- Das, G., Jenny, A., Klein, T.J., Eaton, S., and Mlodzik, M. (2004). Diego interacts with Prickle and Strabismus/Van Gogh to localize planar cell polarity complexes. *Development* 131, 4467–4476.
- Davey, C.F., Mathewson, A.W., and Moens, C.B. (2016). PCP Signaling between Migrating Neurons and their Planar-Polarized Neuroepithelial Environment Controls Filopodial Dynamics and Directional Migration. *PLOS Genet* 12, e1005934.

- de Anda, F.C., Pollarolo, G., Da Silva, J.S., Camoletto, P.G., Feiguin, F., and Dotti, C.G. (2005). Centrosome localization determines neuronal polarity. *Nature* 436, 704–708.
- Deans, M.R., Antic, D., Suyama, K., Scott, M.P., Axelrod, J.D., and Goodrich, L.V. (2007). Asymmetric Distribution of Prickle-Like 2 Reveals an Early Underlying Polarization of Vestibular Sensory Epithelia in the Inner Ear. *J. Neurosci.* 27, 3139–3147.
- Deardorff, M.A., Tan, C., Conrad, L.J., and Klein, P.S. (1998). Frizzled-8 is expressed in the Spemann organizer and plays a role in early morphogenesis. *Development* 125, 2687–2700.
- Deb, A. (2014). Cell–cell interaction in the heart via Wnt/ β -catenin pathway after cardiac injury. *Cardiovascular Research* 102, 214–223.
- Dent, E.W., and Gertler, F.B. (2003). Cytoskeletal Dynamics and Transport in Growth Cone Motility and Axon Guidance. *Neuron* 40, 209–227.
- Dent, E.W., and Kalil, K. (2001). Axon Branching Requires Interactions between Dynamic Microtubules and Actin Filaments. *J. Neurosci.* 21, 9757–9769.
- Detrick, R., Dickey, D., and Kintner, C. (1990). The Effects of N-Cadherin Misexpression on Morphogenesis in *Xenopus* Embryos. *Neuron* 4, 493–506.
- Devenport, D. (2016). Tissue morphodynamics: Translating planar polarity cues into polarized cell behaviors. *Seminars in Cell & Developmental Biology* 55, 99–110.
- Devenport, D., and Fuchs, E. (2008). Planar polarization in embryonic epidermis orchestrates global asymmetric morphogenesis of hair follicles. *Nat Cell Biol* 10, 1257–1268.
- Dombeck, D.A., Harvey, C.D., Tian, L., Looger, L.L., and Tank, D.W. (2010). Functional imaging of hippocampal place cells at cellular resolution during virtual navigation. *Nat Neurosci* 13, 1433–1440.
- Drees, F., Pokutta, S., Yamada, S., Nelson, W.J., and Weis, W.I. (2005). α -Catenin Is a Molecular Switch that Binds E-Cadherin- β -Catenin and Regulates Actin-Filament Assembly. *Cell* 123, 903–915.
- Dudchenko, P.A. (2004). An overview of the tasks used to test working memory in rodents. *Neurosci Biobehav Rev* 28, 699–709.

- Dupret, D., Revest, J.-M., Koehl, M., Ichas, F., Giorgi, F.D., Costet, P., Abrous, D.N., and Piazza, P.V. (2008). Spatial Relational Memory Requires Hippocampal Adult Neurogenesis. *PLOS ONE* 3, e1959.
- Ernst, A., Alkass, K., Bernard, S., Salehpour, M., Perl, S., Tisdale, J., Possnert, G., Druid, H., and Frisén, J. (2014). Neurogenesis in the Striatum of the Adult Human Brain. *Cell* 156, 1072–1083.
- Etchamendy, N., Enderlin, V., Marighetto, A., Vouimba, R.M., Pallet, V., Jaffard, R., and Higeret, P. (2001). Alleviation of a selective age-related relational memory deficit in mice by pharmacologically induced normalization of brain retinoid signaling. *J. Neurosci.* 21, 6423–6429.
- Etchamendy, N., Konishi, K., Pike, G.B., Marighetto, A., and Bohbot, V.D. (2012). Evidence for a virtual human analog of a rodent relational memory task: a study of aging and fMRI in young adults. *Hippocampus* 22, 869–880.
- Etheridge, S.L., Ray, S., Li, S., Hamblet, N.S., Lijam, N., Tsang, M., Greer, J., Kardos, N., Wang, J., Sussman, D.J., et al. (2008). Murine Dishevelled 3 Functions in Redundant Pathways with Dishevelled 1 and 2 in Normal Cardiac Outflow Tract, Cochlea, and Neural Tube Development. *PLOS Genet* 4, e1000259.
- Ezan, J., and Montcouquiol, M. (2013). Revisiting planar cell polarity in the inner ear. *Seminars in Cell & Developmental Biology* 24, 499–506.
- Fannon, A.M., and Colman, D.R. (1996). A Model for Central Synaptic Junctional Complex Formation Based on the Differential Adhesive Specificities of the Cadherins. *Neuron* 17, 423–434.
- Fanto, M., Clayton, L., Meredith, J., Hardiman, K., Charroux, B., Kerridge, S., and McNeill, H. (2003). The tumor-suppressor and cell adhesion molecule Fat controls planar polarity via physical interactions with Atrophin, a transcriptional co-repressor. *Development* 130, 763–774.
- Fenstermaker, A.G., Prasad, A.A., Bechara, A., Adolfs, Y., Tissir, F., Goffinet, A., Zou, Y., and Pasterkamp, R.J. (2010). Wnt/Planar Cell Polarity Signaling Controls the Anterior–Posterior Organization of Monoaminergic Axons in the Brainstem. *J. Neurosci.* 30, 16053–16064.
- Franke, J.D., Montague, R.A., and Kiehart, D.P. (2010). Nonmuscle myosin II is required for cell proliferation, cell sheet adhesion and wing hair morphology during wing morphogenesis. *Developmental Biology* 345, 117–132.

- Fredette, B.J., Miller, J., and Ranscht, B. (1996). Inhibition of motor axon growth by T-cadherin substrata. *Development* 122, 3163–3171.
- Galimberti, I., Gogolla, N., Alberi, S., Santos, A.F., Muller, D., and Caroni, P. (2006). Long-Term Rearrangements of Hippocampal Mossy Fiber Terminal Connectivity in the Adult Regulated by Experience. *Neuron* 50, 749–763.
- Galimberti, I., Bednarek, E., Donato, F., and Caroni, P. (2010). EphA4 Signaling in Juveniles Establishes Topographic Specificity of Structural Plasticity in the Hippocampus. *Neuron* 65, 627–642.
- Gammill, L.S., and Bronner-Fraser, M. (2003). Neural crest specification: migrating into genomics. *Nat Rev Neurosci* 4, 795–805.
- Gao, F.-B., Kohwi, M., Brenman, J.E., Jan, L.Y., and Jan, Y.N. (2000). Control of Dendritic Field Formation in *Drosophila*: The Roles of Flamingo and Competition between Homologous Neurons. *Neuron* 28, 91–101.
- Garcia, M., Leduc, C., Lagardère, M., Argento, A., Sibarita, J.-B., and Thoumine, O. (2015). Two-tiered coupling between flowing actin and immobilized N-cadherin/catenin complexes in neuronal growth cones. *PNAS* 112, 6997–7002.
- Giannone, G., Mège, R.-M., and Thoumine, O. (2009). Multi-level molecular clutches in motile cell processes. *Trends in Cell Biology* 19, 475–486.
- Giese, A.P., Ezan, J., Wang, L., Lasvaux, L., Lembo, F., Mazzocco, C., Richard, E., Reboul, J., Borg, J.-P., Kelley, M.W., et al. (2012). Gipc1 has a dual role in Vangl2 trafficking and hair bundle integrity in the inner ear. *Development* 139, 3775–3785.
- Gilman, S.R., Iossifov, I., Levy, D., Ronemus, M., Wigler, M., and Vitkup, D. (2011). Rare De Novo Variants Associated with Autism Implicate a Large Functional Network of Genes Involved in Formation and Function of Synapses. *Neuron* 70, 898–907.
- Gogolla, N., Galimberti, I., Deguchi, Y., and Caroni, P. (2009). Wnt Signaling Mediates Experience-Related Regulation of Synapse Numbers and Mossy Fiber Connectivities in the Adult Hippocampus. *Neuron* 62, 510–525.
- Gold, A.E., and Kesner, R.P. (2005). The role of the CA3 subregion of the dorsal hippocampus in spatial pattern completion in the rat. *Hippocampus* 15, 808–814.

- Gonzales, R.B., DeLeon Galvan, C.J., Rangel, Y.M., and Claiborne, B.J. (2001). Distribution of thorny excrescences on CA3 pyramidal neurons in the rat hippocampus. *J. Comp. Neurol.* **430**, 357–368.
- Gordon-Weeks, P.R. (2004). Microtubules and growth cone function. *J. Neurobiol.* **58**, 70–83.
- Goto, T., and Keller, R. (2002). The Planar Cell Polarity Gene *Strabismus* Regulates Convergence and Extension and Neural Fold Closure in *Xenopus*. *Developmental Biology* **247**, 165–181.
- Goto, T., Davidson, L., Asashima, M., and Keller, R. (2005). Planar Cell Polarity Genes Regulate Polarized Extracellular Matrix Deposition during Frog Gastrulation. *Current Biology* **15**, 787–793.
- Götz, M., and Huttner, W.B. (2005). The cell biology of neurogenesis. *Nat Rev Mol Cell Biol* **6**, 777–788.
- Gumbiner, B.M. (2005). Regulation of cadherin-mediated adhesion in morphogenesis. *Nat Rev Mol Cell Biol* **6**, 622–634.
- Guo, Y., Zanetti, G., and Schekman, R. (2013). A novel GTP-binding protein–adaptor protein complex responsible for export of Vangl2 from the trans Golgi network. *eLife* **2**, e00160.
- Guyot, M.-C., Bosoi, C.M., Kharfallah, F., Reynolds, A., Drapeau, P., Justice, M., Gros, P., and Kibar, Z. (2011). A novel hypomorphic Looptail allele at the planar cell polarity Vangl2 gene. *Dev. Dyn.* **240**, 839–849.
- Hagen, T., and Vidal-Puig, A. (2002). Characterisation of the phosphorylation of β -catenin at the GSK-3 priming site Ser45. *Biochemical and Biophysical Research Communications* **294**, 324–328.
- Hagiwara, A., Yasumura, M., Hida, Y., Inoue, E., and Ohtsuka, T. (2014). The planar cell polarity protein Vangl2 bidirectionally regulates dendritic branching in cultured hippocampal neurons. *Molecular Brain* **7**.
- Hakeda-Suzuki, S., Ng, J., Tzu, J., Dietzl, G., Sun, Y., Harms, M., Nardine, T., Luo, L., and Dickson, B.J. (2002). Rac function and regulation during *Drosophila* development. *Nature* **416**, 438–442.
- Halbleib, J.M., and Nelson, W.J. (2006). Cadherins in development: cell adhesion, sorting, and tissue morphogenesis. *Genes Dev.* **20**, 3199–3214.

Hall, A., and Nobes, C.D. (2000). Rho GTPases: molecular switches that control the organization and dynamics of the actin cytoskeleton. *Philosophical Transactions of the Royal Society B: Biological Sciences* 355, 965–970.

Han, S.P., and Yap, A.S. (2012). The Cytoskeleton and Classical Cadherin Adhesions. In *Adherens Junctions: From Molecular Mechanisms to Tissue Development and Disease*, T. Harris, ed. (Springer Netherlands), pp. 111–135.

Harrington, M.J., Hong, E., Fasanmi, O., and Brewster, R. (2007). Cadherin-mediated adhesion regulates posterior body formation. *BMC Developmental Biology* 7, 130.

Harris, T.J.C., and Tepass, U. (2010). Adherens junctions: from molecules to morphogenesis. *Nat Rev Mol Cell Biol* 11, 502–514.

Hartfuss, E., Galli, R., Heins, N., and Götz, M. (2001). Characterization of CNS Precursor Subtypes and Radial Glia. *Developmental Biology* 229, 15–30.

Haubensak, W., Attardo, A., Denk, W., and Huttner, W.B. (2004). Neurons arise in the basal neuroepithelium of the early mammalian telencephalon: A major site of neurogenesis. *PNAS* 101, 3196–3201.

Hauser, K.F., Khurdayan, V.K., Goody, R.J., Nath, A., Saria, A., and Pauly, J.R. Selective vulnerability of cerebellar granule neuroblasts and their progeny to drugs with abuse liability. *Cerebellum* 2, 184–195.

Hegazy, S.A., Alshareef, A., Gelebart, P., Anand, M., Armanious, H., Ingham, R.J., and Lai, R. (2013). Disheveled proteins promote cell growth and tumorigenicity in ALK-positive anaplastic large cell lymphoma. *Cellular Signalling* 25, 295–307.

Heisenberg, C.-P., Tada, M., Rauch, G.-J., Saúde, L., Concha, M.L., Geisler, R., Stemple, D.L., Smith, J.C., and Wilson, S.W. (2000). Silberblick/Wnt11 mediates convergent extension movements during zebrafish gastrulation. *Nature* 405, 76–81.

Henderson, D.J., Conway, S.J., Greene, N.D.E., Gerrelli, D., Murdoch, J.N., Anderson, R.H., and Copp, A.J. (2001). Cardiovascular Defects Associated With Abnormalities in Midline Development in the Loop-tail Mouse Mutant. *Circ Res* 89, 6–12.

Henze, D.A., Urban, N.N., and Barrionuevo, G. (2000). The multifarious hippocampal mossy fiber pathway: a review. *Neuroscience* 98, 407–427.

Hering, H., and Sheng, M. (2001). Dendritic spines : structure, dynamics and regulation. *Nat Rev Neurosci* 2, 880–888.

Heyers, D., Luksch, H., and Redies, C. (2004). Selective synaptic cadherin expression by traced neurons of the chicken visual system¹. *Neuroscience* 127, 901–912.

Hong, E., and Brewster, R. (2006). N-cadherin is required for the polarized cell behaviors that drive neurulation in the zebrafish. *Development* 133, 3895–3905.

Honig, M.G., Petersen, G.G., Rutishauser, U.S., and Camilli, S.J. (1998). In Vitro Studies of Growth Cone Behavior Support a Role for Fasciculation Mediated by Cell Adhesion Molecules in Sensory Axon Guidance during Development. *Developmental Biology* 204, 317–326.

Hou, R., Liu, L., Anees, S., Hiroyasu, S., and Sibinga, N.E.S. (2006). The Fat1 cadherin integrates vascular smooth muscle cell growth and migration signals. *J Cell Biol* 173, 417–429.

Hsieh, S.H.-K., Ferraro, G.B., and Fournier, A.E. (2006). Myelin-Associated Inhibitors Regulate Cofilin Phosphorylation and Neuronal Inhibition through LIM Kinase and Slingshot Phosphatase. *J. Neurosci.* 26, 1006–1015.

Hua, Z.L., Smallwood, P.M., and Nathans, J. (2013). *Frizzled3* controls axonal development in distinct populations of cranial and spinal motor neurons. *eLife* 2.

Hua, Z.L., Jeon, S., Caterina, M.J., and Nathans, J. (2014). *Frizzled3* is required for the development of multiple axon tracts in the mouse central nervous system. *PNAS* 111, E3005–E3014.

Huttenlocher, A., and Horwitz, A.R. (2011). Integrins in Cell Migration. *Cold Spring Harb Perspect Biol* 3, a005074.

Iliescu, A., Gravel, M., Horth, C., Kibar, Z., and Gros, P. (2011). Loss of Membrane Targeting of Vangl Proteins Causes Neural Tube Defects. *Biochemistry* 50, 795–804.

Iliescu, A., Gravel, M., Horth, C., and Gros, P. (2014). Independent Mutations at Arg181 and Arg274 of Vangl Proteins That Are Associated with Neural Tube Defects in Humans Decrease Protein Stability and Impair Membrane Targeting. *Biochemistry* 53, 5356–5364.

- Imamura, Y., Itoh, M., Maeno, Y., Tsukita, S., and Nagafuchi, A. (1999). Functional Domains of α -Catenin Required for the Strong State of Cadherin-based Cell Adhesion. *J Cell Biol* *144*, 1311–1322.
- Imayoshi, I., Sakamoto, M., Ohtsuka, T., Takao, K., Miyakawa, T., Yamaguchi, M., Mori, K., Ikeda, T., Itohara, S., and Kageyama, R. (2008). Roles of continuous neurogenesis in the structural and functional integrity of the adult forebrain. *Nat Neurosci* *11*, 1153–1161.
- Inoue, A., and Sanes, J.R. (1997). Lamina-Specific Connectivity in the Brain: Regulation by N-Cadherin, Neurotrophins, and Glycoconjugates. *Science* *276*, 1428–1431.
- Iwai, Y., Usui, T., Hirano, S., Steward, R., Takeichi, M., and Uemura, T. (1997). Axon Patterning Requires D N-cadherin, a Novel Neuronal Adhesion Receptor, in the Drosophila Embryonic CNS. *Neuron* *19*, 77–89.
- Jenny, A., Darken, R.S., Wilson, P.A., and Mlodzik, M. (2003). Prickle and Strabismus form a functional complex to generate a correct axis during planar cell polarity signaling. *The EMBO Journal* *22*, 4409–4420.
- Jessen, J.R., and Solnica-Krezel, L. (2004). Identification and developmental expression pattern of van gogh-like 1, a second zebrafish strabismus homologue. *Gene Expression Patterns* *4*, 339–344.
- Jessen, J.R., Topczewski, J., Bingham, S., Sepich, D.S., Marlow, F., Chandrasekhar, A., and Solnica-Krezel, L. (2002). Zebrafish trilobite identifies new roles for Strabismus in gastrulation and neuronal movements. *Nat Cell Biol* *4*, 610–615.
- Jin, X. (2016). The role of neurogenesis during development and in the adult brain. *Eur J Neurosci* n/a-n/a.
- Kamiguchi, H. (2007). The Role of Cell Adhesion Molecules in Axon Growth and Guidance. In *Axon Growth and Guidance*, D. Bagnard, ed. (Springer New York), pp. 95–102.
- Kane, D.A., McFarland, K.N., and Warga, R.M. (2005). Mutations in half baked/E-cadherin block cell behaviors that are necessary for teleost epiboly. *Development* *132*, 1105–1116.
- Kaplan, M.S., and Hinds, J.W. (1977). Neurogenesis in the adult rat: electron microscopic analysis of light radioautographs. *Science* *197*, 1092–1094.

- Kapustina, M., Vitriol, E., Elston, T.C., Loew, L.M., and Jacobson, K. (2010). Modeling capping protein FRAP and CALI experiments reveals in vivo regulation of actin dynamics. *Cytoskeleton* 67, 519–534.
- Katsu, T., Ujike, H., Nakano, T., Tanaka, Y., Nomura, A., Nakata, K., Takaki, M., Sakai, A., Uchida, N., Imamura, T., et al. (2003). The human frizzled-3 (FZD3) gene on chromosome 8p21, a receptor gene for Wnt ligands, is associated with the susceptibility to schizophrenia. *Neuroscience Letters* 353, 53–56.
- Kaufmann, N., Wills, Z.P., and Vactor, D.V. (1998). *Drosophila* Rac1 controls motor axon guidance. *Development* 125, 453–461.
- Keller, R., Shih, J., and Domingo, C. (1992). The patterning and functioning of protrusive activity during convergence and extension of the *Xenopus* organiser. *Development* 116, 81–91.
- Kempermann, G., Song, H., and Gage, F.H. (2015). Neurogenesis in the Adult Hippocampus. *Cold Spring Harb Perspect Biol* 7, a018812.
- Kesner, R.P., and Rolls, E.T. (2015). A computational theory of hippocampal function, and tests of the theory: New developments. *Neuroscience & Biobehavioral Reviews* 48, 92–147.
- Kesner, R.P., and Warthen, D.K. (2010). Implications of CA3 NMDA and opiate receptors for spatial pattern completion in rats. *Hippocampus* 20, 550–557.
- Kheirbek, M.A., Tannenholz, L., and Hen, R. (2012). NR2B-Dependent Plasticity of Adult-Born Granule Cells is Necessary for Context Discrimination. *J. Neurosci.* 32, 8696–8702.
- Kibar, Z., Underhill, D.A., Canonne-Hergaux, F., Gauthier, S., Justice, M.J., and Gros, P. (2001b). Identification of a New Chemically Induced Allele (Lpm1Jus) at the Loop-Tail Locus: Morphology, Histology, and Genetic Mapping. *Genomics* 72, 331–337.
- Kibar, Z., Vogan, K.J., Groulx, N., Justice, M.J., Underhill, D.A., and Gros, P. (2001a). Ltap, a mammalian homolog of *Drosophila* Strabismus/Van Gogh, is altered in the mouse neural tube mutant Loop-tail. *Nat Genet* 28, 251–255.
- Kibar, Z., Torban, E., McDearmid, J.R., Reynolds, A., Berghout, J., Mathieu, M., Kirillova, I., De Marco, P., Merello, E., Hayes, J.M., et al. (2007). Mutations in VANG1 Associated with Neural-Tube Defects. *New England Journal of Medicine* 356, 1432–1437.

- Kibar, Z., Bosoi, C.M., Kooistra, M., Salem, S., Finnell, R.H., De Marco, P., Merello, E., Bassuk, A.G., Capra, V., and Gros, P. (2009). Novel mutations in VANG1 in neural tube defects. *Hum. Mutat.* 30, E706–E715.
- Kibar, Z., Salem, S., Bosoi, C., Pauwels, E., De Marco, P., Merello, E., Bassuk, A., Capra, V., and Gros, P. (2011). Contribution of VANG2 mutations to isolated neural tube defects. *Clinical Genetics* 80, 76–82.
- Klein, T.J., and Mlodzik, M. (2005). PLANAR CELL POLARIZATION: An Emerging Model Points in the Right Direction. *Annual Review of Cell and Developmental Biology* 21, 155–176.
- Knierim, J.J. (2015). The hippocampus. *Current Biology* 25, R1116–R1121.
- Knudsen, K.A., Soler, A.P., Johnson, K.R., and Wheelock, M.J. (1995). Interaction of alpha-actinin with the cadherin/catenin cell-cell adhesion complex via alpha-catenin. *J Cell Biol* 130, 67–77.
- Kobielak, A., Pasolli, H.A., and Fuchs, E. (2004). Mammalian formin-1 participates in adherens junctions and polymerization of linear actin cables. *Nat Cell Biol* 6, 21–30.
- Kolodkin, A.L., and Tessier-Lavigne, M. (2011). Mechanisms and Molecules of Neuronal Wiring: A Primer. *Cold Spring Harb Perspect Biol* 3, a001727.
- Kriegstein, A., and Alvarez-Buylla, A. (2009). The Glial Nature of Embryonic and Adult Neural Stem Cells. *Annu. Rev. Neurosci.* 32, 149–184.
- Kriegstein, A.R., and Götz, M. (2003). Radial glia diversity: A matter of cell fate. *Glia* 43, 37–43.
- Kropff, E., Yang, S.M., and Schinder, A.F. (2015). Dynamic role of adult-born dentate granule cells in memory processing. *Current Opinion in Neurobiology* 35, 21–26.
- Kuhn, H.G., Dickinson-Anson, H., and Gage, F.H. (1996). Neurogenesis in the dentate gyrus of the adult rat: age-related decrease of neuronal progenitor proliferation. *J. Neurosci.* 16, 2027–2033.
- Kuhn, T.B., Meberg, P.J., Brown, M.D., Bernstein, B.W., Minamide, L.S., Jensen, J.R., Okada, K., Soda, E.A., and Bamburg, J.R. (2000). Regulating actin dynamics in neuronal growth cones by ADF/cofilin and rho family GTPases. *Journal of Neurobiology* 44, 126–144.

- Lafont, F., Rouget, M., Rousselet, A., Valenza, C., and Prochiantz, A. (1993). Specific responses of axons and dendrites to cytoskeleton perturbations: an in vitro study. *Journal of Cell Science* *104*, 433–443.
- Lake, B.B., and Sokol, S.Y. (2009). Strabismus regulates asymmetric cell divisions and cell fate determination in the mouse brain. *J Cell Biol* *185*, 59–66.
- Lazarov, O., and Hollands, C. (2016). Hippocampal neurogenesis: Learning to remember. *Progress in Neurobiology* *138–140*, 1–18.
- Lee, A.C., and Suter, D.M. (2008). Quantitative analysis of microtubule dynamics during adhesion-mediated growth cone guidance. *Devel Neurobio* *68*, 1363–1377.
- Lee, C.-H., Herman, T., Clandinin, T.R., Lee, R., and Zipursky, S.L. (2001). N-Cadherin Regulates Target Specificity in the Drosophila Visual System. *Neuron* *30*, 437–450.
- Lee, O.-K., Frese, K.K., James, J.S., Chadda, D., Chen, Z.-H., Javier, R.T., and Cho, K.-O. (2003a). Discs-Large and Strabismus are functionally linked to plasma membrane formation. *Nat Cell Biol* *5*, 987–993.
- Lee, R.C., Clandinin, T.R., Lee, C.-H., Chen, P.-L., Meinertzhagen, I.A., and Zipursky, S.L. (2003b). The protocadherin Flamingo is required for axon target selection in the Drosophila visual system. *Nat Neurosci* *6*, 557–563.
- Lee, S., Song, Y.-A., Park, Y.-L., Cho, S.-B., Lee, W.-S., Lee, J.-H., Chung, I.-J., Kim, K.-K., Rew, J.-S., and Joo, Y.-E. (2011). Expression of KITENIN in human colorectal cancer and its relation to tumor behavior and progression. *Pathology International* *61*, 210–220.
- Lei, Y.-P., Zhang, T., Li, H., Wu, B.-L., Jin, L., and Wang, H.-Y. (2010). VANGL2 Mutations in Human Cranial Neural-Tube Defects. *New England Journal of Medicine* *362*, 2232–2235.
- Lele, Z., Folchert, A., Concha, M., Rauch, G.-J., Geisler, R., Rosa, F., Wilson, S.W., Hammerschmidt, M., and Bally-Cuif, L. (2002). parachute/n-cadherin is required for morphogenesis and maintained integrity of the zebrafish neural tube. *Development* *129*, 3281–3294.
- Letourneau, P.C. (1983). Differences in the organization of actin in the growth cones compared with the neurites of cultured neurons from chick embryos. *J Cell Biol* *97*, 963–973.

Leutgeb, J.K., Leutgeb, S., Moser, M.-B., and Moser, E.I. (2007). Pattern Separation in the Dentate Gyrus and CA3 of the Hippocampus. *Science* 315, 961–966.

Levitt, P., and Rakic, P. (1980). Immunoperoxidase localization of glial fibrillary acidic protein in radial glial cells and astrocytes of the developing rhesus monkey brain. *J. Comp. Neurol.* 193, 815–840.

Li, P., Zhang, H.Z., Huff, S., Nimmakayalu, M., Qumsiyeh, M., Yu, J., Szekely, A., Xu, T., and Pober, B.R. (2006). Karyotype–phenotype insights from 11q14.1-q23.2 interstitial deletions: FZD4 haploinsufficiency and exudative vitreoretinopathy in a patient with a complex chromosome rearrangement. *Am. J. Med. Genet.* 140A, 2721–2729.

Li, W., Lee, J., Vikis, H.G., Lee, S.-H., Liu, G., Aurandt, J., Shen, T.-L., Fearon, E.R., Guan, J.-L., Han, M., et al. (2004). Activation of FAK and Src are receptor-proximal events required for netrin signaling. *Nat Neurosci* 7, 1213–1221.

Lin, A.C., and Holt, C.E. (2007). Local translation and directional steering in axons. *The EMBO Journal* 26, 3729–3736.

Lin, C.H., and Forscher, P. (1993). Cytoskeletal remodeling during growth cone-target interactions. *J Cell Biol* 121, 1369–1383.

Lin, C.H., Espreafico, E.M., Mooseker, M.S., and Forscher, P. (1996). Myosin Drives Retrograde F-Actin Flow in Neuronal Growth Cones. *Neuron* 16, 769–782.

Lindqvist, M., Horn, Z., Bryja, V., Schulte, G., Papachristou, P., Ajima, R., Dyberg, C., Arenas, E., Yamaguchi, T.P., Lagercrantz, H., et al. (2010). Vang-like protein 2 and Rac1 interact to regulate adherens junctions. *J Cell Sci* 123, 472–483.

Loudon, R.P., Silver, L.D., Yee, H.F., and Gallo, G. (2006). RhoA-kinase and myosin II are required for the maintenance of growth cone polarity and guidance by nerve growth factor. *J. Neurobiol.* 66, 847–867.

Lowery, L.A., and Vactor, D.V. (2009). The trip of the tip: understanding the growth cone machinery. *Nat Rev Mol Cell Biol* 10, 332–343.

Lu, Q., and Adler, P.N. (2015). The diaphanous Gene of *Drosophila* Interacts Antagonistically with multiple wing hairs and Plays a Key Role in Wing Hair Morphogenesis. *PLOS ONE* 10, e0115623.

- Lu, Q., Schafer, D.A., and Adler, P.N. (2015). The *Drosophila* planar polarity gene multiple wing hairs directly regulates the actin cytoskeleton. *Development* 142, 2478–2486.
- Lucassen, P.J., Meerlo, P., Naylor, A.S., van Dam, A.M., Dayer, A.G., Fuchs, E., Oomen, C.A., and Czéh, B. (2010). Regulation of adult neurogenesis by stress, sleep disruption, exercise and inflammation: Implications for depression and antidepressant action. *European Neuropsychopharmacology* 20, 1–17.
- Lyuksyutova, A.I., Lu, C.-C., Milanesio, N., King, L.A., Guo, N., Wang, Y., Nathans, J., Tessier-Lavigne, M., and Zou, Y. (2003). Anterior-Posterior Guidance of Commissural Axons by Wnt-Frizzled Signaling. *Science* 302, 1984–1988.
- Maciver, S.K. (1998). How ADF/cofilin depolymerizes actin filaments. *Current Opinion in Cell Biology* 10, 140–144.
- Mahoney, P.A., Weber, U., Onofrechuk, P., Biessmann, H., Bryant, P.J., and Goodman, C.S. (1991). The fat tumor suppressor gene in *Drosophila* encodes a novel member of the cadherin gene superfamily. *Cell* 67, 853–868.
- Majima, T., Ogita, H., Yamada, T., Amano, H., Togashi, H., Sakisaka, T., Tanaka-Okamoto, M., Ishizaki, H., Miyoshi, J., and Takai, Y. (2009). Involvement of afadin in the formation and remodeling of synapses in the hippocampus. *Biochemical and Biophysical Research Communications* 385, 539–544.
- Maness, P.F., and Schachner, M. (2007). Neural recognition molecules of the immunoglobulin superfamily: signaling transducers of axon guidance and neuronal migration. *Nat Neurosci* 10, 19–26.
- Mapp, O.M., Walsh, G.S., Moens, C.B., Tada, M., and Prince, V.E. (2011). Zebrafish Prickle1b mediates facial branchiomotor neuron migration via a farnesylation-dependent nuclear activity. *Development* 138, 2121–2132.
- Marighetto, A., Etchamendy, N., Touzani, K., Torrea, C.C., Yee, B.K., Rawlins, J.N., and Jaffard, R. (1999). Knowing which and knowing what: a potential mouse model for age-related human declarative memory decline. *Eur. J. Neurosci.* 11, 3312–3322.
- Marsh, L., and Letourneau, P.C. (1984). Growth of neurites without filopodial or lamellipodial activity in the presence of cytochalasin B. *J Cell Biol* 99, 2041–2047.

- Marthiens, V., Gavard, J., Padilla, F., Monnet, C., Castellani, V., Lambert, M., and Mège, R.-M. (2005). A novel function for cadherin-11 in the regulation of motor axon elongation and fasciculation. *Molecular and Cellular Neuroscience* 28, 715–726.
- Masai, I., Lele, Z., Yamaguchi, M., Komori, A., Nakata, A., Nishiwaki, Y., Wada, H., Tanaka, H., Nojima, Y., Hammerschmidt, M., et al. (2003). N-cadherin mediates retinal lamination, maintenance of forebrain compartments and patterning of retinal neurites. *Development* 130, 2479–2494.
- Matakatsu, H., and Blair, S.S. (2006). Separating the adhesive and signaling functions of the Fat and Dachsous protocadherins. *Development* 133, 2315–2324.
- Matsunaga, M., Hatta, K., Nagafuchi, A., and Takeichi, M. (1988). Guidance of optic nerve fibres by N-cadherin adhesion molecules. *Nature* 334, 62–64.
- May-Simera, H.L., Kai, M., Hernandez, V., Osborn, D.P.S., Tada, M., and Beales, P.L. (2010). Bbs8, together with the planar cell polarity protein Vangl2, is required to establish left–right asymmetry in zebrafish. *Developmental Biology* 345, 215–225.
- McAuliffe, J.J., Bronson, S.L., Hester, M.S., Murphy, B.L., Dahlquist-Topalá, R., Richards, D.A., and Danzer, S.C. (2011). Altered patterning of dentate granule cell mossy fiber inputs onto CA3 pyramidal cells in limbic epilepsy. *Hippocampus* 21, 93–107.
- McConnell, S.K. (1995). Constructing the cerebral cortex: Neurogenesis and fate determination. *Neuron* 15, 761–768.
- Meberg, P.J., Ono, S., Minamide, L.S., Takahashi, M., and Bamburg, J.R. (1998). Actin depolymerizing factor and cofilin phosphorylation dynamics: Response to signals that regulate neurite extension. *Cell Motil. Cytoskeleton* 39, 172–190.
- Medeiros, N.A., Burnette, D.T., and Forscher, P. (2006). Myosin II functions in actin-bundle turnover in neuronal growth cones. *Nat Cell Biol* 8, 216–226.
- Mejillano, M.R., Kojima, S., Applewhite, D.A., Gertler, F.B., Svitkina, T.M., and Borisy, G.G. (2004). Lamellipodial Versus Filopodial Mode of the Actin Nanomachinery: Pivotal Role of the Filament Barbed End. *Cell* 118, 363–373.
- Merla, G., Brunetti-Pierri, N., Micale, L., and Fusco, C. (2010). Copy number variants at Williams–Beuren syndrome 7q11.23 region. *Hum Genet* 128, 3–26.

- Merte, J., Jensen, D., Wright, K., Sarsfield, S., Wang, Y., Schekman, R., and Ginty, D.D. (2010). Sec24b selectively sorts Vangl2 to regulate planar cell polarity during neural tube closure. *Nat Cell Biol* 12, 41–46.
- Mingaud, F., Le Moine, C., Etchamendy, N., Mormède, C., Jaffard, R., and Marighetto, A. (2007). The hippocampus plays a critical role at encoding discontinuous events for subsequent declarative memory expression in mice. *Hippocampus* 17, 264–270.
- Mingaud, F., Mormede, C., Etchamendy, N., Mons, N., Niedergang, B., Wietrzyk, M., Pallet, V., Jaffard, R., Krezel, W., Higuieret, P., et al. (2008). Retinoid hyposignaling contributes to aging-related decline in hippocampal function in short-term/working memory organization and long-term declarative memory encoding in mice. *J. Neurosci.* 28, 279–291.
- Mitchison, T., and Kirschner, M. (1988). Cytoskeletal dynamics and nerve growth. *Neuron* 1, 761–772.
- Mitra, S.K., Hanson, D.A., and Schlaepfer, D.D. (2005). Focal adhesion kinase: in command and control of cell motility. *Nat Rev Mol Cell Biol* 6, 56–68.
- Mizoguchi, A., Nakanishi, H., Kimura, K., Matsubara, K., Ozaki-Kuroda, K., Katata, T., Honda, T., Kiyohara, Y., Heo, K., Higashi, M., et al. (2002). Nectin an adhesion molecule involved in formation of synapses. *J Cell Biol* 156, 555–565.
- Montcouquiol, M., Rachel, R.A., Lanford, P.J., Copeland, N.G., Jenkins, N.A., and Kelley, M.W. (2003). Identification of Vangl2 and Scrb1 as planar polarity genes in mammals. *Nature* 423, 173–177.
- Montcouquiol, M., Sans, N., Huss, D., Kach, J., Dickman, J.D., Forge, A., Rachel, R.A., Copeland, N.G., Jenkins, N.A., Bogani, D., et al. (2006). Asymmetric Localization of Vangl2 and Fz3 Indicate Novel Mechanisms for Planar Cell Polarity in Mammals. *J. Neurosci.* 26, 5265–5275.
- Moreau, M.M., Piguel, N., Papouin, T., Koehl, M., Durand, C.M., Rubio, M.E., Loll, F., Richard, E.M., Mazzocco, C., Racca, C., et al. (2010). The Planar Polarity Protein Scribble1 Is Essential for Neuronal Plasticity and Brain Function. *J. Neurosci.* 30, 9738–9752.
- Moser, E.I., Kropff, E., and Moser, M.-B. (2008). Place Cells, Grid Cells, and the Brain's Spatial Representation System. *Annual Review of Neuroscience* 31, 69–89.

- Mrkusich, E.M., Flanagan, D.J., and Whittington, P.M. (2011). The core planar cell polarity gene *prickle* interacts with *flamingo* to promote sensory axon advance in the *Drosophila* embryo. *Developmental Biology* 358, 224–230.
- Myers, J.P., and Gomez, T.M. (2011). Focal Adhesion Kinase Promotes Integrin Adhesion Dynamics Necessary for Chemotropic Turning of Nerve Growth Cones. *J. Neurosci.* 31, 13585–13595.
- Myers, Jonathan P., Santiago-Medina, M., and Gomez, T.M. (2011). Regulation of axonal outgrowth and pathfinding by integrin–ecm interactions. *Devel Neurobio* 71, 901–923.
- Nagaoka, T., and Kishi, M. (2016). The planar cell polarity protein Vangl2 is involved in postsynaptic compartmentalization. *Neuroscience Letters* 612, 251–255.
- Nagaoka, T., Inutsuka, A., Begum, K., Hafiz, K. Musabbir bin, and Kishi, M. (2014b). Vangl2 Regulates E-Cadherin in Epithelial Cells. *Scientific Reports* 4, 6940.
- Nagaoka, T., Ohashi, R., Inutsuka, A., Sakai, S., Fujisawa, N., Yokoyama, M., Huang, Y.H., Igarashi, M., and Kishi, M. (2014a). The Wnt/Planar Cell Polarity Pathway Component Vangl2 Induces Synapse Formation through Direct Control of N-Cadherin. *Cell Reports* 6, 916–927.
- Nagaoka, T., Tabuchi, K., and Kishi, M. (2015). PDZ interaction of Vangl2 links PSD-95 and Prickle2 but plays only a limited role in the synaptic localisation of Vangl2. *Scientific Reports* 5, 12916.
- Nakashiba, T., Cushman, J.D., Pelkey, K.A., Renaudineau, S., Buhl, D.L., McHugh, T.J., Barrera, V.R., Chittajallu, R., Iwamoto, K.S., McBain, C.J., et al. (2012). Young Dentate Granule Cells Mediate Pattern Separation, whereas Old Granule Cells Facilitate Pattern Completion. *Cell* 149, 188–201.
- Nakayama, M., Nakajima, D., Nagase, T., Nomura, N., Seki, N., and Ohara, O. (1998). Identification of High-Molecular-Weight Proteins with Multiple EGF-like Motifs by Motif-Trap Screening. *Genomics* 51, 27–34.
- Nallathambi, J., Shukla, D., Rajendran, A., Namperumalsamy, P., Muthulakshmi, R., and Sundaresan, P. (2006). Identification of novel FZD4 mutations in Indian patients with familial exudative vitreoretinopathy. *Mol. Vis.* 12, 1086–1092.

Navarro, P., Ruco, L., and Dejana, E. (1998). Differential Localization of VE- and N-Cadherins in Human Endothelial Cells: VE-Cadherin Competes with N-Cadherin for Junctional Localization. *J Cell Biol* 140, 1475–1484.

Neunuebel, J.P., and Knierim, J.J. (2014). CA3 Retrieves Coherent Representations from Degraded Input: Direct Evidence for CA3 Pattern Completion and Dentate Gyrus Pattern Separation. *Neuron* 81, 416–427.

Nieman, M.T., Kim, J.B., Johnson, K.R., and Wheelock, M.J. (1999). Mechanism of extracellular domain-deleted dominant negative cadherins. *Journal of Cell Science* 112, 1621–1632.

Nikitzuk, J.S., Patil, S.B., Matikainen-Ankney, B.A., Scarpa, J., Shapiro, M.L., Benson, D.L., and Huntley, G.W. (2014). N-cadherin regulates molecular organization of excitatory and inhibitory synaptic circuits in adult hippocampus in vivo. *Hippocampus* 24, 943–962.

Noctor, S.C., Flint, A.C., Weissman, T.A., Wong, W.S., Clinton, B.K., and Kriegstein, A.R. (2002). Dividing Precursor Cells of the Embryonic Cortical Ventricular Zone Have Morphological and Molecular Characteristics of Radial Glia. *J. Neurosci.* 22, 3161–3173.

Noctor, S.C., Martínez-Cerdeño, V., Ivic, L., and Kriegstein, A.R. (2004). Cortical neurons arise in symmetric and asymmetric division zones and migrate through specific phases. *Nat Neurosci* 7, 136–144.

Noctor SC, Martínez-Cerdeño V, and Kriegstein AR (2007). COntribution of intermediate progenitor cells to cortical histogenesis. *Arch Neurol* 64, 639–642.

Nollet, F., Kools, P., and van Roy, F. (2000). Phylogenetic analysis of the cadherin superfamily allows identification of six major subfamilies besides several solitary members¹. *Journal of Molecular Biology* 299, 551–572.

O’Keefe, J., and Dostrovsky, J. (1971). The hippocampus as a spatial map. Preliminary evidence from unit activity in the freely-moving rat. *Brain Res.* 34, 171–175.

Oblander, S.A., Ensslen-Craig, S.E., Longo, F.M., and Brady-Kalnay, S.M. (2007). E-cadherin promotes retinal ganglion cell neurite outgrowth in a protein tyrosine phosphatase-mu-dependent manner. *Mol. Cell. Neurosci.* 34, 481–492.

Ozawa, M., and Kemler, R. (1998). The Membrane-proximal Region of the E-Cadherin Cytoplasmic Domain Prevents Dimerization and Negatively Regulates Adhesion Activity. *J Cell Biol* 142, 1605–1613.

Ozawa, M., Engel, J., and Kemler, R. (1990). Single amino acid substitutions in one Ca²⁺ binding site of uvomorulin abolish the adhesive function. *Cell* 63, 1033–1038.

Paemka, L., Mahajan, V.B., Ehaideb, S.N., Skeie, J.M., Tan, M.C., Wu, S., Cox, A.J., Sowers, L.P., Gecz, J., Jolly, L., et al. (2015). Seizures Are Regulated by Ubiquitin-specific Peptidase 9 X-linked (USP9X), a De-Ubiquitinase. *PLOS Genet* 11, e1005022.

Parsons, L., Harris, K.-L., Turner, K., and Whittington, P.M. (2003). Roundabout gene family functions during sensory axon guidance in the drosophila embryo are mediated by both Slit-dependent and Slit-independent mechanisms. *Developmental Biology* 264, 363–375.

Patten, A.R., Yau, S.Y., Fontaine, C.J., Meconi, A., Wortman, R.C., and Christie, B.R. (2015). The Benefits of Exercise on Structural and Functional Plasticity in the Rodent Hippocampus of Different Disease Models. *Brain Plasticity* 1, 97–127.

Paudyal, A., Damrau, C., Patterson, V.L., Ermakov, A., Formstone, C., Lalanne, Z., Wells, S., Lu, X., Norris, D.P., Dean, C.H., et al. (2010). The novel mouse mutant, chuzhoi, has disruption of Ptk7 protein and exhibits defects in neural tube, heart and lung development and abnormal planar cell polarity in the ear. *BMC Developmental Biology* 10, 87.

Pertz, O., Bozic, D., Koch, A.W., Fauser, C., Brancaccio, A., and Engel, J. (1999). A new crystal structure, Ca²⁺ dependence and mutational analysis reveal molecular details of E-cadherin homoassociation. *The EMBO Journal* 18, 1738–1747.

Piazzzi, G., Selgrad, M., Garcia, M., Ceccarelli, C., Fini, L., Bianchi, P., Laghi, L., D'Angelo, L., Paterini, P., Malfertheiner, P., et al. (2013). Van-Gogh-like 2 antagonises the canonical WNT pathway and is methylated in colorectal cancers. *Br J Cancer* 108, 1750–1756.

Piguel, N.H., Fievre, S., Blanc, J.-M., Carta, M., Moreau, M.M., Moutin, E., Pinheiro, V.L., Medina, C., Ezan, J., Lasvaux, L., et al. (2014). Scribble1/AP2 Complex Coordinates NMDA Receptor Endocytic Recycling. *Cell Reports* 9, 712–727.

- Pinto, D., Pagnamenta, A.T., Klei, L., Anney, R., Merico, D., Regan, R., Conroy, J., Magalhaes, T.R., Correia, C., Abrahams, B.S., et al. (2010). Functional impact of global rare copy number variation in autism spectrum disorders. *Nature* 466, 368–372.
- Piper, M., Anderson, R., Dwivedy, A., Weinl, C., van Horck, F., Leung, K.M., Cogill, E., and Holt, C. (2006). Signaling Mechanisms Underlying Slit2-Induced Collapse of Xenopus Retinal Growth Cones. *Neuron* 49, 215–228.
- Pokutta, S., and Weis, W.I. (2000). Structure of the Dimerization and β -Catenin- Binding Region of α -Catenin. *Molecular Cell* 5, 533–543.
- Pokutta, S., Drees, F., Takai, Y., Nelson, W.J., and Weis, W.I. (2002). Biochemical and Structural Definition of the α -Afadin- and Actin-binding Sites of α -Catenin. *J. Biol. Chem.* 277, 18868–18874.
- Pokutta, S., Drees, F., Yamada, S., Nelson, W.J., and Weis, W.I. (2008). Biochemical and structural analysis of α -catenin in cell–cell contacts. *Biochemical Society Transactions* 36, 141–147.
- Pollard, T.D., Blanchoin, L., and Mullins, R.D. (2000). Molecular Mechanisms Controlling Actin Filament Dynamics in Nonmuscle Cells. *Annu. Rev. Biophys. Biomol. Struct.* 29, 545–576.
- Popov, V.I., Kleschevnikov, A.M., Klimenko, O.A., Stewart, M.G., and Belichenko, P.V. (2011). Three-dimensional synaptic ultrastructure in the dentate gyrus and hippocampal area CA3 in the Ts65Dn mouse model of Down syndrome. *J. Comp. Neurol.* 519, 1338–1354.
- Price, D.J., Kennedy, H., Dehay, C., Zhou, L., Mercier, M., Jossin, Y., Goffinet, A.M., Tissir, F., Blakey, D., and Molnár, Z. (2006). The development of cortical connections. *European Journal of Neuroscience* 23, 910–920.
- Qu, Y., Glasco, D.M., Zhou, L., Sawant, A., Ravni, A., Fritzsche, B., Damrau, C., Murdoch, J.N., Evans, S., Pfaff, S.L., et al. (2010). Atypical Cadherins Celsr1-3 Differentially Regulate Migration of Facial Branchiomotor Neurons in Mice. *J. Neurosci.* 30, 9392–9401.
- Qu, Y., Huang, Y., Feng, J., Alvarez-Bolado, G., Grove, E.A., Yang, Y., Tissir, F., Zhou, L., and Goffinet, A.M. (2014). Genetic evidence that Celsr3 and Celsr2, together with Fzd3, regulate forebrain wiring in a Vangl-independent manner. *Proc. Natl. Acad. Sci. U.S.A.* 111, E2996-3004.
- Rachel, R.A., Murdoch, J.N., Beermann, F., Copp, A.J., and Mason, C.A. (2000). Retinal axon misrouting at the optic chiasm in mice with neural tube closure defects. *Genesis* 27, 32–47.

- Radice, G.L., Rayburn, H., Matsunami, H., Knudsen, K.A., Takeichi, M., and Hynes, R.O. (1997). Developmental Defects in Mouse Embryos Lacking N-Cadherin. *Developmental Biology* 181, 64–78.
- Ramsbottom, S.A., Sharma, V., Rhee, H.J., Eley, L., Phillips, H.M., Rigby, H.F., Dean, C., Chaudhry, B., and Henderson, D.J. (2014). Vangl2-regulated polarisation of second heart field-derived cells is required for outflow tract lengthening during cardiac development. *PLoS Genet.* 10, e1004871.
- Rao, M.S., and Mayer-Proschel, M. (1997). Glial-Restricted Precursors Are Derived from Multipotent Neuroepithelial Stem Cells. *Developmental Biology* 188, 48–63.
- Rawls, A.S., and Wolff, T. (2003). Strabismus requires Flamingo and Prickle function to regulate tissue polarity in the *Drosophila* eye. *Development* 130, 1877–1887.
- Redies, C., Inuzuka, H., and Takeichi, M. (1992). Restricted expression of N- and R-cadherin on neurites of the developing chicken CNS. *J. Neurosci.* 12, 3525–3534.
- Redish, A.D., Rosenzweig, E.S., Bohanick, J.D., McNaughton, B.L., and Barnes, C.A. (2000). Dynamics of Hippocampal Ensemble Activity Realignment: Time versus Space. *J. Neurosci.* 20, 9298–9309.
- Riehl, R., Johnson, K., Bradley, R., Grunwald, G.B., Cornel, E., Lilienbaum, A., and Holt, C.E. (1996). Cadherin Function Is Required for Axon Outgrowth in Retinal Ganglion Cells In Vivo. *Neuron* 17, 837–848.
- Rivero, O., Selten, M.M., Sich, S., Popp, S., Bacmeister, L., Amendola, E., Negwer, M., Schubert, D., Proft, F., Kiser, D., et al. (2015). Cadherin-13, a risk gene for ADHD and comorbid disorders, impacts GABAergic function in hippocampus and cognition. *Transl Psychiatry* 5, e655.
- Roberts, J.L., Hovanes, K., Dasouki, M., Manzardo, A.M., and Butler, M.G. (2014). Chromosomal microarray analysis of consecutive individuals with autism spectrum disorders or learning disability presenting for genetic services. *Gene* 535, 70–78.
- Robitaille, J., MacDonald, M.L.E., Kaykas, A., Sheldahl, L.C., Zeisler, J., Dubé, M.-P., Zhang, L.-H., Singaraja, R.R., Guernsey, D.L., Zheng, B., et al. (2002). Mutant frizzled-4 disrupts retinal angiogenesis in familial exudative vitreoretinopathy. *Nat Genet* 32, 326–330.

- Rodríguez, I. (2004). The dachsous gene, a member of the cadherin family, is required for Wg-dependent pattern formation in the *Drosophila* wing disc. *Development* 131, 3195–3206.
- Rodriguez, O.C., Schaefer, A.W., Mandato, C.A., Forscher, P., Bement, W.M., and Waterman-Storer, C.M. (2003). Conserved microtubule–actin interactions in cell movement and morphogenesis. *Nat Cell Biol* 5, 599–609.
- Rohrschneider, M.R., Elsen, G.E., and Prince, V.E. (2007). Zebrafish *Hoxb1a* regulates multiple downstream genes including *prickle1b*. *Developmental Biology* 309, 358–372.
- Rollenhagen, A., Sätzler, K., Rodríguez, E.P., Jonas, P., Frotscher, M., and Lübke, J.H.R. (2007). Structural Determinants of Transmission at Large Hippocampal Mossy Fiber Synapses. *J. Neurosci.* 27, 10434–10444.
- Rolls, E. (2013). The mechanisms for pattern completion and pattern separation in the hippocampus. *Front. Syst. Neurosci* 7, 74.
- Ryu, H.-S., Park, Y.-L., Park, S.-J., Lee, J.-H., Cho, S.-B., Lee, W.-S., Chung, I.-J., Kim, K.-K., Lee, K.-H., Kweon, S.-S., et al. (2010). KITENIN Is Associated with Tumor Progression in Human Gastric Cancer. *Anticancer Res* 30, 3479–3486.
- Sahay, A., Scobie, K.N., Hill, A.S., O’Carroll, C.M., Kheirbek, M.A., Burghardt, N.S., Fenton, A.A., Dranovsky, A., and Hen, R. (2011a). Increasing adult hippocampal neurogenesis is sufficient to improve pattern separation. *Nature* 472, 466–470.
- Sahay, A., Wilson, D.A., and Hen, R. (2011b). Pattern Separation: A Common Function for New Neurons in Hippocampus and Olfactory Bulb. *Neuron* 70, 582–588.
- Sajan, S.A., Fernandez, L., Nieh, S.E., Rider, E., Bukshpun, P., Wakahiro, M., Christian, S.L., Rivière, J.-B., Sullivan, C.T., Sudi, J., et al. (2013). Both Rare and De Novo Copy Number Variants Are Prevalent in Agenesis of the Corpus Callosum but Not in Cerebellar Hypoplasia or Polymicrogyria. *PLOS Genet* 9, e1003823.
- Salomon, D., Ayalon, O., Patel-King, R., Hynes, R.O., and Geiger, B. (1992). Extrajunctional distribution of N-cadherin in cultured human endothelial cells. *Journal of Cell Science* 102, 7–17.
- Sanchez-Alvarez, L., Visanuvimol, J., McEwan, A., Su, A., Imai, J.H., and Colavita, A. (2011). VANG-1 and PRKL-1 Cooperate to Negatively Regulate Neurite Formation in *Caenorhabditis elegans*. *PLOS Genet* 7, e1002257.

- Sans, N., Ezan, J., Moreau, M.M., and Montcouquiol, M. (2016). Planar Cell Polarity Gene Mutations in Autism Spectrum Disorder, Intellectual Disabilities, and Related Deletion/Duplication Syndromes. In *Neuronal and Synaptic Dysfunction in Autism Spectrum Disorder and Intellectual Disability*, (Elsevier), pp. 189–219.
- Sarmiere, P.D., and Bamburg, J.R. (2004). Regulation of the neuronal actin cytoskeleton by ADF/cofilin. *J. Neurobiol.* *58*, 103–117.
- Sasselli, V., Boesmans, W., Vanden Berghe, P., Tissir, F., Goffinet, A.M., and Pachnis, V. (2013). Planar cell polarity genes control the connectivity of enteric neurons. *Journal of Clinical Investigation* *123*, 1763–1772.
- Schaefer, A.W., Schoonderwoert, V.T.G., Ji, L., Mederios, N., Danuser, G., and Forscher, P. (2008). Coordination of Actin Filament and Microtubule Dynamics during Neurite Outgrowth. *Developmental Cell* *15*, 146–162.
- Schafer, S.T., Han, J., Pena, M., Halbach, O. von B. und, Peters, J., and Gage, F.H. (2015). The Wnt Adaptor Protein ATP6AP2 Regulates Multiple Stages of Adult Hippocampal Neurogenesis. *J. Neurosci.* *35*, 4983–4998.
- Scott, J.A., Shewan, A.M., Elzen, N.R. den, Loureiro, J.J., Gertler, F.B., and Yap, A.S. (2006). Ena/VASP Proteins Can Regulate Distinct Modes of Actin Organization at Cadherin-adhesive Contacts. *Mol. Biol. Cell* *17*, 1085–1095.
- Scoville, W.B., and Milner, B. (1957). Loss of recent memory after bilateral hippocampal lesions. *J. Neurol. Neurosurg. Psychiatr.* *20*, 11–21.
- Seifert, J.R.K., and Mlodzik, M. (2007). Frizzled/PCP signalling: a conserved mechanism regulating cell polarity and directed motility. *Nat Rev Genet* *8*, 126–138.
- Senti, K.-A., Usui, T., Boucke, K., Greber, U., Uemura, T., and Dickson, B.J. (2003). Flamingo Regulates R8 Axon-Axon and Axon-Target Interactions in the Drosophila Visual System. *Current Biology* *13*, 828–832.
- Shafer, B., Onishi, K., Lo, C., Colakoglu, G., and Zou, Y. (2011). Vangl2 Promotes Wnt/Planar Cell Polarity-like Signaling by Antagonizing Dvl1-Mediated Feedback Inhibition in Growth Cone Guidance. *Developmental Cell* *20*, 177–191.

- Sheng, M., and Hoogenraad, C.C. (2007). The Postsynaptic Architecture of Excitatory Synapses: A More Quantitative View. *Annual Review of Biochemistry* 76, 823–847.
- Shih, J., and Keller, R. (1992). Cell motility driving mediolateral intercalation in explants of *Xenopus laevis*. *Development* 116, 901–914.
- Shima, Y., Kengaku, M., Hirano, T., Takeichi, M., and Uemura, T. (2004). Regulation of Dendritic Maintenance and Growth by a Mammalian 7-Pass Transmembrane Cadherin. *Developmental Cell* 7, 205–216.
- Shimizu, T., Yabe, T., Muraoka, O., Yonemura, S., Aramaki, S., Hatta, K., Bae, Y.-K., Nojima, H., and Hibi, M. (2005). E-cadherin is required for gastrulation cell movements in zebrafish. *Mechanisms of Development* 122, 747–763.
- Singh, J., and Mlodzik, M. (2012). Planar cell polarity signaling: coordination of cellular orientation across tissues. *WIREs Dev Biol* 1, 479–499.
- Sittaramane, V., Pan, X., Glasco, D.M., Huang, P., Gurung, S., Bock, A., Li, S., Wang, H., Kawakami, K., Matisse, M.P., et al. (2013). The PCP protein Vangl2 regulates migration of hindbrain motor neurons by acting in floor plate cells, and independently of cilia function. *Developmental Biology* 382, 400–412.
- Small, J.V., Isenberg, G., and Celis, J.E. (1978). Polarity of actin at the leading edge of cultured cells. *Nature* 272, 638–639.
- Sokol, S.Y. (1996). Analysis of Dishevelled signalling pathways during *Xenopus* development. *Current Biology* 6, 1456–1467.
- Sokol, S.Y. (2015). Spatial and temporal aspects of Wnt signaling and planar cell polarity during vertebrate embryonic development. *Seminars in Cell & Developmental Biology* 42, 78–85.
- Song, H., Hu, J., Chen, W., Elliott, G., Andre, P., Gao, B., and Yang, Y. (2010). Planar cell polarity breaks bilateral symmetry by controlling ciliary positioning. *Nature* 466, 378–382.
- Sowers, L.P., Loo, L., Wu, Y., Campbell, E., Ulrich, J.D., Wu, S., Paemka, L., Wassink, T., Meyer, K., Bing, X., et al. (2013). Disruption of the non-canonical Wnt gene PRICKLE2 leads to autism-like behaviors with evidence for hippocampal synaptic dysfunction. *Mol Psychiatry* 18, 1077–1089.

- Stark, S.M., Yassa, M.A., and Stark, C.E.L. (2010). Individual differences in spatial pattern separation performance associated with healthy aging in humans. *Learn. Mem.* *17*, 284–288.
- Steimel, A., Wong, L., Najarro, E.H., Ackley, B.D., Garriga, G., and Hutter, H. (2010). The Flamingo ortholog FMI-1 controls pioneer-dependent navigation of follower axons in *C. elegans*. *Development* *137*, 3663–3673.
- Stein, K.F., and Mackensen, J.A. (1957). Abnormal development of the thoracic skeleton in mice homozygous for the gene for looped-tail. *Am. J. Anat.* *100*, 205–223.
- Stockinger, A., Eger, A., Wolf, J., Beug, H., and Foisner, R. (2001). E-cadherin regulates cell growth by modulating proliferation-dependent beta-catenin transcriptional activity. *J. Cell Biol.* *154*, 1185–1196.
- Strale, P.-O., Duchesne, L., Peyret, G., Montel, L., Nguyen, T., Png, E., Tampé, R., Troyanovsky, S., Hénon, S., Ladoux, B., et al. (2015). The formation of ordered nanoclusters controls cadherin anchoring to actin and cell–cell contact fluidity. *J Cell Biol* *210*, 333–346.
- Strong, L.C., and Hollander, W.F. (1949). Hereditary loop-tail in the house mouse accompanied by imperforate vagina and with lethal craniorachischisis when homozygous. *Journal of Heredity* *40*, 329–334.
- Strutt, D. (2003). Frizzled signalling and cell polarisation in *Drosophila* and vertebrates. *Development* *130*, 4501–4513.
- Strutt, D., and Warrington, S.J. (2008). Planar polarity genes in the *Drosophila* wing regulate the localisation of the FH3-domain protein Multiple Wing Hairs to control the site of hair production. *Development* *135*, 3103–3111.
- Strutt, H., and Strutt, D. (2009). Asymmetric localisation of planar polarity proteins: Mechanisms and consequences. *Seminars in Cell & Developmental Biology* *20*, 957–963.
- Strutt, D.I., Weber, U., and Mlodzik, M. (1997). The role of RhoA in tissue polarity and Frizzled signalling. *Nature* *387*, 292–295.
- Strutt, H., Warrington, S.J., and Strutt, D. (2011). Dynamics of Core Planar Polarity Protein Turnover and Stable Assembly into Discrete Membrane Subdomains. *Developmental Cell* *20*, 511–525.

- Suter, D.M., and Forscher, P. (1998). An emerging link between cytoskeletal dynamics and cell adhesion molecules in growth cone guidance. *Current Opinion in Neurobiology* 8, 106–116.
- Suter, D.M., and Forscher, P. (2000). Substrate-cytoskeletal coupling as a mechanism for the regulation of growth cone motility and guidance. *Journal of Neurobiology* 44, 97–113.
- Suter, D.M., and Forscher, P. (2001). Transmission of growth cone traction force through apCAM–cytoskeletal linkages is regulated by Src family tyrosine kinase activity. *J Cell Biol* 155, 427–438.
- Suto, F., Tsuboi, M., Kamiya, H., Mizuno, H., Kiyama, Y., Komai, S., Shimizu, M., Sanbo, M., Yagi, T., Hiromi, Y., et al. (2007). Interactions between Plexin-A2, Plexin-A4, and Semaphorin 6A Control Lamina-Restricted Projection of Hippocampal Mossy Fibers. *Neuron* 53, 535–547.
- Tabarés-Seisdedos, R., and Rubenstein, J.L.R. (2009). Chromosome 8p as a potential hub for developmental neuropsychiatric disorders: implications for schizophrenia, autism and cancer. *Mol Psychiatry* 14, 563–589.
- Takai, Y., Shimizu, K., and Ohtsuka, T. (2003). The roles of cadherins and nectins in interneuronal synapse formation. *Current Opinion in Neurobiology* 13, 520–526.
- Takeda, H., Shimoyama, Y., Nagafuchi, A., and Hirohashi, S. (1999). E-cadherin functions as a cis-dimer at the cell–cell adhesive interface in vivo. *Nat Struct Mol Biol* 6, 310–312.
- Takeichi, M. (1988). The cadherins: cell-cell adhesion molecules controlling animal morphogenesis. *Development* 102, 639–655.
- Tamura, M., Koyama, R., Ikegaya, Y., Matsuki, N., and Yamada, M.K. (2006). K252a, an inhibitor of Trk, disturbs pathfinding of hippocampal mossy fibers: *NeuroReport* 17, 481–486.
- Tamura, M., Tamura, N., Ikeda, T., Koyama, R., Ikegaya, Y., Matsuki, N., and Yamada, M.K. (2009). Influence of brain-derived neurotrophic factor on pathfinding of dentate granule cell axons, the hippocampal mossy fibers. *Molecular Brain* 2, 2.
- Tanaka, H., Shan, W., Phillips, G.R., Arndt, K., Bozdagi, O., Shapiro, L., Huntley, G.W., Benson, D.L., and Colman, D.R. (2000). Molecular Modification of N-Cadherin in Response to Synaptic Activity. *Neuron* 25, 93–107.

- Tao, H., Manak, J.R., Sowers, L., Mei, X., Kiyonari, H., Abe, T., Dahdaleh, N.S., Yang, T., Wu, S., Chen, S., et al. (2011). Mutations in Prickle Orthologs Cause Seizures in Flies, Mice, and Humans. *The American Journal of Human Genetics* 88, 138–149.
- Taylor, J., Abramova, N., Charlton, J., and Adler, P.N. (1998). Van Gogh: A New *Drosophila* Tissue Polarity Gene. *Genetics* 150, 199–210.
- Tessier-Lavigne, M., and Placzek, M. (1991). Target attraction: Are developing axons guided by chemotropism? *Trends in Neurosciences* 14, 303–310.
- Thoumine, O. (2008). Interplay between adhesion turnover and cytoskeleton dynamics in the control of growth cone migration. *Cell Adhesion & Migration* 2, 263.
- Timsit, S., Martinez, S., Allinquant, B., Peyron, F., Puellas, L., and Zalc, B. (1995). Oligodendrocytes originate in a restricted zone of the embryonic ventral neural tube defined by DM-20 mRNA expression. *J. Neurosci.* 15, 1012–1024.
- Tissir, F., and Goffinet, A.M. (2006). Expression of planar cell polarity genes during development of the mouse CNS. *European Journal of Neuroscience* 23, 597–607.
- Tissir, F., and Goffinet, A.M. (2013). Shaping the nervous system: role of the core planar cell polarity genes. *Nat Rev Neurosci* 14, 525–535.
- Tissir, F., Qu, Y., Montcouquiol, M., Zhou, L., Komatsu, K., Shi, D., Fujimori, T., Labeau, J., Tyteca, D., Courtoy, P., et al. (2010). Lack of cadherins Celsr2 and Celsr3 impairs ependymal ciliogenesis, leading to fatal hydrocephalus. *Nat Neurosci* 13, 700–707.
- Togashi, H., Abe, K., Mizoguchi, A., Takaoka, K., Chisaka, O., and Takeichi, M. (2002). Cadherin Regulates Dendritic Spine Morphogenesis. *Neuron* 35, 77–89.
- Tønnesen, J., Katona, G., Rózsa, B., and Nägerl, U.V. (2014). Spine neck plasticity regulates compartmentalization of synapses. *Nat Neurosci* 17, 678–685.
- Torban, E., Patenaude, A.-M., Leclerc, S., Rakowiecki, S., Gauthier, S., Andelfinger, G., Epstein, D.J., and Gros, P. (2008). Genetic interaction between members of the Vangl family causes neural tube defects in mice. *PNAS* 105, 3449–3454.

- Torban, E., Iliescu, A., and Gros, P. (2012). Chapter Ten - An Expanding Role of Vangl Proteins in Embryonic Development. In *Current Topics in Developmental Biology*, Y. Yang, ed. (Academic Press), pp. 237–261.
- Touzani, K., Marighetto, A., and Jaffard, R. (2003). Fos imaging reveals ageing-related changes in hippocampal response to radial maze discrimination testing in mice. *Eur. J. Neurosci.* 17, 628–640.
- Tree, D.R.P., Shulman, J.M., Rousset, R., Scott, M.P., Gubb, D., and Axelrod, J.D. (2002). Prickle Mediates Feedback Amplification to Generate Asymmetric Planar Cell Polarity Signaling. *Cell* 109, 371–381.
- Tronel, S., Belnoue, L., Grosjean, N., Revest, J.-M., Piazza, P.-V., Koehl, M., and Abrous, D.N. (2012). Adult-born neurons are necessary for extended contextual discrimination. *Hippocampus* 22, 292–298.
- Tsukiura, T., Suzuki, C., Shigemune, Y., and Mochizuki-Kawai, H. (2008). Differential contributions of the anterior temporal and medial temporal lobe to the retrieval of memory for person identity information. *Hum Brain Mapp* 29, 1343–1354.
- Uchida, N., Honjo, Y., Johnson, K.R., Wheelock, M.J., and Takeichi, M. (1996). The catenin/cadherin adhesion system is localized in synaptic junctions bordering transmitter release zones. *J Cell Biol* 135, 767–779.
- Veeman, M.T., Slusarski, D.C., Kaykas, A., Louie, S.H., and Moon, R.T. (2003). Zebrafish Prickle, a Modulator of Noncanonical Wnt/Fz Signaling, Regulates Gastrulation Movements. *Current Biology* 13, 680–685.
- Verma, S., Shewan, A.M., Scott, J.A., Helwani, F.M., Elzen, N.R. den, Miki, H., Takenawa, T., and Yap, A.S. (2004). Arp2/3 Activity Is Necessary for Efficient Formation of E-cadherin Adhesive Contacts. *J. Biol. Chem.* 279, 34062–34070.
- Vinson, C.R., and Adler, P.N. (1987). Directional non-cell autonomy and the transmission of polarity information by the frizzled gene of *Drosophila*. *Nature* 329, 549–551.
- Vitriol, E.A., and Zheng, J.Q. (2012). Growth Cone Travel in Space and Time: the Cellular Ensemble of Cytoskeleton, Adhesion, and Membrane. *Neuron* 73, 1068–1081.

- Vitriol, E.A., Uetrecht, A.C., Shen, F., Jacobson, K., and Bear, J.E. (2007). Enhanced EGFP-chromophore-assisted laser inactivation using deficient cells rescued with functional EGFP-fusion proteins. *PNAS* *104*, 6702–6707.
- Vivancos, V., Chen, P., Spassky, N., Qian, D., Dabdoub, A., Kelley, M., Studer, M., and Guthrie, S. (2009). Wnt activity guides facial branchiomotor neuron migration, and involves the PCP pathway and JNK and ROCK kinases. *Neural Development* *4*, 7.
- Vladar, E.K., Bayly, R.D., Sangoram, A.M., Scott, M.P., and Axelrod, J.D. (2012). Microtubules Enable the Planar Cell Polarity of Airway Cilia. *Current Biology* *22*, 2203–2212.
- Wada, H., Iwasaki, M., Sato, T., Masai, I., Nishiwaki, Y., Tanaka, H., Sato, A., Nojima, Y., and Okamoto, H. (2005). Dual roles of zygotic and maternal Scribble1 in neural migration and convergent extension movements in zebrafish embryos. *Development* *132*, 2273–2285.
- Wada, H., Tanaka, H., Nakayama, S., Iwasaki, M., and Okamoto, H. (2006). Frizzled3a and Celsr2 function in the neuroepithelium to regulate migration of facial motor neurons in the developing zebrafish hindbrain. *Development* *133*, 4749–4759.
- Wallingford, J.B. (2012). Planar cell polarity and the developmental control of cell behavior in vertebrate embryos. *Annu. Rev. Cell Dev. Biol.* *28*, 627–653.
- Wallingford, J.B., and Habas, R. (2005). The developmental biology of Dishevelled: an enigmatic protein governing cell fate and cell polarity. *Development* *132*, 4421–4436.
- Wallingford, J.B., and Harland, R.M. (2002). Neural tube closure requires Dishevelled-dependent convergent extension of the midline. *Development* *129*, 5815–5825.
- Wallingford, J.B., and Mitchell, B. (2011). Strange as it may seem: the many links between Wnt signaling, planar cell polarity, and cilia. *Genes Dev.* *25*, 201–213.
- Wallingford, J.B., Rowling, B.A., Vogeli, K.M., Rothbacher, U., Fraser, S.E., and Harland, R.M. (2000). Dishevelled controls cell polarity during *Xenopus* gastrulation. *Nature* *405*, 81–85.
- Walsh, G.S., Grant, P.K., Morgan, J.A., and Moens, C.B. (2011). Planar polarity pathway and Nance-Horan syndrome-like 1b have essential cell-autonomous functions in neuronal migration. *Development* *138*, 3033–3042.

- Wang, J., Hamblet, N.S., Mark, S., Dickinson, M.E., Brinkman, B.C., Segil, N., Fraser, S.E., Chen, P., Wallingford, J.B., and Wynshaw-Boris, A. (2006a). Dishevelled genes mediate a conserved mammalian PCP pathway to regulate convergent extension during neurulation. *Development* 133, 1767–1778.
- Wang, Y., and Nathans, J. (2007). Tissue/planar cell polarity in vertebrates: new insights and new questions. *Development* 134, 647–658.
- Wang, Y., Zhang, J., Mori, S., and Nathans, J. (2006b). Axonal Growth and Guidance Defects in Frizzled3 Knock-Out Mice: A Comparison of Diffusion Tensor Magnetic Resonance Imaging, Neurofilament Staining, and Genetically Directed Cell Labeling. *J. Neurosci.* 26, 355–364.
- Wang, Y.-K., Samos, C.H., Peoples, R., Pérez-Jurado, L.A., Nusse, R., and Francke, U. (1997). A novel human homologue of the *Drosophila* frizzled wnt receptor gene binds wingless protein and is in the Williams syndrome deletion at 7q11.23. *Hum. Mol. Genet.* 6, 465–472.
- Wansleben, C., Feitsma, H., Montcouquiol, M., Kroon, C., Cuppen, E., and Meijlink, F. (2010). Planar cell polarity defects and defective Vangl2 trafficking in mutants for the COPII gene Sec24b. *Development* 137, 1067–1073.
- Warrington, S.J., Strutt, H., and Strutt, D. (2013). The Frizzled-dependent planar polarity pathway locally promotes E-cadherin turnover via recruitment of RhoGEF2. *Development* 140, 1045–1054.
- Weiss, E.E., Kroemker, M., Rüdiger, A.-H., Jockusch, B.M., and Rüdiger, M. (1998). Vinculin Is Part of the Cadherin–Catenin Junctional Complex: Complex Formation between α -Catenin and Vinculin. *J Cell Biol* 141, 755–764.
- Wen, S., Zhu, H., Lu, W., Mitchell, L.E., Shaw, G.M., Lammer, E.J., and Finnell, R.H. (2010). Planar cell polarity pathway genes and risk for spina bifida. *Am. J. Med. Genet.* 152A, 299–304.
- Wen, Z., Han, L., Bamburg, J.R., Shim, S., Ming, G., and Zheng, J.Q. (2007). BMP gradients steer nerve growth cones by a balancing act of LIM kinase and Slingshot phosphatase on ADF/cofilin. *J Cell Biol* 178, 107–119.
- White, J., Mazzeu, J.F., Hoischen, A., Jhangiani, S.N., Gambin, T., Alcino, M.C., Penney, S., Saraiva, J.M., Hove, H., Skovby, F., et al. (2015). DVL1 Frameshift Mutations Clustering in the

Penultimate Exon Cause Autosomal-Dominant Robinow Syndrome. *The American Journal of Human Genetics* 96, 612–622.

Wijetunge, L.S., Angibaud, J., Frick, A., Kind, P.C., and Nägerl, U.V. (2014). Stimulated Emission Depletion (STED) Microscopy Reveals Nanoscale Defects in the Developmental Trajectory of Dendritic Spine Morphogenesis in a Mouse Model of Fragile X Syndrome. *J. Neurosci.* 34, 6405–6412.

Wilke, S.A., Raam, T., Antonios, J.K., Bushong, E.A., Koo, E.H., Ellisman, M.H., and Ghosh, A. (2014). Specific disruption of hippocampal mossy fiber synapses in a mouse model of familial Alzheimer's disease. *PLoS ONE* 9, e84349.

Williams, B.B., Cantrell, V.A., Mundell, N.A., Bennett, A.C., Quick, R.E., and Jessen, J.R. (2012). VANGL2 regulates membrane trafficking of MMP14 to control cell polarity and migration. *J Cell Sci* 125, 2141–2147.

Williams, E.J., Furness, J., Walsh, F.S., and Doherty, P. (1994). Activation of the FGF receptor underlies neurite outgrowth stimulated by L1, N-CAM, and N-cadherin. *Neuron* 13, 583–594.

Williams, M.E., Wilke, S.A., Daggett, A., Davis, E., Otto, S., Ravi, D., Ripley, B., Bushong, E.A., Ellisman, M.H., Klein, G., et al. (2011). Cadherin-9 Regulates Synapse-Specific Differentiation in the Developing Hippocampus. *Neuron* 71, 640–655.

Wilson, N.H., and Stoeckli, E.T. (2012). Chapter eight - Sonic Hedgehog Regulates Wnt Activity During Neural Circuit Formation. In *Vitamins & Hormones*, G. Litwack, ed. (Academic Press), pp. 173–209.

Wilson, P., and Keller, R. (1991). Cell rearrangement during gastrulation of *Xenopus*: direct observation of cultured explants. *Development* 112, 289–300.

Winter, C.G., Wang, B., Ballew, A., Royou, A., Karess, R., Axelrod, J.D., and Luo, L. (2001). *Drosophila* Rho-Associated Kinase (Drok) Links Frizzled-Mediated Planar Cell Polarity Signaling to the Actin Cytoskeleton. *Cell* 105, 81–91.

Wixted, J.T., and Squire, L.R. (2011). The medial temporal lobe and the attributes of memory. *Trends Cogn. Sci. (Regul. Ed.)* 15, 210–217.

Wolff, T., and Rubin, G.M. (1998). Strabismus, a novel gene that regulates tissue polarity and cell fate decisions in *Drosophila*. *Development* 125, 1149–1159.

- Wong, L.L., and Adler, P.N. (1993). Tissue polarity genes of *Drosophila* regulate the subcellular location for prehair initiation in pupal wing cells. *J Cell Biol* *123*, 209–221.
- Wu, J., and Mlodzik, M. (2008). The Frizzled Extracellular Domain Is a Ligand for Van Gogh/Stbm during Nonautonomous Planar Cell Polarity Signaling. *Developmental Cell* *15*, 462–469.
- Xu, G., Craig, A.W.B., Greer, P., Miller, M., Anastasiadis, P.Z., Lilien, J., and Balsamo, J. (2004). Continuous association of cadherin with β -catenin requires the non-receptor tyrosine-kinase Fer. *Journal of Cell Science* *117*, 3207–3219.
- Yamada, K.M., Spooner, B.S., and Wessells, N.K. (1971). Ultrastructure and Function of Growth Cones and Axons of Cultured Nerve Cells. *J Cell Biol* *49*, 614–635.
- Yamada, S., Pokutta, S., Drees, F., Weis, W.I., and Nelson, W.J. (2005). Deconstructing the Cadherin-Catenin-Actin Complex. *Cell* *123*, 889–901.
- Yan, J., Lu, Q., Fang, X., and Adler, P.N. (2009). Rho1 has multiple functions in *Drosophila* wing planar polarity. *Developmental Biology* *333*, 186–199.
- Yang, C., Axelrod, J.D., and Simon, M.A. (2002). Regulation of Frizzled by Fat-like Cadherins during Planar Polarity Signaling in the *Drosophila* Compound Eye. *Cell* *108*, 675–688.
- Yates, L.L., Papakrivopoulou, J., Long, D.A., Goggolidou, P., Connolly, J.O., Woolf, A.S., and Dean, C.H. (2010a). The planar cell polarity gene *Vangl2* is required for mammalian kidney-branching morphogenesis and glomerular maturation. *Hum. Mol. Genet.* *19*, 4663–4676.
- Yates, L.L., Schnatwinkel, C., Murdoch, J.N., Bogani, D., Formstone, C.J., Townsend, S., Greenfield, A., Niswander, L.A., and Dean, C.H. (2010b). The PCP genes *Celsr1* and *Vangl2* are required for normal lung branching morphogenesis. *Hum. Mol. Genet.* *19*, 2251–2267.
- Yin, H., Copley, C.O., Goodrich, L.V., and Deans, M.R. (2012). Comparison of Phenotypes between Different *vangl2* Mutants Demonstrates Dominant Effects of the Looptail Mutation during Hair Cell Development. *PLOS ONE* *7*, e31988.
- Yoon, T.M., Kim, S.-A., Lee, J.K., Park, Y.-L., Kim, G.Y., Joo, Y.-E., Lee, J.H., Kim, K.K., and Lim, S.C. (2013). Expression of KITENIN and its association with tumor progression in oral squamous cell carcinoma. *Auris Nasus Larynx* *40*, 222–226.

Yoshioka, T., Hagiwara, A., Hida, Y., and Ohtsuka, T. (2013). Vangl2, the planner cell polarity protein, is complexed with postsynaptic density protein PSD-95. *FEBS Letters* 587, 1453–1459.

Zeesman, S., Kjaergaard, S., Hove, H.D., Kirchhoff, M., Stevens, J.M., and Nowaczyk, M.J.M. (2012). Microdeletion in distal 17p13.1: A recognizable phenotype with microcephaly, distinctive facial features, and intellectual disability. *Am. J. Med. Genet.* 158A, 1832–1836.

Zhang, C.-L., Zou, Y., He, W., Gage, F.H., and Evans, R.M. (2008). A role for adult TLX-positive neural stem cells in learning and behaviour. *Nature* 451, 1004–1007.

Zhang, J., Shemezis, J.R., McQuinn, E.R., Wang, J., Sverdlov, M., and Chenn, A. (2013). AKT activation by N-cadherin regulates beta-catenin signaling and neuronal differentiation during cortical development. *Neural Development* 8, 7.

Zhong, W., and Chia, W. (2008). Neurogenesis and asymmetric cell division. *Current Opinion in Neurobiology* 18, 4–11.

Zhou, F.-Q., and Cohan, C.S. (2004). How actin filaments and microtubules steer growth cones to their targets. *J. Neurobiol.* 58, 84–91.

Zhou, L., Bar, I., Achouri, Y., Campbell, K., Backer, O.D., Hebert, J.M., Jones, K., Kessaris, N., Rouvroit, C.L. de, O’Leary, D., et al. (2008). Early Forebrain Wiring: Genetic Dissection Using Conditional *Celsr3* Mutant Mice. *Science* 320, 946–949.

Zicha, D., Dobbie, I.M., Holt, M.R., Monypenny, J., Soong, D.Y.H., Gray, C., and Dunn, G.A. (2003). Rapid Actin Transport During Cell Protrusion. *Science* 300, 142–145.

La Polarité Cellulaire Planaire (PCP) est une voie de signalisation originellement identifiée chez les invertébrés pour son rôle dans l'établissement d'une asymétrie cellulaire perpendiculaire à l'axe apico-basal. Elle définit une polarité dans le plan d'un épithélium et coordonne cette polarité dans tout l'épithélium. L'activation de la voie PCP conduit à une réorganisation du cytosquelette en passant par une modulation des zones d'adhésion, régulant ainsi la forme et les mouvements des cellules. La voie de signalisation de la PCP est conservée tout au long de l'évolution jusqu'au mammifères, et contrôle la morphogénèse de divers tissus dont les tissus épithéliaux et mésenchymateux, ainsi que pour les tissus cardiaques, osseux, pulmonaire ou encore rénaux, mais aussi le système nerveux pour n'en citer que quelques-uns.

Afin d'identifier le rôle de *vangl2*, un des gènes centraux de la PCP, dans la mise en place de la circuiterie hippocampale, nous avons créé un modèle murin où *vangl2* est supprimé de façon conditionnelle (cKO) dans le télencéphale à des stades précoces de l'embryogénèse.

J'ai d'abord montré que Vangl2 est enrichi dans les neurones immatures de la zone sous-granulaire du DG, ainsi que dans l'arborisation des neurites (axones et dendrites) des cellules granulaires (CG) du gyrus denté (DG) de l'hippocampe. Ainsi, Vangl2 est enrichi dans le *stratum lucidum* (sl), une région dense en contacts synaptiques entre le DG et le CA3. Dans cette région a lieu une synapse très particulière entre l'axone des CG, la fibre moussue (Mf) qui forme des boutons géants (MfB) et les excroissances épineuse (TE) issues de la partie proximale des dendrites apicaux. L'analyse structurale et ultrastructurale de ces épines démontre que l'élargissement et la complexification de la synapse MfB/TE est bloquée dans nos mutants, alors que les zones actives (PSD) des épines sont présentes, mais réorganisées. De façon intéressante, dans une zone plus distale des dendrites des neurones du CA3 (sl), les épines sont, elles, plus grosses, suggérant un remodelage complexe du réseau en l'absence de *vangl2*. Enfin, j'ai pu montrer que ces défauts morphologiques étaient corrélés à des problèmes de mémoire complexe (mémoire déclarative) qui dépendent de l'hippocampe mais aussi du cortex. Cette étude montre pour la première fois l'importance du signal PCP dans maturation *in vivo* d'un circuit hippocampique spécifique ainsi que ces conséquences cognitives.

D'autres résultats *in vitro* montrent que la suppression de *vangl2* augmente la vitesse de déplacement des cônes de croissance sur des substrats de N-cadhérine. J'ai utilisé la microscopie en super résolution spt-PALM-TIRF pour montrer que cette augmentation de croissance est inversement proportionnelle à la vitesse du flux rétrograde d'actine. Des expériences de FRAP permettent de suggérer que les molécules de N-cadhérine engagées dans des interactions hémophiliques (adhésion) est plus importante dans les mutants *vangl2*.

Je propose que Vangl2 contrôle le recyclage et la stabilité des protéines N-cadhérine dans les sites d'adhésion afin de réguler localement les dynamiques d'actine et par conséquent la croissance neuronale.